REVISTA PORTUGUESA DE QUÍMICA

RPTQAT 28 (1/4) 1-141 (1986)
ISSN 0035-0419

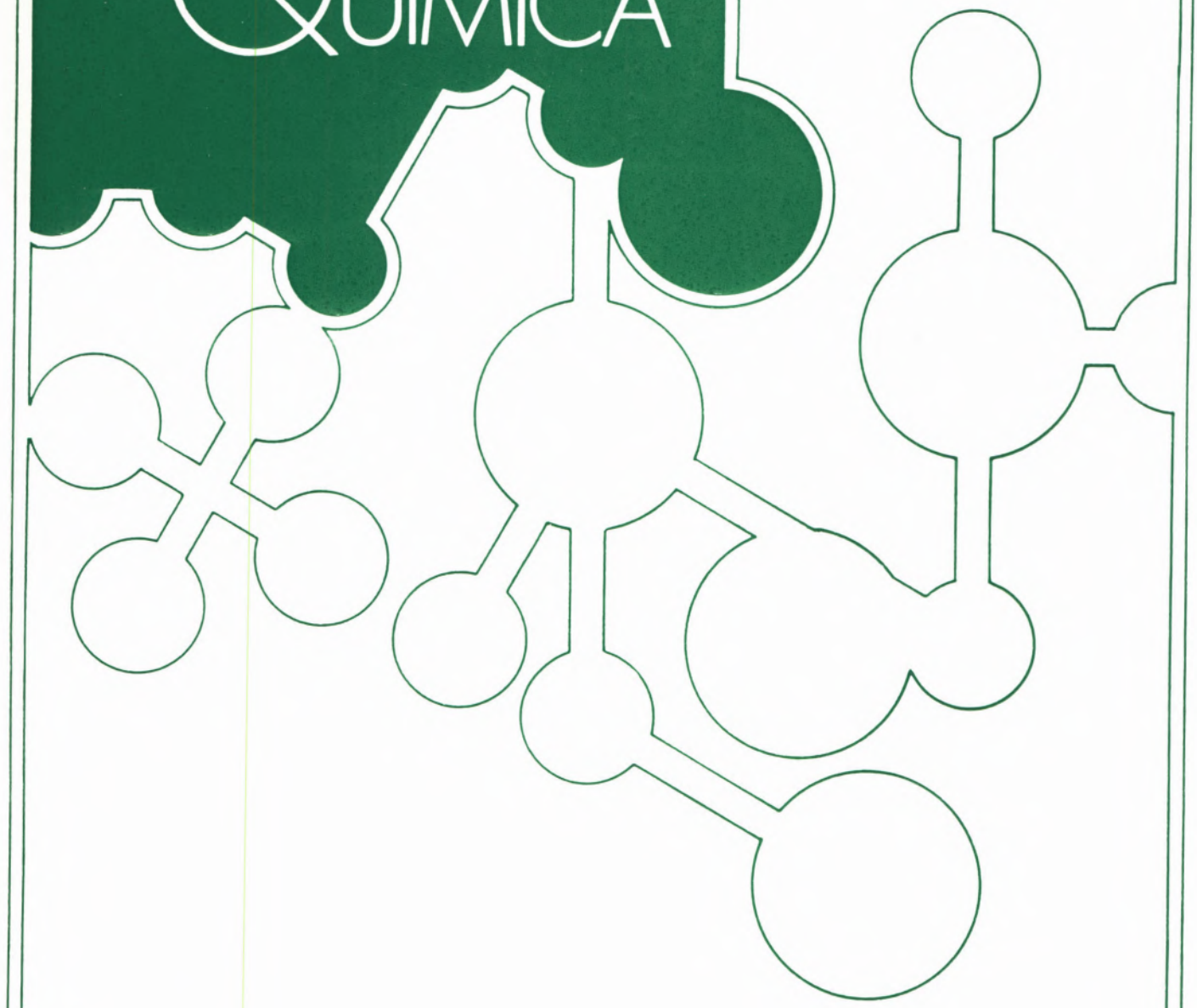

Rev. Port. Quím., Vol. 28, N.º 1/4
Pp. 1 - 141 — Porto, 1986

REVISTA PORTUGUESA DE QUÍMICA

Propriedade e edição da
SOCIEDADE PORTUGUESA DE QUÍMICA
em continuação da
REVISTA DE QUÍMICA PURA E APLICADA
fundada em 1905 por
Ferreira da Silva.
Subsidiada pelo
INSTITUTO NACIONAL DE INVESTIGAÇÃO CIENTÍFICA

Redacção e administração — Departamento de Química-Faculdade de Ciências-Porto

Composição, impressão e acabamento — Imprensa Portuguesa
Rua Formosa, 108-116 - Porto

Capa — Luís Filipe de Abreu

Publicação trimestral. Número avulso: 500$00. Assinatura (quatro números), Portugal 1600$00, outros países: U.S. $12 por número, $40 por assinatura

índice

J. J. R. Fraústo da Silda A. J. L. Pombeiro	1	Nuclear Quadrupole Resonance Study of Anilinium Bromides and Iodides
Maria José Bação Madruga	11	Separação e Identificação das Formas Físico-Químicas do ^{60}Co na Água do Mar e na Água Doce
C. A. Nieto de Castro R. D. Trengove W. A. Wakeham	17	The Density Dependence of the Thermal Conductivity of Toluene
F. Capitán F. Molina P. Espinosa L. F. Capitán-Vallvey	22	A Study of the Ni(II)-2-(*o*-Hydroxyphenylimino-methyl)Pyrrole System. Determination of Ni(II)
M. R. Bermejo M. Gayoso M. Isabel Fernández A. Hermida M. Ester Gómez	26	Coordination Chemistry of TI(III) With Azoles I Compounds of $TlXX'_2$ With Pyrazole
Sebastião J. Formosinho António J. C. Varandas	33	A Simple Theoretical Model for the Energy Barrier in Unimolecular Reactions
Sebastião J. Formosinho	38	The Role of Bond Order and Entropy of Transition States in Electron Transfer Reactions Part 1. — Outer-sphere electron exchange processes
Sebastião J. Formosinho	48	The Role of Bond Order and Entropy of Transition States in Electron Transfer Reactions Part 2. — Reaction Energy Effects on Outer-sphere and Inner-sphere Reactions
Hugh D. Burrows Sebastião J. Formosinho	57	The Role of Bond Order and Entropy of Transition States in Electron Transfer Reactions Part 3. — Cross-reaction Relationships
Sebastião J. Formosinho	61	The Role of Bond Order and Entropy of Transition States in Electron Transfer Reactions Part 4. — Electrochemical Reactions and the Anodic-Cathodic Asymmetry of the Tafel Plots

M. F. Ribeiro F. Ramôa Ribeiro P. Dufresne C. Marcilly	**68**	Effect of Calcination Conditions on the Catalytic Properties of NiH Mordenite in Toluene Disproportionation
A. M. Amorim da Costa	**71**	Carbon-Hydrogen Stretching Raman Modes and Lateral Interaction in N-Dodecyl Compounds
M. Brotas de Carvalho M. Regina Sales Grade Ana P. Carvalho M. J. Belzunce S. Mendioroz J. A. Pajares	**77**	Diatomitos de Rio Maior e de Óbidos: Composição Química e Características Mineralógicas e Texturais
Carlos F. G. C. Geraldes Victor M. S. Gil M. Helena S. F. Teixeira F. Teixeira	**85**	Nuclear Magnetic Resonance Studies of Cimetidine and Ranitidine in Solution: Acide Base Equilibria and Effect of Antacids
Nosrat M. Abed Abdel-Ghani A. Elagamey Salah Z. Sowellim Abdel-Fattah A. Harb	**95**	Some Reactions With α,β-Unsaturated Acyl Isothiocyanates
A. M. M. Cardoso M. G. Santana Marques A. J. Ferrer Correia	**101**	Metastable Mapping: Bidimensional Mass Spectrometry in a Reserve Geometry Instrument
António R. T. Calado César A. N. Viana Lídia M. P. C. Albuquerque Raquel M. C. Gonçalves	**110**	Método Estatístico Aplicado à Cinética de Reacções de 2.ª Ordem 1 — Reacção de Menschutkin do iodeto de etilo com a trietilamina em butanol-2
M. Teresa S. D. Vasconcelos Adélio A. S. C. Machado	**120**	Calibração do Eléctrodo de Vidro para Determinação de Constantes de Formação em Meio nem muito Ácido nem muito Alcalino (pH 4-10)

J.J.R. FRAÚSTO DA SILVA
A.J.L. POMBEIRO
Centro de Química Estrutural,
Complexo I
Instituto Superior Técnico,
Av. Rovisco Pais,
1096 Lisboa, Portugal

NUCLEAR QUADRUPOLE RESONANCE STUDY OF ANILINIUM BROMIDES AND IODIDES

Br^{79} (and Br^{81}) and I^{127} nuclear quadrupole resonance frequencies (ν) were detected for the anilinium salts $YC_6H_4NH_3^+X^-$ (Y = o-,m-,p-,CH_3; o-, m-, p -NO_2; p-CF_3. X = Br and/or I). The asymmetry parameter η (for X = I) and the fraction of ionic character of the halide bond were estimated for these compounds and the results demonstrate a polarisation of the halide electron cloud which was interpreted by considering the conceivable formation of $\overset{+}{N}H\ldots X^-$ hydrogen bonds with predominant electrostatic character.

Linear dependences of ν upon Hammett's σ constants for the para *and the* meta *Y substituent were observed and are object of discussion.*

I — INTRODUCTION

Hydrogen-bonding plays an important role in various chemical and biological systems but, although it has been widely studied, the examples selected usually involve the most commonly accepted hydrogen bond former atoms and groups. The halogens have received comparatively less attention, to the exception of their hydracids, notably HF, perhaps for lack of suitable experimental techniques. Indeed, a wide variety of methods has been applied to the detection of this type of bonding, namely based on the measurement of vapour pressure, density, molecular weight, molar volume, dielectric constant, thermal and electric conductivity, refractive index, etc., but they are all indirect and hydrogen bonding is postulated on the basis of some deviation from expected «normal» physical properties. More direct evidence for formation of this type of bonds has been achieved by X-ray analysis and spectroscopic techniques (infrared, Raman and nuclear magnetic resonance) [1]. In the last decade, nuclear quadrupole resonance (N.Q.R.) spectroscopy (which has a more specific character than those spectroscopic methods and provides a quantitative interpretation of the results) has also been applied to the detection of this type of bonding, but only a few examples have been reported, *e.g.*, on studies of ammonia and ammonium hydrate [2], guanidinium ion [3], hexamethylenetetramine and its complexes [4], hexamethylenetetramine triphenol [5], 2,5-dichlorophenol [6], trichloroacetic acid [7], carboxylic acids and alcohols [8], systems involving carbonyl groups [9], HCl_2^- salts [10], aducts of chloroacetic acids with pyridine [11], aducts of 2,6-dichloro-4-nitrophenol with amine [12] and systems with nonlinear hydrogen (deuterium) bonds [13].

Fraústo da Silva and Vilas-Boas have also reported [14] the results obtained with a variety of alkylammonium bromides and iodides, $R_3NH^+X^-$ (R_3=Me_3,Me_2H,MeH_2,Et_3,Et_2H,EtH_2

or PrH_2; X=Br or I) which were interpreted [14] on the basis of formation of hydrogen bonding of the type $N^+H \ldots X^-$, with predominant electrostatic character; the effects of temperature and deuteration on the hydrogen bonds of some of these alkylammonium halides were also studied by N.Q.R. by other authors [15].

The present work extends the N.Q.R. study to the related anilinium bromides and iodides of the type $YC_6H_4NH_3^+X^-$ (Y = o-,m-p-Me; o-,m-,p-NO_2; p-CF_3; p-Cl) and $C_6H_5NMeH_2^+X^-$ which afford further information on these less studied hydrogen bond formers. The corresponding chloride salts were not studied since their N.Q.R. frequencies are lower than the measuring range of the spetrometer used. The investigation by N.Q.R. of the hydrogen bonding, the ^1H-^2D isotope efect and the order-disorder phase transition in the anilinium bromides $C_6H_5NH_3^+Br^-$, $C_6H_5ND_3^+Br^-$ and $C_6D_5NH_3^+Br^-$ has been reported by other authors [16].

II—THEORETICAL BASIS OF THE METHOD

Nuclei with spin equal or greater than one present a non-spherical charge distribution which can be interpreted in terms of a nuclear quadrupole moment given by eQ where e is the elementary charge and Q is the electric quadrupole which measures the deviation from the spherical symmetry.

If such a nucleus lies within a non-homogeneous (non-spherical) electric field (due to the electrons which are in its vicinity and which belong to the same atom or which are involved in the bonding to this atom), an interaction occurs between its nuclear quadrupole moment and the electric field gradient and the energy of this nuclear quadrupole coupling is given by

$$E_Q = eQq_{zz}\,\frac{3m_I^2 - I(I+1)}{4I(2I-1)} \qquad (1)$$

In this expression eQ is the quadrupole moment, eQq_{zz} is the nuclear quadrupole coupling constant, I is the nuclear spin, m_I is the magnetic nuclear quantum number and q_{zz} is the maximum electric field gradient given by

$$q_{zz} = \frac{\partial^2 V}{\partial z^2} \qquad (2)$$

where V is the electrostatic potential due to the charges in the vicinity of the nucleus and z is the direction of the maximum gradient. Equation [1] is valid only when the electric field gradient has axial symmetry, *i.e.*, when q_{xx} equals q_{yy} and the following relationship is obbeyed:

$$q_{xx} = \frac{\partial^2 V}{\partial x^2} = q_{yy} = \frac{\partial^2 V}{\partial y^2} \qquad (3)$$

In other cases, an asymmetry parameter, η, may be defined as

$$\eta = \frac{q_{xx} - q_{yy}}{q_{zz}} \qquad (4)$$

and it has to be considered in the expression which allows to estimate E_Q, which is then more complex than equation (1) [17].

Equation (1) shows that the nuclear energy levels are doubly degenerate (E_Q depends on m_I^2 and, hence, on $|m_I|$) and, according to the selection rule $\Delta m_I = \pm 1$, the frequency of the allowed transitions is given by

$$\nu_r = E'_Q - E''_Q = \frac{3eQ\,q_{zz}}{4hI(2I-1)}(2M_I - 1) \qquad (5)$$

where M_I is the highest value of m_I corresponding to each energy level (m_I may have a total of $2I+1$ possible values: $-I, -I+1, \ldots, I-1, I$).

Since Br^{79} (and Br^{81}) and I^{127} nuclei have $I = 3/2$ and $5/2$, respectively, only one transition ($\pm 3/2 \leftarrow \pm 1/2$) and two transitions ($\pm 5/2 \leftarrow \pm 3/2$ and $\pm 3/2 \leftarrow \pm 1/2$), respectively, are expected to be observed and

their frequencies are given by the following equations:

For I = 3/2 (Br^{79} or Br^{81}):

$$\nu_r = \frac{eQ\,q_{zz}}{2h}(1 + \eta^2/3)^{1/2} \qquad (6)$$

For I = 5/2 (I^{127}):

$$\nu_1 = \frac{3eQ\,q_{zz}}{20h}(1 + 1.092\ \eta^2 - 0.634\ \eta^4) \qquad (7)$$

$$\nu_2 = \frac{3eQ\,q_{zz}}{10h}(1 - 0.203\ \eta^2 + 0.162\ \eta^4) \qquad (8)$$

In the latter case (I = 5/2), since two resonance frequencies are observed, it is possible to estimate both the nuclear quadrupole coupling constant ($eQ\,q_{zz}$) and the η parameter of the electric field gradient.

Moreover, from the knowledge of the quadrupole coupling constant, it is possible [18] to estimate roughly the fraction of ionic character of the bond according to the following simplified expression:

$$i = 1 - \frac{|\,eQ\,q_{mol}\,|}{|\,eQ\,q_{at}\,|} \qquad (9)$$

where eQq_{mol} is the quadrupole coupling constant of the halogen atom in the molecule under study and eQq_{at} is the quadrupole coupling constant of the *free* halogen atom [eQq_{at} (Br^{79}) = — 769.756 and eQq_{at} (I^{127}) = +2292.712].

It should also be pointed out that the above mentioned transitions will only occur if the halogen nucleus is surrounded by a non-spherical electronic distribution ($q_{zz} \neq 0$), as it will happen if the electronic cloud is directionally polarized by some kind of interaction, *e.g.*, hydrogen bonding.

III — RESULTS AND DISCUSSION

General aspects

In the compounds studied in the present work a single nuclear quadrupole resonance for Br^{79} (or Br^{81}) and two resonances for I^{127} were observed, in the bromide and iodide salts, respectively, at the frequencies given by Table I, which also shows the estimated fraction of ionic character of the postulated $^{+}NH \ldots X^-$ bond and the asymmetry parameter of the field gradient in the case of the iodides. This parameter, η_I, was estimated from equations (7) and (8) whereas the corresponding fraction of ionic character of the $^{+}NH \ldots I^-$ bond, i_I, was estimated from equation (9) where $|\,eQq_{mol}\,|$ was $|\,eQ\,q_{zz}\,|$ calculated from expressions (7) and (8).

Since the evaluation of η_{Br} was not possible in this study, $|\,eQ\,q_{mol}\,|$ [to be used in expression (9)] was estimated from equation (6) by considering $(1 + \eta^2/3)^{1/2} \simeq 1$; this simplification leads to an error for i_{Br} which is not greater than *ca.* 0.2 %, assuming that η_{Br} is not higher than η_I for the analogous iodide salts (the highest and, hence, the least favourable value is 0.47 ≃ 0.5 observed for N-methylanilinium iodide).

Apart from the compounds listed in Table I, other anilinium salts were prepared and tested but no nuclear quadrupole resonance frequencies could be observed even after repeated crystallisations and thermal treatments possibly due to lattice defects that were not removed by these treatments. Among these are the following: *p*-$CH_3OC_6H_4NH_3^+.Br^-$, *p*-$CH_3COC_6H_4NH_3^+.Br^-$, *o*-$HOC_6H_4NH_3^+.Br^-$ and *p*-$ClC_6H_4NH_3^+.Br^-$. However, a frequency, assigned to the chorine atom, was observed at 34.4 MHz (at *ca.* 300 K) for *p*-$ClC_6H_4NH_3Br$. This value is higher than that known [19] for *p*-chloroaniline (at the same temperature, the frequency is lower than 33.974 MHz which is the value observed [19] at 196 K) possibly on account of the electron withdrawing inductive ability of the $-NH_3^+$ group which leads to an increase of the electric field gradient (q_{zz}) at the Cl atom; a similar effect results from the elimination of the possibility of the $-NH_2$ group (with a + R resonance effect) to con-

Table I

Nuclear quadrupole resonance frequencies (ν) [a]) of anilinium bromide and iodide salts, fraction of ionic character of the halide bond (i) and asymmetry parameter (η) of the iodide electric field

Anilinium salt	X = Br [b])			X = I			
	ν (Br^{79})	ν (Br^{81})	i (Br^{79})	ν (I^{127}) $\nu_1(3/2 \leftarrow 1/2)$	ν (I^{127}) $\nu_2(5/2 \leftarrow 3/2)$	i (I^{127})	η (I^{127})
$C_6H_5NH_3^+X^-$	16.9 [c])	14.2	0.956	15.0	24.9	0.963	0.42
p-$CH_3C_6H_4NH_3^+X^-$	16.3	13.9	0.958	17.3	23.8 [d])	0.963	0.68
m-$CH_3C_6H_4NH_3^+X^-$ [e])	16.25	13.8	0.958				
o-$CH_3C_6H_4NH_3^+X^-$	25.9	21.9	0.933	15.8	28.6	0.958	0.29
p-$NO_2C_6H_4NH_3^+X^-$ [e])	17.9	15.2	0.954				
m-$NO_2C_6H_4NH_3^+X^-$ [e])	22.9	19.4	0.941				
o-$NO_2C_6H_4NH_3^+X^-$ [e])	20.4	17.2	0.947				
p-$CF_3C_6H_4NH_3^+X^-$ [f])				24.5	33.2	0.948	0.70
$C_6H_5N(CH_3)H_2^+X^-$	18.5	15.5	0.952	21.9	35.0	0.948	0.47

a) Values (with an estimated error below *ca.* 0.1 %) in MHz measured at *ca.* 298 K.

b) $\nu(Br^{79})/\nu(Br^{81}) \simeq Q(Br^{79})/Q(Br^{81}) = 1.197$.

c) A more precise value, $\nu(Br^{79}) = 16.664$ MHz at T = 289.8 K, is reported in reference [15].

d) Weak resonance.

e) N.Q.R. frequency not observed for X = I.

f) N.Q.R. frequency not observed for X = Br.

jugate with the aromatic ring as a result of its protonation to give $-NH_3^+$.

The data quoted in Table I deserves a few general comments:

a) The observation of nuclear quadrupole resonance frequencies evidences a non-spherical electronic distribution ($q_{zz} \neq 0$) around the bromide or iodide nucleus which rules out an unperturbed s^2p^6 spherical electronic distribution in the halide ion. Since they are unlikely to arise from second order lattice effects in a 100 % ionic compound, these results may be interpreted, as proposed [14] in the N.Q.R. study of alkylammonium bromide and iodide salts, in terms of the involvement of the balide ion in hydrogen bonding, *i.e.*, polarization of the electron clouds of the bromide and iodide ions caused by the hydrogens of the ammonium groups. The high value of $\nu(^{79}Br)$ observed in anilinium bromide (and its deuterated analogues), the large ^1H-^2D isotopic shift of this frequency (*ca.* 400KHz at 77K) by deuteration of the ammonium group, the lack of free rotation of the $-NH_3^+$ group and the fact that the dis-

tance $N \ldots Br^-$ is shorter than that corresponding to the van der Waal's radius of $-NH_4^+$ plus the ionic radius of Br^- have also been considered by other authors [16,20c] as evidence for $N^+H \ldots Br^-$ hydrogen bonding. Short $N \ldots I^-$ distances have also been taken as evidence for $\overset{+}{N}H \ldots I^-$ bonds in trimethylammonium iodide [25b].

b) The estimated fraction of ionic character of the halide bond is high (i_{Br}, $i_I \tilde{>} 0.94$); hence the corresponding hydrogen bonds have predominant electrostatic nature, $\overset{+}{N}H \ldots X^-$. In other terms, the deformation of the electron cloud of the bromide and iodide ions is small.

c) The η asymmetry parameter (estimated for the iodide ion) presents values which are well above zero (mainly for the *para* substituted anilinium salts, p-$CF_3C_6H_4NH_3^+I^-$ and p-$CH_3C_6H_4NH_3^+I^-$), thus showing a non-axial electric field around the iodide nucleus and suggesting an interaction of this ion with neighbouring hydrogen atoms which is more complex than that resulting from a single hydrogen-bonding per halide ion (an axial symmetry, $\eta = 0$, would then be expected).

A similar observation was reported [14] for the ethyl- and diethyl-ammonium iodide salts where the formation of three hydrogen bonds per iodide is suspected [20].

d) The N.Q.R. frequency of the halide ion and the asymmetry parameter appear to be strongly dependent on the organic group(s) bound to the nitrogen atom of the ammonium salt, but no general trends can be recognized.

Hence, although the comparison among $C_6H_5NH_3^+X^-$, $CH_3NH_3^+X^-$ [14] and $C_3H_7NH_3^+X^-$ [14], and between $C_6H_5N(CH_3)H_2^+X^-$ and $(CH_3)_2NH_2^+X^-$ [14], may suggest that the replacement of an alkyl by a phenyl group at the nitrogen in a primary or secondary amine appears to lead to an increase of the N.Q.R. frequency and of the asymmetry parameter and to a decrease of the ionic character of the $N^+H \ldots X^-$ bond, these trends are not followed by the ethylammonium salts which present a very high N.Q.R. frequency and asymmetry parameter (even higher than those observed for the anilinium salts).

Moreover, in the anilinium series, the secondary ammonium salt $C_6H_5N(CH_4)H_2^+X^-$ presents N.Q.R. halide frequencies which are higher than those exhibited by the primary anilinium salt $C_6H_5NH_3^+X^-$. Hence, the replacement of a hydrogen atom by a methyl group leads to an increase of the halide frequency.

Although the main reason for such a behaviour cannot be ascertained, a few tentative explanations may be put forward: in the secondary ammonium salt the positive charge is localized in a smaller number of hydrogen atoms and a stronger polarizing distortion of the electronic charge distribution in the neighboring halide may result with an increase of q_{zz} and, hence, of the N.Q.R. frequency; an effect of the same kind may also result from the polarizing effect (of the induced positive charge) of the methyl group (as a result of its resonance and inductive electron donor character) on the halide electronic cloud.

Within the group of aryl ammonium salts, the N.Q.R. frequency depends also on the phenyl substituent but this behaviour is discussed separately.

N.Q.R. halide frequency and Hammett's σ constant of the phenyl substituent.

The electron donor/acceptor ability of a substituent at a phenyl ring may be expressed by the known Hammett's σ constant and since the postulated hydrogen bond to the halide ions in the compounds studied in the present work would be expected to be

dependent on such an ability, the possibility of a correlation between the Hammett's σ constant and the N.Q.R. halide frequency (ν) may be anticipated (which is also, if verified, a confirmation of the soundness of the hypothesis of occurrence of hydrogen bonding in the system studied).

Figure 1 shows a plot of ν (Br^{79} or I^{127}) for the anilinium ion and its derivative salts, $YC_6H_4NH_3^+X^-$, versus the Hammett's σ constant [21] for the Y substituent (in *para* or *meta* position); as can be seen, the halide N.Q.R. frequency appears to increase linearly with σ, except in the case of ν_1 (I^{127}). Hence, an increase of the electron withdrawing ability of the substituent leads to a distortion of the electronic charge distribution in the halide (X^-) ion (increase of q_{zz} and, hence, of ν) with an increase in the covalent component of the $NH^+ \ldots X^-$ bond, as commented on later.

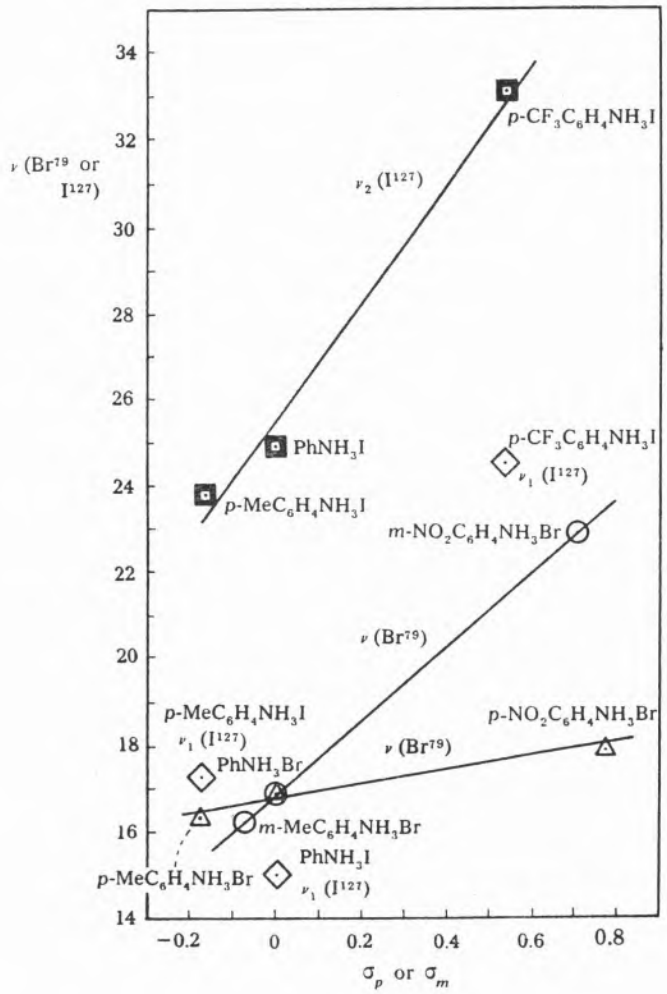

Fig. 1

Plot of ν (Br^{79} or I^{127}) versus the Hammett's σ constant of the substituent (Y) in compounds $YC_6H_4NH_3X$ (X = Br or I)

△ — ν (Br^{79}) *in compounds with* para-Y.
⊙ — ν (Br^{79}) *in compounds with* meta-Y.
◇ — ν_1 (I^{127}) *in compounds with* para-Y.
□ — ν_2 (I^{127}) *in compounds with* para-Y.

It we consider the Taft σ_I constant [21] (which only takes into consideration the inductive contribution of the substituent) instead of the Hammett's constant, a better linear correlation is observed for ν_2 (I^{127}) and the points corresponding to ν_1 (I^{127}) become closer to obeying a linear correlation. However, if the Taft σ_R^o constant [21] (which measures the polar resonance effect of the substituent) is considered instead of the Hammett's σ consant, a general deviation from the linearity is observed for all sets of frequencies.

These observations suggest that the N.Q.R. halide frequency follows the phenyl substituent inductive effect closer than its resonance effect.

Moreover, ν (Br^{79}) is more sensitive to a change of electronic properties of the phenyl substituent (measured by Hammett's σ constant) when this is in the *meta* rather than in the *para* position, in accordance with the higher importance of the inductive effects and the weaker resonance effects associated to the former position relative to the latter.

From the slopes of the plots of figure 1, it may also be observed that ν (I^{127}) is more sensitive than ν (Br^{79}) to a variation in the electronic properties of the sustituent (Hammett's σ constant), in agreement with the higher polarizability of the iodide relative to the bromide ion.

In the above mentioned discussion, only the *para* and the *meta* substituent positions were considered, since ν (X) for compounds with

an *ortho* substituent presents a more complex dependence on the substituent and on the halide [*e.g.*, the bromide salt $o\text{-}CH_3C_6H_4NH_3^+Br^-$ has the highest $\nu(Br^{79})$ value observed in this study, whereas the analogous iodide salt has a very low $\nu(I^{127})$ and $o\text{-}NO_2C_6H_4NH_3^+Br^-$ exhibits $\nu(Br^{79})$ at an intermediate value between the corresponding *meta* and *para* compounds].

Anomalies of behaviour associated to *ortho* substituents are well known and have also been reported in N.Q.R. studies by other authors [22]. Among the reasons for the anomalies, stereochemical effects, which, *e.g.*, may cause steric hindrance or decrease the planarity of the molecule (hence, the N-phenyl ring resonance with resulting decrease of ν) may be cited as prominent factors; different crystalline structures; polarizing effect of the charge of the *ortho* substituent (as a result of resonance and inductive effects) upon the electronic shell of the halide are other possible reasons.

Linear correlations of halogen N.Q.R. coupling frequencies with the Hammett's σ constant have also been referred to by other authors [19, 23, 24] in different compounds (*e.g.*, chlorobenzene derivatives), and, in some cases, it was observed [24] that the changes in the N.Q.R. frequency were mainly determined by the inductive rather than the resonance effect which, in some instances, only leads to small differences which are of the same order of magnitude as those due to crystalline field effects.

N.Q.R. halide frequency and the fraction of ionic character of the halide bond

From equations (6) to (9) and for a constant asymmetry parameter (η), an inverse linear relationship is expected between the halide N.Q.R. frequency (ν) and the fraction of ionic character (i) of the halide-hydrogen bond, *i.e.*, the greater the deviation from the spherical symmetry of the electronic cloud around the nucleus (increase of q_{zz} and of ν) the lower the ionic character of the $NH^+ \ldots X^-$ bond. However, if the asymmetry parameter η varies along a series of compounds, the above mentioned general correlation is no longer valid.

The plots of the N.Q.R. frequency for Br^{79} and I^{127} of the salts $YC_6H_4NH_3^+X^-$ *versus* the fraction of ionic character, $i(Br^{79})$ and $i(I^{127})$, are depicted in figures 2 and 3, respectively, where, for comparison, is also included the data previously reported [14] for the related alkylammonium salts.

The expected linear variation is observed (figure 2) for the bromide salts since, as mentioned above, the fraction of ionic character of the bromide bond was estimated by neglecting the effect of η. The highest ionic character of the bromide bond (with the corresponding lowest N.Q.R. frequency) is found in some alkylammonium bromides whereas some substituted anilinium bromides display the lowest ionic character of the bromide-hydrogen bond.

However, for the iodide salts (figure 3), families of plots of $\nu(I^{127})$ *versus* $i(I^{127})$ have to be considered according to the estimated values of the asymmetry parameter. An increase of this parameter results in an increase of $\nu_1(I^{127})$ but in a decrease of $\nu_2(I^{127})$. Each line was drawn for each group of compounds with similar η values, and it corresponds roughly to the plot of the equation, which relates $\nu(I^{127})$ with $i(I^{127})$, obtained from expressions (7) [or (8)] and (9) for η equal to the average of the η values of those compounds.

The lowest value of the asymmetry parameter η is observed for some of the alkylammonium iodide salts (methyl-, trimethyl- and propyl-ammonium iodides), whereas the *para*-substituted anilinium salts display the highest η values conceivably as a result of a more complex multi-hydrogen bonding between the halide ion and various hydrogen atoms belonging to different molecules as it was pointed out earlier [14] and is supported by some X-ray studies, *e.g.*, of anilinium- [16,20b,20c] and monoethylammonium- [15,20a] -halide (bromide or iodide) salts (high η values are displayed by the

iodide compounds); moreover, a higher axial symmetry of the hydrogen-bonds around the halide ion is shown also by X-ray data, *e.g.*, on methylammonium salts [15,25] and accordingly, low η (iodide) values are observed. In conclusion, it can be said that alkylammonium and arylammonium halides exhibit $N^+H \ldots X^-$ interactions whose single/multiple character depend on the halide considered and are highly sensitive to the organic group bound to nitrogen in the ammonium salt.

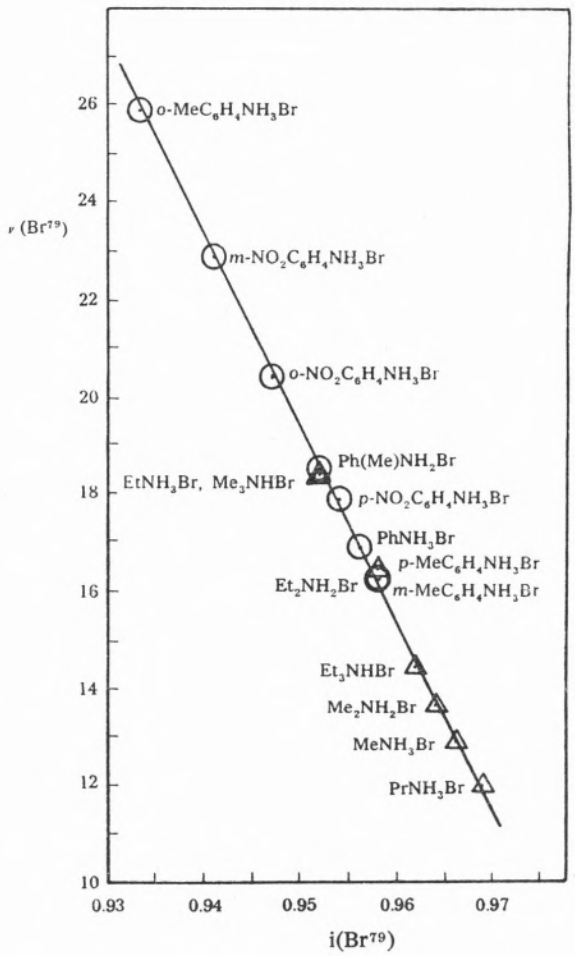

Fig. 2

Plot of $\nu(Br^{79})$ versus the fraction of ionic character of the bromide bond, $i(Br^{79})$

⊙ — *Arylammonium bromide salts*
△ — *Alkylammonium bromide salts* [14]

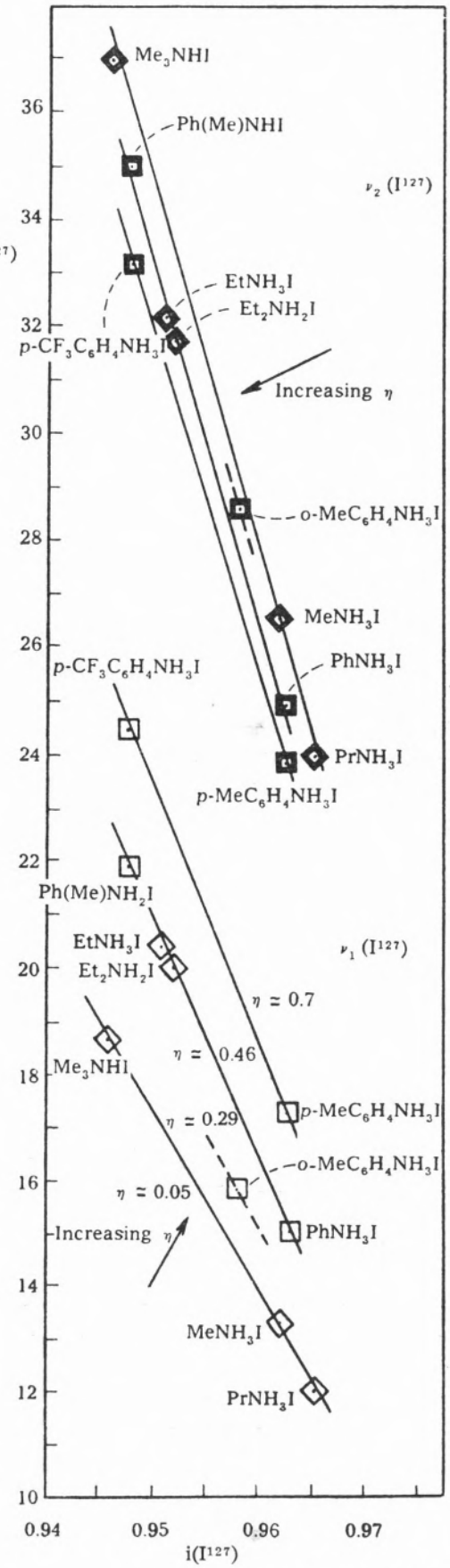

Fig. 3

Plot of $\nu_1(I^{127})$ and $\nu_2(I^{127})$ versus the fraction of ionic character of the iodide bond, $i(I^{127})$

□ — *Arylammonium iodide salts (ν_2)*
◇ — *Alkylammonium iodide salts (ν_1)* [14]
◇ — *Alkylammonium iodide salts (ν_2)* [14].

The correlations observed and the changes found on going from primary to secondary amines are consistent with a directional character of these interactions of the type normally referred to as hydrogen bonding. Although this type of bonds is not usually invoked in systems with the less electronegative halides Br^- and I^-, there is no theoretical objection to their inclusion even if the corresponding interactions are naturally weaker than those with F^-, Cl^-, nitrogen or oxygen.

IV — EXPERIMENTAL

The anilinium salts were prepared by reaction of the corresponding base with an excess of the appropriate acid (HBr or HI); ethanol or dichloromethane were used as solvents in a few cases (for the preparation of *p*-$CH_3C_6H_4NH_3X$ and *o*-$NO_2C_6H_4NH_3X$ or *p*-$ClC_6H_4NH_3X$, respectively). The isolated products were purified by repeated recrystallization from ethanol or ethanol/dichloromethane.

The N.Q.R. studies were performed on crystalline samples (ca. 2-3g) contained in a 12mm thin-walled tube, at a temperature of 298K, by using a WILKS N.Q.R.-1A spectrophotometer equiped with a General Radio Co. frequency meter.

The accuracy of the measurements is of the order of 0.1 % due to the instrument error and uncertainty in locating the fundamental bands.

Received, 15th May 1985

ACKNOWLEDGEMENTS

The experimental assistance and helpful discussions with Prof. Luís Vilas-Boas in the early stages of this study are greatly acknowledged.

REFERENCES

[1] G.C. PIMENTEL, A.L. MCCLELLAN, «The Hydrogen Bond», W.H. Freeman & Co., San Francisco, 1960; W.A. Bueno, «Ligação de Hidrogénio», Ed. Universidade de S. Paulo, Brasil (Ed. McGraw-Hill do Brasil), 1978.

[2] C.T. O'KONSKI, T.J. FLANTT, *J. Chem. Phys.*, **27**, 815 (1957), S. ELETR, C.T. O'KONSKI, *J. Chem. Phys.*, **54**, 4312 (1971).

[3] T. OJA, *Adv. Nucl. Quadrupole Reson.*, **7**, 401 (1974).

[4] B.V. DRESVYANK, V.S. GRECHISHKIN, T.G. BALICHEVA, I.V. POLOGIKH, *Teor. Eksp. Khim.*, **1**, 276 (1975).
R.A. MARINO, *Adv. Nucl. Quadrupole Reson.*, 7,391 (1974)..

[5] R.A. MARINO, *J. Chem. Phys.*, **57**, 4560 (1972).

[6] A. INDUMATHY, J. RAMAKRISHNA, *Proc. Nucl. Phys. Solid State Phys. Symp.*, **21c**, 678 (1978).

[7] O. KH. POLESHCHUK, YU. K. MAKSYUTIN, O.F. SYCHEV, K.K. KOSHELEV, I.G. ORLOV, *Izv. Akad. Nauk SSSR. Ser. Kim.*, **6**, 1431 (1975).

[8] J.W. CLYMER, *Diss. Abstr. Int. B.*, **43**, 2568 (1983).

[9] M. SUHARA, J.A.S. SMITH, *J. Magn. Reson.*, **50**, 237 (1982).

[10] C J. LUDMAN, J. Waddington, J.A. SALTHOUSE, R.J. LYNCH, J.A.S. SMITH, *Chem. Comm.*, **6**, 405 (1970).

[11] H. CHIHARA, N. NAKAMURA, *Bull. Chem. Soc. Japan*, **44**, 1971 (1980).

[12] E. GRECH, J. KALENIK, Z. MALARSKI, L. SOBCZYK, *J. Chem. Soc., Faraday Trans.*, **79**, 2005 (1983).

[13] T.L. BROWN, L.G. BUTLER, D.Y. CURTIN, Y. HIYAMA, I.C. PAUL, R.B. WILSON, *J. Am. Chem. Soc.*, **104**, 1172 (1982).

[14] J.J.R. FRAÚSTO DA SILVA, L.F. VILAS-BOAS, *Rev. Portug. Quím.*, **14**, 115 (1972).

[15] G. JUGIE, J.A.S. SMITH, *J. Chem. Soc., Faraday Trans.*, **74**, 994 (1978).

[16] W. PIES, A. WEISS, *Bull. Chem. Soc. Japan*, **51**, 1051 (1978).

[17] G.K. SEMIN, E.I. FEDIN, «Use of NQR in Chemical Crystalography», *in* «The Mössbauer Effect and its Application to Chemistry», van Nostrand Co., New York, 1966.

[18] C.H. TOWNES, B.P. DAILEY, *J. Chem. Phys.*, **17**, 782 (1949).
S.A.C. LUCKEN, «Nuclear Quadrupole Coupling Constants», Academic Press, 1970.

[19] H.C. MEAL, *J. Amer. Chem. Soc.*, **74**, 6121 (1952).

[20] a) F. JELLINEK, *Acta Cryst.*, **11**, 626 (1958).
b) I. TAGUCHI, *Bull. Chem. Soc. Japan*, **34**, 392 (1961).
c) I. NITTA, T. WATANABI, I. TAGUCHI, *Bull. Chem. Soc. Japan*, **34**, 1405 (1961).

[21] C. LAURENCE, B. WOJTKOWIAK, *Ann. Chim.*, **5**, 163 (1970).

[22] See, *e.g.*, P.J. BRAY, *J. Chem. Phys.*, **22**, 950 (1954).

[23] See, *e.g.*:
P.J. BRAY, R.G. BARNES, *J. Chem. Phys.*, **27**, 551 (1957);
P.J. BRAY, *J. CHEM. Phys.*, **22**. 1787 (1954);
H.O. HOOPER, P.J. BRAY, *J. Chem. Phys.*, **33**, 334 (1960).

[24] D. BIEDENKAPP, A. WEISS, *J. Chem. Phys.*, **49**, 3933 (1968).

[25] a) E.J. GABE, *Acta Cryst.*, **14**, 1296 (1961).
b) G.M. SHELDRICK, W.S. SHELDRICK, *Acta Cryst.*, B**26**, 1334 (1970).

RESUMO

Estudo de ressonância de quadripolo nuclear de brometos e iodetos de anilínio.

As frequências de ressonância de quadripolo nuclear (ν) de Br^{79} (e Br^{81}) e I^{127} foram detectadas nos sais de anilínio $YC_6H_4NH_3^+X^-$ (Y = o-,m-,p-CH_3; o-,m-,p-NO_2; p-CF_3. X = Br e/ou I). O parâmetro de assimetria η (para X = I) e a fracção de carácter iónico da ligação do halogeneto foram estimados para estes compostos e os resultados obtidos demonstraram a ocorrência de polarização da núvem electrónica do halogeneto, o que foi interpretado considerando a possível formação de ligações de hidrogénio $N^+H \ldots X^-$ com carácter electrostático predominante.

Observaram-se ainda dependências lineares, que são objecto de discussão, entre ν e as constantes σ de Hammett para os substituintes em posição para *e* meta.

MARIA JOSÉ BAÇÃO MADRUGA
LNETI - DPSR
Serviço de Radioactividade Ambiente
Estrada Nacional n.º 10
2685 Sacavém

SEPARAÇÃO E IDENTIFICAÇÃO DAS FORMAS FÍSICO-QUÍMICAS DO ^{60}Co NA ÁGUA DO MAR E NA ÁGUA DOCE

The purpose of the present work is to accomplish the partition and identification of the possible physico-chemical forms of the ^{60}Co in sea and fresh water. This was carried out with two types of resins, an cationic exchange and an ionic chelating resin.

Results show that, in the case of the sea water and with the ionic exchange resin, the anionic and neutral (0,16 %), cationic (85,2 %) and insoluble (6,6 %) physico-chemical forms of ^{60}Co were identified.

In what concerns fresh water, using both resins, only one physico-chemical form was identified, probably the cationic one, with a high recovery.

1 — INTRODUÇÃO

As centrais nucleares, através dos seus efluentes líquidos, rejeitam para o meio ambiente uma grande variedade de radionuclidos. Esses efluentes quando lançados, quer na rede hidrográfica (rios, lagos, etc.), quer no mar, podem sofrer diferentes graus de diluição e transformações físico-químicas.

Dos radionuclidos lançados no ambiente, o ^{60}Co, com um período de semi-desintegração relativamente elevado, 5,2 anos, representa uma grande percentagem da actividade total rejeitada.

O cobalto é um elemento essencial à grande maioria dos organismos vegetais e animais. Com efeito, diminui a decomposição da clorofila na escuridão, activa alguns enzimas dos vegetais e participa ainda na edificação de moléculas de vitamina B_{12}, que é um complexo de cobalto trivalente e um constituinte essencial do fenómeno de fixação do azoto. Por isto, e pelo já referido, torna-se este radionuclido objecto de particular atenção quanto ao seu impacto na natureza em particular para o Homem.

Em consequência de experiências de radioecologia em que se torna essencial o conhecimento das diferentes formas fisico-químicas dos radionuclidos, porque elas intervêm de maneira diversa no modo e intensidade de fixação pelos organismos, o presente trabalho tem como objectivo separar e identificar as possíveis formas fisico-químicas do ^{60}Co na água do mar e na água doce.

Com esta finalidade utilizaram-se duas espécies de resinas: uma resina de troca catiónica, a qual contém catiões que vão permutar com outros que existam em solução; e uma resina iónica que contém iões actuando como grupos complexantes na ligação a iões metálicos. A separação e identificação dessas diferentes formas são feitas por meio da medida da radiação gama emitida pelo radionuclido associado às diferentes fracções do eluído.

2 — MÉTODO EXPERIMENTAL

2.1 — *DESCRIÇÃO DA TÉCNICA*

A técnica, consiste fundamentalmente na fixação duma solução radioactiva de ^{60}Co em resinas e na sua eluição com diferentes eluentes [1].

Assim introduz-se por via húmida, numa coluna de vidro com 0,8 cm de diâmetro e 16 cm de altura, a resina adequada. Trata-se essa resina por passagens sucessivas de água até que o pH do eluído seja idêntico ao da água inicial, o que só se consegue, nalguns casos, com o tratamento da resina com uma solução 0,1 N de NaOH.

Com a resina a pH determinado, deita-se em seguida no topo da coluna 3 ml duma solução radioactiva, cuja actividade em ^{60}Co é de 16 $nCi.ml^{-1}$. Esta solução obtém-se a partir da contaminação da água a utilizar com um certo volume de uma solução de cloreto de cobalto, as quais se mantêm em contacto durante três dias, podendo contudo este tempo não ser suficiente para que se estabeleça o equilíbrio químico entre os iões envolvidos.

Procede-se depois à eluição do cobalto, com os eluentes a estudar, recolhendo-se os eluídos em fracções de 5 ml para tubos de plástico. Mede-se em seguida, a actividade de cada fracção em equipamento adequado.

2.2 — *EQUIPAMENTO DE MEDIDA*

O equipamento de medida utilizado foi um sistema de detecção gama monocanal, constituído por um detector de NaI (T1) 4″ × 4″, de poço, com as dimensões de 1 ¼″ de diâmetro interior e de 2 ½″ de profundidade, ligado a um conjunto de módulos (fonte de alta tensão, amplificador, discriminador, contador e relógio) e previamente calibrado para o ^{60}Co.

2.3 — *ENSAIOS REALIZADOS*

a) Água do mar

Utilizando a técnica descrita anteriormente realizaram-se experiências com a resina de troca catiónica, Dowex 50W - X8, forma H^+, 100-200 mesh, usando como eluentes, água do mar e HNO_3 3N.

b) Água doce

Adaptando-se a técnica já descrita, à água doce, realizaram-se ensaios, a diferentes pH usando como eluentes água doce e HNO_3 3N. Com base num trabalho de LOWMAN F. G. & TING R. Y. [2], incidindo sobre a água do mar e utilizando uma resina iónica quelatante, Chelex 100, forma sódica, 200-400 mesh, realizaram-se ensaios usando como eluentes água doce, HCl 1N e HNO_3 3N.

Seguindo-se a teoria de COLEMAN, G. H. [3], realizaram-se ensaios, em que se utilizou a mesma resina Chelex 100, e como eluentes ácido clorídrico com diferentes concentrações.

3 — DISCUSSÃO DOS RESULTADOS

3.1 — *ÁGUA DO MAR*

Com os resultados das actividades medidas nas várias alíquotas, traçou-se o gráfico representado na figura 1. O perfil obtido está em perfeita concordância com o publicado por MARCHAND, M. [1]. Considerou-se, assim, lógico atribuir às fracções correspondentes dos dois gráficos as mesmas formas fisico-químicas do cobalto, embora as percentagens das mesmas sejam ligeiramente diferentes.

Identificaram-se, portanto, as formas aniónicas ou neutras e as formas catiónicas, com rendimentos respectivamente de 0,16 % e 85,2 % na eluição com água do mar e as formas insolúveis, com um rendimento de 6,6 % na eluição com HNO_3 3N. Parece contudo necessário proceder-se posteriormente a uma confirmação das formas aniónicas, através da utilização duma resina aniónica, uma

vez que dando o cobalto origem a várias formas complexas, o que se identificou no gráfico da figura 1, como formas aniónicas ou neutras poderá corresponder não só à forma aniónica do cobalto, como também a formas complexas como os cloretos, carbonatos, sulfatos, etc.

Segundo MARCHAND, M. [1], as formas aniónicas ou neutras correspondem provavelmente à formação de complexos com o ligando Cl^-: $CoCl_2$, $CoCl_3^-$ e $CoCl_4^{2-}$ e as formas catiónicas correspondem aos iões $CoCl^+$ e Co^{2+}. Contudo, poderão ainda existir outras formas catiónicas como, por exemplo, as espécies hidratadas $Co(H_2O)_6^{2+}$.

3.2 — *ÁGUA DOCE*

A figura 2 representa graficamente a separação das formas fisico-químicas do cobalto em água doce com a resina Dowex 50 W - X8.

Verifica-se que na eluição com água doce não se consegue a separação de qualquer forma; na eluição com HNO_3 e com a resina a pH = 7 (figura 2-I), pH = 2 (figura 2-II) e pH = 3 (figura 2-III), se consegue a obtenção de um só pico correspondente a uma única forma com um rendimento elevado.

A figura 3 representa graficamente a separação das formas fisico-químicas do cobalto em água doce com a resina Chelex 100.

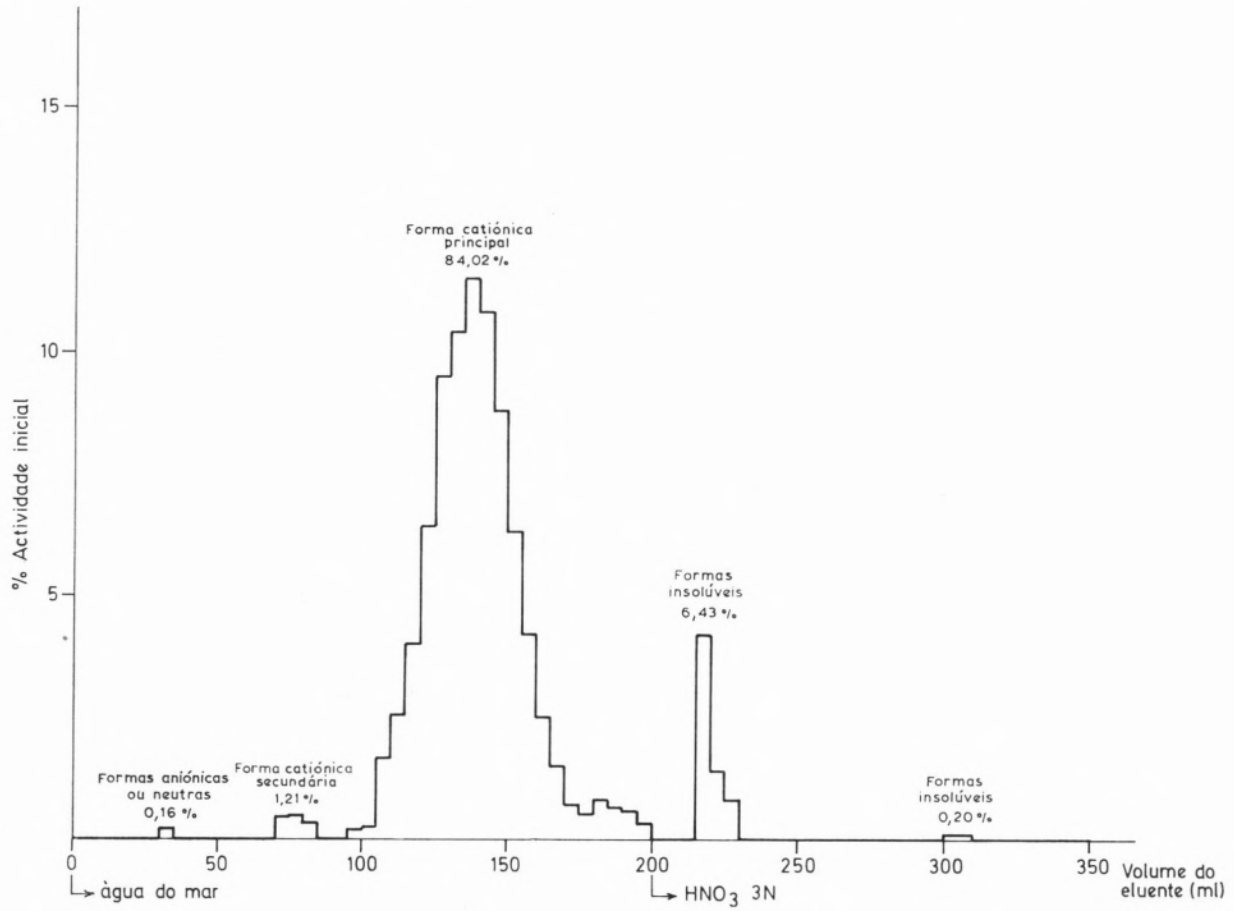

Fig. 1

Separação das formas fisico-químicas do cobalto em água do mar com resina Dowex 50W - X8

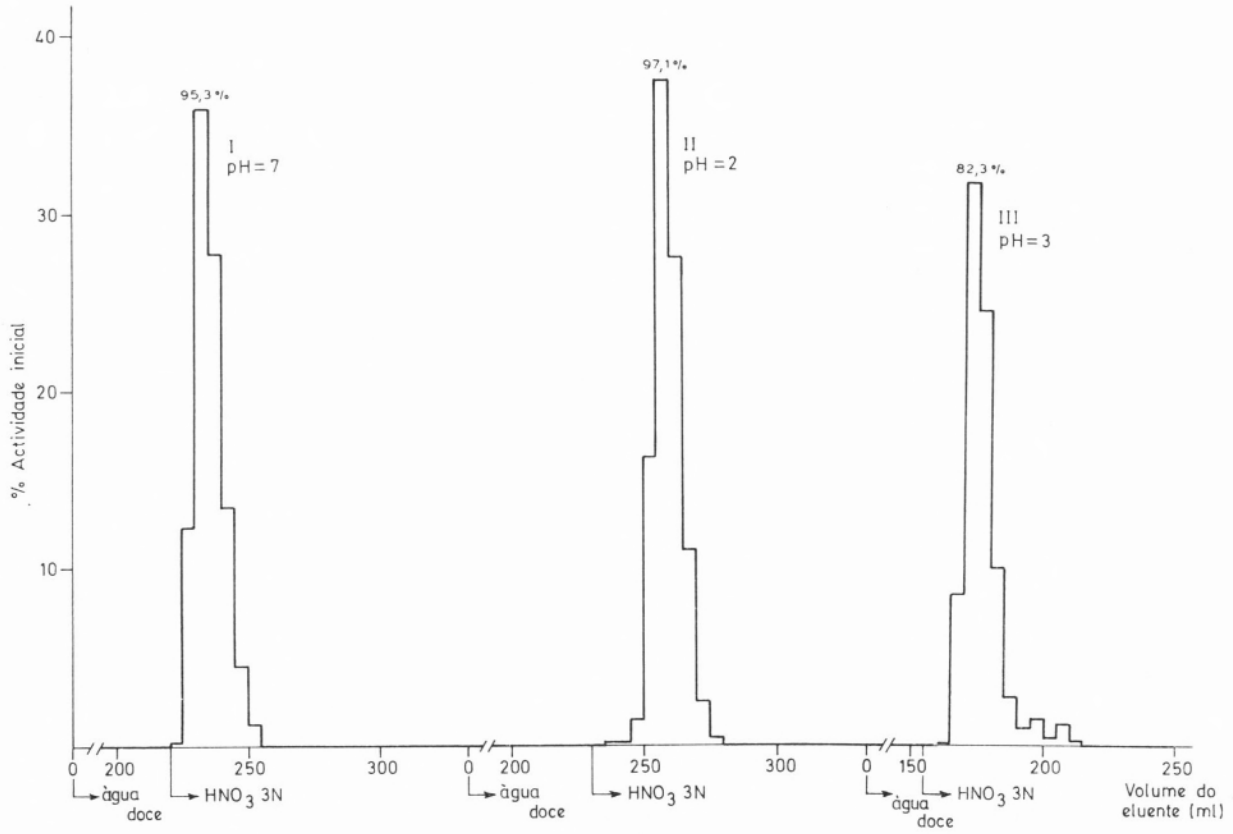

Fig. 2

Separação das formas fisico-químicas do cobalto em água doce com resina Dowex 50W - X8

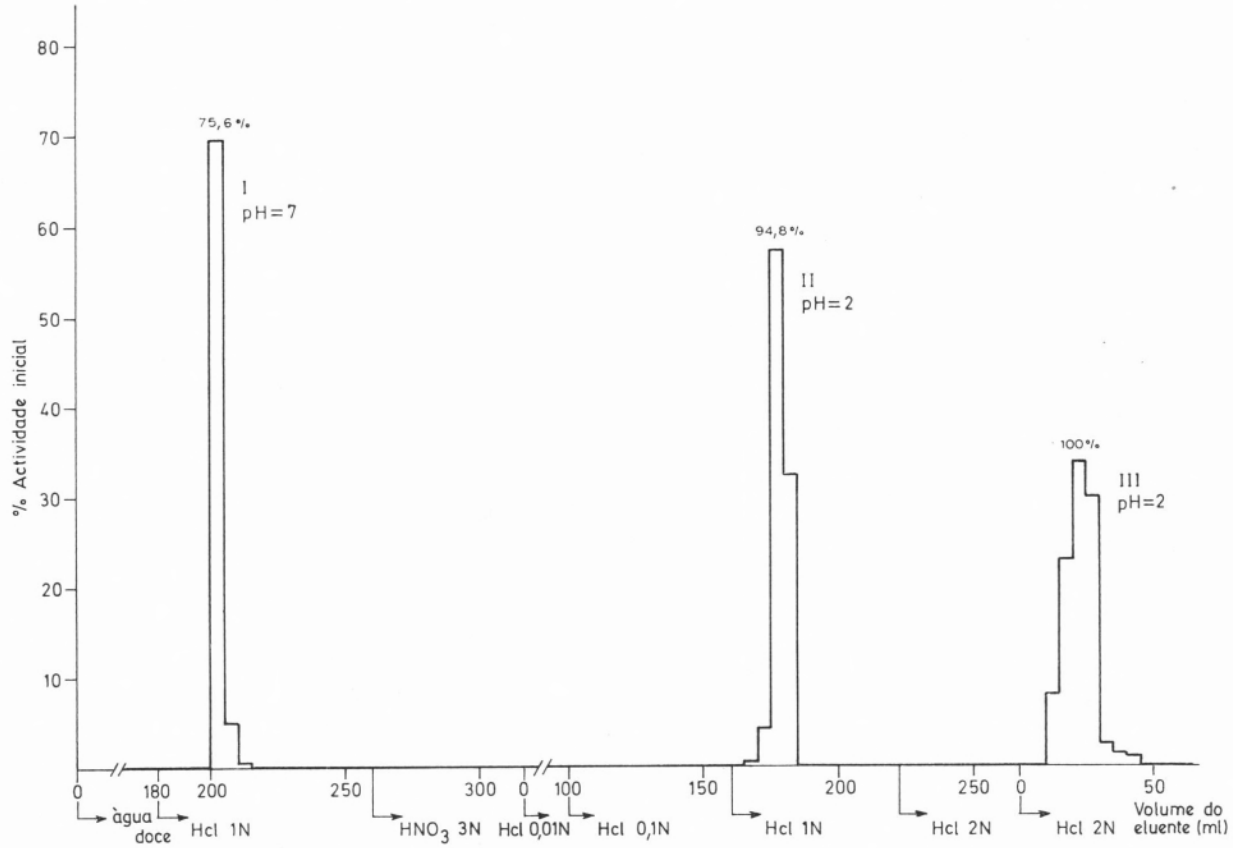

Fig. 3

Separação das formas fisico-químicas do cobalto em água doce com resina Chelex 100

Analogamente, ao já verificado na situação anterior, não se consegue qualquer separação dessas formas quando se utiliza a água doce como eluente.

Como se pode ainda verificar na figura 3, à medida que a concentração do ácido vai aumentando, o rendimento da eluição aumenta também, obtendo-se o valor de 100 % quando a concentração do ácido clorídrico é de 2N.

Estes resultados estão de acordo com o trabalho, já referido, de COLEMAN, G. H. [3], sendo de concluir que ao diminuir o coeficiente de distribuição do cobalto na resina, se verifica uma eluição mais completa.

Comparando os resultados obtidos para a água do mar e para a água doce, verifica-se o seguinte:

1.º — Utilizando a resina Dowex 50 W - X8 e eluindo com as respectivas águas, conseguiu-se, para a água do mar a separação de algumas formas fisico-químicas, enquanto que para a água doce, não ocorreu qualquer separação.
2.º — Utilizando a resina Dowex 50 - X8, mas HNO_3 3N como eluente, constatou-se que para a água do mar se separaram as formas insolúveis, enquanto que para a água doce se obteve uma única forma.

4 — CONCLUSÕES

Poder-se-á, pois, concluir que o cobalto, quando introduzido na água do mar, pode sofrer alterações químicas, enquanto que quando introduzido na água doce, permanece sem alterações, ou seja, na forma catiónica, pelo menos durante períodos relativamente pequenos, como aqueles aqui estudados.

A confirmá-lo, os resultados de SAAS, A. & GRAUBY, A. [4] ao verificarem que num suporte de silica gel impregnado de resina Dowex 50 W - X8 e utilizando como eluente água doce as formas catiónicas do cobalto se mantinham estacionárias enquanto que, com água do mar, havia uma migração e mesmo uma separação entre as formas catiónicas e as aniónicas ou complexas.

Os resultados de FERRER, M. C. [5], que encontrou 100 % de cobalto sob a forma catiónica em água doce leva a admitir que é essa igualmente a conclusão a tirar dos resultados obtidos, apesar de os rendimentos terem variado de acordo com as resinas e os eluentes utilizados.

Como conclusões finais poder-se-á dizer que, para a água doce com qualquer das duas resinas utilizadas, se conseguem rendimentos elevados na obtenção da forma catiónica, aplicando como eluentes quer HCl 1N ou 2N, quer HNO_3 3N, e, que tanto para a água do mar como para a água doce, a forma catiónica é sempre a forma predominante.

AGRADECIMENTOS

A autora agradece à Dr.ª Maria Carolina Vaz Carreiro, a valiosa contribuição prestada no decorrer do trabalho.

Agradece também ao Dr. António Ortins de Bettencourt, director do Serviço de Radioactividade Ambiente, pela revisão final do trabalho e às Dr.as Maria Manuela Godinho e Maria Manuela Simões pelas sugestões apresentadas para melhoria de ordenação e apresentação do texto.

(Recebido em 25.Outubro.1984; em versão corrigida em 27.Dezembro.1985)

RESUMO

Pretendeu-se com este trabalho efectuar a separação e identificação das possíveis formas fisico-químicas do ^{60}Co em água do mar e água doce, usando dois tipos de resinas, uma resina de troca catiónica e uma resina iónica quelatante.

Os resultados obtidos mostram que para a água do mar e com a resina catiónica é possível a separação e identificação de todas as formas fisico-químicas do ^{60}Co encontrando-se valores de 0,16 % para as

aniónicas ou neutras, 85,2 % para as catiónicas e 6,6 % para as insolúveis.
Para a água doce e com ambas as resinas, somente se conseguiu, e com um elevado rendimento, a identificação de uma única forma fisico-química, provavelmente a catiónica.

BIBLIOGRAFIA

[1] MARCHAND, M. "Considérations sur les formes physico-chimiques du cobalt, manganése, zinc, chrome et fer dans une de mer enrichie ou non de matière organique". *J. Cons. Int. Explor. Mer*, **35** (2), 130-142 (1974).

[2] LOWMAN, F. G. & TING, R. Y. "The state of cobalt in seawater and its uptake by marine organisms and sediments" Radioactive Contamination of the Marine Environment, IAEA (1973).

[3] COLEMAN, G. H. "The radiochemistry of plutonium" NAS-NS-3058 USAEC (1965).

[4] SAAS, A. & GRAUBY, A. "Techniques de determination rapide des effects de synergie radionucleides-polluants" Combined effects of radioactive, chemical and thermal releases to the environment, IAEA (1975).

[5] FERRER, M. C. "Étude experimentale du comportement de huit radionucleides artificiels dans le cours terminal du Rhone" These de Docteur en Geologie Appliquée (1983).

C. A. NIETO DE CASTRO
Departamento de Química,
Faculdade de Ciências da Universidade de Lisboa,
and Centro de Química Estrutural, Complexo I,
1096 Lisboa Codex.

R. D. TRENGOVE
W. A. WAKEHAM
Imperial College Thermophysical Properties Data Centre,
Department of Chemical Engineering and Chemical Technology,
Imperial College, Prince Consort Road
London SW7 2BY, U.K.

THE DENSITY DEPENDENCE OF THE THERMAL CONDUCTIVITY OF TOLUENE

The paper describes a new interpretation of the density dependence of the thermal conductivity of liquid toluene in terms of an equation based upon the van der Waals model of a dense fluid. The new analysis is carried out on accurate thermal conductivity data reported previously with the aid of results for the density of toluene published more recently. A simple correlation, basead on the van der Waals model, is found to relate the thermal conductivity to the molar volume of the liquid with an accuracy commensurate with the uncertainty in the former.

1 — INTRODUCTION

In an earlier publication [1] we reported measurements of the thermal conductivity of liquid toluene over the pressure range 0.1 to 585 MPa, and in the temperature range 35-87°C. The estimated accuracy of the reported experimental data is one of ±0.3 %. However, at the time of publication there were no available density data for the liquid with a comparable accuracy over the same range of conditions. It was therefore not possible to analyse the density dependence of the thermal conductivity in the manner which has proved successful for many other liquids [2]. Furthermore, it was not possible to deduce from the measurements thermal conductivities on the saturation line of toluene which have been proposed as standard reference values for liquid thermal conductivity. This is because only an extrapolation of the thermal conductivity to the saturation line which is carried out using density as the independent variable has a secure foundation [3]. The availability of new, accurate values of the density of toluene over a range of temperatures and pressures [4,5] has now made it possible to re-analyse the thermal conductivity data in order to fulfil both of the objectives set out above.

2 — DENSITY DEPENDENCE OF THE THERMAL CONDUCTIVITY

Accurate density measurements for liquid toluene have recently been reported independently by Kashiwagi et *al.* [4], and Easteal and Woolf [5]. The experiments of the former authors extend over the pressure range up to 250 MPa and the temperature range 0 to 100°C, and have a claimed accuracy of ± 0.1 %. The results of the latter authors cover the more limited temperature range 5-50°C and extend to pressures as high as 500 MPa. The estimated accuracy of this second set of data is also ±0.1%. The most accurate thermal conductivity

data [1] extend along five isotherms in the range 35-87°C and up to 585 MPa. Consequently, the combination of the two new sets of experimental densities allow us to prepare a table of thermal conductivity as a function of density over at least part of the complete range of thermodynamic states. In preparing this table, which comprises Table I, we have combined the representations of density as a function of pressure along several isotherms given by Kashiwagi *et al.* [4] and Easteal and Woolf [5]. For each experimental pressure employed in the thermal conductivity measurements the density at the temperature of interest has then been obtained by interpolation using a procedure described elsewhere [6]. When the densities obtained from the two independent sources are compared in an overlaping range of thermodynamic states the values never differ by more than $\pm$ 0.2 %, and usually by much less. This value is taken as an upper limit to the uncertainty in the densities quoted in Table I. The corresponding uncertainty in the thermal conductivity is one of $\pm$ 0.3 %.

3 — REPRESENTATION OF THE DATA

An analysis of the thermal conductivity of a dense fluid, [7,8] based on the rough hard-sphere model of the fluid suggests that to a good approximation the quantity

$$\lambda^* = \frac{\lambda}{(\lambda_{tr,0})} \left(\frac{V}{V_o} \right)^{2/3} = F(V/V_o) \quad (1)$$

should be a function of (V/V_o) alone. Here, λ is the thermal conductivity of the dense fluid at a molar volume V. The quantity $\lambda_{tr,0}$ is the translational contribution to the thermal conductivity of the gas in the limit of zero-density and V_o is the close-packed volume of the hard-sphere system [7, 8]. Owing to the fact that the real molecules have repulsive potential wells that are not infinitely steep, V_o will possess a weak temperature dependence.

Table I

The thermal conductivity of toluene as a funcion of density

T = 308.15 K		T = 320.15 K		T = 330.15 K		T = 345.15 K		T = 360.15 K	
ρ / kg m^{-3}	λ / mW m^{-1} K^{-1}	ρ / kg m^{-3}	λ / mW m^{-1} K^{-1}	ρ / kg m^{-3}	λ / mW m^{-1} K^{-1}	ρ / kg m^{-3}	λ / mW m^{-1} K^{-1}	ρ / kg m^{-3}	λ / mW m^{-1} K^{-1}
854.7	128.9	843.2	125.2	838.9	124.4	821.3	118.4	806.6	113.4
855.2	129.1	844.3	126.6	842.6	125.2	821.4	118.7	829.6	123.2
856.5	129.6	861.6	133.7	849.7	128.3	832.0	122.1	848.1	131.1
862.6	132.4	867.7	135.6	860.5	132.8	840.3	126.5	849.1	130.2
866.9	134.6	884.9	143.7	862.9	135.1	862.0	136.0	865.3	139.5
878.3	139.6	899.4	150.6	872.2	138.1	891.6	150.0	882.2	146.6
889.7	145.5	911.5	156.3	888.6	146.1	904.1	155.8	893.7	152.1
892.3	146.3	921.9	161.8	901.1	152.1	915.4	161.4	905.0	158.0
897.1	148.6	924.5	168.3	912.9	158.4	924.5	166.0	925.5	168.1
898.2	149.1	948.5	175.4	924.3	163.9	934.8	171.0		
928.7	163.8			933.6	169.0				
938.1	168.1			942.5	173.1				
955.8	177.6								

In order to test the hypothesis of equation (1) for toluene it is sufficient to demonstrate that the lines of λ^* against ln V for each isotherm can be superimposed upon each other by shifts along the ln V axis. The shift necessary along this axis for two isotherms represents the change in V_o between the two temperatures. For this purpose experimental values of λ^* may be evaluated from the equation [7, 8].

$$\lambda^* = 1.936 \times 10^7 \lambda V^{2/3} (M/RT)^{1/2} \quad (2)$$

wherein M is the molecular weight of the fluid, R the universal gas constant and T the absolute temperature. For definiteness we adopt a value for V_o at 308 K deduced from viscosity measurements made by Kashiwagi and Makita [9]. Figure 1 then shows the result of the superposition of the remaining thermal conductivity isotherms on the reference line at 308 K by shifts along the ln V axis. It can be seen that the agreement between the various isotherms is remarkable which confirms the hypothesis of equation (1). The values of V_o which secure .this agrement are listed in Table II.

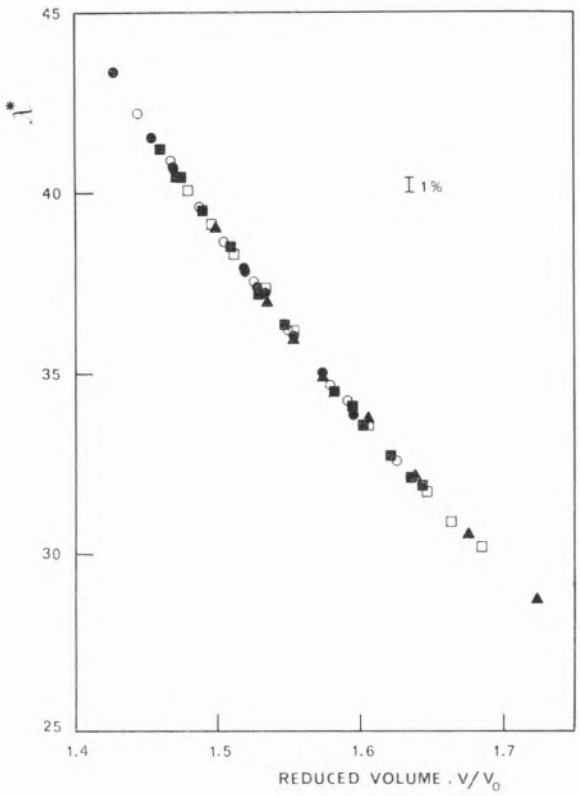

Figure 1

The reduced thermal conductivity, λ^*, for toluene as a function of V/V_0.

●; *308.15 K;* o: *320.15 K;* ■: *330.15 K;* □: *345.15 K;* ▲: *360.15 K.*

Table II

The temperature dependence of the core volume V_0 for toluene

T/K	$10^6 V_0/m^3\ mol^{-1}$
308.15	67.51
320.15	67.18
330.15	66.86
345.15	66.59
360.15	66.25

It follows from this discussion that the experimental data for the thermal conductivity along all isotherms may be represented by a single equation for which the simple form

$$\ln \lambda^* = 4.5540 - 2.1989 \ln (V/V_o) \quad (3)$$

is found to be an optimum by least squares regression. Figure 2 shows deviations of the original thermal conductivity data [1] from the correlation together with the recent results of other workers [4]. The data on which the correlation is based depart by no more than $\pm$ 1 % from the universal equation and have a standard deviation of only $\pm$ 0.3 %. Furthermore, although the data of Kashiwagi *et al.* [4] depart by as much as 1.5 % from the correlation at the highest temperatures and pressures, the deviation is usually much less and is within the mutual uncertainty of the data and the correlation.

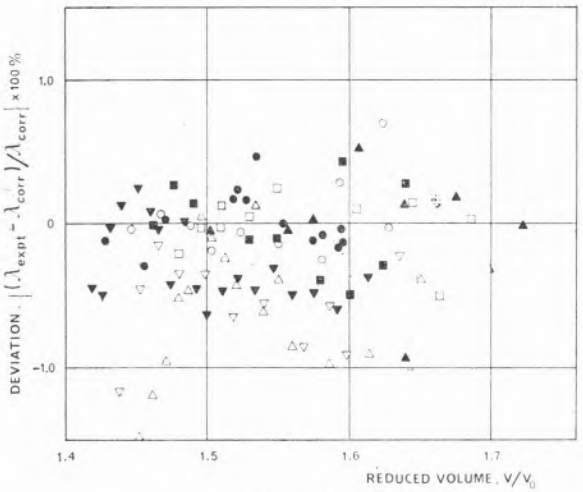

Figure 2

Deviations of experimental thermal conductivity data from the correlation of equations (1) and (2) and Table II.

Present work — ●: 308.15 K; o: 320.15 K; ■: 330.15 K; □: 345.15; ▲: 360.15 K. Kashiwagi et al. [4] —▲: 313.15 K; ∇: 323.15 K; Δ: 348.15 K.

4 — THE THERMAL CONDUCTIVITY ALONG THE SATURATION LINE

The desirability of establishing standard reference values for the thermal conductivity of liquids is vividly illustrated by the wide range of values reported for almost any liquid [10]. Toluene itself has often been proposed as a suitable reference material. The accuracy of the thermal conductivity data discussed in this paper makes them suitable for inclusion in the establishment of such standard rerefence values. However, since the normal reference conditions pertain to the saturation line or to 0.1 MPa the data considered require extrapolation in order to be used in this fashion. The preceding section has illustrated that an extrapolation based on the dependence of the thermal conductivity on density is both reliable and simple. Accordingly, we have fitted an equation of the form of equation (2) to the thermal conductivity data for each isotherm and used the fit to derive the thermal conductivity at saturation. The values are listed in Table III. Inevitably this extrapolation degrades the accuracy of the original experimental data to some extent, but the extrapolation is not large and it is estimated that the reported saturation line values should not be in error by more than $\pm$ 1 %.

Table III

The thermal conductivity of toluene along the saturation line

T/K	λ/mW m^{-1} K^{-1}
308.15	128.5
320.15	124.9
330.15	121.0
345.15	116.9
360.15	112.0

ACKNOWLEDGEMENTS

The authors are grateful to the United Kingdom Department of Trade and Industry, the United Kingdom Science and Engineering Research Council and the Instituto Nacional de Investigação Científica, Portugal for financial support of this work. They also wish to express their thanks to Drs. A. J. Easteal and L. Woolf for performing the high pressure density measurements and allowing them to use the data prior to publication.

(received, 5.th July 1985;
in revised form, 31th December 1985)

REFERENCES

[1] C.A. Nieto de Castro, S.F.Y. Li, G.C. Maitland and W.A. Wakeham, *Int. J. Thermophys.* **4**, 311 (1983).

[2] S.F.Y. Li, G.C. Maitland and W.A. Wakeham, *Int. J. Thermophys.* **5**, 351 (1984).

[3] J. Menashe, M. Mustafa, M. Sage and W.A. Wakeham, *Proc. 8th Symp. Thermophys. Properties*, J.V. Sengers, Ed., (ASME, New York, 1981), p. 254.

[4] H. KASHIWAGI, T. HASHIMOTO, Y. TANAKA, H. KUBOTA AND T. MAKITA, *Int. J. Thermophys.* **3**, 201 (1982).

[5] A.J. EASTEAL AND L. WOOLF, *Int. J. Thermophys*, **6**, 331 (1985).

[6] J. MFNASHE AND W.A. WAKEHAM, BER. BUNSENGES. *Phys. Chem.* **85**: 340 (1981).

[7] S.F.Y. LI, G.C. MAITLAND AND W.A. WAKEHAM, *High Temp.-High Press.*, **17**, 241 (1985).

[8] S.F.Y. LI, *PhD Thesis*, Imperial College (1984).

[9] H. KASHIWAGI AND T. MAKITA, *Int. J. Thermophys.* **3**, 289 (1892).

[10] D.T. JAMIESON AND J.S. TUDHOPE, «*Thermal Conductivity of Liquids. A Data Survey to 1973*», (HMSO, Edinburgh, 1974).

RESUMO

A dependência da densidade na condutibilidade térmica do tolueno

Este trabalho descreve uma nova interpretação da dependência da densidade da condutibilidade térmica do tolueno em termos de uma equação baseada no modelo de van der Waals para um fluido denso. A nova análise é baseada em valores precisos da condutibilidade térmica anteriormente publicados e de valores de densidade do tolueno publicados recentemente. Verifica-se que, existe uma correlação simples baseada no modelo de van der Waals, entre a condutibilidade térmica e o volume molar do líquido, com uma exactidão compatível com a incerteza dos dados experimentais.

F. CAPITÁN
F. MOLINA
P. ESPINOSA
L.F. CAPITÁN-VALLVEY

Department of Analytical Chemistry
Faculty of Sciences
University of Granada
Granada
Spain

A STUDY OF THE Ni(II)-2-(*o*-HYDROXYPHENYLIMINOMETHYL)PYRROLE SYSTEM. DETERMINATION OF Ni(II)

The Schiff base 2-(o-hydroxyphenyliminomethyl)pyrrole reacts with the Ni(II) ion to produce a red complex with a stoicheiometric ratio of 1:1 (λ_{max} = 500 nm, $\varepsilon = 6.3 \times 10^3$ $dm^3.mol.^{-1}.cm^{-1}$). The optimum conditions for the formation of the complex are studied and a method for the quantitative determination of Ni(II) within the range 1-12 ppm is proposed A method of identifiying Ni(II) is also suggested (detection limit = 0.2 μg), using the retention of the reaction product of 2-(o-hydroxyphenyliminomethyl)pyrrole with the Ni(II) ion by an ion-exchange resin.

1 — INTRODUCTION

In a previous publication [1] we have reported on the results obtained with regard to the synthesis, chemicophysical characteristics and reaction capacity of the Schiff base 2-(o-hydroxyphenyliminomethyl) pyrrole with inorganic ions. As we indicated, one of the most sensitive reactions is that which takes place with the Ni(II) ion, which produces a red colour in basic media (pD = 5.7) and a yellow precipitate in neutral media. An analysis of the solid yellow compound showed clearly that the stoicheiometric ratio of the complex was 2:1 (ligand:cation) and its structure was tetrahedric [2].

In this paper we study the Ni(II)-2-(o-hydroxyphenyliminomethyl) pyrrole system in solution and propose a new spectrophotometric method for determining the Ni(II) ion. Furthermore, we propose a new resin spot test, based on the intense colouring of the complex, for the qualitative detection of Ni(II).

2 — EXPERIMENTAL

APPARATUS

Beckman Acta III spectrophotometer.

Crisom mod. 501 pH-meter equipped with glass and saturated calomel electrodes.

REAGENTS

All chemicals used were of analytical-reagent grade.

Nickel(II) solution 0.1 mol.dm^{-3}. Prepared from $Ni(NO_3)_2.6H_2O$ and standardised gravimetrically with dimethylglyoxime. The working solutions were prepared by appropriate dilution.

2-(o-hydroxyphenyliminomethyl) pyrrole. The Schiff base was synthesized by condensing equimolar amounts of o-aminophenol and pyrrole-2-aldehyde in ethanol under reflux,

and recrystallized from ethanol-water [1]. Solutions 5×10^{-3} mol.dm^{-3} and 1 g.dm^{-3} were prepared by disolving the appropriate amounts in ethanol.

Cationic - exchange resin Dowex 50×8 (100 — 200 mesh) sodium form.

PROCEDURE FOR THE SPECTROPHOTOMETRIC DETERMINATION OF Ni(II)

Into a 25-cm^3 calibrated flask transfer an aliquot of solution to make a concentration of nickel(II) of between 2 and 8 ppm and add 2.5 cm^3 of 0.1 mol. dm^{-3} NH_4Cl/NH_3 buffer solution to adjust the pH to 10.2. Add 1 cm^3 of the 5×10^{-3} mol. dm^{-3} Schiff base solution in ethanol and complete up to 25 cm^3 with the appropriate volumes of ethanol and water so that the final mixture results in 60 % v/v ethanol-water. After 15 minutes, measure the absorbance of the solutions at 500 nm against a spectrophotometric blank of the Schiff base prepared in the same way.

PROCEDURE FOR THE IDENTIFICATION OF Ni(II)

A couple of drops of the solution to be analysed are added to a few cationic-exchange resin beads and the mixture is shaken. After waiting a minute or two to attain equilibrium 1 drop of the reagent solution 1 g.dm^{-3} is added, plus one or two drops of NaOH 2 mol.dm^{-3}, shaking again for a few moments. The presence of Ni(II) is indicated if the resin beads turn red.

3 — RESULTS AND DISCUSSION

3.1 — *A STUDY OF THE Ni(II)-2-(O-HYDROXYPHENYLIMINOMETHYL) PYRROLE SYSTEM IN SOLUTION*

Ni (II) with the Schiff base 2-(o-hydroxyphenyliminomethyl) pyrrole in a basic hydroalcoholic medium produces a red colouring with maximum absorption at 500 nm.

The optimum pH for the formation of the complex appears to be between 9.5 — 10.5 (fig. 1). To obtain this we found a buffer solution of NH_4Cl/NH_3 0.1 mol. dm^{-3} to be the most suitable. The absorbance reaches its maximum value 15 mins. after the preparation of the solution and remains stable for 30 minutes more.

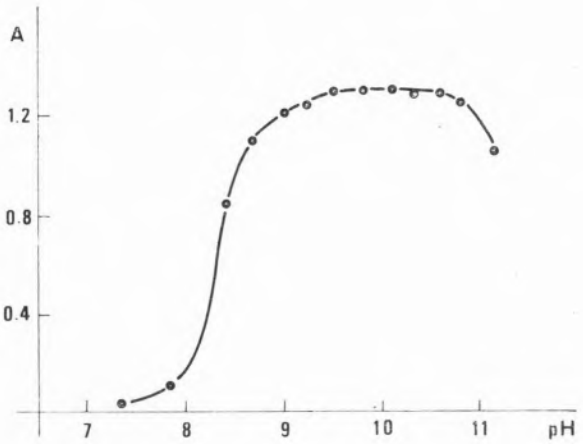

Fig. 1

The influence of the pH on the absorbance ($\lambda = 500$ nm).

The optimum ethanol concentration is 60 % (v/v).

A higher concentration of ethanol results in a slight displacement in the longer wavelengths (from 490 to 500 nm) and greater absorption values.

Our experiments have shown that the order in which the reagents are added does not affect the final outcome.

The stoicheiometry of the complex was determined according to the YOE-JONES [3] and JOB [4] methods, and on each occasion the ratio was found to be 1:1. The conditional

stability constant of the chelate, determined by MEITES and TOMAS' method [5] at pH=10.2 showed a value of 2.2×10^6.

3.2 — *THE SPECTROPHOTOMETRIC DETERMINATION OF Ni(II)*

Fullfilment of Beer's law and reproduceability

Once the optimum conditions had been established for the formation of the Ni(II)-2-(o-hydroxyphenyliminomethyl) pyrrole complex we carried out experiments which showed that Beer's law is obeyed within the range 1 to 12 ppm of Ni(II) ($c=-0.04+9.51A$, $r^2 = 0.999$); the molar absorptivity at 500 nm is 6.3×10^3 $dm^3 . mol^{-1} . cm^{-1}$.

The zone of least error, determined by using Ringbom's graph, is between 2 and 8 ppm of Ni(II).

In 10 analogous samples containing 4 ppm of Ni(II) the relative error (P=0.05) was found to be 1.1 %.

Interference study

We carried out tests in order to determine the effect which variable quantities of foreign ions might have on solutions containing 6 ppm of Ni(II).

The following ions, of those which we studied, produce interference:

Cu(II), Cd(II), Tl(III), Pd(II), Fe(III), U(VI), Zn(II) and Ga(III) interfere negatively when present at concentrations of 1 ppm.

Pb(II), Co(II), Bi(III), Au(III), In(III), Ti(IV) and V(V) interfere negatively when present at concentrations of more than 3 ppm.

3.3. — *THE IDENTIFICATION OF Ni(II)*

Preliminary evidence showed that 2-(o-hydroxyphenyliminomethyl) pyrrole is capable of reacting with the Ni(II) ion when this is attached to an ionic-exchange resin; the reaction product is retained by the resin.

The reaction only takes place in highly basic NaOH medium, and the NaOH solution must be added after that of the Schiff base.

The formation time and the intensity of the colour of the resin depend on the quantity of Ni(II) present. It may take up to five minutes, for example, to clearly identify the colouring if the concentration of Ni(II) is close to the limits of identification.

Given the red colouring which the resin beads acquire in the presence of the Ni(II)-2-(o-hydroxyphenyliminomethyl)pyrrole system it might be reasonable to presume that the product retained by them is the complex with a stoicheiometric ratio of 1:1 studied in the previous section of this paper. This stoicheiometry may correspond to a cationic compound.

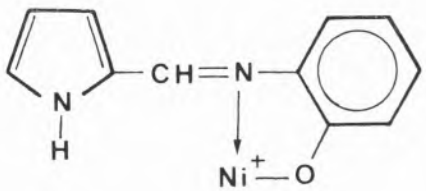

On the other hand the fact the red compound only forms in a basic medium might suggest that the reagent behaves as a dibasic ligand, binding to the Ni(II) ion through the deprotonated pyrrolic N, as well as through the azomethinic N and thus forming a neutral polymeric compound [6], which would be absorbed onto the resin.

Sensitivity

Using our experimental method we have established that the detection limit and the dilution limit for Ni(II) are 0.2μg and 0.4 ppm, respectively.

Foreign ion interference

Table I shows the results obtained from experiments with 4μg of Ni(II) in the presence of various quantities of potentially interfering ions.

Table I

The tolerance of various different inorganic ions in the qualitative detection of Ni(II) (4 μg)

Foreign ion	Foreign ion/Ni(II)
Ti(IV), Ga(III), Pb(II), In(III), Bi(III)	200
U(VI), Zn(II)	
Au(III), Pd(II), Tl(III)	100
Cd(II), Fe(III)*	50
V(V)	25
Cu(II)	3
Co(II)	1

* In the presence of a few drops of triethanolamine at 1%.

(Received, 21st June 1985;
in revised forms 10th October 1985)

REFERENCES

[1] F. CAPITÁN, L.F. CAPITÁN-VALLVEY, P. ESPINOSA, F. MOLINA, *Quím. Anal.* **4** , 335 (1985).
[2] F. CAPITÁN, F. MOLINA, P. ESPINOSA, L.F. CAPITÁN-VALLEY, *Acta Chimica Hungarica* **121**, 373 (1986).
[3] J.H. YOE, A.L. JONES, *Ind. Eng. Chem, Anal.*, **16**, 11 (1944).
[4] P. JOB, *Ann. Chim.*, **9**, 114 (1927).
[5] L. MEITES, H.C. TOMAS, «Advanced Analytical Chemistry», McGraw Hill Book Company. Inc., 1958.
[6] A. SYAMAL, K.S. KALE, *Curr. Sci.*, **44**, 256 (1974).

RESUMO

Estudo do sistema Ni(II)-2-(0-hidroxifeniliminometil) pirrol. Determinação de Ni(II)

A base de Schiff 2-(o-Hidroxifeniliminometil) pirrol reage com o ião Ni(II) dando um complexo vermelho na proporção estequiométrica 1:1 (λ_{max} = 500 nm; $\varepsilon = 6.3 \times 10^3$ $dm^3.mol^{-1}.cm^{-1}$). Estudaram-se as condições óptimas para a formação do complexo e propõe-se um método para o doseamento de Ni(II) no intervalo 1-12 ppm. Sugere-se, também, um método para a identificação de Ni(II) (limite de identificação = 0,2 μg), fundamentado na retenção do produto da reacção entre 2-(o-hidroxifeniliminometil)pirrol e Ni(II) por uma resina permutadora de iões.

M. R. BERMEJO **
M. GAYOSO
Departamento de Química Inorgánica,
Facultad de Química
Universidad de Santiago de Compostela,
Espanha

M. ISABEL FERNÁNDEZ
A. HERMIDA
M. ESTER GÓMEZ
Departamento de Química Inorgánica,
Colegio Universitario de Lugo,
Espanha

COORDINATION CHEMISTRY OF TI(III) WITH AZOLES I COMPOUNDS OF $TlXX'_2$ WITH PYRAZOLE *

The complexes $TlCl_2Br.2Pz$; $TlClBr_2.2Pz$; $TlCl_2I.2Pz$; $TlBr_2I.2Pz$; $TlBrI_2.2Pz$; $TlI_3.2Pz$ and $TlClBrI.2Pz$ (where Pz = Pyrazole) have been prepared and characterized. All the solids isolated behave as non ionogenus in acetonitrile solution. The IR spectra are discussed specially the Tl-X stretching vibration modes, molecular structures for the complexes are proposed.

* Presented, in part, at the XXI Reunión Bienal de R.S.E.F.Q., Castellón, España (1984).

** To whom any correspondence may be addressed.

INTRODUCTION

The properties of Tl (III) halides as acceptor are nowadays well known [1, 2], since, twenty years ago, Cotton [3] was able to stabilize compounds of the type TlX_3nL.
Lately, we have studied both the stabilization of interhaloderivatives of thallium, such as $TlXX'_2nL$ (4, 5, 6 and references therein mentioned) and the structure of this kind of complexes (7, 8, 9). We have observed [10] that hard ligands (in Pearson's terminology [11]) are the best stabilizers of these systems. We have studied ligands whose donor atom is oxygen and we are now interested in the study of nitrogen ligands.
Among those ligands nitrogenated heterocycles, particularly pyridine and picolines [14-19], are specially interesting as stabilizers of thallium halides of the TlX_3nL type; but very little is known about the stability of complexes of the $TlXX'_2nL$ type. Recently, we have done some research with $TlClBr_2nL$ complexes (L = pyridines α, β and γ picolines) [20] and we now report results obtained with pyrazole (Pz).
The donor properties of pyrazole as a ligand have been previously studied by us with other systems [21, 22] and we thought it suitable to study the stabilization of the $TlXX'_2nL$ complexes. $TlCl_3$2Pz and $TlBr_3$2Pz have been prepared previously by us [22], and now are compared from the spectral point of view.

EXPERIMENTAL

REAGENTS

TlCl, TlBr, TlI, Br_2, pyrazole (Merck p. s.) and IBr (Shuchart p. s.) were used without further purification. Chlorine was prepared «in situ» in the conventional way. Analema iodine was resublimed. Solvents were purified by standard methods.

PREPARATION OF THE COMPOUNDS

The complexes were prepared following the method proposed by Cotton [3] and

improved by us [6, 12]. The solution with the acceptor was prepared by adding, slowly and with magnetic stirring, a solution of the halogen (X_2) or interhalogen (XX') in acetonitrile to a suspension of the thallium halide (TlX) in the same solvent. When TlX is completely dissolved the addition of the oxidizing agent is stopped and its excess is removed with a current of dry nitrogen. The solution of pyrazole in the stoicheiometric quantity was slowly added to that of the donor and was left with magnetic stirring for 24 hours.

$TlCl_2Br.2Pz$ and $TlClBr_2.2Pz$: These compounds were prepared by previous oxidation of 3.5 mmol of TlBr and 4 mmol of TlCl with the required quantity of Cl_2 and Br_2, using acetonitrile as solvent. 7.5 mmol and 8.7 mmol of pyrazole were aftewards added, and the solution was stirred for 24 hours. The transparent solutions were concentrated under vacuum. A yellow solid ($TlCl_2Br.2Pz$) was obtained which gave a yield of 90 % and an orange solid (yield 67 %).

$TlCl_2I.2Pz$ and $TlClI_2.2Pz$: These compounds were prepared in a similar way to the previous ones. Cl_2 or I_2 in acetonitrile were added to 4 mmol of TlI and 3.5 mmol of TlCl. 7.5 mmol and 8.0 mmol of pyrazole respectively were inmediately added. The resulting solutions are concentrated under vacuum. A yellow solid ($TlCl_2I.2Pz$, yield 94 %) and a

Table 1

Composition and some properties of the complexes

Compounds	Colour	% C	% H	% N	% Tl	M.P./°C	Λ^{**}
$TlI_3.2Pz$	Red	10.1 (10.0)	1.0 (1.1)	7.6 (7.8)	27.5 (28.3)	90	91
TlClBrI.2Pz	Orange	12.2 (12.4)	1.5 (1.4)	9.5 (9.6)	34.6 (35.1)	107	83
$TlCl_3.2Pz$	Yellow	16.2 (16.1)*	1.8 (1.8)	12.6 (12.5)	45.5 (45.7)	95	66
$TlCl_2Br.2Pz$	Yellow	15.2 (14.7)	1.7 (1.6)	12.4 (11.4)	39.1 (41.6)	76	50
$TlCl_2I.2Pz$	Yellow	13.7 (13.4)	1.4 (1.5)	9.1 (10.4)	37.2 (37.9)	77	47
$TlClBr_2.2Pz$	Orange	13.3 (13.5)	1.4 (1.5)	10.5 (10.5)	36.9 (38.1)	63	40
$TlClI_2.2Pz$	Red	11.0 (11.4)	1.3 (1.3)	8.6 (8.9)	32.5 (32.5)	102	77
$TlBr_3.2Pz$	Yellow	12.8 (12.4)	1.6 (1.4)	10.3 (9.7)	36.2 (35.2)	90	31
$TlBr_2I.2Pz$	Orange	10.9 (11.5)	1.4 (1.3)	8.8 (8.9)	32.3 (32.6)	123	85
$TlBrI_2.2Pz$	Granate	10.5 (10.7)	1.3 (1.2)	8.3 (8.3)	28.1 (30.3)	157	91

* The theoretical values are in brackets.

** $ohm^{-1} . cm^2 . mol^{-1}$ dissolution 10^{-3} M in CH_3CN.

red solid ($TlClI_2.2Pz$, yield 67 %) were obtained.

$TlBr_2I.2Pz$ and $TlBrI_2.2Pz$: The solution of the acceptors were prepared with 3 mmol of TlI and 3,6 mmol of TlBr in acetonitrile, wich were oxidized with the required quantities of Br_2 and I_2. 7 mmol and 7.5 mmol of pyrazole respectively, were added to each solution. When the resulting solutions were concentrated, oranges needles ($TlBr_2I.2Pz$, yield 77 %) and a violet solid ($TlBrI_2.2Pz$, yield 71 %) were obtained.

$TlI_3.2Pz$: 3.3 mmol of iodine in acetonitrile were added to 3 mmol of TlI and 7 mmol of pyrazole in the same solvent; a red solid were obtained. The solid was washed with cold acetonitrile and vacuum dried. Yield 83 %.

TlClBrI.2Pz: 7mmol of BrI in acetonitrile were used to oxidize 5.2 mmol of TlCl. 12 mmol of pyrazole in the same solvent were immediately added. The orange solid obtained was washed with acetonitrile. Yield 83 %.

CHEMICAL ANALYSIS

C, H and N microanalyses were performed using a Perkin-Elmer 240-B elemental analyser. Thallium was determined by atomic absorption in a Perkin-Elmer 2.280 absorptiometer equipped with the suitable lamp, at a wavelength of 276.8 nm and using an oxidizing flame air-acetilene. The analytical data are summarized in Table 1, wich also shows some physical properties of the compounds.

PHYSICAL MEASUREMENTS

Conductivity data were obtained in acetonitrile in a WTW Model LF-3 conductimeter. The IR spectra of the ligands and the complexes were recorded as nujol mulls between NaCl (4000-600 cm^{-1}) or polyethylene (600--100 cm^{-1}) windows using a Perkin-Elmer 180 spectrophotomer.

RESULTS AND DISCUSSION

All the complexes were prepared as coloured solids, most of them powdery and difficult to crystallize. They are light stable but decompose slowly in air. In water the hydrolysis is very fast. The values of the melting points are low in all cases, suggesting the presence of molecular forms, with very weak interactions in the solid. They have very low solubilities in polar solvents (n-hexane, benzene, etc.) but the solubility increases in solvents with high dielectric constant (acetone, ethanol, acetonitrile... et.).

The values for the molar conductivities of the complexes in acetonitrile (see Table 1) are lower than 120-180 $ohm^{-1}\ cm^2\ mol^{-1}$ considered characteristic of 1:1 electrolytes (23) and are in agreement with the values obtained for similar systems [10, 13, 20, 22].

The IR study was carried out taking into account the spectrum of the free ligand and observing the modifications that the characteristic bands of the ligands undergo upon coordination. The number and the position of the ν(Tl-X) and ν(Tl-N) bands were also studied, in order to get information about the posible stereochemistry. The assignment of the ligand bands at high vawelengths was made as in the literature [24, 25], particularly following Reedijk's papers. The most significant bands are shown in Table 2.

A strong shift of the ν(N-H) bands towards higher wave numbers (350-400 cm^{-1}) is always observed and is explained as due to important changes of the hydrogen bond in the free associated ligands. It is noteworthy that the position of ν(N-H) in the complexes is lower than the position of that band in the ligands in gas phase, suggesting that there is still a certain amount of hidrogen bond in the complexes [28]. Similar results were obtained in other systems [22, 29]. The stretching bands of the ring (1540-1360)

Table 2

Most important IR bands (4000-600 cm^{-1}) of the ligands and the complexes

Compounds	ν(N-H)	ν(C-H)	Ring streching				C-H, N-H and ring bending modes				
Pz	2900F	3150F,a	1540m	1470F	1400F	1360F	1260d	1135mF	1050F	930F	910F
$TlCl_3$.2Pz	3340F	3140F,a	1540m	1470F	1405F	1370F	1240d	1130F	1050F	920F	910F
$TlCl_2Br$.2Pz	3300F	3130F,a	1530m	1480F	1400F	1370F	1240m	1130F	1050m	920m	910F
$TlCl_2I$.2Pz	3285F	3100F,a	1540m	1470F	1400F	1370F	1250d	1135F	1050F	930F	910F
$TlClBr_2$.2Pz	3300F	3130F,a	1530m	1465F	1410F	1380m	1250d	1130F	1040F	920m	910F
$TlClI_2$.2Pz	3250F	3100F,a	1540m	1465F	1400F	1370F	1250d	1135F	1050F	920m	910F
$TlBr_3$.2Pz	3330F	3145F,a	1530m	1470mF	1395F	1355F	1265m	1130F	1050F	930F	900F
$TlBr_2I$.2Pz	3300F	3100F,a	1540m	1480F	1400F	1355F	1240d	1130F	1040F	930F	910F
$TlBrI_2$.2Pz	3250F	3100F,a	1540m	1470F	1400F	1365m	1240d	1130F	1040F	930F	900m
TlI_3.2Pz	3250F	3100F,a	1530m	1460F	1400F	1370m	1260d	1120F	1050F	930F	910F
TlClBrI.2Pz	3250F	3100F,a	1540m	1480F	1400F	1370m	1250d	1130F	1050F	930F	910F

Table 3

Most important IR bands (400-80 cm^{-1}) of the ligand and the complexes

Compounds	ν (Tl-Cl)	ν (Tl-Br)	ν (Tl-I)	Other bands
Pz				135F
$TlCl_3$.2Pz	290mF, 270mF			192m*, 160m+, 135m, 110d
$TlCl_2Br$.2Pz	300mF	188F		150m+, 120m
$TlCl_2I$.2Pz	283mF, 260mF		157F	128mF, 111F+
$TlClBr_2$.2Pz	307mF	200hF, 190mF		154m+, 120m
$TlClI_2$.2Pz	303F		165mF	190m*, 120m
$TlBr_3$.2Pz		200h, 195mF		137F
$TlBr_2I$.2Pz		180mF	162F	120m
$TlBrI_2$.2Pz		180F	160mF, 155mF	122m
TlI_3.2Pz			157h, 152mF	190m*, 130m
TlClBrI.2Pz	278F	184mF	162F	110m+

* Bands assigned as δ (Tl-Cl).
\+ Bands provisionaly assigned as ν (Tl-N).

undergo small shifts when pyrazole is coordinated, implying that the structure of the ring is only slightly modified and the donor-aceptor bond occurs through the pyridine nitrogen [30]. The other ligand bands do not undergo significant variations.

The bands ν (Tl-X), ν (Tl-N) and δ (Tl-X) which appears below 500 cm^{-1}, offer information about the structure of the complexes. The assignment of the ν (Tl-X) has been accomplished by comparing the spectra of one complexes with each other and with the assignment made in other thallium complexes of the type TlX_3L_2 and $TlXX'_2L_2$ prepared by us [4, 5, 6, 12]. It was also taken into account that according to Carty [31], the ν (Tl-Br)/ν (Tl-Cl) and ν (Tl-I)/ν (Tl-Cl) ratios must be approximately 0,7 and 0,6 respectively. The bands showing below 150 cm^{-1} have been taken as δ (Tl-X) modes, as it has been suggested by WALTON [32] and MCWHINNIE [33]. It is not easy to make the assignment of the ν (Tl-N) band, as it is placed at 200 cm^{-1} [22] and at this wavelength the ν (Tl-Br) bands appears, so that it was assigned only, and in a provisional way, in the case of the complexes $TlCl_3$.2Pz, $TlClI_2$.2Pz and TlI_3.2Pz. The proposed assignment are listed in Table 3. The presence in the solid of ionic and dimeric or polimeric species through association may be rejected due both to the shape of one spectrum and the position of the bands (see Fig. 1). In fact, no bands appear over 320 cm^{-1} belonging to $|TlX_{4-n}|^-$ forms and the spectrum show a small number of bands, excluding the possible presence of two kinds

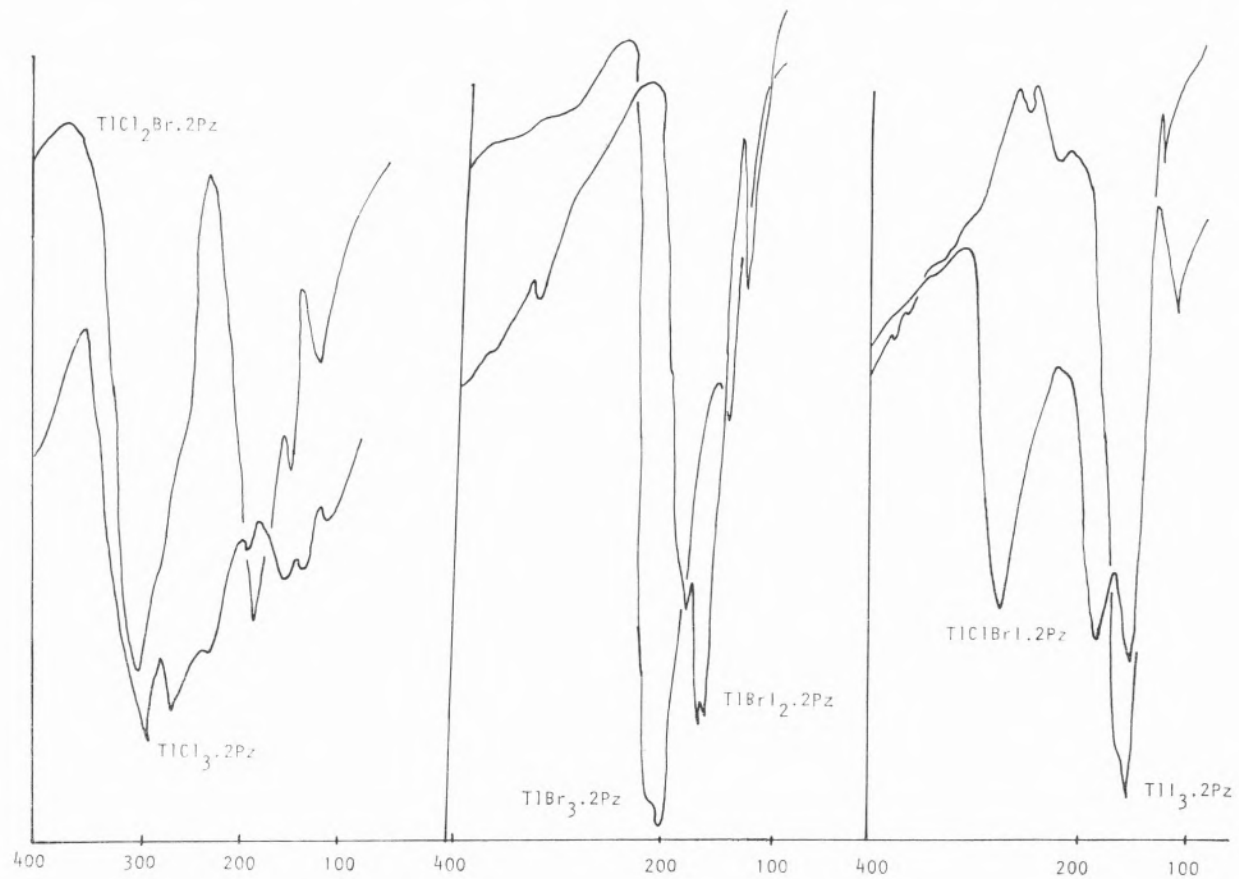

Fig. 1

IR spectra of some complexes and their ligands (400-80 cm^{-1})

of bond: ν (Tl-X)$_{final}$ and ν (Tl-X)$_{bridge}$. We may also mention that coordination around the central atom is 5, as it has been already discussed (12).

Both X-Ray diffraction studies of the complexes prepared by us with oxigenated ligands: $TlI_3(2PicO)_2$ [7]; $TlBr_3(TPPO)_2$, [8]; $TlBr_2I(TPPO)_2$ [36]; $TlBrI_2(4\text{-}PicO)_2$ [37]; $TlClBrI(TPPO)_2$ [38]; and Worral's work [39] with amines and other nitrogenated ligands reveal that these compounds present a monomeric «bpt» structure with the ligands in apical positions.

If the complexes $TlCl_3$.2Pz, $TlBr_3$.2Pz and TlI_3.2Pz present this structure, with approximately D_{3h} symmetry around the central atom, they should present 4 stretching vibrations: one active only in IR, ν_{as} Tl-N(A''_2); two active in Raman, ν_s Tl-N(A'_2) and ν_s Tl-X(A'_1); finally one active both IR and Raman, νTl-X(E'). In our case we find only one ν_{as} Tl-N for the compound $TlCl_3$.2Pz and two bands assigned to the E mode which are the result of the loss of symmetry of the molecule and subsequent splitting of the E mode; a similar situation has been already found [7, 45]. The main conclusion is that these compounds should present a distorted «bpt» structure.

For the complexes of the type $TlXX'_2$.2Pz we observe three bands characteristic of ν (Tl-X) and ν (Tl-X'), but such a situation may also correspond to puntual simmetry C_{2v}, C_s or C_1 around the thallium atom. The vibrational study on its own does not offer definitive solutions, but the spectral study in comparison with compounds of the type $TlXX'_2$2L, for which difractometric studies were carried out [36, 37], allow us to propose that the most probable structure is «bpt» with ligands in the apical positions.

TlClBrI.2Pz offers a spectral situation quite similar to the one discussed in the case of $TlXX'_2$.2Pz, so that we propose the same kind of structure.

(Received, 3rd.July.1985; in revised form, 15th.January.1986)

REFERENCES

[1] R. A. WALTON. *Coord. Chem. Rev.*, **6**, 1 (1971).

[2] A. PIDCOCK. *"M.T.P." Inorg. Chem. Ser. Two*, **1**, 281 (1975).

[3] F. A. COTTON, B. F. G. JOHNSON, R. M. WING. *Inorg. Chem.*, **4**, 502 (1965).

[4] M. V. CASTAÑO, A. SÁNCHEZ, M. R. BERMEJO, M. GAYOSO. *An. Quim.*, **79B**, 357 (1983).

[5] M. R. BERMEJO, F. BOTANA, M. GAYOSO. *Rev. Port. Quim.*, **26**, 113 (1984).

[6] M. R. BERMEJO, J. IRISARRI, M. GAYOSO. *Synth. React. Inorg. Met-org. Chem.*, **15**, 197 (1985).

[7] M. R. BERMEJO, A. CASTIÑEIRAS, M. GAYOSO, W. HILLER, U. ENGLERT, J. STRÄHLE, *Z. Naturforsch*, **39B**, 1159 (1984).

[8] M. R. BERMEJO, F. BOTANA, A. CASTIÑEIRAS, M. GAYOSO, W. HILLER, J. STRÄHLE. *Acta Cientif. Compost.*, **XXII**, 161 (1985).

[9] M. R. BERMEJO, A. CASTIÑEIRAS, M. GAYOSO, W. HILLER and J. STRÄHLE. *Acta Cryst.* (in press).

[10] T. LUCAS, J. CARREIRA, M. R. BERMEJO, M. GAYOSO. *Rev. Port. Quim.*, **22**, 108 (1980).

[11] R. E. PEARSON. *Science*, **151**, 172 (1956).

[12] J. IRISARRI, M. R. BERMEJO, M. V. CASTAÑO, M. GAYOSO, *Rev. Port. Quim.*, **25**, 174 (1983).

[13] J. GARCÍA, M. R. BERMEJO, M. V. CASTAÑO, M. GAYOSO. *Acta Cientif. Compost.*, **XIX**, 487 (1982).

[14] R. J. MEYER. *Z. Anorg. Allgem. Chem.*, **24**, 321 (1900).

[15] C. RENZ. *Chem. Ber.*, **35**, 1110 (1902).

[16] R. K. ABBOTT. *Iowa State Coll. J. Sci.*, **18**, 3 (1943).

[17] F. KUL'BA YA, V. E. MIRONOV, V. I. SAZHINA, T. G. OGIBENINA. *Zhur. Neorg. Khim.*, **8**, 911 (1963).

[18] B. F. G. JOHNSON, R. A. WALTON. *Inorg. Chem.*, **5**, 49 (1966).

[19] F. KUL'BA YA, N. G. ROSLAVSKII YA, L. V. BARSUKOV, V. E. MIRONOV. *Zhur. Neorg. Khim.*, **13**, 153 (1968).

[20] F. BLANCO, M. V. CASTAÑO, M. R. BERMEJO, M. GAYOSO. *An. Quim.*, **81B**, 133 (1985).

[21] J. R. MASAGUER, E. FREIJANES, J. SORDO, J. CASAS, M. R. BERMEJO. *Inorg. Chim. Acta*, **25**, 203 (1977).

[22] M. E. GARCÍA FERNÁNDEZ, J. SORDO, J. S. CASAS, M. GAYOSO, *An. Quim.* **78B**, 27 (1982).

[23] W. GEARY, COORD. *Chem. Rev.*, **7**, 81 (1971).

[24] A. ZECCHINA, L. CERRUTI, S. COLUCCIA, E. BORELLO. *J. Chem. Soc. (B)*, 1363 (1967).

[25] L. J. BELLAMY. "The *Infrared Spectra of Complex Molecules*", Methuen, 2.ª Ed. (1966).

[26] J. REEDIJK, P. *Rec. Trav. Chim.*, **90**, 117 (1971).

[27] J. REEDIJK, J. L. A. WINDHORST, N. H. M. VAN HAM, W. L. GROENEVELD. *Rec. Trav. Chim.*, **90**, 234 (1971).

[28] L. J. BELLAMY. "Infrared Spectra of Complex Molecules", vol. 1. Chapman and Hall, London (1975).
[29] J. REEDIJK. *Rec. Trav. Chim.*, 88, 1139 (1969).
[30] K. M. YUNUSOV, A. O. GARNOVSKII, D. A. OSIPOV, YU V. KOLOOYAZHNYI. *J. Gen. Chem. U.S.S.R.*, **41**, 1329 (1971).
[31] A. J. CARTY. *Coord. Chem. Rev.*, **4**, 29 (1969).
[32] R. A. WALTON. *Inorg. Chem.*, **7**, 640 and 1927 (1968).
[33] J. R. HUDMAN, M. PATEL, W. R. MCWHINNIE. *Inorg. Chim. Acta*, **4**, 161 (1970).
[34] T. E. SPIRO. *Inorg. Chem.*, **6**, 659 (1967).
[35] D. N. STOROPOULOS, J. K. KOUSNIS, N. G. GALINOS. *Inorg. Nucl. Chem. Letters*, **17**, 117 (1981).
[36] M. R. BERMEJO, J. BRAVO, A. CASTIÑEIRAS, M. GAYOSO, W. HILLER, J. STRÄHLE. *Acta Cryst.* (in press).
[37] M. R. BERMEJO, M. E. GARCÍA FERNÁNDEZ, M. GAYOSO, W. HILLER, J. STRÄHLE. *Z. Naturforsch* (in press).
[38] M. R. BERMEJO, A. CASTIÑEIRAS, M. GAYOSO, W. HILLER, J. STRÄHLE. *Acta Cryst.* (submitted).
[39] S. E. JEFFS, R. W. H. SMALL, I. J. WORRALL. *Acta Cryst.*, **C40**, 67, 381 e 1628 (1984).
[40] M. R. BERMEJO, M. ISABEL FERNANDEZ, M. GAYOSO, *An. Quim.*, **82B**, 57 (1986).

SEBASTIÃO J. FORMOSINHO
ANTÓNIO J.C. VARANDAS
Departamento de Química, Universidade de Coimbra
3049 Coimbra Codex, Portugal

A SIMPLE THEORETICAL MODEL FOR THE ENERGY BARRIER IN UNIMOLECULAR REACTIONS

A simple classical intersecting-state model, which estimates energy barriers in terms of thermodynamic, geometric and chemical bond order factors, is employed to calculate $\Delta G^{\ddagger}$ for the isomerizations of cyclopropane and methyl isocyanide and the dissociation of cyclobutane. Within reasonable structural assumptions agreement between theory and experiment is obtained. The large difference in $\Delta G^{\ddagger}$ for the two isomerization reactions is interpreted in terms of differences in the bond orders of the transition states.

INTRODUCTION

The last decade brought a tremendous increase in a number of accurate *ab initio* and even simple MO theory calculations for chemical reactions. However, to unravel trends of reactivity within a family of related processes, theoretical models, which sacrifice rigour to gain simplicity and computational feasibility, are often better than such *ab initio* calculations [1]. They have also a heuristic value, an aspect which has been somewhat neglected in quantum chemistry. We have recently developed a simple model to estimate energy barriers of chemical reactions in terms of geometric, electronic and thermodynamic factors [2]. We can probably say that this model was designed more for viewing the wood rather the individual trees. Nevertheless it presents an unified model for several empirical and semi-empirical relations between kinetics and thermodynamics, namely the Marcus and BEBO theory and Linear Free Energy Relationships [2, 3].

Although theories of absolute reaction rates offer expressions permitting calculations of the energy barrier of unimolecular reactions, virtually the only cases where reasonable predictions of the activation energy have been made by simple methods are simple bond-breaking bond-forming processes and a few elimination reactions [4, 5].

In view of the importance of unimolecular reactions in gas-phase kinetics, we have decided to test the applicability of our model to the estimation of energy barriers for three unimolecular reactions, namely the isomerization of cyclopropane and methyl isocyanide and the dissociation of cyclobutane. We aim also to assess the most important structural factors which determine the magnitude of the chemical energy barriers of these reactions.

THEORETICAL MODEL

The intersecting-state model (ISM) has been described in detail elsewhere [2] and will

only be stated briefly here. The model estimates the energy barrier of the reaction

$$A + BC \rightarrow AB + C$$

from the intersection of the potential energy curves of BC and AB. If one assumes that the potential energy curves can be represented by harmonic oscillators

$$\frac{1}{2} f_r \, x^2 = \frac{1}{2} f_p \, (d - x)^2 + \Delta E^\circ \qquad (1)$$

where f_r and f_p are the force constants of reactant and product, respectively, x the bond distension in the reactant and ΔE° the reaction energy. The parameter d is the sum of the bond distensions in reactant and product, and it has been shown [2] to be proportional to the sum of the equilibrium bond lengths of reactant and product

$$d = \eta \, (l_r + l_p) \qquad (2)$$

The reduced bond distension η is given by

$$\eta = \frac{a' \ln 2}{n^\dagger} + \frac{a'}{2} \left(\frac{\Delta E^\circ}{\lambda} \right)^2 \qquad (3)$$

where a′ is a constant ($a' = 0.156$), $n^\dagger$ is the bond order of the transition state for the thermoneutral situation, and λ, which is the so called «configuration entropy» proposed by Agmon and Levine [6], is a measure the «energy capacity» of the activated complexes. When the bond-forming bond-breaking processes involve a single bond in reactant and another one in the product, the total bond order is assumed to be conserved along the reaction coordinate [7] and consequently $n^\dagger = 1/2$ [2]. However, the present model considers the possibility that the total bond order can be higher than unity. This can occur either for double or triple bonds, with conservation of total bond order, or for cases where the total bond order is not conserved. The latter case occurs when nonbonding or antibonding electrons acquire a bonding character in the transition state. These transition state bond orders can be known from simple molecular orbital diagrams [3]. Consequently all the parameters of the model come from fields outside chemical kinetics, with the exception of λ which, in general, must be estimated empirically from kinetic data. However, for many reactions $|\Delta E^\circ| << \lambda$ and we can neglect the dependence of η on λ and $(\Delta E^\circ)^2$.

Once d is known from eqs (2) and (3), x can be estimated from eq (1) and the energy barrier due to the distension of the reactant is

$$\Delta E^\dagger = \frac{1}{2} f_r \, x^2 \qquad (4)$$

For vapour phase reactions involving the breaking of one bond and the making of another one, ISM gives a good estimation of the activation energy [2]. However, for reactions in condensed media or for vapour phase reactions of complex molecules there are many other degrees of freedom rather then one stretching in reactant and another in product. To keep the model unidimensional, we have to treat such degrees of freedom on a statistical basis by employing free energies rather than internal energies. In fact, under such conditions the model provides good estimations of $\Delta G^\dagger$ for several types of reactions (2, 3, 8, 9).

Although temperature is not an explicit parameter of ISM, ΔG° and λ [3] are temperature dependent parameters.

Furthermore, when the chemical reaction involves bond-breaking bond-forming processes of more than one chemical bond in reactant and product, a judicious choice of the effective force constants along the reaction coordinate has to be made.

The energy barrier due to bending motions can also be estimated within the assumption of harmonic behaviour

$$\Delta G_b = \frac{1}{2} f_b \, (\theta - \theta^\circ)^2 \qquad (5)$$

as long as the change in bond angle, $\theta - \theta^\circ$, is not very large.

ISOMERIZATION OF CYCLOPROPANE

The rearrangement of cyclopropane into propylene is considered to be a simple unimolecular process [10]. In the high pressure region (> 10 Torr) and in a temperature range of 469 to 519°C, the rate constants follow the expression

$$k/s^{-1} = 1.5 \times 10^{15} \exp(-272.0/RT \text{ kJ mol}^{-1})$$

The activation free energy of the reaction can be estimated from

$$k = \frac{k_B T}{h} c_0^{1-m} \exp(-\Delta G^{\ddagger}/RT)$$

where c_0 is the standard concentration ($c_0 = 1$ mol dm^{-3}), m is the molecularity of the reaction and the other symbols have their usual meaning. Whithin the temperature range of the experimental studies, $\Delta G^{\ddagger}_{792} = 242$ kJ mol^{-1} and $\Delta G^{0}_{792} = -57$ kJ mol^{-1}, estimated from the data collected by Benson *et al.* [11].

The following vibrational modes can be considered to be important for this reaction: in the bond-forming bond-breaking processes the stretching of one C-C and one C-H bond in the reactant and one C = C and one C-H bond in the products. The most significant changes in bond angles are the CCC and CCH. Assuming that such changes up to the transition state are one half of the overall change between reactant and product, the bond angle variations are 30° (90°-60°) for CCC and 19.5° (109.5°-90°) for CCH.

The stretching modes can be taken as independent diatomic oscillators and under this assumption the average stretching force constant of two independent modes is $f = \sqrt{f_1^2 + f_2^2}$ [12]. The relevant data are $f_{C-H} = 2.9 \times 10^3$ kJ mol^{-1} Å^{-2}; $f_{C-C} = 2.7 \times 10^3$ kJ mol^{-1} Å^{-2} and $f_{C=C} = 5.77 \times 10^3$ kJ mol^{-1} Å^{-2} [13]. Consequently $f_r = 4.0 \times 10^3$ kJ mol^{-1} Å^{-2} and $f_p = 6.5 \times 10^3$ mol^{-1} Å^{-2}. The bond length data $l_{C-H} = 1.096$ Å, $l_{C-C} = 1.537$ Å and $l_{C=C} = 1.335$ Å, lead to $l_r + l_p = (l_{C-H} + l_{C-C})/2 + (l_{C-H} + l_{C=C})/2 = 2.523$ Å.

Now we can estimate the energy barrier due to the stretching of the chemical bonds, through eqs (1)-(4), for free energies rather than internal energies. The square dependence of η on $(\Delta G^{\circ})^2$ can be neglected because λ is expected to be high ($\lambda >> |\Delta G^{\circ}|$) for molecules with many degrees of freedom, particularly if the activation entropy is positive, as it is the case for the reactions under study (3). With $n^{\dagger} = 1/2$ the estimated energy barrier for stretching is ΔG_{792} (st) = 164 kJ mol^{-1}.

The bending force constants are $f_{CCC} = 0.146$ kJ mol^{-1} deg^{-2} and $f_{CCH} = 0.10$ kJ mol^{-1} deg^{-2} [13]. We can thus estimate the following energy contributions for the bending motions, $\Delta G^{\ddagger}_b$(CCC) = 66 kJ mol^{-1} and $\Delta G^{\ddagger}_b$(CCH) = 20 kJ mol^{-1}. The estimated overall free energy barrier is the sum of all these energy contributions, e., $\Delta G^{\ddagger}_{792} = 250$ kJ mol^{-1} The calculated value is good agreement with the experimental data (242 kJ mol^{-1} [10]). The present calculation reveals also that the main contributions for the energy barrier can be attributed to the stretching of the chemical bonds (65 %).

Other motions could have been considered for the reaction coordinate, such as the in-phase motion of the two oscillators, in reactant and product. However for this case the effective force constant is $f = f_1 + f_2$ and the estimated energy barrier is much higher than the experimental value.

ISOMERIZATION OF METHYL ISOCYANIDE

The thermal unimolecular isomerization of methyl isocyanide CH_3CN, has been investigated by Schneider and Rabinovitch [14]. The activation free energy is $\Delta G^{\ddagger}_{533} = 155$ kJ mol^{-1} at pressures > 5 Torr and temperatures between 200°C and 260°C and $\Delta G^{\circ}_{533} = -68$ kJ mol^{-1} [11].

Two possible situations can be envisaged for the transition state. The first one considers

the only reactive bonds to be C-N in the reactant and a C-C bond in the product because the C≡N bond is unaffected by the reaction. With $f_{C-N} = 2.95 \times 10^3$ kJ mol^{-1} Å^{-2} $f_{C-C} = 2.7 \times 10^3$ kJ mol^{-1} Å^{-2} $l_{C-N} = 1.47$ Å, $l_{C-C} = 1.537$ Å [13] and $n^\dagger = 1/2$, the activation energy barrier for stretching is calculated to be $\Delta G^\ddagger_{533}$ (st) = 117 kJ mol^{-1}.

The second situation considers also the involvement of the C≡N bond in the bond-breaking bond-forming processes in the reactant and the product. The effective force constant is $f_r \cong f_p = 1.1 \times 10^4$ kJ mol^{-1} Å^{-2} because $f_{C\equiv N} = 1.07 \times 10^4$ kJ mol^{-1} Å^{-2} [13]. The average bond order in reactant and product is n = 2, and consequently, if the total bond order is conserved along the reaction coordinate, then $n^\dagger = 1$. With these parameters and $l = (l_{C-N} + l_{C-C} + 2\ l_{C\equiv N})/4$ ($l_{C\equiv N}$ = = 1.157 Å [13]) eqs (1) to (4) lead to $\Delta G^\ddagger_{533}$(st) = 82 kJ mol^{-1} This value is considerably lower than in the previous case, because the transition state bond order is now considerably higher; the effect of an higher force constant on $\Delta G^\dagger$ is compensated by the effect of a shorter bond length.

Assuming a triangular transition state, the change in bond angle CNC is very large (ca. 110°) and consequently the harmonic behaviour is no longer valid. The energy barrier owing to the bending motion can be approximately estimated from the «strain energy» of cyclopropane 105 kJ mol^{-1} [15]. The bending energy in the transition state can be attributed to the strain of only two bonds; the C≡N is assumed to cause no strain. Then the estimated energy barrier is ca. 70 kJ mol^{-1}. With the calculated energy barriers for stretching and bending, the energy barrier is estimated to be $\Delta G^\ddagger_{533} = 152$ kJ mol^{-1} again close to the experimental value.

It is worth an emphasis on the role played by the C≡N bond in the transition state. Transition state bond orders higher than 0.5 have been found with molecular species with apparently nonreactive nonbonding and antibonding electrons [2, 3]. Here we have an example where bonding electrons can act in a similar way by syphoning electronic density into the transition state. This seems to be one of the main reasons (accounts for 35 kJ mol^{-1}) why the isomerization of methylisocyanide has an energy barrier 87 kJ mol^{-1} lower than that in the cyclopropane isomerization. The others are associated with equilibrium bond lengths and force constants which are smaller for the former reaction (account for 30 kJ mol^{-1}). The difference in ΔG° accounts only for a difference of 5 kJ mol^{-1} in the energy barriers.

DISSOCIATION OF CYCLOBUTANE

The dissociation of cyclobutane into two ethylene molecules has been studied experimentally by Walters and coworkers [16]. In the high pressure region the activation free energy of this unimolecular reaction is $\Delta G^\dagger = 228$ kJ mol^{-1} and $\Delta G^\circ = 7.0$ kJ mol^{-1} at 713 K. A correction was applied in ΔS° for the change in the standard state from 1 atm to 1 mol dm^{-3}.

Several possible reaction coordinates can be considered. One is that the four C-C bonds of reactant and two C = C bonds of products act as independent oscillators. With $l = l_{C-C} + l_{C=C}$ and $n^\dagger = 1/2$ this leads to a very high energy barrier ($\Delta G^\ddagger = 310$ kJ mol^{-1}). The alternative coordinate that we can define, a cyclic transition state with a common C-C stretch leads to a very low barrier (123 kJ mol^{-1}). However this is not surprising because the simultaneous stretch of four bonds in cyclobutane does not lead to the formation of two ethylene molecules. This requires the contraction of two CC bonds and the distension of the other two. A possible effective force constant is the one of a cyclic ring, common to reactant and product where there is the composition of these two kinds of motions; $f = \sqrt{2}\ f_{C-C}$ and with $l = 2\ l_{C-C'}$ an energy barrier $\Delta G^\ddagger_{713} \cong 248$ kJ mol^{-1} is estimated for harmonic oscillators. When one compares the energy barrier for the stretching motions of the dissociation of cyclobutane and the isomerization of cyclopropane, conc-

ludes that the higher energy barrier of the former process can be attributed to an higher ΔG° and l.

CONCLUSIONS

We have shown that within reasonable assumptions ISM can provide estimations of energy barriers for simple unimolecular reactions in fair agreement with experiment. In spite of the distorted picture that the model may provide, it has revealed some interesting mechanistic insights such as the role of $C \equiv N$ bond order on decreasing the energy barrier of the isomerization of methyl isocyanide and the role of equilibrium bond lengths and stretching force constants in controlling reaction energy barriers.

Recebido 28.Junho.1986

ACKNOWLEDGMENTS

We are grateful to Instituto Nacional de Investigação Científica for financial support.

REFERENCES

[1] C. TRINDLE. *Croat. Chem. Acta*, **57**, 1231 (1984).
[2] A.J.C. VARANDAS, S.J. FORMOSINHO, *J. Chem. Soc., Chem. Commun*, 163 (1986); *J. Chem. Soc., Faraday Trans.* 2, **82**, 953 (1986).
[3] S.J. FORMOSINHO, *Rev. Port. Quím.*, **27**, 427 (1985).
[4] S.W. BENSON, *Specialist Report Reaction Kinetics*, **1**, 1 (1975).
[5] K.J. LAIDLER, *Theories of Chemical Reaction Rates*, McGraw Hill, New York, 1969.
[6] N. AGMON, R.D. LEVINE, *Chem. Phys. Lett.*, **52**, 197 (1977).
[7] H.S. JOHNSTON, C. PARR, *J. Am. Chem. Soc.*, **85**, 2544 (1963).
[8] S.J. FORMOSINHO, *Tetrahedron*, **42**, 4557 (1986).
[9] H.D. BURROWS, S.J. FORMOSINHO, *J. Chem. Soc. Faraday Trans.* 2, **82**, 1563 (1986).
[10] T.S. CHAMBERS, G.B. KISTIAKOWSKY, *J. Am. Chem. Soc.*, **56**, 399 (1934); B.S. RABINOVITCH, E.W. SCHLAG, K.B. WIBERG, *J. Chem. Phys.*, **28**, 504 (1958).
[11] Data collected in S.W. BENSON, F.R. CRUICKSHANK, D.M. GOLDEN, G.R. HAUGEN, H.E. O'NEAL, A.S. RODGERS, R. SHAW, R. WALSH, *Chem. Rev.*, **69**, 279 (1969).
[12] S.J. FORMOSINHO, *Mol. Photochem.*, **7**, 41 (1976).
[13] A.J. GORDON, R.A. FORD, «The Chemist's Companion», John Wiley, New York, 1972, p. 107 and 114.
[14] F.W. SCHNEIDER, B.S. RABINOVITCH, *J. Phys. Chem.*, **84**, 4215 (1962).
[15] W. WELTNER, *J. Am. Chem. Soc.*, **75**, 4224 (1953).
[16] C.T. GENAUX, F. KERN, W.D. WALTERS, *J. Am. Chem. Soc.*, **75**, 6196 (1953); R.W. CARR, W.D. WALTERS, *J. Phys. Chem.*, **67**, 1370 (1963).

RESUMO

Um modelo teórico simples para a barreira de energia de reacções unimoleculares

Aplica-se um modelo de intersecção de estados para o cálculo de barreiras de energia em termos de parâmetros termodinâmicos, geométricos e de ordem de ligação, ao cálculo de $\Delta G^{\ddagger}$ na isomerização do ciclopropano, isocianeto de metilo e na dissociação do ciclobutano. Utilizando parâmetros estruturais razoáveis obtém-se acordo com os dados experimentais. O estudo revela alguns aspectos mecanísticos relevantes, tais como o do papel de ordens de ligação no estado de transição que explica em grande medida a diferença nas barreiras de energia das duas reacções de isomerização.

SEBASTIÃO J. FORMOSINHO
Departamento de Química, Universidade de Coimbra, 3049 Coimbra Codex, Portugal

THE ROLE OF BOND ORDER AND ENTROPY OF TRANSITION STATES IN ELECTRON TRANSFER REACTIONS

Part 1. — Outer-sphere electron exchange processes.

The current approach of Marcus theory to estimate energy barriers of electron transfer reactions in terms of a least nuclear motion path is questioned. Another approach, based on an expansion of configuration in the transition states is presented. An intersecting-state model is employed to estimate metal-ligand bond distentions at the transition state in terms of bond lengths and force constants, and the transition state bond order. This model can successfully treat electron exchanges, including the case of systems such as $Co^{2+/3+}_{(aq)}$ *and* $Fe(phen)^{2+/3+}_{3}$ *where the Marcus theory estimates rates* 10^7 *times slower and* 10^5 *times faster, respectively, than experiment.*

INTRODUCTION

The history of science reveals that many times the structure of sciences does not possess a powerful logic. Henri Poincaré in his book «La Science et l'Hypothèse» [1] gives an interesting example from the field of classical mechanics. In the absence of any force the velocity of a body does not change; but of equal logic are other conceptions such as that the acceleration or the position of the body do not change. The choice between these different assumptions is not a matter of logic, but of agreement with experimental observations.

In any particular scientific field it is virtually impossible to fit a new theory to all the relevant experimental facts. The facts which are not accounted for by the theory are «enigmas». These can many times be later explained through refinements of the theory, but if they survive as enigmas for a long time and if the disagreement with the theory is of a large magnitude, they become «anomalies». It is the existance of anomalies that reveals the presence of a «crisis» in any scientific field [2], and a crisis requires new theoretical approaches, which should be able to solve the anomalous facts of the old theory.

The theory of Marcus has been the «paradigm» of the field of electron transfer reactions but, in our view, symptoms of a crisis are becoming apparent. For electron exchange reactions there are examples «of an old system, $Co^{2+/3+}$ or $Fe^{2+/3+}$ where, despite the current extensive understanding of electrons transfers, there remains something to be understood» [3]. The aquo $Co^{2+/3+}$ and $Fe^{2+/3+}$ pairs have an anomalous behaviour, because the measured self-exchange rates are about 10^7 and 10^3, respectively, faster than those calculated through the theory of Marcus.

Marcus [4] has predicted nearly three decades ago that an inverted effect on the reaction rates should occur for very exothermic electron transfer reactions. In spite of several

experimental searches, with a few exceptions, the experiments do not conform to this model and other alternative models have been proposed [5-7] to interpret the variety of the energy-gap laws of these reactions. The disagreement between theory and experiment can amount also to several orders of magnitude.

The theory of Marcus predicts also that the rate constants of electron transfer reactions can be obtained from the individual self-exchange reaction rates and the equilibrium constant of the reaction, through the so called «cross-reaction relationship». This simple relation has been perhaps the most widely used and tested in electron transfer theory, but in spite of its sucess there are cases where disagreements of five orders of magnitude do exist [8].

Hupp and Weaver (9) have recently reported the existance of strong anodic-cathodic asymmetries on the Tafel plots for metal-aquo redox couples which cannot be interpreted within the framework of the theory of Marcus. Such effects amount typically to two orders of magnitude in the relative rates for the cathodic and anodic reactions under the extreme experimental conditions employed.

Finally the theory of Marcus gives a special importance to the outer-shell reorganization energy barriers for electron transfer reactions. Recent results for the ferrocenium — ferrocene self-exchange [10] reveal that the rates of electron transfer in a variety solvents, from methanol to dimethylsulfoxide, vary by a factor of 2 whereas the theory of Marcus predicts a ca. 20-fold variation.

In view of these anomalous features, it seems worth exploring alternative theoretical procedures to estimate rates of electron transfer reactions. In this paper we will apply a recently developed intersecting-state model [11] to the study of electron exchange processes and in the following papers of this series the other types of «anomalies» will be considered.

THE EXPANSION OF CONFIGURATIONS IN THE TRANSITION STATE

Transition state bond lengths in electron transfer reactions of coordinated or solvated ions are considered to be intermediate between the metal-ligand bond lengths of the oxidized and reduced species [3, 12, 13], i.e., one ion has contracted and the other has expanded in order to reach the configuration of the transition state. This follows a suggestion of Libby [14] that the more similar the inner coordination shells of donor and acceptor ions, the less difficult would be the electron transfer. Support for such an idea was suggested from, for example, the slowness of the $Co(NH_3)_6^{2+/3+}$ exchange reaction, because there is a large difference in the the Co-N bond lengths ($l_{red} - l_{ox} \simeq 0.21$ Å). Although rates $\leqslant 2 \times 10^{-10}$ mol^{-1} dm^3 s^{-1} were initially estimated [15], a recent redetermination of this self-exchange rate ($4\text{-}8 \times 10^{-6}$ mol^{-1} dm^3 s^{-1}) is at least four orders of magnitude greater [16].

Currently the transition state configuration is determined by finding the lowest potential energy for a system of two bond length coordinates: $Me^{n+} - L$ and $Me^{(n+1)+} - L$. The bond lengths are $l_{ox} < l^{\dagger} < l_{red}$ and the contribution of the inner-shell reorganization for the reaction energy barrier is estimated to be

$$\Delta G_{in}^{\dagger} = \frac{m\ f_{ox}\ f_{red}}{2\ (f_{ox} + f_{red})} (l_{ox} - l_{red})^2 \qquad (1)$$

where m is the number of bonds involved in the reorganization process and f_{ox} and f_{red} are the stretching force constants of the metal-ligand bonds. The bulk solvent reorganization energy barrier [1, 3] is given by

$$\Delta G_{out}^{\dagger} = \frac{(\Delta e)^2}{4} \left(\frac{1}{2a_{ox}} + \frac{1}{2a_{red}} - \frac{1}{r}\right) \left(\frac{1}{D_{op}} - \frac{1}{D_r}\right) \qquad (2)$$

where a_{ox} and a_{red} are the radii of the solvated spherical ions: the ionic radium plus

the van der Waals diameter (2.76 Å) of a water molecule [12]; r is the mean distance between the centers of the reactants in the activated complexes, Δe is the charge transferred in the reaction, D_{op} and D_s are the optical and static dielectric constants of the medium respectively. For one electron transfer in water

$$\Delta G^{\dagger}_{out}/kJ\ mol^{-1} = 188\ (\frac{1}{a} - \frac{1}{r}) \qquad (3)$$

with $a = 2a_{ox}\ a_{red}/(a_{ox} + a_{red})$.

Let us considered a spherical metal ion of charge *n* surrounded, for example, by water molecules in the first and the second coordination shell. When due to the transfer of an electron the charge of the ion changes rapidly to $n + 1$, there is a strong perturbation of the water molecules. Since the energy between an electronic charge and a dipole decreases in absolute value with the increase of the ion-dipole distance, this «instantaneous» perturbation will be stronger for the first-shell and weaker in the second-shell. However, when $l_{ox} = l_{red}$, the theory of Marcus (eq (1)) implies that electron transfer does not cause any energy change in the first-shell, but causes significant energy changes in the second-shell. This is not reasonable, not only in view of the previous argument, but also because the symmetric stretching force constants for the metal-ligand bonds are different in the oxidized and reduced species (vide e.g. the system $Fe(phen)_3^{2+/3+}$ [17, 18]). Any change in the force constants of the first coordination shell has to proceed via changes in the metal-ligand bonds and consequently has an internal energy barrier. The change in frequencies can be though to be included in the preexponential term of the rate constants, but for an electron transfer reaction between an oxidized and a reduced species such a term is an average of the frequencies of both partners.

Such facts suggest a different kind of model for the transition state configuration. If one assumes that there is an «expansion» in the transition state, i.e., $l_{ox} \leqslant l_{red} < l^{\dagger}$, even when $l_{ox} = l_{red}$, there will be an inner-shell reorganizational energy due to the expansion in configuration. A similar suggestion, with some experimental support, is provided by the study of the volumes of activation. Stranks [19] has discussed in detail the inner- and outer-shell contributions to $\Delta V^{\dagger}$ in oxidation-reduction reactions. The outer-shell contribution results from the changes in coulombic forces in bringing charged reactants to the transition state, the solvent rearrangement on the formation of the transition state and the change in activity due to interionic interactions. For For $Fe(H_20)_6^{2+/3+}$, Stranks has estimated $\Delta V^{\dagger}_{out} = -16.5\ cm^3\ mol^{-1}$. Assuming that the ions are spherical with radii of *a* (3.45 Å) ($a = r/2$) and that the transition state compressibility is identical to that of reactants, because the bond lengths are intermediate between the ones of the two reagents, then the change in the inner-shell volume, $\Delta V^{\dagger}_{in}$, ranges between 0 and $-58\ cm^3\ mol^{-1}$. Consequently, $\Delta V^{\dagger}$ ranges between $-16.5\ cm^3\ mol^{-1}$ and $-75\ cm^3\ mol^{-1}$.

The experimental change in the volume of activation, $\Delta V^{\dagger} = -12\ cm^3\ mol^{-1}$ [19], is higher than $\Delta V^{\dagger}_{out}$. This cannot be attributed to the finite compressibility of the solvated-ions, because such a contribution is very small ($\leq 0.5\ cm^3\ mol^{-1}$ [19]). Consequently, such findings may suggest that in the activated complexes there is some expansion of the metal-ligand bonds ($r > 2a$) rather than a small interpenetration of the shells ($r < 2a$). The difference between $\Delta V^{\dagger}$ and $\Delta V^{\dagger}_{out}$ may imply an increase in the metal-ligand bonds at the transition state. The overlap of the electronic wave functions for electron transfer reactions is very small, but can be increased by any spatial increase of those functions due to nuclear motions in the collision complexes. So the electronic coupling, H_{ab}, is expected to be higher for an «explosion» of configuration in the transitions states than for the activated complexes configuration of the theory of Marcus.

INTERSECTING-STATE MODEL

To investigate the logic consequences of an expanded transition state for electron transfer reactions, we will employ a recently developed intersecting-state model (ISM) [11] which estimates energy barriers of chemical reactions in terms of thermodynamic, geometric and electronic factors. The model estimates energy changes caused by an expansion in the bond length from a reactant to the transition state and, consequently, is adequate to estimate energy changes due to the expansion in the transition states of electron transfer processes. Nevertheless this point may be further clarified by the following discussion.

ISM has been developed for the study of bond-breaking bond-forming reactions such as $A + BC \rightarrow AB + C$. Figure 1 shows the

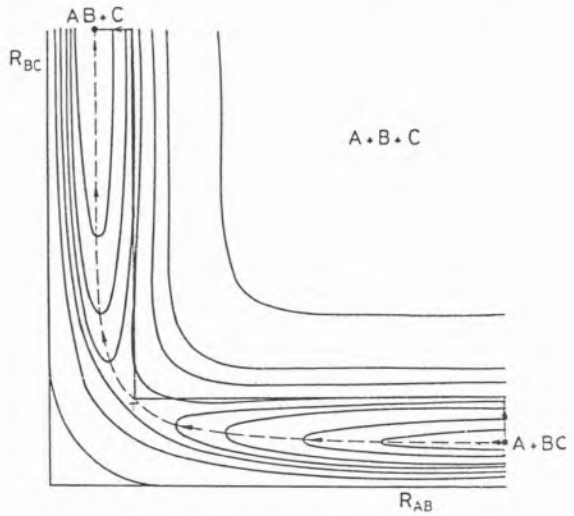

potential energy surface for such a reaction together with the reaction path. This can be simulated by the following nonmonotonous path:

i) BC stretch to $R^{\ddagger}_{BC}$ at a constante R_{AB} (large distance (∞));
ii) a virtually isoenergetic path through the saddle point; R_{AB} decreases from almost infinity to the value $R^{\ddagger}_{AB}$ at a constant $R^{\ddagger}_{BC}$, etc.;
iii) $R^{\ddagger}_{AB}$ decreases to the equilibrium value R^{e}_{AB} at a constant R_{BC} (∞).

This path justifies the estimation of the reaction energy barrier through the intersection of BC and AB potencial energy curves, when $R^{\ddagger}_{AB} > R^{e}_{AB}$ and $R^{\ddagger}_{BC} > R^{e}_{BC}$ (a contraction of the bonds was also possible). However if, for example $R^{\ddagger}_{BC} < R^{e}_{BC}$ and $R^{\ddagger}_{AB} > R^{e}_{AB}$ the energy barrier cannot be estimated through the intersection of two potential energy curves, because the intermediate path through the transition state configuration is no longer an isoenergetic path.

If one considers now an electron transfer reaction such as

$$*Fe(H_2)_6^{2+} + Fe(H_2O)_6^{3+} \rightarrow *Fe(H_2O)_6^{3+} + Fe(H_2O)_6^{2+}$$

one can represent the expansion in the transition state for each one of the reactants on the potential energy surface of Figure 1. For example one should consider:

i) an expansion of $*Fe(II) - O$ equilibrium length up to $R^{\ddagger}_{Fe(II)-O}$;
ii) a jump from this configuration to $R^{\ddagger}_{Fe(II)-O}$, due to the transfer of the electron;
iii) a contraction of the $R^{\ddagger}_{Fe(II)-O}$ to the equilibrium length.

At an infinite distance, e.g., $F_{Fe(II)-O}$ is a virtual distance, because the species $Fe^{(II)}_{(aq)}$ only exists after electron transfer.

Although electron transfer and atom transfer are different kinds of processes, for an expanded transition state configuration, electron transfer can be considered a limiting case of the atom transfer situation when the isoenergetic nuclear path tends to zero. But since this path is not involved in the calculation of $\Delta E^{\ddagger}$, atom and electron transfer reactions or other kinds of no bond-breaking bond-forming processes such as spin exchange [20] can be analyzed through the same intersecting-state model.

A similar procedure will be applicable to the $Fe^{(III)}_{(aq)}$ species. In general one would average the potential energies for the two reactant and the two product species, after taking as

the origin of coordinates the equilibrium bond length of each one of the species involved, and only one reaction coordinate will be employed in the calculations. It might be argued that one should use two reaction coordinates. This is essential in the theory of Marcus, because one of the coordinates is expanded whereas the other is contracted. However, for the present model both coordinates are in expansion and one can use a reaction coordinate where the bond distensions of the two reactants is the same. So a single coordinate will do. In consequence, if f_{ox} and f_{red} are the stretching force constants of the metal-ligand bonds, this assumption leads to an average force constant for the single coordinate $f_{av} = (f_{ox} + f_{red})/2$.

ISM has been presented in detail elsewhere [11] but will be briefly reviewed here. Let us assume, for simplicity, that the potential free energy curve for a reactant and product can be represented by harmonic oscillators of force constants f_r and f_p and equilibrium bond lengths l_r and l_p. The configuration of the transition state can be found at the intersection of the potential energy curves of the reactant and product. Then one can write

$$\frac{1}{2} f_r x^2 = \frac{1}{2} f_p (d - x)^2 + \Delta G^o \qquad (4)$$

where ΔG^o is the reaction free energy, x is the bond distension from the reactant to the transition state, $x = l^\dagger - l_r$, and d ($d > 0$) is the sum of the bond distensions from the reactant and the product species to the transition state,

$$d = (l^\dagger - l_r) + (l^\dagger - l_p) \qquad (5)$$

and represents also the horizontal displacement of the potential energy curves. The activation free energy of the reaction is given by

$$\Delta G^\dagger = \frac{1}{2} f_r x^2 \qquad (6)$$

where x is estimated through eq (4), once d is known.

The sum of bond distensions up to the transition state [11] was shown to be related to the sum of the equilibrium bond lengths of reactants and products

$$d = \eta (l_r + l_p) \qquad (7)$$

where η measures the relative increase in the bond lengths. This equation has a simple physical meaning: when an equilibrium bond length is small its bond distension is expected to be small, but when it is large the bond distension is also expected to be large.

The reduced bond distension η is related [11] to the chemical bond order of the transition state, $n^\dagger$, and a parameter λ which is associated with the so called «configuration entropy»,

$$\eta = \frac{a' \ln 2}{n^\dagger} + \frac{a'}{2\lambda^2} (\Delta G^o)^2 \qquad (8)$$

λ has dimensions of an energy and can be viewed as an energy capacity of the activated complexes; a′ is a constant ($a' = 0.156$). Eq (8) shows that the reduced bond distension depends on $n^\dagger$ and ΔG^o. It is small when the bond order of the transition state is high, and *vice versa*. For a thermoneutral reaction η and d are independent of λ.

When $f_r = f_p = f$ then eqs (4) and (6) lead to

$$\Delta G^\dagger = \frac{(\Delta G^o + (1/2) f d^2)^2}{2 f d^2} \qquad (9)$$

Furthermore when d is independent of ΔG^o, i.e. $\lambda >> |\Delta G^o|$, eq (9) reduces to the Marcus-equation

$$\Delta G^\dagger = \Delta G(0)^\dagger \left(1 + \frac{\Delta G^o}{4 \Delta G(0)^\dagger}\right)^2 \qquad (10)$$

where $\Delta G(0)^\dagger$ is the kinetic energy barrier for the thermoneutral situation, which is

$$\Delta G(0)^\dagger = \frac{1}{8} f \left[\frac{a' \ln 2}{n^\dagger} (l_r + l_p)\right]^2 \qquad (11)$$

On neglecting the work terms of bringing the reactants together, the Marcus-equation is found to be a particular case of ISM. Eq (11)

reveals also that the intrinsic energy barrier for electron exchange reactions is controlled by the metal-ligand force constants and bond lengths, and by the transition state bond order.

ELECTRON EXCHANGE REACTIONS

Coordinated or solvated metal ions have several metal-ligand bonds which are involved in the inner-shell reorganization. In order to keep the model unidimensional, one has to define an effective force constant f for the coordination shell. Let us consider, to start with, two bonds of force constants f_1 and f_2. In general terms the effective force constant is given by

$$f_{eff}^2 = f_1^2 + f_2^2 + 2f_1 f_2 \cos\Theta$$

If the vibrations of the two bonds are in-phase, $\Theta = O^o$ and $f_{eff} = f_1 + f_2$. When the motions have a destructive interference $\Theta^o = 180^o$ and $f_{eff} = |f_1 - f_2|$. For a random motion of the two bonds $\Theta^o = 90^o$ and $f_{eff} = \sqrt{f_1^2 + f_2^2}$. These considerations can be generalized to any number of oscillators.

For a metal-ion with a coordination number of m, then the possible effective force constants are

$$f = m(f_{ox} + f_{red})/2 \qquad (12)$$

as considered in the theory of Marcus, and

$$f = \sqrt{m}(f_{ox} + f_{red})/2 \qquad (13)$$

which we have found appropriate to deal with several chemical reactions [21]. In the calculations we have employed the force constants estimated by Khan and Bockris [22] from metal-ligand symmetric stretching frequencies ν_i; $f_i = 4\pi^2 c^2 \mu \nu_i^2$ where c is the velocity of the light and μ the reduced mass of the vibrating ligand.

Since we are dealing with metal-ligand single bonds and during the electron transfer process there are no chemical bond-breaking process, we take $n^\dagger = 1$ for all cases except where stated otherwise.

Table 1 presents the necessary spectroscopic data for the calculation of the $Fe(H_2O)_6^{2+/3+}$ inner-shell energy barrier [17, 22, 23]. The calculation based on eq (11) and for the random situation (eq (13)) is in good agreement with the experimental value: $\Delta G^\dagger$ (exp) = 72.5 kJ mol^{-1} and $\Delta G^\dagger$ (calc) = 74 kJ mol^{-1}. For the in-phase situation (eq (12)) the calculated energy barrier is too high, 181 kJ mol^{-1}.

The calculated values are only the inner-shell contribution to the energy barrier. The outer-shell contribution can be estimated from the reorganization in the second-shell due to the expansion of the first-shell, where $E = -nZe\mu'/r^2$ is the energy of a metal ion charge Ze surrounded of n dipoles of dipole moment μ' at a metal distance r. When this distance is estimated for a spherical solvated ion, i.e., under the hypothesis that all the bonds had the same distension y ($(6/2)f\,y^2 = (\sqrt{6}/2)f_i\,x^2$) then the outer-shell reorganization energy ($\lesssim 2$ kJ mol^{-1}) is more than an order of magnitude lower than the inner-shell energy barrier. This finding is also in agreement with the negligible (a factor of 2) variation of the rates of ferrocenium-ferrocene self-exchange from methanol to dimethylsulphoxide [10]; these findings also lead to $\Delta G_{out}^\dagger = 1.8$ kJ mol^{-1} in water. In view of these facts we can take the inner-shell reorganization as a good estimation of the reaction energy barrier. Under this assumption ISM estimates the rate constant for $Fe_{(aq)}^{2+/3+}$ within a factor of 2 times slower than the experimental rate, but not 10^3 times as it is the case with the theory of Marcus [3].

Table 1 presents also the $\Delta G^\dagger$ values for several other electron exchange reactions. The agreement with experiment is quite good.

An in-phase motion of all the bonds (eq (12)) is implied by the theory of Marcus [12] and such a force constant leads to an overestimation of the free energy barrier, which is in general balanced by the underestimation of the bond distensions at the transition state,

Table 1

Inner-Shell Reorganization Energy Barrier for Electron Exchange Reactions.

Reaction	l_{Me-X}/Å Me(II)	l_{Me-X}/Å Me(III)	f_{Me-X}/kJ mol^{-1} Å^{-2} (*c*) Me(II)	f_{Me-X}/kJ mol^{-1} Å^{-2} (*c*) Me(III)	$n^{\dagger}$	$\Delta G^{\dagger}$/kJ mol^{-1} (*j*) Marcus tehory (*d*)	Intersecting state model (*e*) In-phase motion (*f*)	Intersecting state model (*e*) Random motion (*g*)	Experimental
$Fe(OH_2)_6^{2+/3+}$	2.123	1.955 (*a*)	9.6×10^2	1.5×10^3	1	20	181	74	72.5 (*a*)
$Cr(OH_2)_6^{2+/3+}$	2.30	1.98 (*a*)	9.6×10^2	1.5×10^3	1	73	203	80	82 (*h*)
$V(OH_2)_6^{2+/3+}$	~2.26	~2.12 (*b*)	9.6×10^2	1.5×10^3	1	—	206	84	84.2 (*i*)
$Co(OH_2)_6^{2+/3+}$ (*k*)	2.12	1.91 (*a*)	9.6×10^2	1.5×10^3	1	77.5	174	71	68.7 (*i*)
$Fe(CN)_6^{4-/3-}$	1.900	1.926 (*a*)	3.1×10^3	2.4×10^3	1.54	3	147	60	57.0 (*h*)
$Mo(CN)_8^{4-/3-}$ (*l*)	—	—	—	—	1.70	—	142	50	48.5

(*a*) Ref. 17; (*b*) Atomic radii + 1.38 Å; (*c*) Data for $Fe^{2+/3+}$ from ref. 22 and 23; other data assumed to be equal to the one of $Fe^{2+/3+}_{(aq)}$; (*d*) Eq. (1) (*e*) Eqs (11) and (7) and (8) with $\Delta G^{\circ} = 0$; (*f*) Eq. (12), $m = 6$; (*g*) Eq. (13), $m = 6$; (*h*) Ref. 24; (*i*) Ref. 25; (*j*) room temperature; (*k*) We have neglected the change from a high spin to a low spin state because it has a very low activation energy; (*l*) Average force constant $f = 6.8 \times 10^3$ kJ mol^{-1} Å^{-2} estimated from the comparison of $\nu = 473$ cm^{-1} for $Mo(CN)_8^{4-}$ and $Fe(CN)_6^{4-/3-}$ with $m = 8$, ref. 23 (b) p. 171, 172; $l_r + l_p = 3.83$ Å as for $Fe(CN)_6^{4-/3-}$; $\Delta G^{\dagger}$ ref. 24 p. 137 with a preexponential factor 10^{13} s^{-1}.

owing to the $l_{ox} < l^{\dagger} < l_{red}$ situation. This cancellation of errors explains the good estimations that the theory of Marcus provides for several electron exchange reactions [12, 13]. However, for $Co(H_2O)_6^{2+/3+}$ where the change in equilibrium bond lengths is large, Sutin [12] overestimates $\Delta G^{\dagger}_{in}$ (vide Table 1) and further considers a significant $\Delta G^{\dagger}_{out}$ contribution. It is not surprising, then, that the rate calculated through such a procedure is eight orders of magnitude slower than experiment. ISM provides an estimation in very good agreement with experiment (2.5 times slower).

Like the other examples presented here, the electron transfer reaction between $Fe(CN)_6^{4-}$ and $Fe(CN)_6^{3-}$ is an outer-sphere process, because the inner coordination spheres are inert to substitution [24-26]. However $\Delta G^{\dagger}$ is smaller than the free energy barrier of the other exchange reactions in Table 1, in spite of the fact that the force constants are higher. This behaviour can be attributed to differences in bond orders at the transition state as a result of interactions between π orbitals of the CN^- ligands and the metal orbitals, leading to a new set of π molecular orbitals. With electronic configurations (only for π bonds) such as $t_{2g}^6(\pi_b)\ t_{1u}^6(\pi_b)\ t_{2g}^6(\pi^*)$ for $Fe(CN)_6^{4-}$ and $t_{2g}^6(\pi_b)\ t_{1u}^6(\pi_b)\ t_{2g}^5(\pi^*)$ for $Fe(CN)_6^{3-}$, the average bond order can be estimated as 1.54. For example, with $Fe(CN)_6^{3-}$ which has 6 bonds in the reagent, the bond order contribution of the π electrons is $(12-5)/2 \times 6$; this contribution should be added to the contribution $n = 1$ from the σ bonds. Considering the bond order of the transition state as $n^{\dagger} = 1.54$, eq (8) shows that the reduced bond distension η is much smaller than when $n^{\dagger} = 1$. Consequently, $\Delta G^{\dagger}$ is also smaller. The calculated value for a random vibrational motion of the bonds is also in good agreement with experiment (Table 1). A similar situation is also found with $Mo(CN)_8^{4-/3-}$ where the estimated bond order is $n^{\dagger} = 1.70$ for d^4 and d^3 metal ion configurations.

The present model can reproduce the experimental $\Delta G^{\dagger}$ values which are not related to any systematic variations in $\Delta H^{\dagger}$ and $T\Delta S^{\dagger}$. For example, typical values [24, 25] for some of the reactions of Table 1 are:

	$\Delta H^{\dagger}$/kJ mol^{-1}	$-T\Delta S^{\dagger}$/kJ mol^{-1} (298K)	$\Delta G^{\dagger}$/kJ mol^{-1}
$V^{2+/3+}_{(aq)}$	53.0	31.0	84
$Fe^{2+/3+}_{(aq)}$	46.4	26.1	72.5
$Co^{2+/3+}_{(aq)}$	52.7	16.0	68.7
$Fe(CN)_6^{4-/3-}$	17.1	39.9	57

Such an agreement is obtained with a simple model of harmonic oscillators. This is not surprising, because the energy barriers are not very high and the crossing point of the curves is still on the region where the potential energy curves have a harmonic behaviour. Furthermore, the close agreement between theory and experiment shows that outer-shell reorganization does not have a significant contribution to the activation free energy barrier. It may have significant contributions for $\Delta H^{\dagger}$ and $T\Delta S^{\dagger}$, but such contributions appear to cancel out.

An interesting case to study is the system $Fe(phen)_3^{2+/3+}$; because $l_{ox} \cong l_{red}$ and, consequently, for the theory of Marcus $\Delta G^{\dagger}_{in} = 0$. This is not the case within the present model. The major difficulty in analysing such a system is the fact that the stretching force constants cannot be estimated from the stretching frequencies, since the effective mass of the oscillator Fe^{n+} — phenanthroline is not accurately known. Considering, however, that the stretching force constant is similar to the one of the ammine complexes, $f \cong 2.7 \times 10^3$ kJ mol^{-1} Å^{-2} [18, 20], with $l_{ox} + l_{red} = 3.94$ Å [17] and $n^{\dagger} = 1$, the energy barrier due to internal reorganization $\Delta G(ISM)^{\dagger} = 60$ kJ mol^{-1} is higher than the experimental value $\Delta G^{\dagger} = 45$ kJ mol^{-1} (1) (ref. 25 p. 475). Such a discrepancy can be attributed to the uncertainty in f and/or to some electronic siphoning from the aromatic rings into the iron-nitrogen bonds at the transition state, as is observed in spin exchange of N-Fe(II) and Fe(III) comlexes ($\eta = 0.098$) [20]. Under these assumptions the estimated energy barrier $\Delta G^{\dagger} = 50$ kJ mol^{-1} is much closer to the experimental value, and the calculated rate is an order of magnitude slower than experiment (10^5 mol^{-1} dm^3 s^{-1}). It is worth comparing such results with those of the theory of Marcus. For this system $\Delta G^{\dagger}_{in} = 0$ and $\Delta G^{\dagger}_{out} = 13$ kJ mol^{-1} with a = 7.5 Å and r = 15 Å. Such a value compares well with data for similar systems, e.g., $Co(bpy)_3^{2+/3+}$ where $\Delta G^{\dagger}_{out} = 13.8$ kJ mol^{-1} with a = 6.8 Å and r = 13.6 Å [12]. With these external and internal energy barriers, the electron exchange rate in $Fe(phen)_3^{2+/3+}$ is calculated to be diffusion controlled. So the theory of Marcus predicts a rate five orders of magnitude higher than experiment.

CONCLUSIONS

We have shown that the hypothesis of an expansion of configuration in the transition states of electron transfer reactions, provides reasonable estimates of the reaction energy barriers in terms of inner-shell reorganization. This does not necessarily mean that there are no contributions from the second-shell reorganization, buy they are certainly smaller than the ones from the first-shell, and both are so intimately connected that they can be dealt with in terms of an overall metal-ligand potential energy curve [27].

Discrepancies on the estimated rates within the Marcus formalism as, for example, $Co^{2+/3+}_{(aq)}$ which proceeds 10^6 - 10^8 times faster than the calculated rate [3, 12], are absent in

(1) The activation free energy is estimated for an adiabatic process

$$k_{et}/\text{mol}^{-1}\ \text{dm}^3\ \text{s}^{-1} = 10^{13} \exp(-\Delta G^{\dagger}/RT)$$

the present model. Previous suggestions [28] for a different pathway for this exchange reaction, are unnecessary to explain the experimental rates. In any case, suggestions of competitive mechanisms for the system $Fe(phen)_3^{2+/3+}$ where the Marcus rate is now 10^5 times faster than the experimental value are not possible.

The theory of Marcus employs essentially the Principle of Least Motion [29] to estimate the inner-shell reorganization for electron transfer reactions. For current chemical reactions it is known that the least-motion path is seldom the least-energy path [30]. It may well be the same for the electron transfer processes. On comparing with the rigorous theoretical treatment of the Marcus theory, the present approach may appear to be *ad hoc* and arbitrary. So we have a rigorous theory that does not account for all the experimental facts which, at present, are considered to be relevant in the field, and a semi-empirical approach which reproduces well the experimental facts. This is a dilemma. None the less ISM can rationalize experimental results and has some predictive value in the field of electron transfer reactions.

ACKNOWLEDGMENTS

I am grateful to Prof. R. A. Marcus for most stimulating and helpful discussions, where points of disagreement, naturally, arose. I am also grateful to Profs H. D. Burrows, S. M. B. Costa, A. J. C. Varandas, B. J. Herold and A. L. Maçanita for helpful discussions and suggestions and to Prof. H. Rau for making available to us some work prior to publication. This work is supported by the Instituto Nacional de Investigação Científica.

Recebido em 17 de Outubro de 1986

REFERENCES

[1] H. POINCARÉ, «La Science et l'Hypothèse», Flammarion, Paris, 1909, p. 112-119.

[2] T.S. KUHN, «The Structure of Scientific Revolutions», University of Chicago Press, Chicago, 2nd ed. 1970; Chaps. 5 to 7.

[3] R.A. MARCUS in «Understanding Molecular Properties» ed A.E. Hansen et al., Reidel, 1986, to be published.

[4] R.A. MARCUS, J. Chem. Phys., **24**, 966 (1956); Disc. Faraday Soc., **29**, 21 (1960); J. Chem. Phys., **43**, 679 (1965).

[5] D. REHM and A. WELLER, Ber. Bunsenges. Phys. Chem., **73**, 834 (1969).

[6] T. KAKITANI and N. MATAGA, Chem. Phys., **93**, 381 (1985); J. Phys. Chem., **90**, 993 (1986).

[7] H. RAU, R. FRANCK and G. GREINER, J. Phys. Chem., **90**, 2476 (1986); H. RAU, J. Am. Chem. Soc., submitted for publication.

[8] See for example C. CREUTZ an N. SUTIN, J. Am. Chem. Soc., **99**, 241 (1977).

[9] J.T. HUPP and M.J. WEAVER, J. Phys. Chem., **88**, 6128 (1984).

[10] T. GENNETT, D.F. MILNER and M.J. WEAVER, J. Phys. Chem., **89**, 2787 (1985).

[11] A.J.C. VARANDAS and S.J. FORMOSINHO, J. Chem. Commun., 163 (1986); J. Chem. Soc. Faraday Trans. 2, **82**, 953 (1986).

[12] N. SUTIN, Prog. Inorg. Chem., **30**, 441 (1983).

[13] For a recent review see R.A. MARCUS and N. SUTIN, Biochem. Biophys. Acta **811**, 265 (1985).

[14] W.F. LIBBY, J. Phys. Chem., **56**, 863 (1952).

[15] D.R. STRANKS, Discuss. Faraday Soc., **29**, 73 73 (1960); N.S. BIRADAR, D.R. STRANKS and M.S. VAIDYA, Trans. Faraday Soc., **58**, 2421 (1962).

[16] A. HAMMERSHØI, D. GASELOWITZ and H. TAUBE, Inorg. Chem., **23**, 979 (1984).

[17] B.S. BRUNSCHWIG, C. CREUTZ, D. H. MCCARTNEY, T.K. SHAM and N. SUTIN, Faraday Disc. Chem. Soc., **74**, 113 (1982).

[18] J.R. FERRARO, «Low Frequency Vibrations of Inorganic and Coordination Compounds», Wiley — Interscience, New York, 1970, chap 7.

[19] D.R. STRANKS, Pure Appl. Chem., **38**, 303 (1974).

[20] H.D. BURROWS and S. J. FORMOSINHO, J. Chem. Soc., Faraday Trans 2, **82**, 1563 (1986).

[21] S.J. FORMOSINHO, Mol. Protochem., **7**, 41 (1976); L.G. ARNAUT, S.J. FORMOSINHO and A.M. SILVA, J. Photochem., **27**, 185 (1984); S.J. FORMOSINHO, Pure Appl. Chem., **58**, 1173 (1986).

[22] S.U.M. KHAN and J.O'.M. BOCKRIS, J. Phys. Chem., **87**, 4012 (1983).

[23] (a) J. NAKAGAWA and T. SHIMANOUCHI, Spectrochim. Acta, **20**, 429 (1964).

(b) K. NAKAMOTO, «Infrared Spectra of Inorganic Coordination Compounds», Wiley, New York, 1970.

[24] W.L. REYNOLDS and R. W. LUMRY, «Mechanisms of Electron Transfer Reactions», Ronald Press, New York, 1966, chapter 3 and p. 34.

[25] F. BASOLO and R. G. PEARSON, «Mechanisms of Inorganic Reactions», Wiley, New York, 2nd ed, 1968, p. 71, p. 466.

[26] H. TAUBE, «Electron Transfer Reactions of Complex Ions in Solutions», Academic Press, New York, 1970, p. 49-70.

[27] E. SACHER and K.J. LAIDLER, Trans. Faraday Soc., **59**, 396 (1963).

[28] J.F. ENDICOTT, B. DURHAM and K. KUMAR, Inorg. Chem., **21**, 2437 (1982); D.H. MACARTNEY and N. SUTIN, Inorg. Chem., **24**, 3403 (1985).

[29] F.O. RICE and E. TELLER, J. Chem. Phys., **6**, 489 (1938); ibid., **7**, 199 (1939).

[30] L. SALEM, «Electrons in Chemical Reactions», John-Wiley, New York, 1982, p. 44-46.

RESUMO

O papel da ordem de ligação e da entropia dos estados de transição nas reacções de transferência de electrões.

Parte 1 — Processos de transferência de electrões de camada externa.

A utilização da teoria de Marcus no cálculo das barreiras de energia das reacções de transferência de electrões é examinada criticamente e, perante as dificuldades desta teoria em explicar algumas destas reacções, propõe-se um modelo teórico alternativo. Este modelo, baseado no Modelo de Intersecção de Estados, admite que no estado de transição as ligações reactivas metal-ligando sofrem uma expansão. As barreiras de energia dependem das constantes de força e comprimentos destas ligações e da ordem de ligação do estado de transição. O novo modelo consegue interpretar as reacções de troca de electrões em solução, nomeadamente $Co^{2+/3+}_{(aq)}$ *e* $Fe(fenantrolina)^{2+/3+}_{3}$*, em que a teoria de Marcus calculava constantes de velocidade* 10^7 *vezes inferior e* 10^5 *vezes superiores aos valores experimentais.*

SEBASTIÃO J. FORMOSINHO
Departamento de Química, Universidade de Coimbra, 3049 Coimbra Codex, Portugal

THE ROLE OF BOND ORDER AND ENTROPY OF TRANSITION STATES IN ELECTRON TRANSFER REACTIONS

Part 2. — Reaction Energy Effects on Outer-sphere and Inner-sphere Reactions.

A classical intersecting-state model, previously developed for gas phase reactions, has been applied to the study of electron transfer reactions. Activation energies depend on the lengths and force constants of metal-ligand bonds and on the bond orders and entropies of the transition states. Two kinds of transition states have been found, one with a bond order or $n^{\dagger} = 1$ *for outer-sphere reactions, and another with* $n^{\dagger} \cong 1.5$ *for inner-sphere and fast outer-sphere reactions. The distensions of the metal-ligand bonds in the transition state increase with an increase in the absolute value of the free energy of the reaction. Such a variation depends on the configuration entropy parameter* λ, *and is strong when* λ *is low. For solvated or coordinated metal-ions* λ *is low when* $\Delta S^{\dagger}$ *is low, with* λ *ranging typically between 350 to 100 kJ mol*$^{-1}$. *Such variation can interpret the occurrence of the different reaction energy laws which can be found in electron transfer reactions. The inverted region is found when* λ *is low, but when* λ *is high only a diffusional plateau is found at low* ΔG°. *Marcus-equation for the variation of* $\Delta G^{\dagger}$ *with* ΔG° *is a particular case of the present model when* $\lambda >> |\Delta G^{\circ}|$.

The effect of the reaction free energy, ΔG°, on the rates of electron transfers has been a field of great controversy. Normally, a decrease in ΔG° increases the rate of electron transfer. However, Marcus [1] has predicted that for very exothermic reactions an inverted region occurs, where the rates of reaction decrease with a further decrease in ΔG°. Although there is recent evidence that the predicted inverted effect can be observed [2-4] there are many well documented cases where the inverted region is not observed, and the rates of reaction attain a plateau for very low ΔG° values. For the latter situation, the Marcus-equation is no longer valid in the inverted region and other equations, such as that of Rehm and Weller [5], have to be employed. This has lead us to suggest [6] that such a discrepancy could be solved if one considers that the distance between the potential energy curves of reactants and products would increase with a decrease in ΔG°, following a similar suggestion of Koeppl and Kresge [7] for hydrogen atom transfer reactions. The physical basis for such a variable distance situation was later found through the development of an intersecting-state model (ISM) [8] to estimate energy barriers of chemical reactions, and a preliminar account on its application to the inverted region problem has been given [9]. Rau and coworkers [10] have also developed a model under similar lines to interpret the energy gap laws in electron transfer reactions, while Kakitani and Mataga [11] have also developed a model based on the motion of the molecules in the solvent shell, to interpret the variety of such laws.

In Part 1 of this series [12] we have suggested that electron transfer reactions can be treated as any other ordinary chemical reaction, and have shown that such a hypothesis leads to calculated self-exchange reaction rates in good agreement with experiment, even for cases where a strong disagreement exists between experiment and values given by the theory of Marcus. Here we intend to further

explore this hypothesis to investigate the effect of ΔG^{o} on the rates of outer- and inner-sphere electron transfer reactions.

ENERGY-GAP LAWS

In the previous paper [12] we have shown that Marcus-equation can be considered as a particular case of the general intersecting-state model [8] which was employed for the estimation of the reaction energy barriers. Marcus-equation is valid when the effective force constants in reactants and products are identical and when the sum of the distensions, d, and the reduced bond distension, η, are independent of ΔG^{o}. The former condition is justified for the systems which will be studied, but the latter one needs investigation. The general expression [8] for η is

$$\eta = \frac{a' \ln 2}{n^{\dagger}} + \frac{a'}{2\lambda^{2}} (\Delta G^{o})^{2} \qquad (1)$$

where $n^{\dagger}$ is the bond order of the transition state and λ is the configuration entropy parameter established by Agmon and Levine [13], which has dimensions of an energy. For a thermoneuaral reaction η is independent of λ. However, for exothermic or endothermic reactions, the reaction energy ΔG^{o} has to be accommodated as internal energy of the activated complexes, through distension of the bonds involved in the reaction and/or in many other degrees of freedom not involved in the reaction coordinate. The parameter λ can be viewed as the activated complex capacity (in terms of free energy) to accommodate the reaction free energy. If λ is high, the activated complexes have many ways to distribute energy and, consequently, only a small fraction of ΔG^{o} is stored as distension of the reactive bonds. However, when λ is low a considerable amount of the reaction energy has to be stored in the reactive bonds, through further bond distension. Consequently, η and d increase with an increase in $|\Delta G^{o}|$ and the effect of exothermicity in the reaction rates is less pronounced than when λ is high. Marcus-equation corresponds to the cases where $\lambda >> |\Delta G^{o}|$ for which the inverted region occurs at $\Delta G^{o} < -fd^{2}/2$.

To illustrate how the effect of ΔG^{o} on the electron transfer rates, k_{et}, depends on the value of λ, Figure 1 presents the calculated

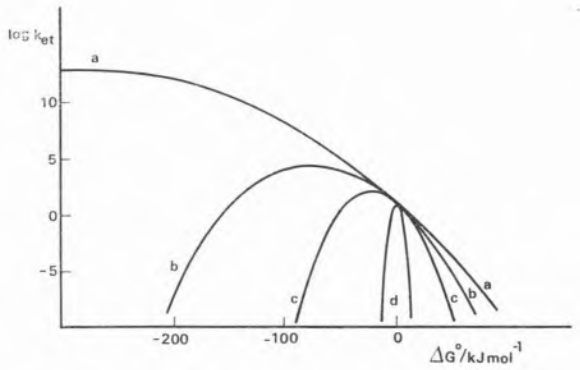

Fig. 1 — Calculated electron transfer rate constants (eq (2)) as a function of ΔG^{o}, for several configuration entropy parameter, λ, values: a) $\lambda \rightarrow \infty$ corresponds to the Marcus-equation; b) $\lambda = 200$ kJ mol^{-1}; c) $\lambda = 100$ kJ mol^{-1}; d) $\lambda = 10$ kJ mol^{-1}. Data employed in the calculation: $l_{ox} + l_{red} = 4$ Å, $f = 2.9 \times 10^{3}$ kJ mol^{-1} Å^{-2} and $n^{\dagger} = 1$.

rates for a prototype situation with k_{et}/mol^{-1} dm^{3} s$^{-1} = 10^{13} \exp(-\Delta G^{\dagger}/RT)$ and

$$\Delta G^{\dagger} = \frac{(\Delta G^{o} + (1/2)\, fd^{2})^{2}}{2fd^{2}} \qquad (2)$$

The parameter d is proportional to the sum of equilibrium bond lengths of the oxidized and reduced species,

$$d = \eta\, (l_{ox} + l_{red}) \qquad (3)$$

The calculations were undertaken with $l_{ox} + l_{red} = 4$ Å, $f = 2.9 \times 10^{3}$ kJ mol^{-1} Å^{-2} and $n^{\dagger} = 1$. Several curves of log k_{et} versus ΔG^{o} are presented for different values of λ and for the Marcus case ($\lambda = \infty$). All the curves share a common point at $\Delta G^{o} = 0$, but in the other regions when λ decreases, the

electron transfer rates decrease, both in the normal and in the inverted region. The electron transfer rate is extremely sensitive to λ when $|\Delta G^o| > \lambda/2$, is moderately sensitive when $\lambda/4 \leq |\Delta G^o| \leq \lambda/2$ and is virtually independent of λ when $|\Delta G^o| < \lambda/4$ (Figure 2).

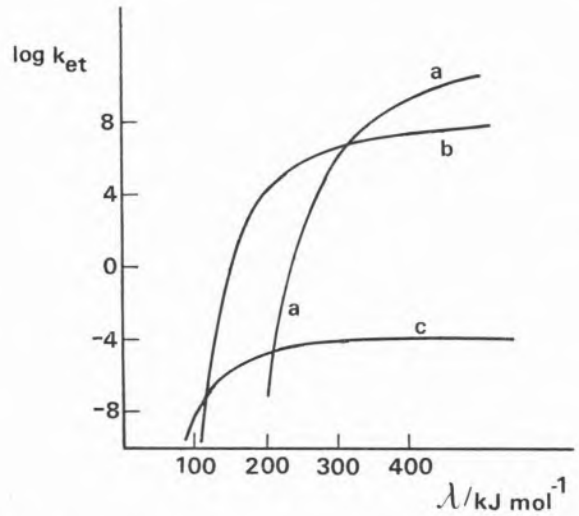

Fig. 2 — Calculated electron transfer rates as a function of λ, for several ΔG^o values: a) -200 kJ mol^{-1}; b) -100 kJ mol^{-1}; c) 50 kJ mol^{-1}.

Far from the $\lambda >> |\Delta G^o|$ limit, the maximum rate does not correspond to the crossing of the potential energy curves at the minumum of the reactant curve where $\Delta G^\dagger = 0$. As Figure 1 shows the position of the inverted region varies with λ (with f, l and $n^\dagger$ constant) ranging between $\Delta G^o = -(1/2)\,fd^2$ $(\lambda \to \infty)$ and $\Delta G^o = 0$ $(\lambda \to 0)$; the maximum rate constant decreases with a decrease in λ.

OUTER-SPHERE REACTIONS

Having examined the energy gap law in a more formal way, it is now useful to investigate the effect of ΔG^o in some real systems. To undergo this task it is more convenient to estimate the distensions (d and η) which reproduce the experimental $\Delta G^\dagger$, rather than to compare activation free energies. For many reactions the $\Delta G^\dagger$ values are not known and have to be estimated from the rate constants of electron transfer (1)

$$k_{et} = \kappa \nu c_0^{1-m'} \exp(-\Delta G^\dagger/RT) \qquad (4)$$

where κ is an electronic factor which takes into account any nonadiabaticity of the reaction, c_0 is the standard concentration 1 mol dm^{-3}, m′ is the molecularity of the reaction, and ν is the frequency of vibration which destroys the activated complexes. We assume, following other authors [14, 15] that the interaction, H_{ab}, between the orbitals of the reactive species is small enough so that it may be neglected in calculating the free energy of activation, but large enough ($H_{ab} \geq 1$ kJ mol^{-1}) so that the reactions are adiabatic, i.e., $\kappa \simeq 1$. We take $\nu = 10^{13}$ s^{-1}. The stretching force constants are based on the set values presented by Khan and Bockris [16] calculated from experimental symmetric stretching frequencies, or were taken from ions of similar structure. The overall force constant is $f = \sqrt{6}\,(f_{ox} + f_{red})/2$ [12]. The length of the metal-ligand bonds [17] when not known, were estimated as the sum of the radius of the central ion and a covalent radius for the atom of the ligand which is linked to the metal ion [18]. Ionic radii were obtained from crystal data [19] and for the ligands we have used 1.38 Å for H_2O [18] and 1.4 Å for NH_3. Force constants were obtained from low frequency vibrational data [20, 21]. Table 1 presents the calculated reduced distension η for several exchange outer-sphere reactions. In spite of the uncertainties on the force constants and the bond length data, the η values are close to the theoretical value of 0.108 for $n^\dagger = 1$, obtained from eq (1)

(1) The observed rate constant is usually expressed as $k_{obs} = K_p\, k_{et}$, where K_p is the equilibrium constant for forming the precursor complex. Therefore $k_{obs} = \kappa \nu c_0^{1-m'} \exp(-\Delta G_p/RT) \exp(-\Delta G'^\dagger/RT)$ where $\Delta G'^\dagger$ is the activation free energy for electron transfer in the precursor complex. As long as the formation of the precursor complex does not alter the energy of the transition state, the activation free energy with respect to the reactants, $\Delta G^\dagger$, is simply $\Delta G^\dagger = \Delta G_p + \Delta G'^\dagger$ and consequently eq (4) is valid.

Table 1

Bond distensions for Electron Transfer Reactions of Aquo-Metal Ions

Reactants	f/kJ mol^{-1} Å^{-2}	$(l_r + l_p)$/Å	$\Delta G^{\ddagger}$/kJ mol^{-1}	d/Å	η
Fe^{2+}/Fe^{3+}	3.0×10^3	4.12	72.5 (*a*)	0.44	0.107
Cr^{2+}/Cr^{3+}	3.0×10^3	4.28	82.0 (*b*)	0.464	0.108
V^{2+}/V^{3+}	3.0×10^3	4.38	84.2 (*c*)	0.474	0.108
Mn^{2+}/Mn^{3+}	3.1×10^3	4.22	93.0 (*c*)	0.49	0.116
Ce^{3+}/Ce^{4+}	2.95×10^3	4.72	82.0 (*c*)	0.47	0.100

(*a*) Ref. 17.
(*b*) W.L. Reynold and R.W. Lumry, «Mechanisms of Electron Transfer Reactions», Ronald Press, New York, 1966, chap. 3 and p. 34.
(*c*) F. Basolo and R.G. Pearson, «Mechanisms of Inorganic Reactions», Wiley, 2nd ed., 1968, p. 466.

when $\Delta G^{\circ} = 0$. As discussed in the previous paper [12], this means that the free energy barrier for electron transfer is due largely to the inner-shell reorganization.

The present model also allows the evaluation of the effect of the reaction free energy, ΔG°, on the electron transfer process. Table 2 presents the bond distension parameters which reproduce the experimental $\Delta G^{\ddagger}$ values, calculated through eq (4); ΔG° values were estimated from redox potentials [19]. Now the reduced distensions are considerably higher than 0.108. According to eq (1) η should increase with an increase in $|\Delta G^{\circ}|$, and a

Table 2

Effect of Reactions Free Energy on the Bond distensions for Electron Transfer Reactions of Aquo-Ions and Ammino-Ions

		f/10^3 kJ mol^{-1} Å^{-2}	$(l_r + l_p)$/Å	$\Delta G^{\dagger}$/kJ mol^{-1} (*a*)	$\Delta S^{\dagger}$/J mol^{-1} K^{-1} (*a*)	ΔG°/kJ mol^{-1}	d/Å	η
1	Np^{4+}/NpO_2^{2+}	3.1	4.485	80.7		— 38.4	0.506	0.1128
2	$Cu^{+}/Fe(OH)^{2+}$	2.5	4.285	43.5		— 58.8	0.473	0.110
3	Ti^{3+}/Fe^{3+}	3.4	4.17	65.3		— 68.3	0.47	0.113
4	Cr^{2+}/Fe^{3+}	3.0	4.21	56.6	— 117	— 113	0.526	0.125
5	Fe^{2+}/Co^{3+}	3.1	4.165	57.7		— 103	0.515	0.1236
6	Eu^{2+}/Fe^{3+}	3.0	4.47	49.0		— 115	0.512	0.115
7	Cr^{2+}/Co^{3+}	3.0	4.195	49.4	— 32.6	— 214	0.596	0.142
8	Mn^{3+}/V^{4+}	3.5	4.175	61.3	— 50.2	— 216	0.585	0.140
9	Ce^{3+}/V^{4+}	3.5	4.422	77.7	+ 25.2	— 235.5	0.634	0.1434
10	V^{4+}/Co^{3+}	3.5	4.045	76.0		— 246	0.638	0.1577
11	$Fe^{2+}/Tl(OH)^{2+}$	3.0	4.94	83.0	— 29.3	— 81.4	0.562	0.114
12	Eu^{2+}/V^{3+}	3.0	4.59	85.0	— 125.4	— 16.8	0.499	0.1087
13	$Eu^{2+}/Co(NH_3)_6^{3+}$	3.2	4.46	89.0	— 175.6	— 51.0	0.533	0.120
14	$Cr^{2+}/Co(NH_3)_6^{3+}$	3.1	4.21	98.8	— 217	— 50.0	0.559	0.133

(*a*) Ref. 22, Chapter 13.

quadratic dependence of η on ΔG° is expected. Figure 3 presents the variation of η with

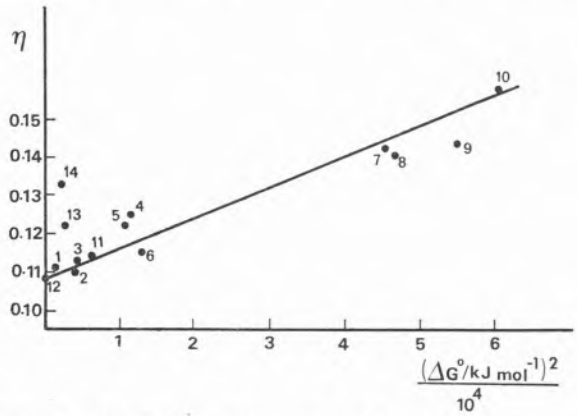

Fig. 3 — Variation of the reduced bond distension, η, with the reaction free energy, ΔG°, for electron transfer reactions of aquo- and hydroxoions. Legend for reactions in Table 2.

$(\Delta G^\circ)^2$. A linear dependence is suggested, although there is considerable scatter. However, such a dependence depends on the parameter λ. In order to test this prediction of the model we have estimated the λ values according to eq (1) and have searched for any possible relationship of λ with the entropic contribution to the activation energy ($-T\Delta S^\dagger$) for electron transfer reactions where the activation entropies are known [22]. Figure 4 reveals a linear relationship between λ and $T\Delta S^\dagger$; for 298 K and a standard state of 1 mol dm^{-3}, the observed relation is

$$\lambda/\text{kJ mol}^{-1} = 360 + 4\ T\ \Delta S^\dagger \qquad (5)$$

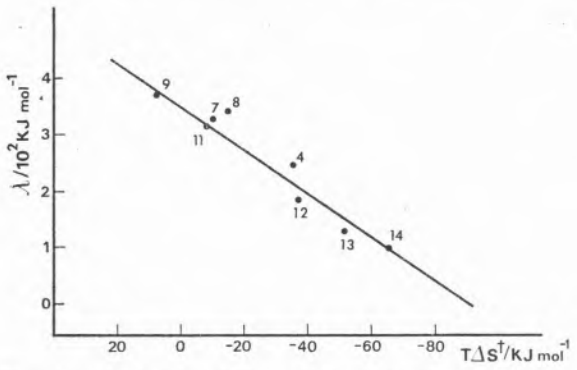

Fig. 4 — Variation of the configuration entropy parameter λ with the activation entropy (standard state 1 mol dm^{-3}; T = 298 K). Legend for reactions in Table 2.

For a positive entropy of activation ($\Delta S^\dagger >> 0$) there is a small dependence of η on $(\Delta G^\circ)^2$, which approaches the situation considered in the theory of Marcus [15], where the distance between the minima of the potential energy curves is independent of ΔG°. However, for large negative activation entropies there is a large increase of η with an increase in $|\Delta G^\circ|$. In this situation the distance between the minumum of the potential energy curves of reactants and products increases with an increase in $|\Delta G^\circ|$, and Marcus-equation is no longer obeyed.

INNER-SPHERE REACTIONS

The essential feature of this kind of electron transfer reactions is that one ligand molecule is shared between the two reacting species forming a bridge between the two metal ions. This requires that the ligand should have at least one pair of electrons available for interaction with the metal orbitals [22]. In general such electron transfer reactions have lower activation free energies than those of outer-sphere reactions. Although Marcus theory is not strictly applicable to inner-sphere reactions, the present model can deal with such a problem.

Let us illustrate the application of ISM to the $Fe(CN)_6^{4-}/IrCl_6^{-}$ system, where both ions share one chloride atom in the reacting complex. Whereas the effective force constant and bond length of $IrCl_6^{-}$ can be taken as that of an outer-sphere reaction, for the other reacting partner ($f = (5f^2_{Fe\text{-}C} + f^2_{Fe\text{-}Cl})^{1/2}$. However since this introduces only a small correction, we have neglected these effects in f and l. Therefore calculations are undertaken with $f = \sqrt{6}\,(f_{Fe(CN)_6}4- + f_{Fe(CN)_6}3- + f_{IrCl_6}- + f_{IrCl_6}2-)/4$ and $l_{ox} + l_{red} = (l_{Fe(II)\text{-}C} + l_{Fe(III)\text{-}C} + l_{Ir(V)\text{-}Cl} + l_{Ir(IV)\text{-}Cl})/2$. Since we are dealing with inner-sphere reactions which are controlled by the electron transfer step, we have assumed a fast formation of the reacting complexes. Therefore activation free energies with respect to reactants can be estimated through eq (4).

Table 3

Bond distensions for Inner-Sphere and Fast Outer-Sphere Electron Transfer Reactions

	Reactants	$f/10^3$ kJ mol^{-1} Å^{-2}	$(l_r + l_p)$/Å	$\Delta G^{\ddagger}$/kJ mol^{-1}	ΔG°/kJ mol^{-1}	d/Å	η
1	$Fe(CN)_6^{4-}/Fe(CN)_6^{3-}$ (*a*)	6.7	3.83 (*e*)	57 (*f*)	0	0.261	0.068
2	$Fe(CN)_6^{4-}/IrCl_6^{-}$	4.4	4.54	38.5 (*b*)	— 63.5	0.344	0.076
3	$Fe(CN)_6^{4-}/OsCl_6^{-}$	4.9	4.74	77.3 (*b*)	— 6.7	0.359	0.0757
4	$Os(dipy)_3^{2+}/Ru(dipy)_3^{3+}$	3.0	4.74	27.2 (*b*)	— 42.0	0.349	0.0736
5	$Os(dipy)_3^{2+}/IrCl_6^{-}$	2.6	4.87	27.2 (*b*)	— 22.2	0.34	0.070
6	$Co(NH_3)_5(OH)^{2+}/Cr^{2+}$	3.2	4.20	38.4 (*c*)	— 49.0	0.389	0.093
7	Fe^{2+}/duroquinone	2.3/3.7 (*d*)	4.14	95.9 (*b*)	84.8	0.362	0.087
8	Fe^{2+}/dichlorosemiquinone	2.3/3.7 (*d*)	4.14	72.5 (*b*)	37.4	0.384	0.093

(*a*) Outer-sphere.
(*b*) Ref. c. of Table 1, 508, 509.
(*c*) Ref. 22, p. 430.
(*d*) Different force constants for reactants and products; in the reactants the force constant for the organic molecules was neglected.
(*e*) Ref. 17.
(*f*) Ref. b of Table 1.

Table 3 presents the calculated bond distensions which reproduce the $\Delta G^{\ddagger}$ values for several inner-sphere reactions, and Figure 5 presents the dependence of η on $(\Delta G^{\circ})^2$. A linear dependence is found for two series of reactions. Just as in the case of outer-sphere reactions, we attribute the differences in slopes to the differences in λ, although we have no experimental data to verify the relationship between λ and $T\Delta S^{\ddagger}$ for this kind of reactions. The most significant difference between the inner-sphere and outer-sphere reactions is the reduced bond distension at $\Delta G^{\circ} = 0$. The intercepts in Figure 5 lead to values of η (0) = 0.067 which corresponds to a transition state bond order of $n^{\ddagger} \cong 1.6$ (eq (1)), which is higher than the value of $n^{\ddagger} = 1$ found for the majority of outer-sphere reactions [12].

For electron transfer reactions $n^{\ddagger}$ values higher than 1 can be expected when there is an increase in the total bond order at the transition state, e.g. when nonbonding or antibonding electrons in reactants (or products) acquire a bonding character in the activated complexes [8, 9]. For example, for the reaction $Cr(H_2O)_6^{2+} / (Co(NH_3)_5X^{2+}$ the bond order of the metal-ligand bonds is 1 in

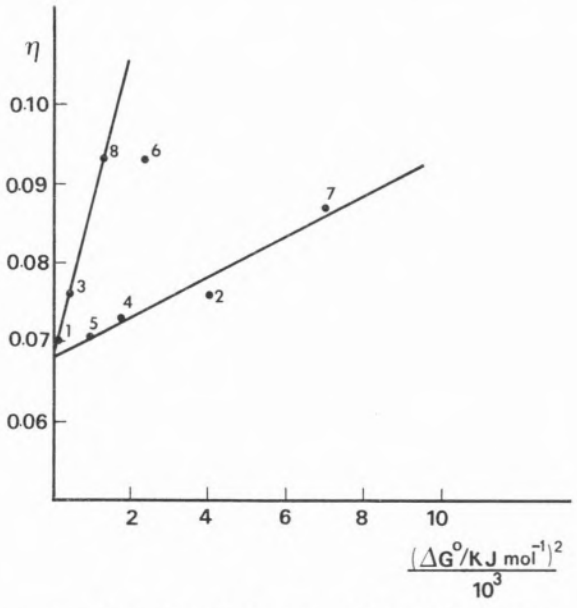

Fig. 5 — Variation of the reduced bond distension, η, with the reaction energy, ΔG°, for inner-sphere electron transfer reactions. Legend for reactions in Table 3.

reactants and products. However, at the transition state some distortion can occur which allows some interaction of the metal d orbitals and the nonbonding p orbitals of the ligands. A better description of the electronic configuration of the transition state is now in terms of molecular orbitals. To estimate the bond order of the metal-ligand bond at the transition state, we can average the bond order for the appropriate electronic configurations. Considering only the highest orbitals the relevant configurations are:

$$\text{Cr(II)}\ \ t_{2g}^6(\pi_b)\ \ t_{1u}^6(\pi_b)\ \ t_{2g}^3(\pi^*)\ \ e_g^1(\sigma^*)\ ;$$
$$\text{Cr(III)}\ \ t_{2g}^6(\pi_b)\ \ \ t_{1u}^6(\pi_u)\ \ t_{2g}^3(\pi^*)$$

$$\text{Co(III)}\ \ t_{2g}^6(\pi_b)\ \ t_{1u}^6(\pi_b)\ \ t_{2g}^6(\pi^*)\ ;$$
$$\text{Co(II)}\ \ t_{2g}^6(\pi_b)\ \ t_{1u}^6(\pi_b)\ \ t_{2g}^6(\pi^*)\ \ e_g^1(\sigma^*)$$

The bond order contribution for one bond from all these configurations is $[(12-4) + (12-3) + (12-6) + (12-7)]/(4 \times 2 \times 6) = 0.583$. This contribution together with the $n = 1$ contribution of the σ bond leads to $n^\dagger = 1.583$. With this value eq (1) gives $\eta(0) = 0.068$, a value in good agreement with the intercept in Figure 5.

Obviously the metal-ligand bonds can already have a bond order higher than 1 in reactants and products, as found in the $Fe(CN)_6^{4-}/Fe(CN)_6^{3-}$ and $Mo(CN)_8^{4-}/Mo(CN)_8^{3-}$ systems. Consequently, such reactions, although mechanistically outer-sphere, as we have discussed in Part 1 of this series [12], are similar to the inner-sphere processes in terms of rate constants.

THE INVERTED REGION

The study of the effect of ΔG° on outer-sphere and inner-sphere reactions within a ISM formalism reveals that for the majority of these systems Marcus theory is not exactly obeyed. The variety of λ values found experimentally (ca. 350 to 100 kJ mol^{-1}) shows that electron transfer reactions can display virtually a continuum of energy gap laws.

In liquid solution the observed rate constants are limited by diffusion,

$$k_{obs} = \frac{k_d\ k_{et}}{k_{-d} + k_{et}} \qquad (6)$$

where k_d is the diffusion rate constant, k_{-d} the back dissociation rate constant of the collision complex and k_{et} the electron transfer rate. Figure 6 presents the calculated

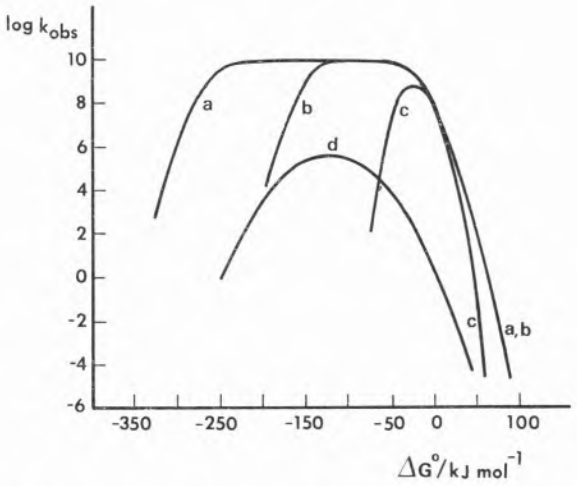

Fig. 6 — Calculated rates of electron transfer reactions in solution with: $n^\dagger = 1.54$ a) $\lambda = 290$ kJ mol^{-1}, b) $\lambda = 145$ kJ mol^{-1} and c) $\lambda = 90$ kJ mol^{-1}; d) $n^\dagger = 1$ and $\lambda = 290$ kJ mol^{-1}. Other parameters: $f = 2.9 \times 10^3$ kJ mol^{-1} Å^{-2}, $l_r + l_p = 4$ Å, $k_d = 10^{10}$ mol^{-1} dm^3 s^{-1}, $k_{-d} = 10^{10}$ s^{-1}; T = 298 K.

rates for typical kinetic data. It is immediately obvious that the occurrence of the inverted region depends on the values of λ and on the nature of the activated complexes. For activated complexes with $n^\dagger = 1$ there is an inverted region at relatively low ΔG°, but for transition states with $n^\dagger \cong 1.5$ the inverted region can only be observed for reasonable ΔG° values when λ is low. For example, with $\lambda = 290$ kJ mol^{-1} the inverted region is only noticeable when $\Delta G^\circ < -240$ kJ mol^{-1}, a value not normally attainable under experimental conditions in solution.

Let us now examine a system where the inverted region has been experimentally

observed. Miller et al. [3] have studied the intramolecular electron transfer in anions of bifunctional steroids (5 α-androstane) A-Sp-B$^-$ (B = 4-biphenyl; A is an acceptor group). The ions are formed on subjecting solutions of these molecules to short pulses of solvated electrons. Figure 7 presents the calculated rate constants for a thermal activation mechanism for solvent reorganization. Good agreement is found with experimental data in the normal and in the inverted regions, with the following set of parameters: $f = 8 \times 10^2$ kJ mol^{-1} Å^{-2}, $\kappa\nu = 10^{13}$ s^{-1}, d = 0.642 Å ($\eta = 0.108$ and $l_r + l_p = 5.94$ Å; or $\eta = 0.072$ and $l_r + l_p = 8.9$ Å), k_d/mol^{-1} dm^3 s^{-1} = k_{-d}/s^{-1} = 3.5×10^{10}; $\lambda = 110$ kJ mol^{-1} In spite of the fact that this reaction is an intramolecular process, we have considered it to be rate determined by rotational and/or translational diffusion of the two reacting moieties linked by a rigid hydrocarbon spacer.

In the intermediate region where $\Delta G^\dagger$ has a minimum, the experimental rates are an order of magnitude lower than the calculated ones (Figure 7). This can be attributed to some

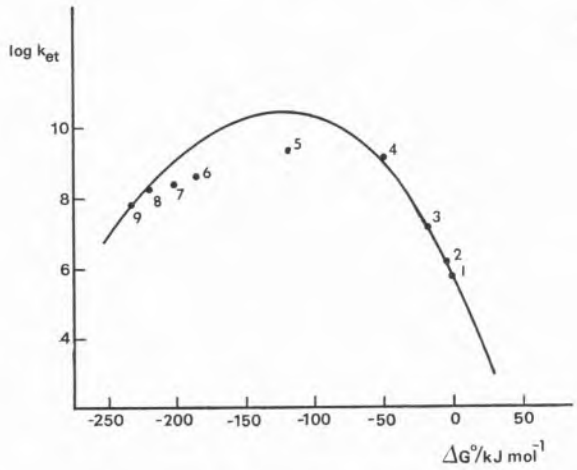

Fig. 7 — Calculated intramolecular electron transfer rate constants in anions of bifunctional steroids A-Sp-B$^-$ as a function of free energy in MTHF solution at 296 K; B = 4-biphenylyl. Experimental data points (ref 3) with the acceptor groupe A: 1. 4-biphenylyl; 2. 2-naphthyl; 3. 9-phenanthryl; 4. 1-pyrenyl; 5. hexahydronaphthoquinon-2-yl; 6. 2-naphthoquinonyl; 7. 2-benzoquinonyl; 8. 5-chlorobenzoquinon-5-yl; 9. 5,6-dichlorobenzoquinon-2-yl.

contribution of an internal rotational energy barrier ($\Delta G^\dagger = 5.5$ kJ mol^{-1}) for the fastest electron transfer processes. Another possible cause of this effect can be a diffusion controlled capture of the electrons by the solute molecules. If nuclear tunnelling was a significant process in the inverted region, we would have expected experimental rates higher than those due to thermal activation, contrary to the present findings.

Different energy gap laws have been reported [11] for three types of electron transfer reactions in polar media: the photoinduced charge separation $A^*...D \rightarrow A^-...D^+$ shows no inverted region; the charge shift $A...D^\pm \rightarrow A^\pm...D$ shows a moderate decrease of rates when $\Delta G°$ is negative; the charge recombination $A^-...D^+ \rightarrow A...D$ shows a strong inverted region effect. Such findings can also be accounted for by ISM in terms of the variation of λ.

For the charge recombination process the final state involves neutral species which interact weakly with the solvent molecules. Consequently, the activated complexes of the type A...D have a small energy of solvation and then λ is low; when λ is low we have shown that the inverted region can be easily observed at moderately negative $\Delta G°$. In contrast the charge separation process involves charged activated complex species $A^{\delta-}...D^{\delta+}$ and the interaction with polar molecules is much stronger than for A...D. Consequently, the solvated activated complexes have a relatively high capacity to store energy and λ is high. For such a situation no inverted effect is observed at normal $\Delta G°$ values.

CONCLUDING REMARKS

The present model provides new insights for the understanding of electron transfer reactions. In contrast to current theories for outer-sphere reactions which consider bulk solvent reorganization as an important part of the activation process, our model suggests that the main activation free energy barrier for outer- and inner-shere reactions is domi-

nated by inner-shell reorganization. The role of the bond order of the transition state is assessed and provides a unifying feature to deal with outer- and inner-sphere reactions within the same theoretical framework. The configuration entropy parameter λ was also found to play a significant role on the driving force effect of ΔG^o for the electron transfer processes. A high λ favours the driving force effect of ΔG^o, but a low λ hinders such an effect. As a consequence, different types of reaction energy gap laws can be found for exothermic reactions. In fact there is a continuum of laws from the strong inverted effect to a constant diffusion rate, when ΔG^o is negative. The fact that, in general, λ is reasonably high for electron transfer reactions of solvated or coordinated metal ions explains the success of the theory of Marcus in the treatment of these systems, except for the inverted region.

ACKNOWLEDGMENTS

We are grateful to Instituto Nacional de Investigação Cientifica for financial support.

Received 19th.October.1986

REFERENCES

[1] R.A. MARCUS, Faraday Disc. Chem. Soc., **29**, 21 (1960).
[2] J.R. MILLER, J.V. BEITZ and R.K. HUDDLESTON, J. Am. Chem. Soc., **106**, 5057 (1984).
[3] J.R. MILLER, L.T. CALCATERRA and G.L. CLOSS, J. Am. Chem. Soc., **106**, 3047 (1984).
[4] M.R. WASIELEWSKI, M.P. NIEMCZYK, W.A. SVEC and E.B. PEWITT, J. Am. Chem. Soc., **107**, 1080 (1985).
[5] D. REHM and A. WELLER, Ber. Bunsenges. Physik. Chem., **73**, 834 (1969); Isr. J. Chem., **8**, 259 (1970).
[6] S.J. FORMORINHO, Rev. Port. Quím., **24**, 74 (1982).
[7] G.W. KOEPPL and A.J. KRESGE, J. Chem. Soc., Chem. Commun., 371 (1973).
[8] A.J.C. VARANDAS and S.J. FORMOSINHO, J. Chem. Soc., Chem. Commun., 163 (1986); J. Chem. Soc., Faraday Trans., **82**, 953 (1986).
[9] S.J. FORMOSINHO, Rev. Port. Quím., **27**, 427 (1985).
[10] H. RAU, R. FRANK and G. GREINER, J. Phys. Chem., **90**, 2476 (1986).
[11] T. KAKITANI and N. MATAGA, Chem. Phys., **93**, 381 (1985); J. Phys. Chem., **90**, 993 (1986).
[12] S.J. FORMOSINHO, Rev. Port. Quím., **28**, 38 (1986).
[13] N. AGMON and R.D. LEVINE, Chem. Phy. Lett., **52**, 197 (1977).
[14] N. SUTIN, Annu. Rev. Sci., **12**, 285 (1962); Prog. Inorg. Chem., **30**, 441 (1983).
[15] R.A. MARCUS, Faraday Discuss. Chem. Soc., **74**, 7 (1982).
[16] S.U.M. KHAN and J.O'.M. BOCKRIS, J. Phys. Chem., **87**, 4012 (1983).
[17] B.S. BRUNSCHWIG, C. CREUTZ, D. H. MACARTNEY, T-K. SHAM and N. SUTIN, Faraday Discuss. Chem. Soc., **74**, 113 (1982).
[18] Y. MARCUS, J. Solution Chem., **12**, 271 (1983).
[19] Handbook of Chemistry and Physics, Chemical Rubber Comp., 52nd edn, 1972, F-177, D-111.
[20] K. NAKAMOTO, «Infrared Spectra of Inorganic Coordination Compounds», Wiley, New York, 1970.
[21] J.R. FERRARO, «Low-Frequency Vibrations of Inorganic and Coordination Compounds», Plenum Press, New York, 1971.
[22] J. BURGESS, «Metal Ions in Solution», Wiley, London, 1978, chap. 13.

RESUMO

O papel da ordem de ligação e da entropia dos estados de transição nas reacções de transferência de electrões.
Parte 2 — O efeito da energia da reacção nas transferências de electrões de camada externa e interna.

O modelo de intersecção de estados, desenvolvido inicialmente para o estudo de reacções em fase gasosa, foi aplicado ao estudo de reacções de transferência de electrões em solução. As barreiras de energia são controladas por comprimentos e constantes de força das ligações metal-ligando e pelas ordens de ligação e entropia dos estados de transição. As reacções de camada externa têm, em geral, $n^\dagger = 1$, *mas quer as reacções rápidas de camada externa, quer as de camada interna tem* $n^\dagger \simeq 1.6$. *As distensões das ligações metal-ligando aumentam com o aumento de* $|\Delta G^o|$. *Esta variação depende do parâmetro da entropia de configuração* λ *e é pequena quando* λ *é elevado e acentuada quando* λ *é baixo.* λ *está relacionado com a entropia de activação, e os seus valores variam tipicamente entre 350 e 100 kJ* mol^{-1}. *Esta variação permite interpretar a existência das diferentes leis de variação das constantes de velocidade com* ΔG^o. *A região invertida ocorre quando* λ *e* $(\Delta S^\dagger)$ *é baixo, mas se* λ *é elevado, as constantes cinéticas são controladas pela difusão quando* ΔG^o *é baixo. A equação de Marcus é um caso particular do presente modelo quando* $\lambda >> |\Delta G^o|$.

HUGH D. BURROWS
SEBASTIÃO J. FORMOSINHO
Departamento de Química, Universidade de Coimbra, 3049 Coimbra Codex, Portugal

THE ROLE OF BOND ORDER AND ENTROPY OF TRANSITION STATES IN ELECTRON TRANSFER REACTIONS

Part 3. — Cross-reaction Relationships.

Discrepancies between Marcus cross-relation rate constants for electron transfer reactions $Co^{3+}_{(aq)}$ ions and experimental values are examined through a general intersecting-state model. The observed rate constant discrepancies are well accounted for by an increase in the distance of the minimum of the potential energy curves with a decrease in the reaction energy.

Within the theory of Marcus [1] the rate constant of the reaction

$$red_1 + ox_2 \xrightarrow{k_{12}} ox_1 + red_2 \qquad (1)$$

can be estimated from the self-exchange reaction rates k_{ii},

$$red_i + ox_i \xrightarrow{k_{ii}} ox_i + red_i \qquad (2)$$

and the equilibrium constant K_{12}, through the equation

$$k_{12} \cong (k_{11}\ k_{22}\ K_{12})^{1/2} \qquad (3)$$

with all processes considered to be adiabatic. Although good agreement with experiment is generally found [2], the rates of a number of very exothermic electron transfer reactions are much slower than predicted by the cross-relations [1-6]. The disagreement between theory and experiment has lead several authors to suggest that the adiabatic approximation cannot be used in the inverted region and suggestions were also made that nuclear tunnelling could be important here [7, 8]. The most proeminent disagreements from theory involve electron transfer reactions of $Co(H_2O)^{3+}_6$ which is a very strong oxidant ($E^o = 1.8$ V [9]). For example, the calculated rates are 2×10^5 times higher than the experimental rate for $Fe(phen)^{2+}_3/Co(H_2O)^{3+}_6$ [4] and 3×10^5 for $Co(terpy)^{2+}_2/Co^{3+}_{(aq)}$ [5]. In this paper we intend to examine such discrepancies, which give further support to the hypothesis that electron transfer reactions can be treated as any other ordinary chemical reaction [10].

ON THE VALIDITY OF MARCUS CROSS-REACTION RELATIONS

For the reaction [1] Marcus has shown that the rate constant can be estimated by eq (3),

neglecting the work terms of bringing the reactants together. This implies that

$$\Delta G^{\dagger}_{12} = (\Delta G^{\dagger}_{11} + \Delta G^{\dagger}_{22} + \Delta G^{o}_{12}) / 2 \qquad (4)$$

where $\Delta G^{\dagger}_{ii}$ are the activation free energies of the self-exchange reactions and ΔG^{o}_{12} the free energy of reaction [1]. Since for electron transfer reactions

$$\Delta G^{\dagger} = [\Delta G^{o} + (1/2) f d^2]^2 / 2 f d^2 \qquad (5)$$

where f is the average metal-ligand stretching force constant and d is the sum of the bond distensions up to the transition state [10], then

$$\Delta G^{\dagger}_{12} = (1/2)\ [(1/4) f_{12} d^2_{12} + \Delta G^{o}_{12} + (\Delta G^{o}_{12})^2 / f_{12} d^2_{12}] \qquad (6)$$

Under conditions where the square term can be neglected ($|\Delta G^{o}_{12}| << 2(\Delta G^{\dagger}_{11} + \Delta G^{\dagger}_{22})$) eqs (4) and (6) imply

$$f_{11}\ d^2_{11} + f_{22}\ d^2_{22} = 2\ f_{12}\ d^2_{12} \qquad (7)$$

As long as the relevant force constants for all reactions have similar values, which is a reasonable assumption if ions of identical carge are involved [11], then

$$d^2_{11} + d^2_{22} = 2\ d^2_{12} \qquad (8)$$

The intersecting-state model (ISM) [10, 12] shows that eq (8) is satisfied when d and the reduced bond distension η are independent of the reaction free energy. Since

$$d = \eta\ l \qquad (9)$$

where l is the sum of the equilibrium lengths of the metal-ligand bonds, $l = l_{ox} + l_{red}$, and

$$\eta = \frac{a'\ \ln 2}{n^{\dagger}} + \frac{a'}{2\ \lambda^2}\ (\Delta G^{o})^2 \qquad (10)$$

this independence requires neglecting the effect of the configuration entropy parameter λ, i.e., $|\Delta G^{o}| << \lambda$. Then eqs (9) and (10) show that

$$[(l_{11}/n^{\dagger}_{11})^2 + (l_{22}/n^{\dagger}_{22})^2] = 2\ (l_{12}/n^{\dagger}_{12})^2 \qquad (11)$$

If there is a constancy of the transition state bond orders, i.e., $n^{\dagger}_{11} = n^{\dagger}_{22} = n^{\dagger}_{12}$, then the equation

$$l^2_{11} + l^2_{22} = 2\ l^2_{12} \qquad (12)$$

is a reasonable estimate of the metal-ligand equilibrium bond lengths and eq (3) is valid. There are several approximations involved in the Marcus cross-reaction relationships, but the most restrictive ones appear to be the constancy of $n^{\dagger}$ and $|\Delta G^{o}_{12}| << \lambda_{12}$. Those are the conditions which are going to be examined for some electron transfer reactions of $Co^{3+}_{(aq)}$.

EFFECT OF THE REACTION ENERGY ON $Co^{3+}_{(aq)}$ ELECTRON TRANSFERS

Electron transfer reactions of Co(III) ions with Co(II) and Fe(II) complexes, with a ΔG^{o} range of 200 kJ mol^{-1}, were studied within the ISM formalism. The bond distension parameter d was estimated from eq (5) in order to reproduce the experimental $\Delta G^{\dagger}$ values, and through $d = \eta\ (l_{ox} + l_{red})$ the reduced bond distensions were calculated (see Table 1). According to eq (10) η should show a square dependence on ΔG^{o}. This is observed in Figure 1 for the data of Table 1, with one slope ($\lambda = 315$ kJ mol^{-1}) for the Co(III)/Co(II) systems and a higher one ($\lambda = 160$ kJ mol^{-1}) for data involving the Fe(III) and Fe(II) species. For metal aquo-ions and a few mixed complexes λ was found empirically to be linearly related with the activation entropy, λ/kJ mol^{-1} = 360 + 4T$\Delta S^{\dagger}$ (standard state 1 mol dm^{-3}) [13]. The same relation may not be exactly valid for the complexes under study, but it can interpret the large change in λ for the reactions of Co(III)/Co(II) and Co(III/Fe(II). For example, the activation entropy for the reaction $Fe^{3+}_{(aq)}/Cr^{2+}_{(aq)}$ is ca.

Table 1

Bond distensions and the effects of the configuration entropy, $k(\eta^o)/k(\eta)$, for Electron Transfer Reactions of $Co^{3+}_{(aq)}$ ions.

	Reaction	$\Delta G^{\ddagger}$/kJ mol^{-1} (*a*)	ΔG^o/kJ mol^{-1}	f/10^3 kJ mol^{-1} Å^{-2} (*e*)	l/Å (*f*)	d/Å	η	$k(\eta(o))/k(\eta)$ (*g*)
1	$Co(terp)^{2+}_2/Co(bipy)^{3+}_3$	58.8	— 62.5	3.5	4.02	0.446	0.111	7
2	$Co(terp)^{2+}_2/Co(phen)^{3+}_3$	55.0	— 68.5	3.5	4.02	0.443	0.110	4
3	$Co(terp)^{2+}_2/Co^{3+}_{(aq)}$	42.9	— 203	3.0	4.12	0.574	0.139	2×10^6
4	$Co(terp)^{2+}_2/Co(phen)^{3+}_2$	45.4	— 95.0	3.2	4.02	0.465	0.116	60
5	$Co^{2+}_{(aq)}/Co^{3+}_{(aq)}$	69.0 (*b*)	0	2.8	4.11	0.449	0.109	—
6	$Co(terpy)^{2+}/Co(phen)^{3+}$	50.5	— 110.5	3.2	4.05	0.494	0.122	2×10^3
7	$Fe^{2+}_{(aq)}/Co^{3+}_{(aq)}$	66.6 (*c*)	— 104	2.7	4.13	0.575	0.139	2×10^7
8	$Fe(phen)^{2+}_3/Co^{3+}_{(aq)}$	55.8 (*d*)	— 64	2.8	4.03	0.497	0.123	2×10^3

(*a*) Estimated from ref. 5 with a preexponential factor of 10^{13} M^{-1} s^{-1}. (*b*) F. Basolo and R.G. Pearson. «Mechanisms of Inorganic Reactions», Wiley, 1968, 2ed, p. 466. (*c*) Ref. 14. (*d*) Ref. 4. (*e*) $f = \sqrt{6}\,(f_{ox} + f_{red})/2$; from the ratio of stretching frequencies (11) of $Co(NH_3)^{2+}_6/Co(NH_3)^{3+}_6$; for the aquo and mixed complexes the metal-oxygen force constants were taken into consideration with a coordination number of 6. (*f*) $l = r_{Me} + r_L$; crystal ionic radii (r_{Me}); $r_L = 1.38$ Å for water and 1.40 Å for nitrogen atoms (Y. Marcus, J. Solution Chem., 1983, **12**, 271). (*g*) $k(\eta(o))/k(\eta)$ is the ratio of the calculated rate by the theory of Marcus, $\lambda >> |\Delta G^o|$, and the experimental rate.

85 J mol^{-1} K^{-1} more negative than for $Co^{3+}_{(aq)}/Cr^{2+}_{(aq)}$ [14].

The intercept of the two reaction systems is the same, $\eta(0) = 0.108$, which corresponds to a transition state bond order of $n^{\ddagger} = 1$, typical of outer-sphere reactions [10, 13]. So, for all the reactions under consideration $n^{\ddagger}$ is constant. However the dependences of η on $(\Delta G^o)^2$ reveal that one cannot neglect the effect of the configuration entropy parameter λ and, consequently, Marcus cross-relations are not obeyed.

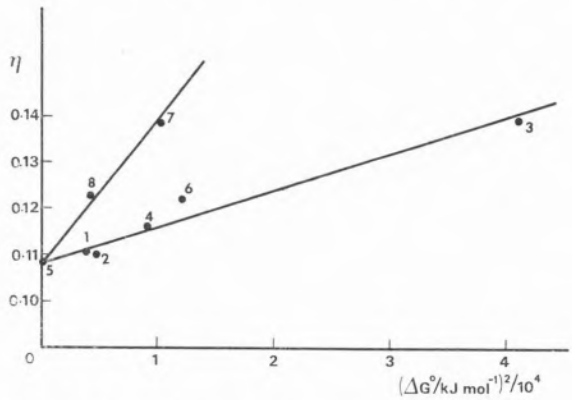

Fig. 1 — Variation of the reduced bond distension, η, with the free energy of reaction, ΔG^o, for electron transfer reactions of $Co^{3+}_{(aq)}$ ions. Legend for reactions in Table 1.

To assess if such an effect is responsible for the discrepancies reported earlier, ISM is employed to calculate the rates of electron transfer neglecting the variation of η with ΔG^o. Table 1 presents the ratio of the calculated rate constants at constant $\eta(0) = 0.108$, $k(\eta(0))$, and the experimental rates, $k(\eta)$. Ratios as high as 10^6-10^7 were found for the reactions $Co(terp)^{2+}_2/Co^{3+}_{(aq)}$ and $Fe^{2+}_{(aq)}/Co^{3+}_{(aq)}$ where the second term in eq (10) is a significant percentage (35 %) of the first term. This reveals that the quadratic dependence of d and η on ΔG^o, not considered in the theory of Marcus, is mainly responsible for the failure of the cross-relations when $|\Delta G^o|$ is high and/or λ is low.

CONCLUDING REMARKS

The view of the ISM formalism that electron transfer reactions can be treated as any other ordinary chemical process has been helpful in interpreting several of the anomalous features observed with the theory of Marcus, where discrepancies between theoretical and experimental rate constants as high as 10^7 have been found [2-8]. This can be attributed mainly to the effect of the configuration entropy which is not considered in the theory of Marcus. However when such an effect is small, Marcus-equation coincides with the ISM-equations and agreement between both treatments exist, although the latter model provides further mechanistic insights. The concept of the transition state bond order accounts basically for the kinetic distinction between normal outer-sphere and inner-sphere reactions, but $n^\dagger$ can also contribute to cases where the Marcus cross-reaction relationships fail, namely systems where reactions of different natures are considered. For relatively slow reactions of $n^\dagger = 1$, we have shown [13] that Marcus-equation is closely verified when $|\Delta G^\circ| \leqq 4\lambda$, i.e. when the second term in the equation of η is ca. 5 % of the first term. However, when the transition state bond order is high, e.g. $n^\dagger = 1.5$ the condition for the validity of the theory of Marcus is slightly more restrictive, $|\Delta G^\circ| \leqq 5\lambda$.

ACKNOWLEDGMENTS

We are grateful to Instituto Nacional de Investigação Cientifica for financial support.

Received, 19th.October.1986

REFERENCES

[1] R.A. MARCUS, J. Chem. Phys., **26**, 867 (1957); Faraday Discuss. Chem. Soc., **29**, 21 (1960).
[2] R.A. MARCUS and N. SUTIN, Biochim. Biophys. Acta, **811**, 265 (1985).
[3] E. KÖNIG and S. HERZOG, J. Inorg. Nucl. Chem., **32**, 585 (1970).
[4] R.J. CAMPION, N. PURDIE and N. SUTIN, Inorg. Chem., **3**, 1091 (1964).
[5] R. FARINA and R.G. WILKINS, Inorg. Chem., **7**, 514 (1968).
[6] C. CREUTZ and N. SUTIN, J. Am. Chem. Soc., **99**, 241 (1977).
[7] S. EFRINA and M. BIXON, Chem. Phys. Lett., **25**, 34 (1974).
[8] R.A. MARCUS and N. SUTIN, Inorg. Chem., **14**, 213 (1975).
[9] D.A. JOHNSON and A.G. SHARPE, J. Chem. Soc., 3490 (1964).
[10] S.J. FORMOSINHO, Rev. Port. Quím., **28**, 38 (1986).
[11] J.R. FERRARO, «Low Frequency Vibrations of Inorganic and Coordination Compounds», Wiley-Interscience, New York, 1970.
[12] A.J.C. VARANDAS and S.J. FORMOSINHO, J. Chem. Commun., 163 (1986); J. Chem. Soc., Faraday Trans. 2, **82**, 953 (1986).
[13] S.J. FORMOSINHO, Rev. Port. Quím., **28**, 48 (1986).
[14] J. BURGESS, «Metal Ions in Solution», Wiley, London, 1978, chap. 13.

RESUMO

O papel da ordem de ligação e da entropia dos estados de transição nas reacções de transferência de electrões.
Parte 3 — «Relações-cruzadas» nas reacções de transferência de electrões.

O uso das «relações-cruzadas» da teoria de Marcus para estimar constantes de velocidades de reacções de transferência do electrão, em especial de $Co^{3+}_{(aq)}$*; dá por vezes valores muito superiores ao experimental. Este desacordo é interpretado, pelo modelo de intersecção de estados, como devido a um aumento da separação das curvas de energia potencial quando* ΔG° *diminui.*

SEBASTIÃO J. FORMOSINHO
Departamento de Química, Universidade de Coimbra, 3049 Coimbra Codex, Portugal

THE ROLE OF BOND ORDER AND ENTROPY OF TRANSITION STATES IN ELECTRON TRANSFER REACTIONS

Part 4. — Electrochemical Reactions and the Anodic-Cathodic Asymmetry of the Tafel Plots.

The free energy barriers of electrochemical electron transfer reactions are found to be dominated by the solvent reorganization in the primary shell of solvated metal ions. Work-corrected heterogeneous and homogeneous electron transfer processes can be treated within the same theoretical framework with the assumption $\Delta G_{hom} = 2\,\Delta G_{het}$, *both for the energy barrier and the reaction free energy. The origins of the anodic cathodic asymmetries of the Tafel plots for metal-aquo redox couples are amenable to interpretation within the intersecting-state model. Whereas the plots are virtually linear when the configuration entropy parameter,* λ, *has no effect on the displacement of the potential energy curves, i.e., when* $\Delta S^{\ddagger}$ *is high, negative curvatures are observed for low values of* λ *and* $\Delta S^{\ddagger}$. *These findings seem to imply that for the very exothermic reactions the «transition state» does not coincide with the «saddle point» owing to configurational effects perpendicular to the reaction coordinate.*

INTRODUCTION

The transfer of electrons between a metal or semiconductor and a dissolved or surface-bound reactant is not essentially different from the same process between two species in homogeneous solution, and the development of theories for these reactions has followed the progresses in the latter field [1-3]. Recently a great effort has been made by Weaver and coworkers [4-6] to assess the role of inner-shell reorganization and the outer-shell reorganization on the energy barrier of electrochemical reactions. Nevertheless, they were unable to explain quantitatively the large anodic-cathodic asymmetry of the Tafel plots for some metal-aquo redox couples in terms of the theory of Marcus [5]. For example, at an overpotential of 700 mV the cathodic reduction of $Cr(H_2O)_6^{3+}$ is 200 times faster than the anodic oxidation of $Cr(H_2O)_6^{2+}$ at the same overpotential. The possible effect of the difference on the force constants of the oxidized and reduced species in Marcus-equation was also considered. Although some of the anodic-cathodic asymmetry is accounted for by this effect, its contribution (6 times) is much smaller than the experimental difference [5].

In previous papers [7, 8] we have shown that electron transfer reactions in solution can be treated as any other ordinary chemical reaction and an intersecting-state model (ISM) [9] has been employed for the study of electron transfer reactions in solution. The model has interpreted satisfactorily several areas where the theory of Marcus failed, such as discrepancies of the calculated and experimental rates of some electron exchange processes [7], the variety of the energy gap laws of electron transfer reactions [8] and «anomalous» cross-reaction relationships [10]. It, thus, seems useful to extend the applications of ISM to the study of electrochemical electron transfer reactions.

Although outer-sphere electron transfer reactions of solvated or coordinated metal ions at metal surfaces and in homogeneous solutions are closely related processes, for the

heterogeneous reactions double-layer effects can be significant. Fortunately most of the experimental data which we are going to analyze were obtained under experimental conditions selected to minimize such effects. These «work-corrected» rate constants [4, 5], in the absence of electrostatic work terms, have been employed in the calculations, except where stated otherwise.

THEORETICAL MODEL

According to the intersecting-state model [9] developed for reactions involving two molecular species, the activation free energy barrier of a chemical reaction can be found at the intersection of two potential energy curves. For harmonic oscillators

$$\frac{1}{2} f_r x^2 = \frac{1}{2} f_p (d-x)^2 + \Delta G^o_{hom} \qquad (1)$$

where x is the bond distension from reactant to the transition state, d represents the horizontal displacement of the potential energy curves and, consequently, represents also the sum of the bond distensions from reactant and product to the transition state; f_i are the appropriate force constants of reactant and product, and ΔG^o_{hom} is the reaction free energy. The activation free energy of the reaction, here represented by $\Delta G^{\ddagger}_{hom}$ in order to be distinguished from that of the heterogeneous electrochemical process ($\Delta G^{\ddagger}_{het}$), is

$$\Delta G^{\ddagger}_{hom} = \frac{1}{2} f_r x^2 \qquad (2)$$

where x is estimated from eq (1), once d is known. This parameter is proportional to the sum of the equilibrium bond lengths [9]

$$d = \eta (l_r + l_p) \qquad (3)$$

with the reduced bond distension, η, given by

$$\eta = \frac{a' \ln 2}{n^{\ddagger}} + \frac{a'}{2 \lambda^2} (\Delta G^o_{hom})^2 \qquad (4)$$

$n^{\ddagger}$ is the transition state bond order, λ is an energy parameter which can be viewed as an energy capacity of the activated complexes and a′ is a constant (a′ = 0.156).

Work-corrected electron transfer rates of electrochemical reactions can be studied in the same manner as the rates of homogeneous processes as long as the assumption $2\Delta G_{het} = \Delta G_{hom}$ is made [11], because two species are undergoing rearrangement in the homogeneous reactions, whereas only one species is involved in the electrochemical process. Consequently eqs (1) (2) and (4) are now written as

$$\frac{1}{2} f_r x^2 = \frac{1}{2} f_p (d-x)^2 + 2 \Delta G^o_{het} \qquad (1')$$

$$2 \Delta G^{\ddagger}_{het} = \frac{1}{2} f_r x^2 \qquad (2')$$

and

$$\eta = \frac{a' \ln 2}{n^{\ddagger}} + \frac{a'}{2 \lambda^2} (2 \Delta G^o_{het})^2 \qquad (4')$$

The rate constant of the heterogeneous electron transfer reaction is related with the activation free energy by

$$k_{het} = \kappa Z \exp (-\Delta G^{\ddagger}_{het}/RT) \qquad (5)$$

where κ is an electronic transmission factor which is 1 for adiabatic processes and $\kappa < 1$ for the nonadiabatic reactions, and Z is the preexponential factor, taken as $Z = 10^4$ cm s^{-1} [11].

THERMONEUTRAL REACTIONS

We have shown that for electron transfer reactions in solution the overall activation free energy is dominated by the inner-shell reorganization process [7, 8] and the same procedure can be employed to study electrochemical reactions. As a preliminary test of the model for these reactions we will analyze some old data collected by Mar-

cus [11]. The inner-shell energy barrier for a thermoneutral situation can be calculated through the expression

$$2\,\Delta G^{\ddagger}_{het} = \frac{1}{8}\ f\ d^2 \qquad (6)$$

where f is the average force constant of the metal-ligand bonds, $f = \sqrt{6}(f_{ox} + f_{red})/2$ [7]. Table 1 presents the calculated bond distension parameters which reproduce $\Delta^{\ddagger}_{het}$, for some electrochemical reactions in aqueous solutions under reversible conditions [8, 12, 13]. The reduced bond distensions, η, are close to 0.108 (eq (4') at $\Delta G^{o}_{het} = 0$), which implies that we are dealing with outer-sphere processes with a bond order at the transition state close to 1. Such values compare well also with those in aqueous solutions [8]. This reveals that for these reactions there are no significant double-layer and nonadiabatic factors, otherwise η would be much higher than the theoretical value 0.108 for $n^{\dagger} = 1$.

The electron transfer reaction $Fe(CN)_6^{4-}/Fe(CN)_6^{3-}$ is an outer-sphere process, but with $\eta = 0.07$ (Table 1), as is found also in solution, since $n^{\dagger} = 1.54$ [7]. All these data reveal that electrochemical electron transfer reactions are also largely dominated by the inner-shell reorganization, similarly to the electron transfer processes in solutions [7, 8].

TAFEL PLOTS

The driving force effect of electrode potential on the electrochemical rates is currently analyzed in terms of a Tafel plot. Hupp and Weaver [5] have analyzed the origins of the anodic-cathodic asymmetries of the Tafel plots for the work-corrected rate constants for the ions $Cr(H_2O)_6^{2+/3+}$ and $Eu(H_2O)_n^{2+/3+}$ at mercury-aqueous interfaces, which contrast with the symmetrical behaviour predicted by the conventional theoretical relationships [11, 14]. These authors have shown that such an asymmetry is not due entirely to differences in force constants between the oxidized and reduced species.

Such studies were based on the least-motion path approach [15] for the estimation of the reorganization energy barrier and on the use of the Marcus-equation [16] to assess the effect of ΔG^{o} on the activation free energy barrier.

Table 1

Calculated bond distensions for electrochemical reactions

	k_{het}/cm s^{-1} (*a*)	$2\Delta G^{\ddagger}_{het}$/kJ mol^{-1}	f/kJ mol^{-1} Å^{-2} (*e*)	d/Å	1/Å (*f*)	η
$Fe^{2+/3+}_{(aq)}$	7×10^{-3}	69.9	3×10^{3}	0.428	4.14	0.104
$V^{2+/3+}_{(aq)}$	4×10^{-3}	72.6	3×10^{3}	0.438	4.38	0.100
$Eu^{2+/3+}_{(aq)}$	3×10^{-4}	85.4	2.7×10^{3}	0.50	4.8	0.104
$Ru^{2+/3+}_{(aq)}$	5×10^{-2} (*b*)	60.2	2.8×10^{3}	0.41	4.15	0.100
$Fe(CN)_6^{4-/3-}$	5.6×10^{-2} (*c*)	59.6	6.74×10^{3}	0.266	3.826	0.070 (*g*)
$Fe(bipy)_3^{2+/3+}$	0.9 (*d*)	45.9	2.3×10^{3}	0.40	3.94	0.102

(*a*) Ref. 11 except where stated otherwise; (*b*) Ref. 6; (*c*) X. Zhang, J. Leddy and A.J. Bard, J. Am. Chem. Soc., 1985, **107**, 3719; (*d*) T. Iwasita, W. Schmickler and J.W. Schultze, Ber. Bunsenges. Phys. Chem., 1985, **89**, 138; (*e*) Ref. 13; (*f*) Ref. 12; (*g*) $n^{\dagger} = 1.54$, Ref. 7.

The least motion approach has been shown to be inadequate for the study of electron transfer reactions between coordinated metal ions [7, 8], and Marcus equation is only obeyed when one can neglect any variation of η and d with the reaction free energy, i.e., when in eqs (4) and (4′) $\lambda >> |\Delta G^{o}|$, a condition which is not valid for all electron transfer reactions [8, 10].

The slope of a Tafel plot ($\alpha = \pm (RT/F)/(d\ \ln k_{het}/d\ E)$) can be estimated from eqs (1′) and (4′) together with the equation

$$\Delta G^{o}_{het} = \pm n_e\ F\ (E\text{-}E_f) \qquad (7)$$

where n_e is the number of electrons transferred ($n_e = 1$), E is the electrode potential, E_f the standard potential and F the Faraday constant (the − sign is for the anodic region and + for the cathodic region). When $f_r = f_p = f$ the slope of $\ln k_{het}$ versus the standard potential is

$$\alpha = \frac{(2\Delta G^{o}_{het} + \frac{1}{2} f\ d^2)}{f\ d^2} \left[(1 + \frac{2f\ d\ a'\ l}{\lambda^2} \right. \qquad (8)$$

$$\left. \Delta G^{o}_{het})d - 2(\Delta G^{o}_{het} + \frac{1}{2} f\ d^2)\ \frac{a'\ l}{\lambda^2}\ \Delta G^{o}_{het} \right]$$

where $l = l_p + l_r$. This equation reveals that $\alpha = 1/2$ when $\Delta G^{o}_{het} \to 0$. Far from this region and when we can neglect the effect of the configuration entropy parameter ($|\Delta G^{o}_{het}| << \lambda$)

$$\alpha \cong \left(\frac{1}{2} + \frac{2\ \Delta G^{o}_{het}}{f\ d^2} \right) \qquad (9)$$

Eq (9) reveals that $\alpha \cong 1/2$ and the Tafel plots are linear as long as $\Delta G^{o}_{het} \leq \Delta G(0)^{\ddagger}_{het}$ where $\Delta G(0)^{\ddagger}_{het}$ is the activation free energy at $\Delta G^{o}_{het} = 0$ ($\Delta G(0)^{\ddagger}_{het} = f\ d^2/16$). Obviously if $f_r \neq f_p$ α is different from 1/2 at $\Delta G^{o}_{het} \to 0$. Table 2 presents the calculated α coefficients for several ratios of f_r/f_p; when $\Delta G^{o}_{het} \to 0$ there is no effect of λ on the electron transfer rate constants. When the effect of λ is significant and $f_r \neq f_p$ eqs (1′)-(4′) and (7) should be used to estimate the transfer coefficient.

Table 2

Calculated transfer coefficients in electrochemical reactions near the standard potential (a)

f_r/f_p	α
10	0.80
6	0.74
3	0.66
1	0.5
0.5	0.47
0.33	0.37
0.17	0.30

(a) Calculations with $f_r = 3 \times 10^3$ kJ mol^{-1} Å^{-2} and d = 0.44 Å.

This shows that the Tafel coefficient α is not a useful tool to analyse the molecular factors which contribute to electron transfer kinetics.

ANODIC-CATHODIC ASYMMETRY OF THE TAFEL PLOTS

Now we would like to discuss the origin of the asymmetry in the Tafel plots for some aquo-ions, reported by Weaver and coworkers [5]. Whereas the plot is virtually linear in the cathodic region it has a strong downward curvature in the anodic region. To explain this, we have to employ eqs (1′) to (4′) and eq (7) without any simplification. We have also to employ different force constants for reactant and product. For example, for the cathodic reduction $f_r = \sqrt{m}\ f_{ox}$ and $f_p = \sqrt{m}\ f_{red}$ where f_{ox} and f_{red} are the single metal-ligand bond stretches for the oxidized and reduced species, and m is the coordination number of the metal ions [7]. Figure 1 compares the observed Tafel plots with the calculated ones for $Cr(H_2O)_6^{3+}$ (cathodic reduction) and $Cr(H_2O)_6^{2+}$ ions. The results show that although an asymmetry of the Tafel plots can be attributed to the differences in force constants of the oxidized

and reduced species, the strong negative curvature of the plot in the anodic region results from the significant dependence of η on $(\Delta G^{\circ})^2$. As eq (4') reveals this can be interpreted in terms of a relatively low value of the configuration entropy parameter ($\lambda = 220$ kJ mol^{-1}; non-Marcus situation). In contrast, in the cathodic region agreement with experiment was found with a constant η, i.e. the parameter λ is reasonably high ($\lambda > 350$ kJ mol^{-1}; Marcus situation).

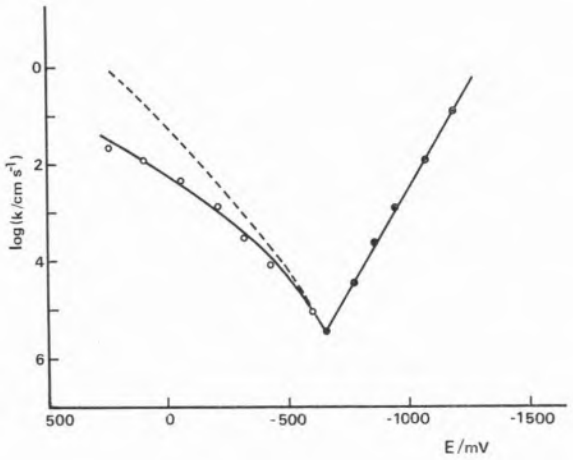

Fig. 1 — Tafel plots for the electron transfer reaction $Cr(H_2O)_6^{2+/3+}$: Experimental plots: ———. Calculated plots: ● cathodic reduction of $Cr(H_2O)_6^{3+}$; $f_r = 3.67 \times 10^3$ kJ mol^{-1} Å^{-2}; $f_p = 2.36 \times 10^3$ kJ mol^{-1} Å^{-2}, d = 0.545 Å independent of the electrode potential; ---- anodic oxidation of $Cr(H_2O)_6^{2+}$: $f_r = 2.36 \times 10^3$ kJ mol^{-1} Å^{-2}; $f_p = 3.67 \times 10^3$ kJ mol^{-1} Å^{-2} and d = 0.545 Å independent of E; O the same set of parameters for the anodic region with d variable with electrode potential, d = 0.545 Å at the standard potential and $a'/2\lambda^2 = 1.6 \times 10^{-6}$ kJ^{2-} mol^2. With $l \cong 4.2$ Å these reactions have $\eta(0) \cong 0.13$ which suggests that they are nonadiabatic processes at a mercury electrode with a common $\kappa \cong 10^{-3}$.

Differences in λ values for solvated and coordinated metal ions were found to be correlated with activation entropies [8], λ/kJ mol^{-1} = 360 + 4 $T\Delta S^{\dagger}$ (standard state 1 mol dm^{-3}). For example, with typical standard entropy values for the hydrated ions [17], $T\Delta S^{\circ}(Cr^{3+}) \cong -87$ kJ mol^{-1} and $T\Delta S^{\circ}(Cr^{2+}) = -25$ kJ mol^{-1} at 298 K, and a transition state entropy which is intermediate between reactant and product, we can reproduce the experimenta data with $T\Delta S^{\circ}[(Cr^{2+}.\, Cr^{3+})^{\dagger}] = -60$ kJ mol^{-1}. Consequently, for the cathodic reduction the energy contribution of the activation entropy is positive, $T\Delta S^{\dagger}_{cat} = 27$ kJ mol^{-1}; λ is high and there is no dependence of η on ΔG°; for the anodic oxidation the activation entropy is very low, $T\Delta S^{\dagger}_{an} = -35$ kJ mol^{-1}, and there is a strong increase of η with $|\Delta G^{\circ}|$.
The calculated curve assumes a constant λ (and $(\Delta S^{\dagger})$ throught the whole electrode potential energy range (Figure 1). A $\Delta S^{\dagger}$ variable with the electrode potential [5], ca. $T\Delta S^{\dagger} = -35$ kJ mol^{-1} at E = 300 mV and $T\Delta S^{\dagger} = 7$ kJ mol^{-1} (298 K) at E = −400 mV will further improve the agreement in the anodic region.

NONEQUILIBRIUM SITUATIONS

Several less empirical theories have been employed to study electrochemical electron transfer reactions, such as the theories of Levich, Dogonadze, Kuznetsov, Ulstrup and coworkers [18]. Nevertheless such treatments can be reduced [19] to the same quadratic form of the theory of Marcus,

$$\Delta G^{\dagger} = c_0 + c_1\ (\Delta G^{\circ}) + c_2\ (\Delta G^{\circ})^2$$

where c_i are coefficients independent of ΔG°. However, we have shown that such a quadratic free energy relation is unable to interpret the asymmetry of the Tafel plots. This requires a more general theoretical model, such as ISM which for harmonic oscillators of a common force constant leads to

$$\Delta G^{\dagger} = c_0 + c_1\ (\Delta G^{\circ}) + c_2\ (\Delta G^{\circ})^2 + c_4\ (\Delta G^{\circ})^4 + c_6\ (\Delta G^{\circ})^6 + \ldots$$

owing to the quadratic dependence of η on $(\Delta G^{\circ})^2$.

The intersecting-state model [9] was developed for equilibrium situations and, consequently, d and η are the same for the forward and backward reactions, i.e. λ is independent of the direction of the reaction. Can the present model go beyond its derivation and contemplate nonequilibrium situations? The answer appears to be yes, because the interpretation of the asymmetry of the Tafel plots requires different λ values for the oxidation and reduction processes. Under the view that λ is a mesure of the «energy capacity» of the activated complexes, different λs imply different generalized transitions states for the anodic and cathodic electron transfers. Variational transition state theories [19-21] show that recrossing, tunnelling, internal state nonequilibrium, and solvent friction effects can introduce significant modifications on the conventional transition state theory. Since the anomalous features appears to be the slowness of the anodic process, the only effects which can contribute to the present findings appear to be recrossing and/or internal state nonequilibrium; frictional effects are only siginficant for high viscosity systems. The dependence of λ on $\Delta S^{\dagger}$ suggests that the former effect is the more important one. A nonequilibrium situation for the internal states implies a relatively inefficient vibrational energy reorganization for the $Cr(H_2O)_6^{2+}$ species, compared with $Cr(H_2O)_6^{3+}$ [22]. Although there are some differences in the stretching frequencies of these aquo-metal ions, these are not very large (1.26 times [23]). Conventional transition state theories are based essentially on the assumption that the passage via the saddle point is rate determining and, consequently, the reaction rate can be computed as the rate of passage at the saddle point. This implies that every trajectory en route from reagents to products crosses the saddle point only once. Having scaled the mountain pass and started its descent into the product region, a trajectory does not turn back. However, under certain conditions, for example at high energies, the saddle point region can lose its strategic importance and other dynamical features of the potential energy surface start to control the probability of reaction [20]. Here we would like to suggest a possible interpretation for the present findings.

Let us consider the model reaction A + BC → AB + C. When the reaction is thermoneutral, the relative kinetic energy of A and BC and AB and C will provide the motion along the reaction coordinate. The trajectories which go over the saddle point do not turn back, and the transition state coincides with the saddle point. However, if the reaction is exothermic or endothermic, the reaction energy must accommodated as internal energy of the activated complexes. Because there is an interconversion of translational and vibrational and rotational energies, the trajectories can suffer the influence of constraints perpendicular to the reaction coordinate, which will be reaction energy dependent. If after the saddle point the reaction valley is a narrow one, because of such constraints some trajectories which have passed the saddle point will be reflected back into the reactants valley. A critical configuration between the regions of «return» and of «no return» can possibly be established [20]. This configuration is crossed only once by the trajectories, but is displaced from the saddle point towards the narrow valley of the products. Consequently, the transition state does not coincide with the saddle point and is displaced towards the products. On the contrary if the valley of products is wide, no constraints will be forced upon the trajectories, after the saddle point. The saddle pass region is only crossed once by the trajectories, and the transition state coincides with the saddle point.

ACKNOWLEDGMENTS

We are grateful to Prof. D.G. Truhlar for a most stimulating and helpful discussion on the nonequilibrium effects. This work is supported by Instituto Nacional de Investigação Cientifica.

Received, 17th.October.1986

REFERENCES

[1] R.A. MARCUS, Ann. Rev. Phys. Chem., **15**, 155 (1964).

[2] P.P. SCHMIDT, «Specialist Report of Electrochem.», The Chemical Society London **5**, chap. 2 (1975); **6**, chap. 4 (1977).

[3] S.U.M. KHAN and J.O'M. BOCKRIS, in «Comprehensive Treatise of Electrochemistry», ed. B.E. CONWAY et al., Eds., Plenum Press, New York, **7**, 41 (1983).

[4] J.T. HUPP, H.Y. LIU, J.K. FARMER, T. GENNETT and M.J. WEAVER, J. Electroanal. Chem., **168**, 313 (1984).

[5] J.T. HUPP and M.J. WEAVER, J. Phys. Chem., **88**, 6128 (1984).

[6] J.T. HUPP and M.J. WEAVER, J. Phys. Chem., **89**, 2795 (1985).

[7] S.J. FORMOSINHO, Rev. Port. Quím., **28**, 38 (1986).

[8] S.J. FORMOSINHO, Rev. Port. Quím., **28**, 48 (1986).

[9] A.J.C. VARANDAS and S.J. FORMOSINHO, J. Chem. Soc. Chem. Commun., 163 (1986); J. Chem. Soc., Faraday Trans. 2, **82**, 953 (1986).

[10] H.D. BURROWS and S.J.FORMOSINHO, Rev. Port. Quím., **28**, 57 (1986).

[11] R.A. MARCUS, J. Phys. Chem., **67**, 853 (1963).

[12] B.S. BRUNSCHWIG, C. CREUTZ, D.H. MACARTNEY, T-K. SHAM and N. SUTIN, Faraday Discuss. Chem. Soc., **74**, 113 (1982).

[13] J.R. FERRARO, «Low-Frequency Vibrations of Inorganic and Coordination Compounds», Plenum Press. New York, 1971.

[14] T.D. TYMA and M.J. WEAVER, J. Electroanal. Chem. Interfacial Electrochem., **111**, 195 (1980).

[15] N. SUTIN, Annu. Rev. Nucl. Sci., **12**, 285 (1962); Prog. Inorg. Chem., **30**, 44 (1983).

[16] R.A. MARCUS, J. Chem. Phys., **24**, 966 (1956); **43**, 679 (1965).

[17] J. BURGESS, «Metal Ions in Solution» Wiley, London, 1978, p. 188.

[18] V.G. LEVICH, Adv. Electrochem. Electrochem. Eng., **4**, 249 (1966); R.R. DOGONADZE, A.M. KUZNETSOV and V.G. LEVICH, Electrochim. Acta, **13**, 1025 (1968); N. BRUNICHE-OLSEN and J. ULSTRUP, J. Chem. Soc. Faraday Trans. 1, **75**, 205, (1979).

[19] M.M. KREEVOY and D.G. TRUHLAR, in «Investigations of Rates and Mechanisms of Reactions», C.F. Bernasconi, Ed., Wiley, New York, 4th ed., part 1, p. 13.

[20] B.C. GARRETT and D.G. TRUHLAR, J. Am. Chem. Soc., **102**, 2559 (1980); P. PECHUKAS, Ber. Bunsenges. Phys. Chem., **86**, 372 (1982).

[21] D.G. TRUHLAR, W.L. HASE and J.T. HYNES, J. Phys. Chem., **87**, 2664 (1983).

[22] Such differences may be related to the large Jahn-Teller distortion in $Cr(H_2O)_6^{2+}$. It would be of interest to consider an electrode couple such as $Cu^{2+}_{(aq)}/Cu^{+}_{(aq)}$, where only one of the species is Jahn-Teller distorted, to see if a similar effect is observed.

[23] K. NAKAMOTO, «Infrared Spectra of Inorganic Coordination Compounds», Wiley-Interscience, New York, 1970.

RESUMO

O papel da ordem de ligação e da entropia dos estados de transição nas reacções de transferência de electrões.
Parte 4 — Reacções electroquímicas e a assimetria dos gráficos de Tafel entre as regiões anódica e catódica.

As barreiras de energia livre das reacções electroquímicas de transferência de electrões são dominadas pela reorganização da primeira camada de coordenação de iões metálicos. As reacções de transferência de electrão, homogéneo e heterogóneo (corrigidos do efeito da dupla camada eléctrica) podem ser estudadas dentro do mesmo formalismo com $\Delta G^{\ddagger}_{hom} = 2\ \Delta G^{\ddagger}_{het}$, *para a energia de reacção e a barreira de energia. A origem da assimetria dos gráficos de Tafel entre a região anódica e catódica é explicado pelo modelo de intersecção de estados nos seguintes termos: se* λ *(e* $\Delta S^{\ddagger}$*) é elevado os gráficos de Tafel são lineares; mas se* λ *(e* $\Delta S^{\ddagger}$*) é baixo os gráficos têm uma curvatura negativa. Estas interpretações parecem implicar que para reacções exotérmicas e* $S^{\ddagger}$ *baixo o ponto de selo não corresponde ao estado de transição devido a restrições dinâmicas ao longo do vale de reacção após o ponto de pela.*

M. F. RIBEIRO
F. RAMÔA RIBEIRO
Grupo de Estudos de Catálise Heterogénea,
Instituto Superior Técnico,
Av. Rovisco Pais,
1096 Lisboa Codex, Portugal

P. DUFRESNE
C. MARCILLY
Institut Français du Pétrole,
B. P. 311,
92500 Rueil-Malmaison, France

EFFECT OF CALCINATION CONDITIONS ON THE CATALYTIC PROPERTIES OF Ni H MORDENITE IN TOLUENE DISPROPORTIONATION

The title reaction has been studied on Ni H mordenites calcined under dry air or wet air. The presence of steam during the calcination increases the activity, selectivity in aromatics and stability of the Ni H mordenite, which can be attributed to the formation of super acid sites.

INTRODUCTION

Disproportionation of toluene catalysed by zeolites is of considerable scientific and industrial interest [1, 2]. The preparation of metal-acid zeolites includes several steps, namely thermal treatments whose experimental conditions have a marked influence on their catalytic properties.

The purpose of this work was to investigate the effect of the presence of steam during the calcination on activity, selectivity and stability of Ni H mordenite in the disproportionation of toluene.

EXPERIMENTAL

Two samples of Ni H mordenite have been prepared. The protonic form was obtained by ion exchange with an ammonium nitrate solution from a large pore sodium mordenite (900 Na zeolon), followed by calcination under dry or wet air (80 wt % H_2O) for 2 hours at 823 K. The nickel was introduced by ion exchange of H mordenite and the samples were again calcined under dry air for 2 hours at 773 K, followed by reduction with hydrogen for 3 hours at 723 K. The calcined catalyst under dry air will be designated as NiHM (d) and under wet air as NiHM (w).

Zeolite crystallinity was estimated from X-ray diffraction. The atomic Si/Al ratios were determined by ^{29}Si-NMR spectroscopy.

Characterization of the acidic function was performed by temperature-programmed desorption of ammonia [3, 4] and of the metallic function by electron probe and transmission electron microscopy (TEM).

The content in nickel was determined by X-ray fluorescence.

The activities were measured in a fixed bed reactor, under a pressure of 2.0 MPa, molar ratio H_2/toluene = 4 and variable temperature, to get toluene conversions, either lower than 10 % with space velocities of 5 h^{-1}, or between 40 and 50 % with space velocities

of 1.5 h^{-1}. The reaction products were analysed by GLC (50 m CP SIL5 capillary column). The coke content of the catalysts was determined by elemental microanalysis.

RESULTS

Both catalysts showed a nickel content of 1.1 wt % and metallic particles of different sizes from 9 to 150 Å. Acid sites of high strength were confirmed by temperature programmed desorption of ammonia, the NiHM (w) presenting a smaller number of acid sites but of higher strength.
The X-ray diffraction confirmed that crystallinity has not changed after calcination under dry or wet air. The atomic Si/Al ratio of NiHM (w) (5.3) is slightly higher than that of NiHM (d) (5.0) explained by Al removal from the lattice after calcination under wet air.
The catalytic performances of NiHM (d) and NiHM (w) in the toluene disproportionation are summarized as follows:

Activity

The values of temperature to obtain similar toluene conversions for both catalysts are presented in Table 1.

Table 1

Comparison of the values of temperature to obtain similar toluene conversions

Catalyst	Temperature (K) to obtain 5% < conv. < 10%	Temperature (K) to obtain 45% < conv. < 50%
NiHM (d)	638 ± 10	683 ± 10
NiHM (w)	588 ± 10	648 ± 10

Selectivity

Disproportionation of toluene lead to the production of benzene and xylenes, but simultaneously other secondary reactions occurred with the formation of non aromatic products (C_1 - C_9), mainly C_1 - C_4 products resulting from hydrogenolysis and hydrocracking reactions.
Both catalysts present a rather low selectivity in aromatics but NiHM (w) is more selective than NiHM (d) (conversion = 45 %, selectivity in aromatics for NiHM (d) = 83 % and for NiHM (w) = 88 %).

Stability

To check the stability, the catalysts have been aged for 6 hours at 793 K, under a pressure of 2.0 MPa, molar ratio H_2/toluene = 4 and a space velocity of 5 h^{-1}, so that coking would occur.
The values of temperature to get similar toluene conversions for both catalysts are presented in Table 2.

Table 2

Comparison between the values of temperature required after ageing to maintain constant toluene conversion

Catalyst	Temperature (K) to obtain 45% < conv. < 50%
NiHM (d)	758 ± 10
NiHM (w)	703 ± 10

NiHM (w) presents a better resistance to deactivation, although both catalysts have suffered a strong deactivation.
The coke content (~1.2 % wt) of both catalysts is quite small.

DISCUSSION

From the analysis of the results we can conclude that the calcination under wet air compared with the calcination under dry air,

increases the catalytic properties of the NiHM mordenite.

The calcination in presence of steam produces Lewis sites [4, 5] that interact with the protonic sites producing super acid sites which are very active in toluene disproportionation. This explains the increase of activity observed for the NiHM (w).

The increase of the selectivity can be explained by an increase of the strength of the acid function compared with the metallic function. Toluene disproportionation is an acid reaction, so the selectivity in aromatics is increased.

The increase of the stability can be attributed to the decrease of the number of Bronsted sites, which are very active in coke formation [6].

The low values of coke obtained for both catalysts after the reaction, suggest that deactivation occurred by blocking of the pores, due to the coke formed in the pore openings. This type of deactivation is usual in mordenites [7, 8]; in fact Guisnet *et al.* [6] showed that in mordenites, 1 % wt. of coke deposited can decrease 95 % of their activity.

Received, 19th June 1986

REFERENCES

[1] N.S. GNEP, M.L. MARTIN DE ARMANDO, M. GUISNET. *React. Kinet. Catal. Lett.*, **13**, 183 1980.

[2] M. FILIPA RIBEIRO, P. DUFRESNE, C. MARCILLY, R. RAMÔA RIBEIRO. *J. Mol. Catal.*, **35**, 227, 1986.

[3] C.V. HIDALGO, H. IOTH, T. HATTORI, M. NIWA, Y. MURAKANI. *J. Catal.*, **85**, 362, 1984.

[4] C. MIRODATOS, B.H. HA, K. OTSUKA, D. BARTHOMEUF. *Proceed. Fifth Int. Conf. on Zeolites*, Naples (Ed. L.V.C. Rees), p. 382, 1980.

[5] C. MIRODATOS, D. BARTHOMEUF. *J. Chem. Soc. Chem. Commun.*, 39, 1981.

[6] N.S. GNEP, M.L. MARTIN DE ARMANDO, C. MARCILLY, B.H. HA, M. GUISNET. *Catalyst Deactivation* (Eds. B. Belmon and G.F. Froment), Elsevier, p. 79, 1980.

[7] J.N. BRECKMAN, G.F. FROMENT. *Ind. Eng. Chem. Fundamentals*, **18**, 245, 1979.

[8] C. MIRODATOS, J.A. DALMON, E.D. GARBOWSKI, D. BARTHOMEUF. *Zeolites*, **2**, 125, 1982.

RESUMO

Influência das condições de calcinação nas propriedades catalíticas de NiH mordenite na dismutação do tolueno.

A reacção de dismutação do tolueno foi estudada sobre NiH mordenites após calcinação sob ar seco e sob ar húmido. A presença de vapor de água durante a calcinação tem um efeito altamente positivo, pois aumenta a actividade, a selectividade em aromáticos e a estabilidade do catalisador NiH mordenite, o que pode ser explicado pela formação de centros activos super ácidos.

A.M. AMORIM DA COSTA
Dept. Chemistry — The University
3000 Coimbra — Portugal

CARBON-HYDROGEN STRETCHING RAMAN MODES AND LATERAL INTERACTION IN N-DODECYL COMPOUNDS

Using spectroscopic data taken from the Raman C-H vibrational region, intramolecular order and lateral chain interactions are studied for solid, liquid-crystalline and normal liquid states in n-dodecane, n-dodecanol, lauric acid, n-dodecanethiol, n-dodecylamine, zinc and lead dodecanoates, n-dodecylamine hydrochloride and dodecylamine-water systems.

1. INTRODUCTION

The features of the C-H stretching vibrational region makes Raman spectroscopy one of the best tools to probe the conformation, environment and dynamics of hydrocarbon systems and of biomembranes which contain long methylene residues [1 and references therein]. In 1972, Brown and co-workers [2] and K. Larsson [3] have shown that when the hydrocarbon chains are in a liquid state the dominant feature in the CH stretching region of the Raman spectra (2800-3000 cm^{-1}) is a peak at about 2850 cm^{-1} which they have assigned to the symmetric stretching vibration of the CH_2 groups; however, when the same chains are in a solid state with close-packing of planar zig-zag chains, the dominant feature in that spectral region would be a peak at about 2885 cm^{-1}, originally interpreted by those authors as due to the symmetric stretching vibrations of the CH_3 groups. Relating the shape of the C-H stretching vibration region to the close-packing arrangements of the hydrocarbon chains and to the effects of different degrees of polar environment of CH_2 and CH_3 groups, those authors have used the ratio of the 2885/2850 cm^{-1} peak intensities as an order/disorder parameter to estimate the degree of disorder of the chains; and the ratio of the 2930/2850 cm^{-1} peak intensities as a measure of the degree of polar environment of the hydrocarbon chains.

Afterwards, the assignments of the vibrational modes appearing in the C-H Raman spectral region have been completely re-examined and it has been shown that the observed Raman scattering due to these modes is strongly determined by several Fermi resonances which depend to a different extent on wether the alkyl residue has an all-trans or a distorted structure [1, 4-8].

This work is an attempt to consider various structural and dynamical aspects of some n-dodecyl systems in relation to the lateral contact among the hydrocarbon chains as estimated from a quantitative analysis of the C-H Raman spectral region.

2. EXPERIMENTAL

Raman spectra were obtained with 514.5 nm excitation from a Spectra—Physics 164 argon ion laser. The scattered light from the sample was focused onto the entrance slit of a Varian Cary 82 Raman Spectrophotometer operating with a spectral slitwidth of 3-4 cm^{-1} (constant over displacement 0-3500 cm^{-1}). The signal from the photon counting system was displayed on a strip chart recorder.

The n-dodecane, lauric acid, n-dodecanol, n-dodecanethiol, and dodecylamine used in this study were of purum grade and have been purified either by destillation or by recrystallization from acetone. Dodecylamine hydrochloride and zinc laurate were prepared, respectively, by reacting a known quantity of dodecylamine with hydrochloride solution and lauric acid with zinc nitrate in solution. The salts were purified by recrystallization from acetone. Mixtures of dodecylamine with water were prepared by measured amounts of amine and double distilled water in sealed glass cells which were allowed phase equilibria during two days in a temperature bath of about 90°C.

The solid samples were contained in 1 mm melting point cappilaries; solution samples were contained into $10 \times 10 \times 50$ mm glass cells.

The accuracy in reported frequencies is estimated to be ± 2 cm^{-1}.

Recordings above room temperature were achieved by a temperature bath design based on an insulated alluminium jacket fitted with ITT Vulcan heater in the solid block. A temperature accuracy better than ± 2°C was obtained for these recordings. In the evaluation of peak intensities, Raman band heights were measured as the spectral heights above a background drawn as a straight line between minima in the spectra which is the combination of broad band luminiscence with the Raman spectrum of the sample. The experimental error in these intensity measurements could be of the order of 10 %.

3. SPECTRAL ANALYSIS AND RESULTS INTERPRETATION

In analyzing the observed changes in the C-H Raman spectral region one must distinguish conformational effects which are intrinsic to the modes from effects due to Fermi resonance interaction with methylene bending mode overtones [9]. Doing that, special attention must be paid to the following experimental observations:

i) the band located between 2845 and 2860 cm^{-1}, referred to as d^+, which is the overlapping scattering from several strong transitions with mostly methylene in-phase symmetric stretching character, does not significantly change with the conformation of the chain. Its peak intensity seems to keep the same average value with respect to the number of gauche defects; and its frequency is shifted upward in a characteristic way depending solely on the length of the longest trans-segment occurring in the chain [10];

ii) the band between 2880 and 2910 cm^{-1}, referred to as d^-, which can be associated mainly with the in-phase CH_2 antisymmetric stretching mode, becomes less intense, broader and eventually structured with frequency shifts upwards by about 8 to 10 wavenumbers, when gauche structures are introduced. The more distorted the molecule, the weaker is the band [1];

iii) a broad, less intense band near 2930 cm^{-1}, referred to as r^+, assigned to the methyl symmetric stretching mixed with a second manifold of overtones and combinations of the CH_2 bendings, exhibits a peak intensity strongly dependent on the number and position of gauche defects in the chain. Its average value increases with gauche content [10].

Two main attempts have been made to give a general interpretation of these observations. The first one [1, 6] treats a highly disordered polymethylene chain as a gas of uncoupled

CH_2 groups with the assumption that gauche structures 'isolate' methylenes from each other. When the concentration of trans structures increases, the spectral features of an 'isolated' CH_2 group are gradually replaced by the spectral pattern predicted for an infinite trans chain: the intensity of the CH_2 symmetric stretching mode near 2850 cm^{-1} substantially decreases since it lends intensity to many levels, and the peak near 2930 cm^{-1} is even less intense because of the change of the shape of the dispersion curve of the methylene bending phonon branch. Thus, the Raman intensities ratio $R = {}_{2930}/I_{2850}$ may be taken as proportional to the relative concentration of conformers. Such a ratio should increase with the increase of gauche structures.

The second attempt has been that of Snyder and co-workers [9, 11] who supposed that the frequency dispersion observed for ordered and disordered methylene chains is very similar, and proposed that the band near 2930 cm^{-1} is a composite of two overlapping bands, one from the methyl group at about 2938 cm^{-1}, and one from the methylene chain at about 2922 cm^{-1}. The latter component would be affected by chain conformation, while the former component is affected by the solvent. Thus, the intensity ratio $R = I_{2930}/I_{2850}$ would be a quantity sensitive both to chain conformation and to solvent, though not necessarily to solvent polarity. Thus, the absolute values of this Raman intensities ratio would depend both on the order due to intrachain structure and that due to lateral crystalline interactions associated with the molecular packing.

Developing an order parameter which will allow an analysis of the lateral crystalline interactions, the intensity of the band at about 2880 cm^{-1} has been considered in a comparison with the intensity of the band at 2850 cm^{-1}. Actually, differences in this peak intensities ratio result primarily from changes in the intensity of the 2850 cm^{-1} band due to different chain packing involving different lateral chain interactions and leading to different halfwidths of the 2850 cm^{-1} line. The CH_2 antisymmetric stretching fundamental at about 2880 cm^{-1} is quite insensitive to chain packing [9-10, 12].

Using such an intensities ratio, a quantitative measure of the lateral order in hydrocarbon systems has been proposed by Gaber and Peticolas [13] defined by the following expressio

$$S_{lat} = (r - 0.7)/1.5$$

where r is the Raman intensities ratio I_{2880}/I_{2850} for the sample under study; 0.7 is the value of r for liquid hexadecane; and 1.5 is the difference between the r values for crystalline and liquid hexadecane. In terms of this relation, $S_{lat} = 1$ will correspond to chains in the crystalline state, whereas $S_{lat} = 0$ corresponds to chains in the liquid state.

It must be noted, however, that only the peak intensities ratio (not integrated intensities) will be environmentally sensitive since the Fermi resonance interaction although affecting the distribution of intensity does not significantly affect the total integrated intensity of the fundamentals themselves. It must be also noted that r is a hybrid quantity because the intensity at both 2880 and 2850 cm^{-1} originates from multiple vibrational modes, as it is obvious with unsaturated alkyl chains [12]

Experimental values of the C-H Raman region of studied n-dodecyl compounds are presented in Table I. Figure 1 illustrates the main features of this spectral region in the case of liquid, solid and aqueous dodecylamine.

The intrachain structure order parameter, i.e., the I_{r+}/I_{d+} peak intensities ratio shows that the intramolecular order degree depends quite siginifcantly on the end groups, mainly in the solid state. It is known that in n-paraffins most efficient chain packing, from an energetic point of view, corresponds to a triclinic packing where all chain planes parallel, or to an othorrhombic packing where every second

Table I

C-H Raman stretching frequencies, peak intensities ratio and lateral interactions parameter values for some n-dodecyl systems

System	ν/cm^{-1}			Intensities ratio		
	$\nu_{(d+)}$	$\nu_{(d-)}$	$\nu_{(r+)}$	$\frac{I_{d-}}{I_{d+}}$	$\frac{I_{r+}}{I_{d+}}$	$S_{lat.} = \frac{a-g}{b-g}$ (*)
n-dodecane						
solid (77K)	2845	2868	2930	2.20	0.25	1.00
liquid (295K)	2848	2871	2932	0.80	0.61	0.00
n-dodecanol						
solid (290K)	2845	2870	2925	1.75	0.39	0.68
liquid (300K)	2850	2876	2925	0.77	0.65	—0.02
lauric acid						
solid (295K)	2846	2879	2925	1.66	0.53	0.61
liquid (328K)	2852	2905	2927	0.85	0.85	0.04
n-dodecanethiol						
solid (260K)	2845	2870	2925	1.70	0.30	0.64
liquid (295K)	2848	2870	2923	0.65	0.74	—0.11
n-dodecylamine						
solid (295K)	2845	2880	2925	1.82	0.31	0.73
liquid (323K)	2850	2888	2925	0.77	0.64	—0.02
n-dodecylamine hydrochloride						
solid (295K)	2846	2880	2925	2.01	0.61	0.86
zinc dodecanoate						
solid (295K)	2848	2879	2925	2.04	0.61	0.89
Lead dodecanoate						
solid (295K)	2847	2880	2925	1.87	0.60	0.76
smectic (373K)	2852	2898	2925	1.16	0.87	0.26
Cubic (378K)	2852	2898	2925	0.87	0.87	0.05
liquid (383K)	2853	2898	2925	0.87	0.89	0.05
25 % dodecylamine-water						
smectic (295K)	2845	2878	2930	1.18	0.44	0.27
nematic (308K)	2850	2888	2930	1.14	0.47	0.24
liquid (333K)	2850	2900	2930	0.68	0.50	0.09

(*) These S_{lat} values have been calculated relative to crystalline n-dodecane, assuming the same magnitude for the interchain vibrational coupling and the phonon dispersion broadening due to chain shortening, i.e., $a = I_{d-}/I_{d+}$ intensities ratio for the sample: $b = I_{d-}/_{d+}$ intensities ratio for crystalline n-dodecane; and $g = I_{d-}/I_{d+}$ intensities ratio for liquid n-dodecane.

chain plane is perpendicular to the rest [14]. In these close-packing arrangements the hydrocarbon chains are always in the extended planar zig-zag conformation, with rotational freedom. This will be the characteristic chain packing of crystalline n-dodecane, at 77K.

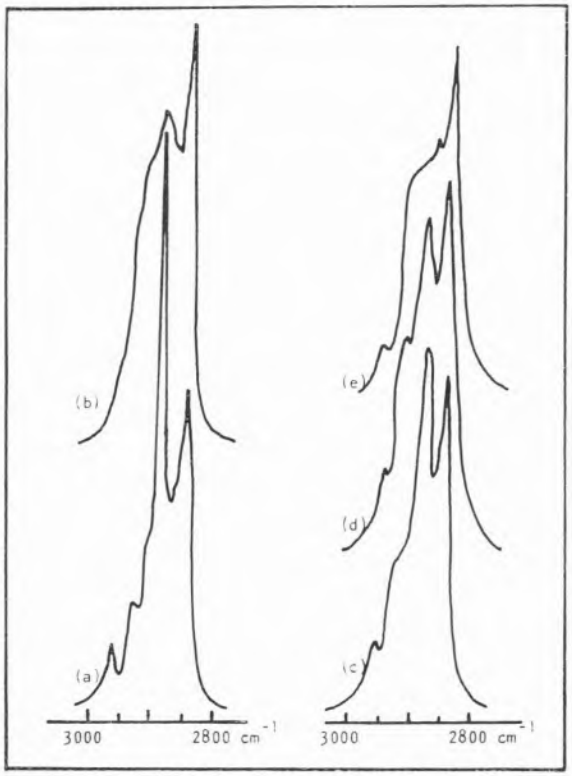

Fig. 1

The C-H stretching vibration region in the Raman spectra of (a) solid dodecylamine at 295K; (b) liquid dodecylamine at 323K; (c), (d), (e), respectively, smetic (295K), nematic (308K) and isotropic solution (333K) 25 % (w/w) dodecylamine in water.

When the end methyl groups are substituted by heavier and/or polar groups the chains may be anchored at the position of those groups, and in such a situation only oscillational movements of the chains are possible.

In n-faty acids association through hydrogen bonds of the polar carboxylic group leads to dimerization with an increase of the effective chain length. Moreover, the carboxylic group may act like an anchor fixing the chain end and leading to possible tight chain folding. From crystalline n-dodecane to lauric acid there is a significant increase of molecular disorder. This increase is much less in the case of n-dodecanol where the association through the head group is not so strong; and even less in the cases of n-dodecanethiol and n-dodecylamine.

In n-dodecylamine hydrochloride, zinc dodecanoate and lead dodecanoate, the bulky end ionic groups instead of anchoring the chain seem to have a great amount of mobility from which result oscillational movements of the chains that lead to a quite high degree of chain distortion [15].

A decrement of about 30 to 50 % is observed in the chain order on going from the solid to liquid-crystalline, as much as the observed on going directly from solid to normal liquid. It is not surprising, since the requirement for formation of a lipid-water liquid crystal is that the hydrocarbon chains are transformed into a state with intramolecular disorder such as that in the liquid [14].

Concerning the lateral order parameter values, it is observed that the dodecylhydrocarbon chains in the solid state are characterized by a value of S_{lat} ca. 0.6-0.9, and a value of S_{lat} about 0.25 for the chains in anisotropic liquid crystalline mesophases. Like in the liquid, the isotropic mesophases are characterized by very small S_{lat} values which characterize an almost complete loss of lateral chain interaction.

From anisotropic to isotropic liquid-crystalline like to isotropic liquid the main changes are due to the contribution of interchain interactions. The parallel mean orientation of the molecules which is a common feature to the solid and the scmetic and the nematic mesophases [16] is a molecular arrangement determined by interchain interactions. The differences in the S_{lat} values for the solid and the liquid-crystalline do not come from differences in lateral interactions, but from the intrachain structures: in the solid state the chains constitute one (all trans) species, whereas in liquid-crystals, like in normal liquids, multiple rotameric forms are present.

4. CONCLUSION

The foregoing analysis leads to the conclusion that in liquid crystal and normal liquid systems the intramolecular vibration of the chains are essentially the same, whereas the intermolecular interactions are quite different. In solids and liquid crystalline mesophases the lateral interactions are similar, but the intrachain order is very much different due to an higher degree of mobility of the chains. In solid and liquid-crystalline states the chains are in lateral contact so that rotational mobility about the long axis of the molecules is very constrained [17-18].

ACKNOWLEDGEMENTS

The financial support from INIC and the work facilities in the Department of Chemistry of the University of Coimbra are greatly acknowledged.

Receibed, 17th.November.1986

REFERENCES

[1] L. RICARD, S. ABBATE and G. ZERBI, *J. Phys. Chem.*, **89**, 4793 (1985).
[2] R.G. BROWN, W.L. PETICOLAS and E. BROWN, *Biochem. Biophys. Res. Commun.*, **54**, 358 (1972).
[3] K. LARSSON, *Chem. Phys. Lipids*, **9**, 181 (1972).
[4] R.G. SNYDER and J.R. SHERER, *J. Chem. Phys.*, **71**, 5221 (1979).
[5] G. ZERBI and S. ABBATE, *Chem. Phys. Lett.*, **80**, 455 (1981).
[6] S. ABBATE, G. ZERBI and S.L. WUNDER, *J. Phys. Chem.*, **86**, 3140 (1982).
[7] R.G. SNYDER, S.L. HSU and S. KRIMM, *Spectrochim. Acta*, **34A**, 395 (1978).
[8] S. ABBATE, S.L. WUNDER and G. ZERBI, *J. Phys. Chem.*, **88**, 593 (1984).
[9] R.G. SNYDER, H.L. STRAUSS and C.A. ELLIGER, *J. Phys. Chem.*, **86**, 5145 (1982).
[10] R.A. MACPHAIL, H.L. STRAUSS, R.G. SNYDER and C.A. ELLIGER, *J. Phys. Chem.*, **88**, 334 (1984).
[11] R.G. SNYDER, *J. Chem. Phys.*, **76**, 3342 (1982).
[12] D.F. WALLACH, S.P. VERMA and J. FOOKSON, *Biochim. Biophys. Acta*, **559**, 153 (1979).
[13] B. GABER and W.L. PETICOLAS, *Biochim. Biophys. Acta*, **465**, 260 (1977).
[14] K. LARSSON, *Physicochimie des composées amphiphiles* (Colloques Nationaux du C.N.R.S., Bordeaux-Lac, 1978) pp. 17-25.
[15] A.M. AMORIM DA COSTA, *Rev. Port. Quim.*, **25**, 57 (1983).
[16] G.W. GRAY and P.A. WINSOR, *Liquid Crystals and Plastic Crystals* (John Wiley and Sons, Chichester, 1974), vol. 1, pg. 6.
[17] R.G. SNYDER, J.R. SCHERER and B.P. GABER, *Biochim. Biophys. Acta*, **601**, 47 (1980).
[18] M.G. BROADHURST, *J. Res. Nat. Bur. Stand., Sect. A*, **66**, 261 (1962).

RESUMO

Uso das vibrações de elongação carbono-hidrogénio do espectro de Raman no estudo de interacções laterais em compostos de n-dodecilo.

Por análise da frequência e intensidade relativa das bandas devidas às elongações carbono-hidrogénio do espectro de Raman, procura estimar-se o grau de ordem intra- e inter-molecular das cadeias hidrocarbonadas de alguns compostos de n-dodecilo em diferentes estados de cristalinidade.

M. BROTAS DE CARVALHO
M. REGINA SALES GRADE,
ANA P. CARVALHO
Centro de Química-Física e Radioquímica, INIC
Universidade de Lisboa, Portugal

M. J. BELZUNCE
S. MENDIOROZ
J. A. PAJARES
Instituto de Catálisis y Petroleoquímica,
C.S.I.C., Madrid, España

DIATOMITOS DE RIO MAIOR E DE ÓBIDOS: COMPOSIÇÃO QUÍMICA E CARACTERÍSTICAS MINERALÓGICAS E TEXTURAIS

Realizou-se um estudo sobre a composição química, características estruturais e propriedades adsortivas de amostras de diatomitos de jazigos de Rio Maior e de Óbidos.

A sua composição química, características estruturais e propriedades de adsorção foram determinadas recorrendo à absorção atómica, análise termogravimétrica, difracção de Raios X, espectroscopia do infravermelho, adsorção de azoto a 77 K e adsorção de corantes em solução.

Os resultados mostram que os minerais apresentam uma grande analogia química, com uma percentagem de sílica de aproximadamente 80 % e de alumina de 6 %, nos diferentes minerais estudados constituídos principalmente por opalo A, com impurezas de quartzo α (de origem possivelmente detrítica), argilas, elevada percentagem de matéria orgânica, e ainda feldspatos (apenas nos diatomitos de Óbidos).

A área específica dos diatomitos de Rio Maior é cerca do dobro da área dos de Óbidos.

INTRODUÇÃO

Os diatomitos, também designados por terras de infusórios, são rochas sedimentares, constituídas por restos de esqueletos fossilizados de organismos unicelulares aquáticos, cuja identificação, quer nos fósseis quer nos seres vivos, tem sido objecto de vários trabalhos a partir de 1880. No entanto, só em 1946, apareceu a primeira sistematização das diatomáceas fósseis existentes em Portugal (jazigos de Rio Maior, Óbidos e Alpiarça) numa publicação de Andrade da Silva [1].

Estas rochas, com aparência terrosa, de cor branca a amarelo rosado, friáveis e suaves ao tacto, são constituídas essencialmente por sílica amorfa, que pode atingir os 94 % para as de melhor qualidade, e por outros elementos, em baixa percentagem, como alumínio, ferro, cálcio, magnésio, potássio, titânio, etc. Os materiais que frequentemente acompanham os depósitos de diatomitos são as argilas, cristais insolúveis de quartzo, materiais inorgânicos como carbonatos, sulfatos e halogenetos e ainda matéria orgânica de origem animal ou vegetal.

A estrutura e a composição das diatomáceas fósseis conferem a estas rochas características como a baixa densidade, elevada porosidade e inércia química, tornando-as particularmente importantes em certas aplicações industriais.

Actualmente os diatomitos nacionais utilizam-se quase exclusivamente como aditivos no fabrico de cimento, papel e borracha. Comprovando-se a boa qualidade destes materiais poderão encarar-se outras aplicações, por exemplo, como adsorventes na indústria alimentar, para a purificação de açúcar, azeite, vinhos e vinagres, na indústria farmacêutica e de produtos químicos, na produção de produtos refractários e ainda como material de suporte de catalisadores metálicos.

De entre os jazigos portugueses, classificados por Leandro [2] em grupos de acordo com a sua posição geológica, salientam-se os diatomitos pliocénicos de Óbidos e de Rio Maior,

tendo estes uma reserva estimada em 20 milhões de toneladas.

Os diatomitos de Rio Maior estão depositados sobre jazigos de lenhite, cuja exploração parece estar prevista no Plano Energético Nacional, pelo que se pensa que a possibilidade de exploração conjunta dos dois minerais abrirá novas perspectivas aos diatomitos nacionais.

O estudo agora apresentado sobre a caracterização química, mineralógica e textural destes materiais, embora incompleto, destina-se a contribuir para o seu conhecimento e valorização.

PARTE EXPERIMENTAL

MATERIAIS ESTUDADOS

Os diatomitos foram colhidos directamente nos jazigos do couto mineiro n.º 3 de Rio Maior e do couto mineiro n.º 36 da Quinta do Jardim [2] de Óbidos, sob a forma de blocos de muito baixa densidade e volume entre 0,5 e 2 dm^3, com aspecto homogéneo e cor branca acinzentada.

Estes materiais foram divididos pelo Centro de Química-Física e Radioquímica de Lisboa e pelo Instituto de Catalisis y Petroleoquímica de Madrid (cerca de 1 Kg de cada um por cada Centro). As amostras para os diferentes ensaios foram retirados daquelas fracções depois do minério ter sido triturado, homogeneizado e mantido em ambiente de humidade constante.

ANÁLISE QUÍMICA

A sílica, componente mais abundante dos diatomitos, foi determinada em várias amostras, segundo um dos métodos clássicos de análise deste composto [3]. Numa primeira fase, procedeu-se à calcinação do material, para eliminação da matéria orgânica e transformação em óxidos dos possíveis carbonatos, determinando-se a perda de peso sofrida nesta operação. O produto calcinado foi então atacado com ácido fluorídrico e algumas gotas de ácido sulfúrico, evaporado até à secura, e de novo calcinado. Os valores de sílica, calculados a partir da perda de peso dos produtos calcinados, foram referidos, em percentagem, aos pesos iniciais das amostras secas a 140ºC. De entre os componentes menores determinaram-se, por absorção atómica, os teores em ferro, alumínio, magnésio e cálcio, após solubilização, por fusão com carbonato de sódio anidro, dos resíduos calcinados resultantes da eliminação da sílica pelo ácido fluorídrico, tendo sido utilizados dois espectrofotómetros de absorção atómica Perkin-Elmer 3030 (em Madrid) e 403 (em Lisboa).

ANÁLISE TERMOGRAVIMÉTRICA

A análise termogravimétrica foi realizada num aparelho Perkin-Elmer constituído por uma microbalança TGS-2, um controlador de temperatura e um registador XY directamente ligado ao sistema de armazenamento de dados, com uma sensibilidade de 2 μg, sendo a perda de peso dada directamente em percentagem do peso da amostra.

As análises foram efectuadas em atmosfera de ar até 900ºC, com uma velocidade de aquecimento de 10º/min., com amostras de 20 a 50 mg previamente mantidas durante 24 horas em excicador com cloreto de cálcio anidro.

ANÁLISE POR ESPECTROFOTOMETRIA DO INFRAVERMELHO

A análise espectral foi realizada num espectrofotómetro de infravermelho Perkin-Elmer 682 de feixe duplo, com registador e microprocessador electrónico, e com a sensibilidade de ± 4 cm^{-1} no intervalo 4000-2000 cm^{-1} e de ± 2 cm^{-1} entre 2000-400 cm^{-1}.

Na preparação das amostras foram utilizadas pastilhas de brometo de potássio, com uma percentagem de 2-3 % de amostra.

ANÁLISE POR DIFRACÇÃO DE RAIOS X

Os difractogramas de Raios X, para o estudo da composição mineralógica, foram obtidas com duas instalações da marca Philips, modelos PW 1865 (em Lisboa) e PW 1710 (em Madrid), sempre com a radiação Kα do cobre, $\lambda = 1{,}5418$ Å, e uma velocidade de varrimento de 2°/min. Nas duas instalações e com amostras diferentes (de Óbidos e de Rio Maior), obtiveram-se espectros idênticos.

ADSORÇÃO DE GASES

Recorreu-se à adsorção física de gases para determinar as propriedades texturais dos diatomitos.
Nestes estudos foi utilizada uma instalação para volumetria de adsorção do tipo convencional, medindo-se a adsorção de N_2 a 77 K, nas amostras de diatomito previamente desadsorvidas a 100°C, durante 1 hora, em vazio melhor do que 10^{-3} Pa.

ADSORÇÃO DE CORANTES

Na caracterização dos diatomitos por adsorção em fase líquida e após ensaios prévios realizados com uma vasta gama de corantes, foram utilizadas soluções aquosas de azul de metileno (AM) (Erba) e de violeta de cristal (VC) (Merck).

As experiências foram realizadas em pequenos frascos tapados, mantidos num banho termostatizado a 25°C, com agitação, sendo os tempos de contacto de cerca de 2 horas. A variação de concentração da fase líquida foi determinada por espectrofotometria do visível, utilizando um espectrofotómetro Pye-Unicam SP 1800, nos comprimentos de onda 610 nm, para o azul de metileno, e 590 nm, para o violeta de cristal.
Optimizaram-se as condições experimentais para obter um número suficiente de resultados de equilíbrio de adsorção, de modo a poder traçar as respectivas isotérmicas até um patamar bem definido.

RESULTADOS

ANÁLISE QUÍMICA

Os teores encontrados para os componentes mais comuns dos diatomitos, referidos a amostras secas a 140°C, estão indicados na Tabela I. Os valores inscritos nas colunas I, II e III, correspondem em cada caso a análises realizadas em Lisboa com amostras diferentes retiradas de 1 Kg de material homogeneizado proveniente de Rio Maior ou de Óbidos. Na coluna IV, indicam-se os resultados de análises idênticas realizadas em Madrid a partir de uma outra fracção de 1 Kg do material homogeneizado.
O exame da Tabela I mostra que o desvio relativo para os teores em sílica é sem-

Tabela I

Resultados da análise química, para alguns componentes dos diatomitos de Rio Maior e de Óbidos.

	Rio Maior					Óbidos			
	I	II	III	IV	Média	I	II	III	Média
SiO_2	77.5	77.7	81.0	78.02	78.6	76.0	81.0	81.0	79.3
Al_2O_3	5.7	5.7	5.7	6.11	5.8	7.0	5.1	5.6	5.9
Fe_2O_3	1.6	1.7	1.4	1.12	1.5	1.1	1.0	1.6	1.2
CaO	0.2	0.2	0.3	0.74	0.4	0.3	0.2	0.2	0.2
MgO	0.5	0.5	0.3	0.12	0.4	0.4	0.3	0.3	0.3
Perda por calcinação	11.2	11.9	9.2	12.16	11.1	11.3	10.3	10.4	10.7

pre $< 2\ \%$. Os valores registados para os componentes menores foram obtidos por absorção atómica, a partir de rectas padrão, traçadas pelo método dos mínimos quadrados com coeficientes de correlação superiores a 0,998.

números de onda de 1250-400 cm^{-1}, sendo a mais intensa a que se situa a 1098 cm^{-1}. No intervalo referido o quartzo, a cristobalite, a tridimite e a sílica natural hidratada apresentam espectros similares, sendo difícil a distinção entre estas fases [5]. Distinguem-se,

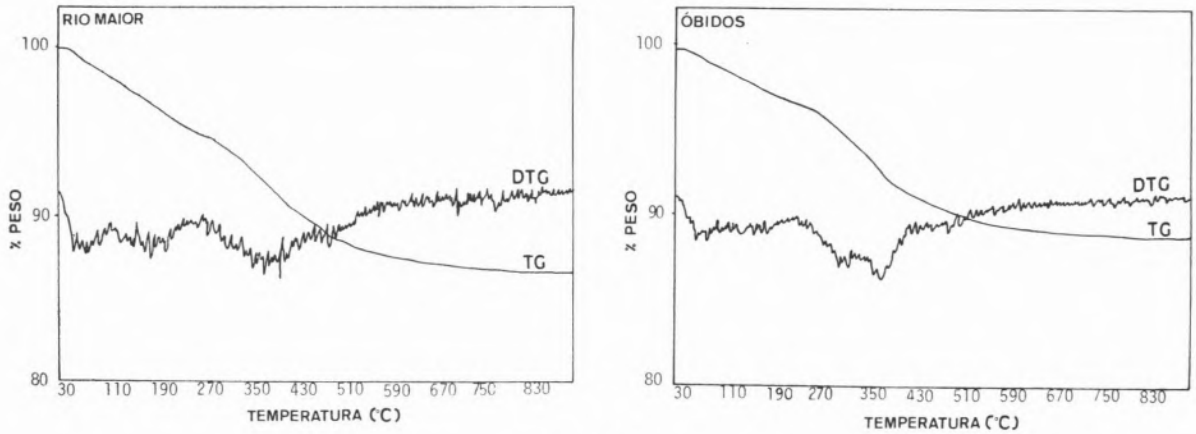

Fig. 1

Termogramas (TG) curvas diferenciais (DTG).

ANÁLISE TERMOGRAVIMÉTRICA

Na Fig. 1 estão representados os termogramas (TG) e as curvas diferenciais (DTG) correspondentes.

Os resultados obtidos com os dois diatomitos são similares, e mostram, praticamente, a inexistência de carbonatos, os quais, se existissem em quantidade apreciável, deviam originar um pico na zona dos 600°C, que não se detecta. A diminuição de peso, até 600°C, traduzida pelas curvas TG, embora acentuada, não apresenta patamares bem definidos, pelo que apenas se pode afirmar que deve ser atribuída à água e matéria orgânica incorporadas no material [4].

ANÁLISE POR ESPECTROFOTOMETRIA DO INFRAVERMELHO

Os espectros traçados em percentagem de transmitância versus número de onda, apresentam-se na Fig. 2.

As bandas mais características são as correspondentes à sílica e localizam-se entre os

no entanto, nos espectros obtidos com as duas amostras de diatomitos (Fig. 2) e mais nitidamente no caso da amostra de Rio Maior, um doblete a 790-780 cm^{-1}, e uma banda mais fraca a 600 cm^{-1}, características do quartzo α.

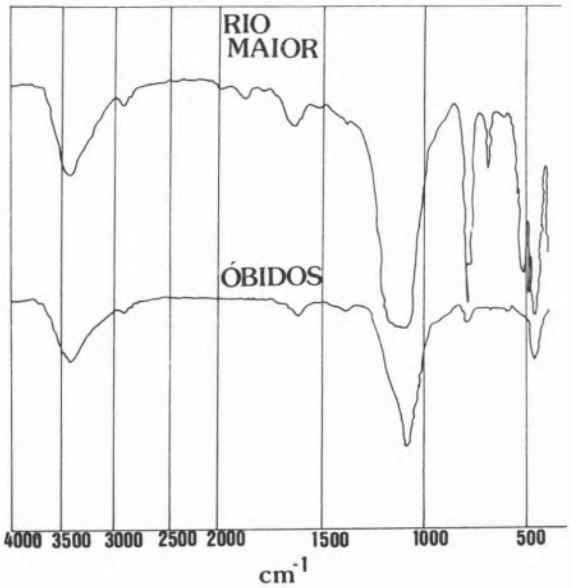

Fig. 2

Espectros de Infravermelho.

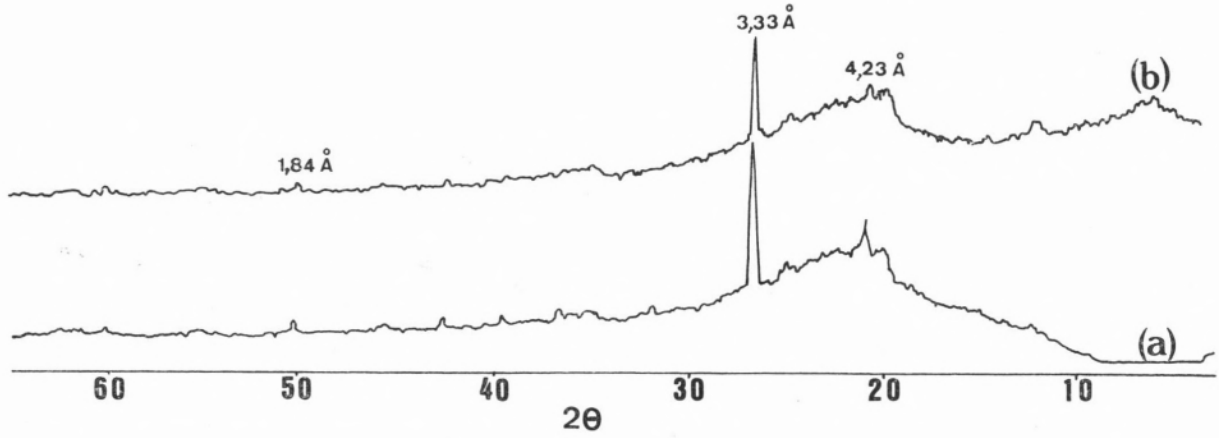

Fig. 3

Difractogramas da amostra de Rio Maior: (a) sem tratramento; (b) após tratamento com água oxigenada.

A banda de absorção a 3422 cm^{-1} corresponde à vibração de elongamento de moléculos de água unidas por pontes de hidrogénio e a banda a 1622 cm^{-1} à vibração de flexão dos grupos SiOH.

A pequena banda a 1440 cm^{-1} pode atribuir-se a presença de vestígios de carbonatos, principalmente na amostra de Óbidos. A ocorrência de bandas nos intervalos de 1970-1900 cm^{-1} e 3000-2800 cm^{-1} revelam a existência duma

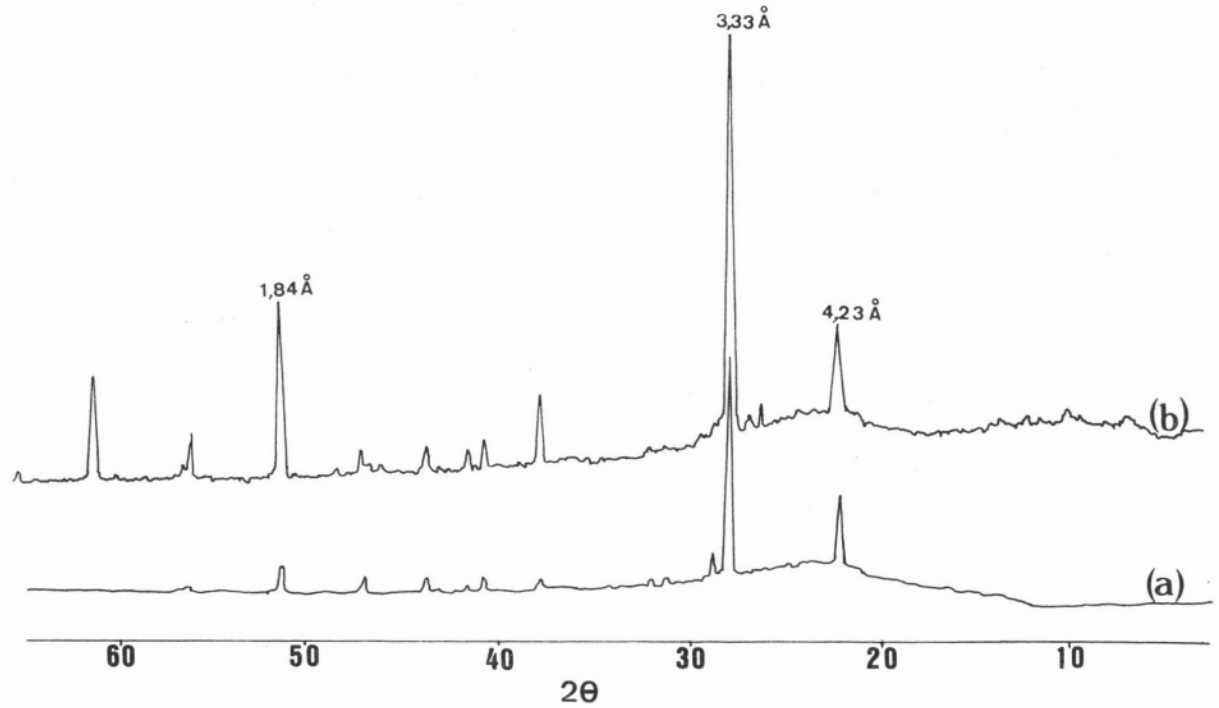

Fig. 4

Difractogramas da amostra de Óbidos: (a) sem tratamento; (b) após tratamento com água oxigenada.

maior percentagem de matéria orgânica nos diatomitos de Rio Maior.

ANÁLISE POR DIFRACÇÃO DE RAIOS X

Nas Figs. 3 e 4 estão representados os difractogramas das amostras de Rio Maior e de Óbidos antes e depois de tratamento com água oxigenada a 50 volumes. A identificação dos minerais foi feita recorrendo às tabelas Hanawatt e ASTM [6].
As riscas a 3,33; 4,23 e 1,84 Å evidenciam claramente a presença de quartzo α nas amostras das duas origens.

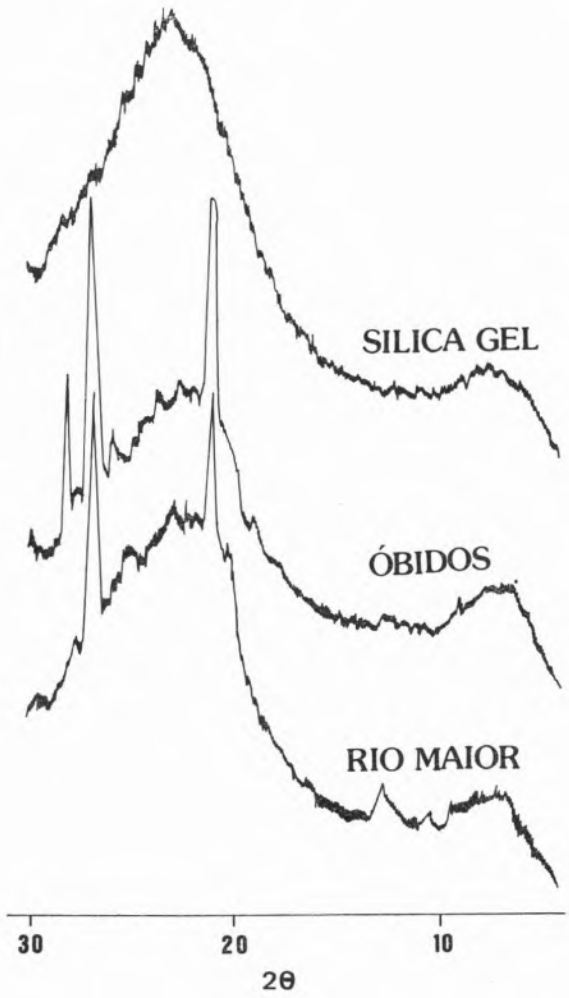

Fig. 5

Difractogramas de amostras de diatomitos e de um gel de sílica após tratamento com ácido clorídrico.

Com o propósito de identificar melhor outras formas de sílica ou aluminosilicatos presentes nos diatomitos, realizaram-se difractogramas de amostras previamente tratadas com ácido clorídrico, para eliminar os possíveis vestígios de carbonatos e alguma matéria orgânica, e compararam-se com o difractograma de um gel de sílica tratado nas mesmas condições (Fig. 5). A natureza difusa da banda centrada aproximadamente a 4,1 Å ($2\theta = 24$) traduz o estado desordenado e próximo do amorfo do opalo A, que é o principal constituinte dos diatomitos.
Tanto nos diatomitos de Rio Maior, como nos de Óbidos, a presença de bandas, na zona compreendida entre 6° e 20°, deve atribuir-se à presença de uma fracção argilosa, cujos componentes não foram identificados.
Na amostra de Óbidos, pode considerar-se a presença de feldspatos, caracterizados pelas riscas a 3,31; 3,77; 4,22 e 3,24 Å, embora algumas se confundam nos difractogramas com as riscas de quartzo α.

PROPRIEDADES DE SUPERFÍCIE

ADSORÇÃO DE GASES

A análise das isotérmicas de N_2 a 77 K, determinadas até um valor da pressão relativa de 0,98, permitiu avaliar, pelo método BET, a área específica, e, pela regra de Gurvitch [7], o volume total de mesoporos, tal como se apresenta na Tabela II. Nesta tabela figura também o valor da área BET, determinado numa amostra de Rio Maior, previamente tratada com ácido nítrico concentrado.

ADSORÇÃO DE CORANTES

As isotérmicas de adsorção do azul de metileno e do violeta de cristal nos diatomitos, como a título de exemplo se mostra na Fig. 6, têm a forma de isotérmicas do tipo Langmuir, permitindo assim a avaliação quantitativa das capacidades das respectivas monocamadas. A partir destes resultados e dos valores das áreas ocupadas pelos iões dos dois corantes

nas monocamadas da generalidade dos óxidos [8], estimaram-se as áreas específicas dos sólidos.

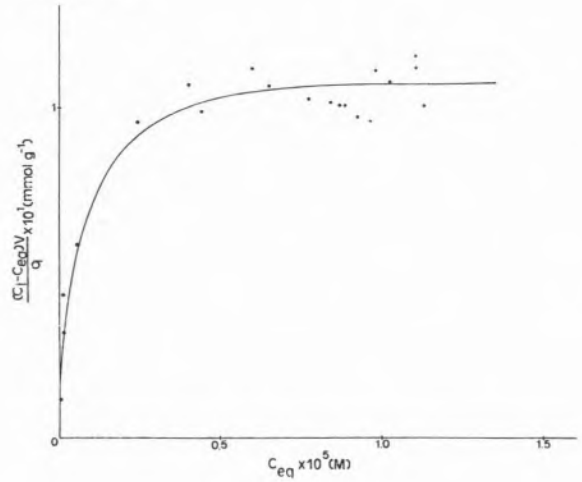

Fig. 6

Isotérmica de adsorção de violeta de cristal, a 25°C, em diatomito de Rio Maior.

Os resultados obtidos para o diatomito de Rio Maior, sem e com um tratamento prévio de ácido azótico concentrado, figuram na Tabela II. A análise desta Tabela permite concluir que, desde que a matéria orgânica seja removida, neste caso pelo tratamento ácido, os valores da área específica determinada com corantes ou com azoto passam a concordar razoavelmente.

CONCLUSÕES

As amostras de diatomitos de Rio Maior e de Óbidos estudadas apresentam uma grande analogia, tanto do ponto de vista químico como mineralógico.

Os resultados da análise química obtidos em Lisboa e em Madrid, com amostras diferentes do produto seco a 140°C, são muito semelhantes (Tabela I) e são concordantes com os valores obtidos por Leandro [2] com material calcinado.

Em qualquer dos casos os minerais contêm sempre aproximadamente 80 % de sílica, 6 % de alumina e uma percentagem em óxidos de ferro superior a 1 %.

A sílica apresenta-se fundamentalmente no estado amorfo e a alumina, pelo menos parcialmente, é um dos constituintes de uma fracção argilosa cujos componentes não foram ainda identificados. Nas amostras de Óbidos detectou-se a presença de feldspatos.

Estes materiais estão praticamente isentos de carbonatos, mas contêm uma elevada quantidade de matéria orgânica incorporada, que no caso de Rio Maior se justifica plenamente pela presença de jazigos de lenhites subjacentes aos de diatomitos.

Em relação à percentagem de sílica (com cerca de 80 %) os diatomitos de Rio Maior e de Óbidos são comparáveis aos de melhor qualidade de Espanha (Elche de la Sierra, Hellin CS e Cenejo CAR e Lebiga [9]). No entanto, enquanto que estes apresentam uma percentagem significativa de carbonatos, as impurezas dos diatomitos por nós estudados são fundamentalmente constituídos por minerais argilosos e materiais orgânicos.

Do ponto de vista da textura, é curioso notar que sendo química e mineralogicamente tão semelhantes, os diatomitos de Rio Maior apresentam uma área específica ($A_{(BET)N}$ = = 18 $m^2\ g^{-1}$) dupla da de Óbidos. Este valor, para o caso de diatomitos espanhóis citados

Tabela II

Características texturais dos diatomitos

Diatomitos	Volume de poros ($cm^3\ g^{-1}$)	Área$_{BET}$(N_2) ($m^2\ g^{-1}$)	Área (A.M.) ($m^2\ g^{-1}$)	Área (V.C.) ($m^2\ g^{-1}$)
Rio Maior	0,048	18	23	30
Rio Maior tratada c/ HNO_3 (conc.)	—	19	20	21 —
Óbidos	0,023	9	—	

só é excedido pelos diatomitos de Elche de la Sierra, que apresentam áreas específicas de cerca de 25 m^2/g [9].

A matéria orgânica que contamina os diatomitos, adsorvendo preferencialmente os iões dos corantes orgânicos, faz aumentar os valores medidos para as «áreas em azul de metileno» e «área em violeta de cristal». Pelo contrário, a presença daquela impureza, provoca uma ligeira diminuição da $area_{(BET)N}$ provavelmente por colmatar os poros do adsorvente.

Dos estudos de adsorção pode ainda concluir-se que a acessibilidade das moléculas de azoto e dos iões de azul de metileno ou de violeta de cristal à superfície dos diatomitos é semelhante, o que demonstra a ausência de microporosidade nestes materiais.

Com estas características de composição e textura os diatomitos portugueses estudados apresentam um potencial interesse como adsorventes, necessitando no entanto de serem beneficiados, com eliminação da matéria orgânica e remoção de impurezas (particularmente ferro), que lhes conferem uma cor cinzenta amarelada.

Realizaram-se experiências prévias de tratamentos com calor, água oxigenada e ácido azótico concentrado que resultaram infrutíferas quanto ao branqueamento, o qual, provavelmente, só será possível com a remoção das argilas onde estão inseridos irreversivelmente os iões ferro e alumínio.

Na continuação deste trabalho tentar-se-á separar a fracção argilosa dos diatomitos, e caracterizar os produtos resultantes.

Recebido em 18 de Novembro de 1985
em forma revista, 6 de Junho de 1986

AGRADECIMENTOS

As autoras agradecem a colaboração do Dr. C.A. Costa Almeida na selecção e recolha do material estudado.

BIBLIOGRAFIA

[1] ANDRADE DA SILVA, A. Publicações do Instituto de Botânica Dr. Gonçalo Sampaio da F.C.U.P. — Porto 1946.

[2] ZBYSEWSKY, G., LEANDRO, G.C., I Cong. Hispano-Luso-Americano, p. 707 (1971).

[3] VOGEL, ARTUR I., «A Text-book of Quantitative Inorganic Analysis», 3th Ed., Longmans, London (1961) p. 580.

[4] KNAUTH, L.P., Epstein, S. Amn Miner, 67 510 (1982).

[5] FARMER et al., «The Infrared Spectra of Minerals», Ed. V.C. Farmer (1974).

[6] Amer. Soc. for Testing Materials, «Data Cards Identification on Crystalline Materials», Philadhelphia, Pa.

[7] GREGG, S.J., SING, K.S.W., «Adsorption, Surface Area and Porosity», Academic Press, London, New York (1967).

[8] GILES, G.H., D'SILVA, A.P., TRIVEDI, A.S., Bristol Symp., Butterworths, London (1969) p. 317.

[9] BELZUNCE, M.J., MENDIOROZ, S., PAJARES, J. A. y PELÁEZ, J.R., Revista de la Real Academia de Ciencias Exactas, Físicas y Naturales, Tomo LXXIX, 3.º, Madrid 1985.

RESUMO

Diatomites from Rio Maior and Óbidos. Chemical composition, mineralogic and textural characteristic.

A study have been made on Diatomites Kieselghurs samples, from deposits at Rio Maior and Óbidos.
Their chemical composition, structure characteristics and adsorption properties were determined using atomic absorption, termogravimetry analysis, X Rays diffraction, I.R. spectroscopy, and adsorption of nitrogen at 77 K and of dyes in solution.
The results show that both minerals have a chemical analogy, in fact, they have about 80 % of silica, and 6 % of alumina, and they are essentially formed by opal A, quartz α as impurities, which are probably detritus, clays, great deal of organic material, and only in Óbidos Kieselghurs, a little of feldspars.
The specific area of Kieselghur from Rio Maior is almost twice the Óbidos one.

CARLOS F.G.C. GERALDES *
VICTOR M.S. GIL
M. HELENA S.F. TEIXEIRA
Chemistry Department, University of Coimbra
3000 Coimbra, Portugal

F. TEIXEIRA
Department of Pharmacology, Faculty of Medicine
University of Coimbra
3000 Coimbra, Portugal

NUCLEAR MAGNETIC RESONANCE STUDIES OF CIMETIDINE AND RANITIDINE IN SOLUTION: ACID-BASE EQUILIBRIA AND EFFECTS OF ANTACIDS

^1H and ^{13}C NMR data is presented for the antiulcer agents cimetidine and ranitidine in aqueous (D_2O) solution at various pH values as well as in DMSO-d_6 solution, and interpreted in terms of acid-base, tautomeric and configurational equilibria. The interaction with Al^{3+} and Mg^{2+} is also investigated, in relation to effects of antacids on the gastrointestinal absorption of those drugs.

* Author to whom correspondence should be adressed.

INTRODUCTION

Cimetidine (N-Cyano-N'methyl-N'' [2-[[(5-methyl-1H-imidazol-4-yl) methyl]thio]ethyl]guanidine) and ranitidine (N-[2-[[[5-[(dimethylamino) methyl]-2-furanyl]-methyl]thio ethyl]-N'-methyl-2-nitro-1, 1-ethenodiamine)—Fig. 1 — are the most effective antiulcer agents among a number of recently introduced similar histamine H_2-receptor antagonists, which effectively inhibit secretion of gastric acid [1-6].

The imidazole moiety of cimetidine, regarded as an essential structural feature of histamine H_2-receptor antagonists [1], is replaced in ranitidine by a substituted aminoalkyl furan ring, with increased drug efficiency [3, 6]. Recently an important role of the N-cyanoazomethyne and nitroethylene units in the pharmacological activity of cimetidine and ranitidine has been proposed [7].

The antacids are still being used in the therapy of peptic ulcer, as a consequence of their quick relief of pain and action on stomach acidity. It has long been verified that the simultaneous use of cimetidine and antacids containing aluminium and/or magnesium salts causes a decrease of about 40 % in the gastrointestinal absorption of that drug, as monitored by its mean peak blood concentration and area under its blood concentration curve [8, 12]. The causes of this have not been reported but an increase of the intragastric pH, a change of gastroduodenal motility [12] and adsorption phenomena [13] have been excluded. A process of complexation of cimetidine with the ions Al^{3+} and Mg^{2+} has been proposed as cause for its reduced gastrointestinal absorption, but not demonstrated [12]. The early work on the simultaneous use of ranitidine and antacids did not demonstrate any decreased gastrointestinal absorption of the drug. Recently that possibility has been reported for a large excess of antacids containing aluminium and magnesium salts [14].

The purpose of the present work is two-fold: to study the pH dependent tautomeric and configurational equilibria of cimetidine and

ranitidine and to investigate the eventual complexation of these drugs with the Al^{3+} or Mg^{2+} ions in aqueous solution in various conditions of pH using proton and ^{13}C Nuclear Magnetic Resonance (NMR) Spectroscopy [15], in an effort to rationalize the drug gastrointestinal absorption data.

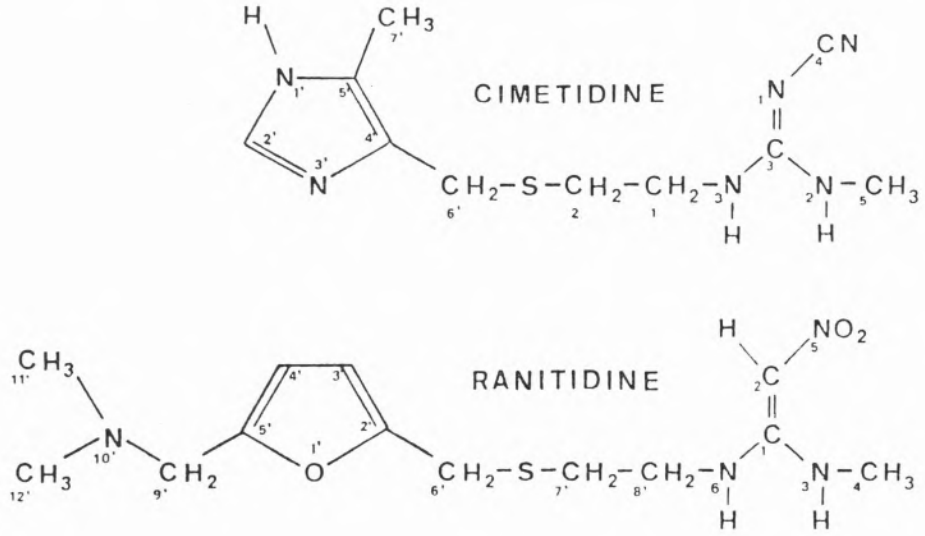

Fig. 1

Chemical structure and numbering scheme of cimetidine and ranitidine

EXPERIMENTAL

Cimetidine and ranitidine hydrochlorides, obtained respectively from Instituto Luso Fármaco, Lisbon, Portugal and Glaxo Group Research Ltd, Middlesex, England, were used without further purification. Magnesium sulphate and aluminium sulphate were obtained from E. Merck AG, Darmstadt. Solutions of cimetidine and ranitidine were made up in the deuteriated solvents, 99,8 % D_2O, $CDCl_3$ or dimethylsulphoxide-d_6 (from Stohler Isotope Chemicals). The pH* values quoted are the directly measured values in D_2O solutions after standardization of the pH meter with H_2O-buffer solutions; pH* was adjusted with dilute solutions of DCl or NaOD (from Stohler Isotope Chemicals) in D_2O using a Metrohm pH-meter E 520 equipped with a Ingold 405-M3A glass electrode. Proton NMR spectra were obtained at 200 MHz and ^{13}C spectra at 50.3 MHz both using a Varian XL-200 spectrometer operating on the Fourier Transform (FT) mode. Sodium 3-trimethylsilyl [2,2,3,3-D_4] propionate (TSS) and dioxane were used as internal standards, respectively for measurements of proton and ^{13}C chemical shifts.

RESULTS AND DISCUSSION

EFFECT OF pH

The proton and ^{13}C NMR spectra of cimetidine in D_2O are shown in Fig. 2. The proton assignments are straightforward and the ^{13}C assignements are based on signal multiplicities as obtained from comparison of proton broadband decoupled and single off-resonance decoupled ^{13}C spectra, and on known ^{13}C chemical shift correlations [15, 16].

Both the proton and ^{13}C chemical shifts of the imidazole moiety of cimetidine are found to be pH dependent, due to its protonation, with a $pK_a = 6,8$ [17]. The ^{13}C chemical shift-pH profiles of the imidazole ring carbons were obtained only from pH = 3.0 up to pH = 7.0 due to insolubility of cimetidine at higher pH. The neutral ring can exist in two tautomeric structures: the H (1′) tautomer or the H (3′) tautomer. Table 1 shows a comparison of the protonation shifts observed for the imidazole carbons of some histidine derivatives [18] with the shifts observed for cimetidine upon changing the pH from 7.0 to 3.0. Histidine is known to exist predominantly as the H (1′) tautomer, in agreement with protonation shifts closer to those of 1-methylhistidine than to those of the 3-methyl isomer (approximately 80 % of H (1′) tautomer) [18]. The protonation shifts for cimetidine are not much different from those of histidine, being again closer to the protonation shifts of 1-methylhistidine. We can thus conclude for the predominance of the H (1′) tautomer of cimetidine in aqueous solution. In fact, if we take the observed protonation shifts for C (4′) and C (5′) of cimetidine as weighted averages of the corresponding values for 1-methylhistidine and 3-methylhistidine, as was done for histidine [18], estimated populations of 60 % and 75 % are obtained for the H (1′) tautomer, using the C (4′) and the C (5′) shifts, respectively. This is in agreement with X-ray crystal structure studies of neutral cimetidine which show that only the N (1′) atom is bonded to H [19, 20].

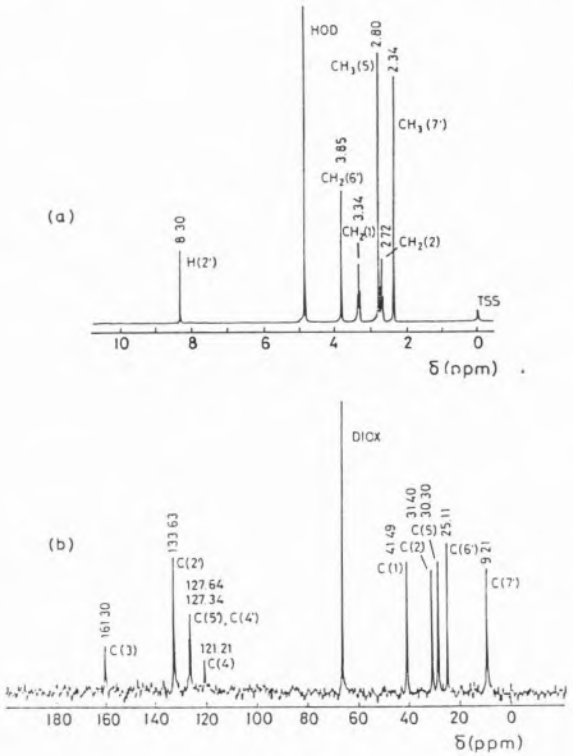

Fig. 2

NMR spectra of 0.2 M cimetidine in D_2O, pH = 5.0: (a) Proton spectrum (δ vs. TSS); (b) ^{13}C spectrum (δ vs. TMS)*

Table 1

Changes in ^{13}C chemical shift of imidazole ring carbons of histidine related compounds upon protonation of the neutral imidazole ring (low field shifts are positive)

Compound	C (2′)	C (4′)	C (5′)	pK [a]	Ref.
Histidine	— 2.4	— 4.8	+ 0.7	6.2	(18)
1-Methylhistidine	— 3.4	— 6.8	+ 2.1	6.7	(18)
3-Methylhistidine	— 3.5	+ 2.3	— 7.1	6.3	(18)
Cimetidine	— 2.1	— 3.0	— 0.1	6.8	b

[a] Average value of the individual carbon-pH profile pK′s.
[b] This work: shifts observed upon changing the pH from 7.0 to 3.0.

The effect of pH* on the proton and ^{13}C spectra of ranitidine was also investigated. The proton spectrum at pH* = 5.0 (Fig. 3 b) was assigned according to the literature [21]. From pH* = 5.0 to pH* = 9.0 several proton resonances move to low frequency specially the CH_3 (11′), CH_3 (12′), CH_2 (9′), CH (4′) and CH_2 (6′) groups (Table 2), due to deprotonation of the N (10′) atom, ($pK_a = 8.2$ [17]). This observation is in agreement with the X-ray crystal structure of ranitidine hydrogen oxalate, where the ranitidine molecule is

protonated at the dimethylamino group [22]. Whatever the pH conditions used, the CH (2) proton signal of the nitroethylenic moiety of ranitidine was not observed in D_2O, due to

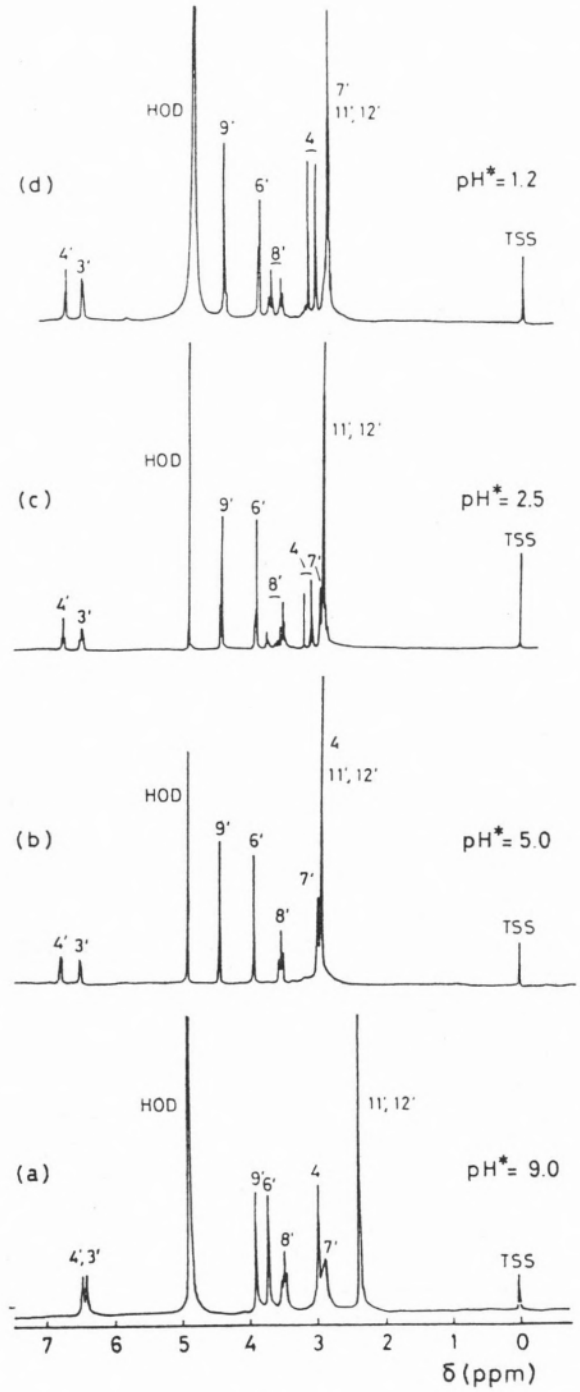

Fig. 3

^1H NMR spectrum of 0.2 M ranitidine in D_2O at different pH values*

Table 2

Proton and ^{13}C chemical shifts of 0.2 M ranitidine in D_2O solution at different pH values*[a]

Nuclei observed	pH*														
^1H					δ (ppm) vs. TSS										
		CH(2)	CH_3(4)	CH(3')	CH(4')	CH_2(6')	CH_2(7')	CH_2(8')	CH_2(9')	CH_3(11', 12')					
	9.0	b	2.92	6.33	6.38	3.66	2.84	3.44	3.84	2.34					
	5.0 Form A	b	2.87	6.40	6.67	3.86	2.92	3.47	4.34	2.87					
	1.2 Form B	b	3.15	6.42	6.69	3.86	2.88	3.55	4.37	2.88					
	1.2 Form C	b	3.04	6.42	6.69	3.88	2.88	3.69	4.37	2.88					
^{13}C							δ (ppm) vs. TMS								
		C(1)	C(2)	C(4)	C(2')	C(3')	C(4')	C(5')	C(6')	C(7')	C(8')	C(9')	C(11', 12')		
	5.0 Form A	156.68	101.21 [c]	28.89 [c]	144.01	110.20	116.47	154.55	28.36	31.28 [c]	41.54 [c]	53.73	42.91		

[a] See Scheme 1 for structures of protonated forms A, B, C.
[b] Not observed due to H/D exchange with the solvent.
[c] Broadened at room temperature (Fig. 6).

fast H/D exchange with the solvent [23]. This phenomenon, which has also been observed for other compounds containing the nitroethylenic group, has been interpreted in terms of an acid-catalysed intramolecular deuterium transfer within the nitrolic form of the compounds, following deuteration at one of the amino groups, with inversion of configuration at the carbon-carbon double bond [23]. This process also leads to E/Z isomerization of the nitroethylenic group, which in D_2O at pH* higher than 3.0 is fast in the proton NMR time scale, leading to an average spectrum corresponding to species A (Scheme 1). The rotation barrier around the carbon-carbon bond of nitroenamines is often low, as determined by NMR studies [23-26] and in accordance with the long $C_1 - C_2$ bond (1.433 Å) observed for ranitidine by X-rays [22].

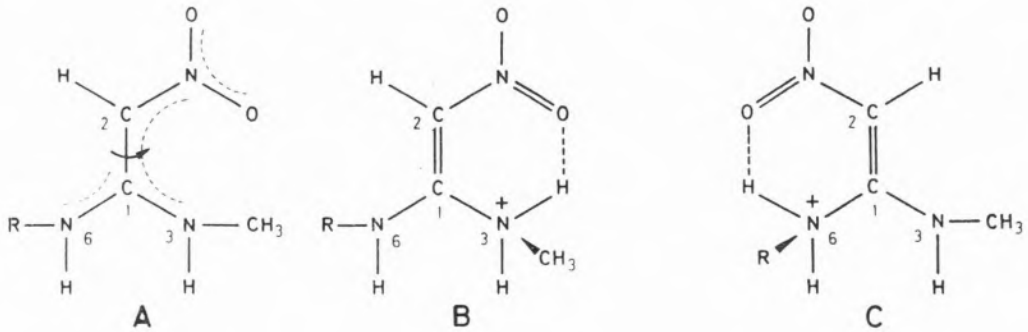

Scheme 1

At pH* values below 3.0, besides the spectrum detected at higher pH* two new sets of ^1H NMR lines appear (Fig. 3 c), revealing the presence of three species in slow exchange. At pH* = 1.2 the new species, B and C, are the only ones present (Fig. 3 d). The assignment of the corresponding signals, shown in Table 2, was helped by spin decoupling techniques (at pH* = 2.5, irradiation of the CH_2 (7′) protons at $\delta \simeq 2.9$ ppm simultaneously decoupled the three CH_2 (8′) triplets), relative intensity considerations and shifts expected upon protonation at N (6) an N (3). Species B and C are the diprotonated E and Z isomers — protonated at N (10′) and also at N (3) or N (6) respectively (Scheme 1). Intramolecular hydrogen bonding in both configurations explains the slow rotation about the bond, which leads to slow exchange.

Fig. 4 shows how the populations of these species revealed by the spectral intensities of the signals due to CH_3 (4) and CH_2 (8′) vary with pH*. One isomer is only slightly more stable than the other. We note that protonated isomer B has been proposed as playing a crucial part in the mechanism of isomerization of ranitidine [23].

The existence of diprotonated forms B and C suggests the possibility of observing the corresponding monoprotonated E/Z isomers in slow exchange (Scheme 2).

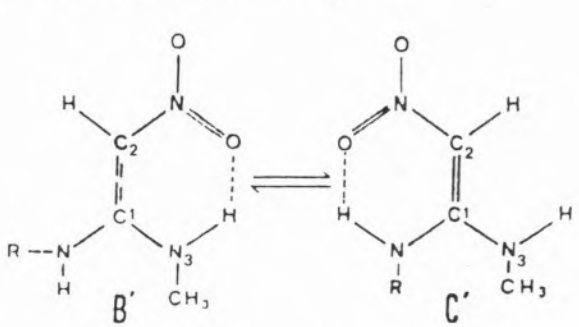

Scheme 2

The major difference expected in the proton NMR spectrum upon conversion of B′ in C′ lies in the NH (3) signal which should undergo a noticeable shift (to low frequency)

and in NH (6) with a similar shift but in opposite direction. These shifts are associated to the hydrogen bonding effect. Those signals, which are not observed separate from the HDO signal in D_2O solutions due to proton exchange, can however be detected in a non-protonating solvent. We have therefore obtained spectra in $CDCl_3$, DMSO-d_6 and

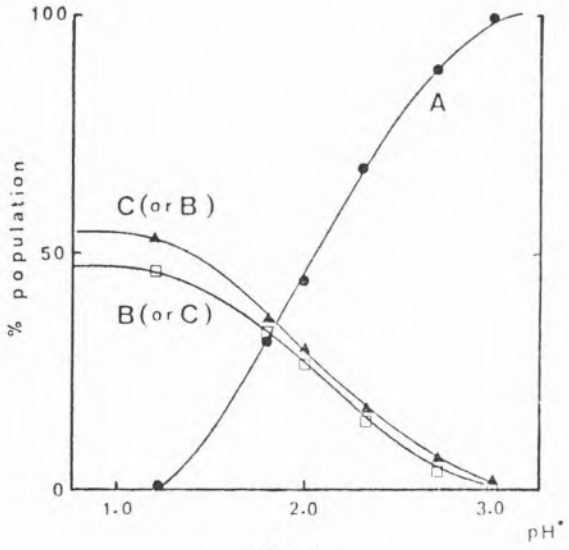

Fig. 4

pH dependence of the populations of the diprotonated E and Z isomers (B and C) and the monoprotonated form of ranitidine (A)

mixtures of these solvents. All the resonances except those due to the NH (3) and NH (6) protons appear as common peaks of B′ and C′. The CH (2) proton signal, which is not observed in D_2O solution, is a broad peak near the resonances due to the ring protons CH (4′) and CH (3′). The NH (3) and NH (6) protons give rise to four signals, two at higher frequency ($\delta \simeq 10$ ppm) corresponding to the internally hydrogen bonded NH protons of the B′ and C′ isomers, respectively (Scheme 2), and a similar pattern at lower frequency ($\delta \simeq 7$ ppm) assigned to the NH protons of B′ and C′ not involved in internal hydrogen bonding. Whereas in $CDCl_3$ the populations of the two isomers are about the same, they are approximately in the ratio 1:2 when DMSO-d_6 is used as solvent (Fig. 5). However, on the basis of these data alone, it was not possible to decide which form is the most stable. In DMSO-d_6 an additional peak at $\delta = 10.7$ ppm can be detected and is assigned to the NH (10′) proton. (We note that solutions are prepared from ranitidine hydrochloride). This signal broadens considerably upon addition of $CDCl_3$ and completely disapears in this solvent, due to exchange phenomena.

Fig. 5 shows the low field part of the proton NMR spectrum of ranitidine hydrochloride in DMSO-d_6 at various temperatures. A temperature increase leads to an increase of the rate of exchange between B′ and C′ and this produces a sharpening of the CH (2) signal; simultaneously, as expected, the NH (3) and NH (6) proton signals broaden and eventually coallesce into a broad resonance at about

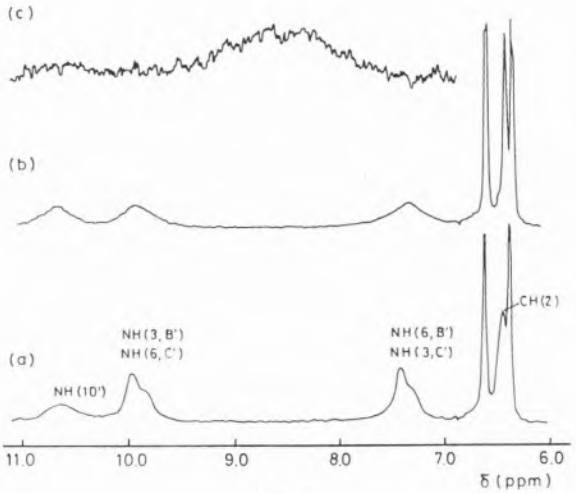

Fig. 5

Temperature dependence of the low field region of the proton NMR spectrum of 0.2 M ranitidine in DMSO — d_6. (a) $T = 20°C$; (b) $T = 40°C$; (c) $T = 90°C$

90°C. This observation enables an estimation of the rate of exchange between B′ and C′ at this temperature of about 10^3 s^{-1} and a free energy of activation ($\Delta G^{\ddagger}$) for exchange of the order of 70 kJ mol^{-1} [27]. This value for $\Delta G^{\ddagger}$ lies within the range of values previously found for various 2,2-disubstituted nitroethylene compounds [23]. We note that the NH (10′) signal at = 10.7 ppm, although broader at high temperature, is still observed at 90°C as

a separate resonance, indicating that the exchange of this proton with the N (3) and N (6) protons is slow.

resonances as is the case with ^1H NMR. Figure 6 shows the spectrum for pH* = 5.0; the assignement was made with help of off-

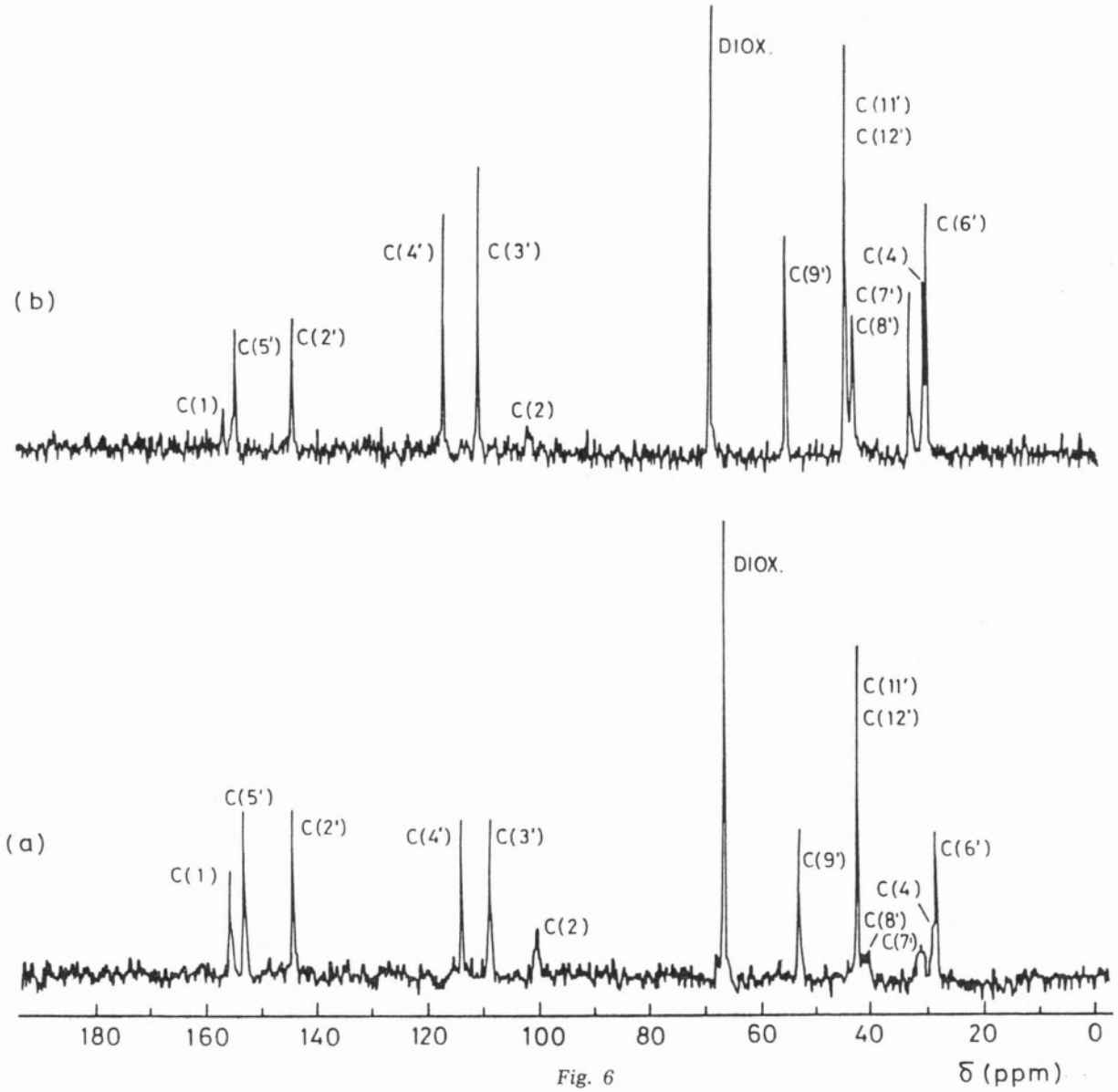

Fig. 6

^{13}C NMR spectrum of 0.2 M ranitidine in D_2O. (a) pH = 5.0, T = 25°C; (b) pH* = 5.0, T = 70°C*

The effect of addition of a small amount of trifluoroacetic acid on the proton NMR spectrum of ranitidine in DMSO-d_6 reveals the presence of the diprotoneted forms B and C (Scheme 1), again in slow exchange, as was previously observed in aqueous solution at low pH.

The ^{13}C NMR spectrum of ranitidine in D_2O at pH* > 3.0 consists of only one set of resonance decoupling techniques and chemical shift correlations (Table 2). At room temperature, the C (2), C (8′), C (7′) and C (4) resonances are very broad and, except C (2), sharpen at high temperature (Fig. 6). This is a clear indication that, at room temperature, an exchange process involving forms B′ and C′ is ocurring at a rate not high enough to lead to completely averaged ^{13}C signals. The

resonances due to ^{13}C nuclei further away from the nitroketenediamine moiety are expected to be almost identical for B′ and C′ and thus lead to a single set of sharp lines even at room temperature. The fact that the C (2) signal does not sharpen at higher temperature is attributed to H/D exchange. Support for this explanation comes from the observation of a sharp (2) signal in DMSO-d_6 solution, where deuteration is not occurring. Regarding the ^{13}C chemical shifts at pH*>3.0, we note the big difference between C (2) and C (1) (a separation of 55 ppm). In particular, the very low δ value for C (2) reflects the negative contribution due to the two nitrogen atoms two bonds away which offsets the low field effect due to -NO_2 [16].

In a similar way to what was found with proton spectra, at pH* < 3.0 additional peaks appear in the ^{13}C spectrum of ranitidine, corresponding to contribution from the species B and C. In these species most ^{13}C resonances coincide with the corresponding resonances of A, except in the C (4), C (6′), C (7′) signal region, where the number of signals doubles. However, due to the proximity of these signals and the uncertainty in interpreting ^{13}C protonation shifts, we did not pursue this analysis further.

EFFECT OF Al^{3+} AND Mg^{2+} IONS

The eventual complexation of cimetidine or ranitidine with the Al^{3+} or Mg^{2+} ions in aqueous solutions at different pH values was investigated using proton and ^{13}C chemical shift measurements. In all cases the proton induced shifts by Mg^{2+} or Al^{3+} were very small. However some useful conclusions could be obtained from the ^{13}C shifts, which are much more sensitive than protons to complexation by closed shell cations [28-30]. The chemical structures of cimetidine and ranitidine (Fig. 1) indicate the potential binding sites of these molecules to Al^{3+} an Mg^{2+}, which are the nitrogen and oxygen atoms. Table 3 shows that addition of aluminum nitrate or magnesium nitrate to aqueous

Table 3

^{13}C chemical shifts, Δ (ppm), induced by Al^{3+} and Mg^{2+} binding to cimetidine and ranitidine (1:1 ligand to metal ratio at 0.2 M concentrations) at pH = 5.0* [a]

Compound	Ion	Carbon Number											
Cimetidine		C(1)	C(2)	C(3)	C(4)	C(5)	C(2′)	C(4′)	C(5′)	C(6′)	C(7′)		
	Al^{3+}	+ 0.18	+ 0.11	− 3.50	[b]	+ 0.53	− 0.36	− 0.96	+ 0.17	− 0.46	− 0.41		
	Mg^{2+}	− 0.16	− 0.08	− 0.20	− 0.10	− 0.08	− 0.55	− 0.69	− 0.12	− 0.58	− 0.21		
Ranitidine		C(1)	C(2)	C(4)	C(2′)	C(3′)	C(4′)	C(5′)	C(6′)	C(7′)	C(8′)	C(9′)	C(11′,12′)
	Al^{3+}	− 0.10	0.00	0.00	− 0.04	− 0.06	− 0.07	− 0.07	− 0.13	0.00	0.00	− 0.08	− 0.16
	Mg^{2+}	− 0.08	0.00	− 0.02	− 0.86	− 0.14	− 0.61	− 0.31	− 0.07	0.00	0.00	− 0.07	− 0.20

[a] A negative Δ value means a shift to high field.
[b] Not observed.

solutions of those compounds in the ratio of 1:1 at pH* = 5.0 has selective effects on their ^{13}C chemical shifts. As the ^{13}C chemical shifts are usually dominated by the local paramagnetic contribution to nuclear shielding [28-30], the largest cation-induced shifts are expected to occur at carbon atoms close to the metal binding sites.

In the case of cimetidine, the large shifts observed with Al^{3+} for the C (2′) and C (4′) atoms of the imidazole ring, the neighboring atoms C (6′) and C (7′) and the C (3) and C (5) atoms of the chain indicate a definite complexation, probably through the chelation of Al^{3+} to N (3′) and N (1). The chelate formation in this case does not involve special strain as shown by a molecular model of cimetidine. With Mg^{2+} the large shifts occur only in the imidazole ring, indicating weaker non-chelating complexation at N (3′). In both cases, these effects are only observed between pH* = 5 and pH* = 6 (at pH* above 6 metal hydroxide precipitation made the investigation impossible). The lack of complexation of cimetidine to the cations at low pH is due to protonation of the N (3′) atom.

In the case of ranitidine, the very small shifts induced by both Al^{3+} or Mg^{2+} show that metal binding is practically inexistent with the former and very weak with the latter, involving most probably the oxygen atom of the furan ring in the latter case. This situation contrasts with the reported preferential binding of lanthanide (III) complexes to ranitidine in $CDCl_3$, through the tert-nitrogen atom N (10′) and the nitro group [21].

The present NMR data are in accordance with gastrointestinal drug absorption studies [9-12] In the case of ranitidine the very weak complexation agrees with the small decrease of gastrointestinal drug absorption only observed in the presence of very large doses of antacids containing aluminium and magnesium salts [14].

CONCLUSIONS

We can summarize the main conclusions of this work as follows:

a) In aqueous solution neutral cimetidine exists mainly in the form of the H (1′) tautomer, in agreement with its crystal structure. A rough calculation based on the ^{13}C protonation shifts of the model compounds 1-methylhistidine and 3-methylhistidine gives a population of 60-75 % for the H (1′) tautomer.

b) Room temperature E/Z isomerization of monoprotonated (at N (10′)) ranitidine in aqueous solution is rapid in the NMR time scale, but becomes slow for the diprotonated species due to intramolecular hydrogen bonding between the $-NO_2$ group and a neighboring $-N_1H_2^+$ group. This gives support to the previously proposed mechanism of isomerization of ranitidine.

c) A free energy of activation of the order of 70 kJ mol^{-1} was estimated for the E/Z isomerization of ranitidine in the non-protonating solvent DMSO-d_6. This value agrees with those previously found for various 2,2-disubstituted nitroethylene compound, taken as models for ranitidine [23].

d) Al^{3+} is found to complex with cimetidine, probably through formation of a chelate involving N (3′) and N (1). Complexation with Mg^{2+} is weaker and seems to involve only the imidazole ring. Complexation of both ions with ranitidine, if present, is very weak. These results are in accordance with studies of the effect of antacids containing aluminium and/or magnesium salts on the gastrointestinal absorption of those drugs [8-12, 14].

ACKNOWLEDGEMENTS

This work was supported by a grant from Instituto Nacional de Investigação Científica (Portuguese Ministry of Education).

The authors thank Instituto Luso-Fármaco and Glaxo Group Research for providing samples of cimetidine and ranitidine, respectively.

Received, 9th December 1985
in revised form, 18th April 1986

REFERENCES

[1] J.W. BLACK, W.A.M. DUNCAN, G.M. DURANT, C.R. GAMELLIN and M.E. PARSONS — *Nature* (London), **236**, 385 (1972).

[2] W.L. BURLAND, H.A. SIMKINS EDS — Proceding of the 2 nd International Symposium of Histamine H_2 — Receptor Antagonist — *Excerpta Medica*, Amsterdam-Oxford, 1977.

[3] J. BRADSHAW, R.T. BRITTAIN, J.W. CLITHEROW, M.J. DALY, D. JACK, B.J. PRICE and R. STABLES — *Br. J. Pharmacol*, **66**, 464P (1979).

[4] W. DOMSCHKE, G. LUX and S. DOMSCHKE — *Lancet*, 320 (1979).

[5] IST SYMPOSIUM ON RANITIDINE, HAMBURG, 1980 — *Scand. J. Pharmacol*, 16 (1981).

[6] N.R. PEDEN, J.H.B. SAUNDERS and K.G. WORMSLEY — *Lancet*, 690 (1979).

[7] L. KLASINC, V. BUTKOVIC, I. NOVAK, M. MIHALIC, R. TOSO and V. SUNJIC — *Gazz. Chim. Ital.*, **110**, 287 (1980).

[8] G. BODEMAR, J.G. MILLS, B. NORLANDER, P. OSBORNE, W.L. BURLAND and A. WALAN — *Gut*, **19**, A990 (1978).

[9] G. BODEMAR, B. NORLANDER and A. WALAN — *Lancet, L.* 444 (1979).

[10] W.M. STEINBERG and J.H. LEWIS — *Gastroenterology*, **78**, 1869 (1980).

[11] R. GUGLER, M. BRAND and A. SOMOGYI — *Eur. J. Clin. Pharmacol.*, **20**, 225 (1981).

[12] W.M. STEINBERG, J.H. LEWIS and D.M. KATZ — *N. Engl. J. Med.*, **307**, 400 (1982).

[13] F. GANIIAN, A.J. CUTIÉ and T. JOCHSBERGER — *J. Pharmac. Sci.*, **69**, 352 (1980).

[14] G.W. MIHALY, A.T. MARINO, L.K. WEBSTER, D.B. JONES, W.J. LOUIS and R.A. SMALLWOOD — *Brit. Med. J.*, **285**, 998 (1982).

[15] F.W. WEHRLI and T. WIRTHLIN «Interpretation of Carbon — 13 NMR Spectra», Heyden an Son, Ltd., Mondon, 1976.

[16] G.C. LEVY and G.L. NELSON — «Carbon - 13 Nuclear Magnetic Resonance for Organic Chemists», Wiley, New York, 1972.

[17] «THE CLINICAL USE OF RANITIDINE», Procedings of the Second International Symposium on Ranitidine. Ed. J.J. Misiewicz and K.G. Wormsley, *Medicine Publishing Foundation*, Oxford, 1982, p. 78.

[18] W.F. REYNOLDS, I.R. PEAT, M.H. FREEDMAN and J.R. LYERLA, Jr., — *J. Amer. Chem. Soc.*, **95**, 328 328 (1973).

[19] E. HADICKE, F. FRICKEL *and* FRANKE — *Chem. Ber.*, **111**, 3222 (1978).

[20] B. KOJIC-PRODIC and Z. RUIC-TOROS — *Acta Cryst.*, **B36**, 1223 (1980).

[21] A. SEGA, F. MOIMAS, E. DECORTE, R. TOSO and V. SUNJIC — *Gazz. Chim. Ital.*, **112**, 421 (1982).

[22] B. KOJIC-PRODIC *and* Z. RUZIC-TOROS and R. TOSO — *Acta Cryst.*, **B38**, 1837 (1982).

[23] A. SEGA, R. TOSO, V. SUNJIC, L. KLASINC, A. SABLJIC and D. SRZIC — *Gazz. Chim. Ita.*, **111**, 217 (1981).

[24] S. RAJAPPA, R. SREENIVASAN, B.G. ADVANI, R.H. SUMMERVILLE and R. HOFFMANN — *Ind. J. Chem.*, **15B**, 297 (1977).

[25] A.I. FETELL and H. FEUER — *J. Org. Chem.*, **43**, 497 (1978).

[26] S. RAJAPPA — *Tetrahedron*, **37**, 1453 (1981).

[27] SEE FOR EXAMPLE, R.J. ABRAHAM and P. LOFTUS, «Proton and Carbon-13 NMR Sepctroscopy — An Integrated Approach», Heyden and Son, Ltd., London, 1978.

[28] E.W. RANDALL and D.G. GILLIES — *Prog. Nucl. Magn. Resonance Spectrosc.*, **6**, 119 (1971).

[29] R.L. LICHTER, «Determination of Organic Structures by Physical Methods», Vol. 4, F.C. Nachod and J.J. Zuckerman, Ed., Academic Press, New York, N.Y., 1971.

[30] R. HAGEN, J.P. WARREN, D.H. HUNTER and J.D. ROBERTS — *J. Chem. Soc.* **95**, 5712 (1973).

RESUMO

Apresentam-se resultados experimentais de RMN de ^1H e de ^{13}C para os agentes anti-úlcera gástrica Cimetidina e Ranitidina em solução aquosa a vários valores de pH bem como em DMSO-d_6, os quais são interpretados em termos de equilíbrios ácido-base, tautoméricos e configuracionais. Investiga-se também a interacção destes fármacos com os iões Al^{3+} e Mg^{2+}, em relação com os efeitos observados de anti-ácidos sobre a absorção gastrointestinal daquelas drogas.

NOSRAT M. ABED
SALAH Z. SOWELLIM
Department of Chemistry, Faculty of Science, Cairo Univ., Giza, A. R. Egypt

ABDEL-GHANI A. ELAGAMEY
Faculty of Science (Damietta), Mansoura University, A. R. Egypt

ABDEL-FATTAH A. HARB
Faculty of Science, Qena University, A. R. Egypt

SOME REACTIONS WITH α, β-UNSATURATED ACYL ISOTHIOCYANATES

Nucleophilic addition reactions of α, β-unsaturated acyl isothiocyanates with aromatic and heteroaromatic amines have been studied. Compound 12 was also prepared which afforded pyrazolo [1,5-a]-s-triazine, coumarine and pyrazolo [1,5-c]-as-triazine derivatives on treatment with 5 % potassium hydroxide, salicylaldehyde and diazotised aminopyrazole respectively.

RESULTS AND DISCUSSION

Aroyl and acyl isothiocyanates are versatile reagents and their chemistry has received considerable recent interest [1-4]. These reagents can react with a variety of polyfunctional molecules either via addition followed by cyclisation or via cycloaddition to yield a variety of heterocyclic derivatives. In the present study, we investigate additions of aromatic and heteroaromatic amines to α, β-unsaturated acyl isothiocyanates with the aim to obtain intermediates suitable for further cyclisation. Thus, treatment of 1a, b with 4-aminoantipyrine has resulted in the formation of the corresponding thiourea derivatives 2a, b in high yield. Similarly, 4-aminopyridine and 2-aminopyrimidine reacted smoothly with 1c to afford the expected adducts 3 and 4, respectively. On the other hand, 3-amino-1,2,4-triazole (5) and 2-aminothiazole (6) reacted with 1a, c to yield the acyl amino derivatives 7 and 8 respectively. The same products could be also obtained from the reaction of each of the amines 5 or 6 and the appropriate acid chloride in dry pyridine (Chart 1).

The formation of 8 from the reaction of 1 with 6 is assumed to proceed via intermediate formation of adduct 9, which readily decompose to give 8 via HCNS elimination. Also, compound 7 may be formed under a similar mechanism (Chart 1).

In contrast, the experiments indicate that in the case of aromatic compounds carrying both a thiol and an amino group, a preferential attack occurs on the thiol group. Thus, by mixing acetone solution of 1a and o-aminothiophenol in equimolecular proportions, a rapid exothermic reaction took place, and solid product of 10 separates which readily losses H_2S upon crystallization to afford 2-acylaminobenzothiazole 11, the latter product could be also obtained directly from the reaction of 2-aminobenzothiazole and p-methoxycinnamoyl chloride (chart 1).

2-Cyanoethanoic acid hydrazide reacted with 1c to yield a product which may be formulated as 12 or isomeric 13. Structure 12 could be established for the reaction product based on IR spectrum. Since the obtained product is insufficiently soluble in the commonly used ^{1}H-NMR solvents, another evidences for the structure could be inferred from its chemical behaviour.

Similar to the recently reported [5], compound 12 could be also cyclized to the pyrazolo [1,5-a]-s-triazine derivative 14 upon treatment with 5 % aqueous potassium hydroxide solution (chart 2).

Compound 12 condensed readily with aromatic aldehydes to afford the corresponding arylidene derivatives 15a, b and with salicylaldehyde to give the coumarine derivative 16.

Compound 12 also coupled with aromatic diazonium salts to yield coupling products for which the hydrozone structure 17 was established for the reaction product based on the presence of a conjugated -CN group in the IR spectra of the coupling products. Similarly, compound 12 coupled with diazotised aminopyrazole to afford the corresponding pyrazolo [1,5-c]-astriazine derivative 18. The formation of the cyclic product 18 is assumed to proceed via formation of the acyclic hydrazones 19 which cyclize readily under the reaction condition.

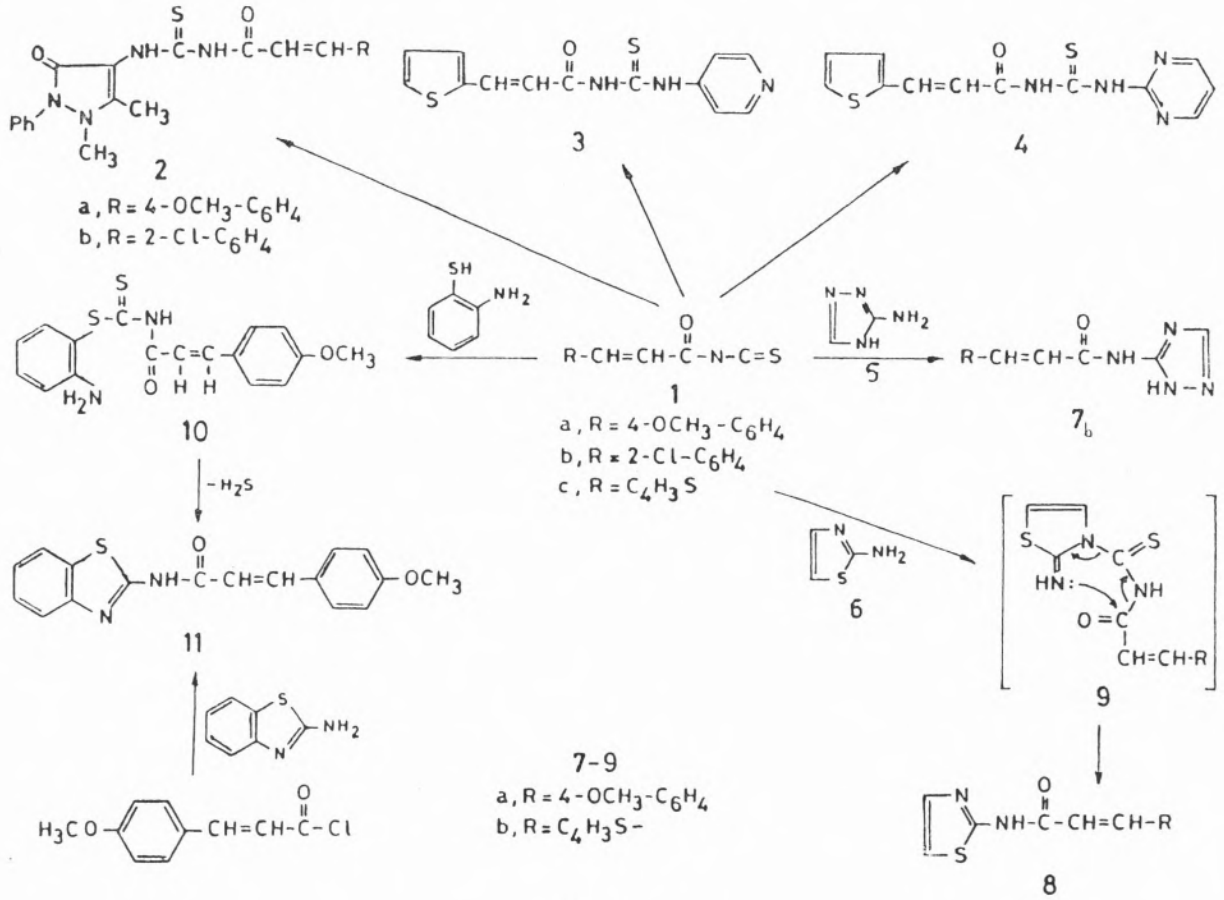

Chart 1

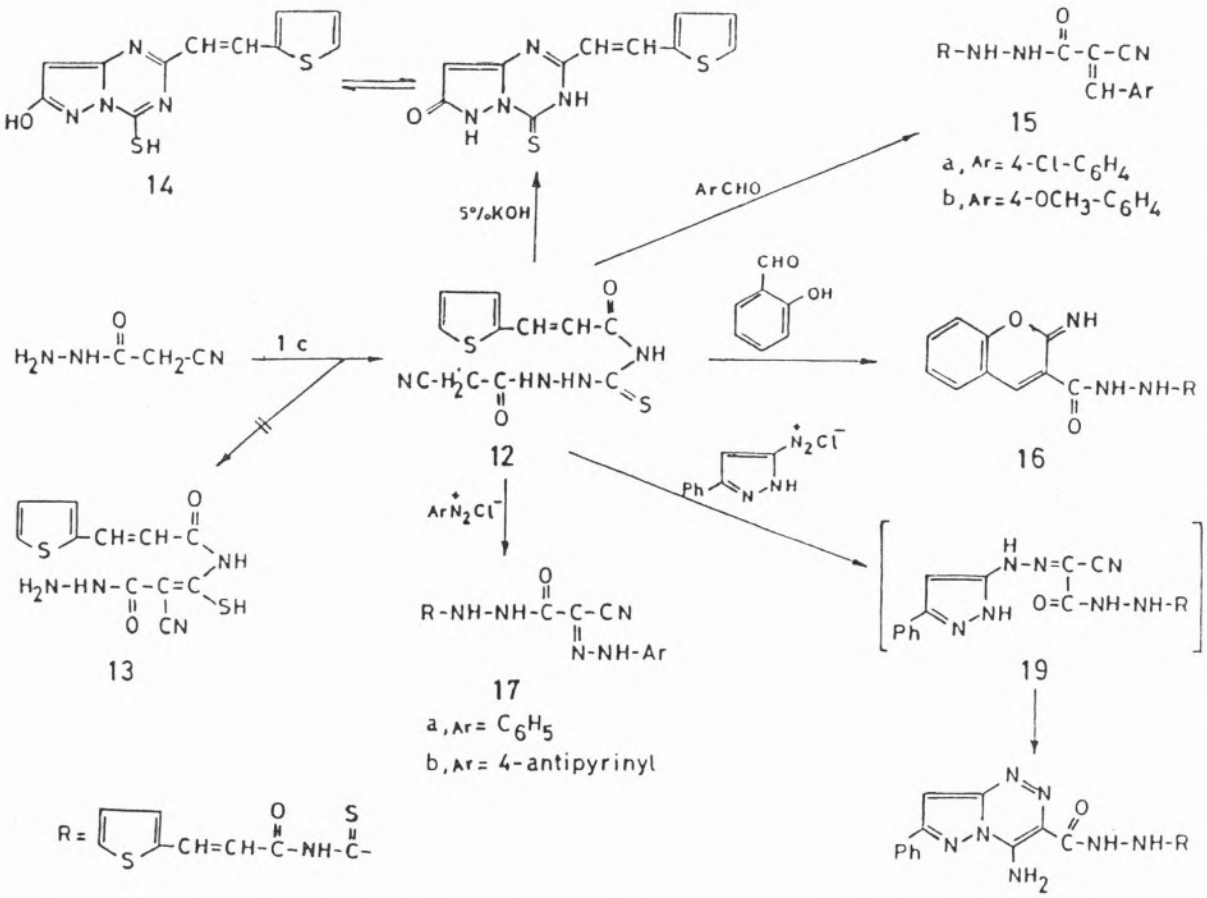

Chart 2

Trials to isolate the acyclic hydrazone 19 were unsuccessful. The direct isolation of triazines on coupling 12 with heterocyclic diazonium salts finds parallelism to Tisler's finding, as he reported isolation of triazines [6] on attempted coupling of diazotized aminoheterocycles with similar systems.

EXPERIMENTAL

All melting points are uncorrected. IR spectra were recorded on a Pye-Unicam SP-1100 spectrophotometer. ^{1}H-NMR spectra were recorded on a Varian EM-390-spectrometer using TMS as the internal standard and chemical shifts are expressed in ppm as δ values. Analytical data were obtained from an analytical Unit at the Cairo University. No attempt has been made to optimize the yields of the described reactions.

The acyl isothiocyanates 1a-c used in the described reactions were prepared by literature methods [7].

Reactions of amines with isothiocyanates. General procedure:

To a solution of compound 1(0.12 mol) in 150 ml of dry acetone, a solution of the appropriate amine (0.1 mol) in dry acetone (50 ml) was added. The reaction mixture was refluxed for 3 hrs and then evaporated in vacuo. The remaining solid product was filtered off, washed with water and crystallized from the appropriate solvent (cf. Table II).

Reactions of amines with acid halides:

To a solution of each of compounds 5 or 6, or 2-aminobenzothiazole (0.01 mol) in dry pyridine (20 ml) the equivalent quantity of

Table I

Spectral data of compounds 2-12

Product N.°	IR, (KBr), cm^{-1}	^{1}H-NMR; δ ppm
2a	3310, 3200 (NH); 1680 (CO); 1610 (C = C).	2.15 (s, 3H, CH_3); 3.25 (s, 3H, CH_3); 3.8 (s, 3H, CH_3); 6.75-7.7 (m, 11H, ethylenic and aromatic protons); 11.5 (br, 2H, 2NH).
2b	3290, 3230 (NH); 1690 (CO); 1620 (C = C).	2.3 (s, 3H, CH_3); 3.3 (s, 3H, CH_3); 6.5 (d, ethylenic CH); 7.0-7.95 (m, 10H, aromatic and ethylenic protons).
3	3210, 3100 (NH); 1690 (CO); 1615 (C = C).	6.3 (d, ethylenic protons); 7.25-8 (m, ethylenic, thienyl and pyridyl protons).
4	3220, 3150 (NH); 1675 (CO); 1610 (C = C).	7.1 (d, J = 15 Hz, trans ethylenic proton); 7.25-7.9 (thienyl and ν_5 pyrimidine); 8.1 (d, J = 15 Hz, trans ethylenic proton); 8.8, 8.9 (ν_4 and ν_6 pyrimidine); 12 and 13.2 (two NH groups).
7b	3400, 3300 (NH); 1700 (CO); 1610 (C = C).	Insufficiently soluble in commonly used ^{1}H-NMR solvents.
8a	3450, 3100 (NH); 1680 (CO); 1620 (C = C).	3.8 (s, 3H, CH_3); 6.9-7.75 (m, 8H, ethylenic, aromatic and thiazole protons).
8b	3360, 3210 (NH); 1700 (CO); 1610 (C = C).	6.8 (d, J = 15 Hz, trans ethylenic proton); 7.25-7.8 (thiophene and thiazole protons); 8 (d, J = 15 Hz, trans ethylenic proton); 12 and 12.8 (two NH groups).
11	3450, 3200 (NH); 1680 (CO); 1620 (C = C).	3.8 (s, 3H, CH_3); 6.7-7.95 (m, 10H, aromatic and ethylenic protons).
12	3450, 3340, 3210 (NH,NH_2); 1690 (CO); 1620 (C = C).	Insufficiently soluble in commonly used ^{1}H-NMR solvents.

the appropriate acid halide was added (chart 1). The reaction mixture was heated on a water bath for 15 min., left to cool and the solid product, so formed, was collected by filtration to give 7, 8 and 11, respectively, which proved to be identical with those obtained from the above procedure.

6-Hyidroxy-2-(thien-2'-ylvinyl)-4 mercapto--pyrazolo [1,5-a]-1,3,5-triazine (14):

A solution of compound 12 (0.01 mol) in potassium hydroxide solution (30 ml, 5 %), was refluxed for two hours, left to cool then acidified with dilute hydrochloric acid. The precipitated material was filtered off, washed with water and crystallized from DMF. compound 14 formed colourless crystals, m.p. > 300°C, yield 55 %; IR: 3300-2400 (NH and OH dimer); 1680 (C = O); 1640 (C = N); 1610 (C = C).

$C_{11}H_8N_4OS_2$ (276.33); Calcd. C, 47.12 %; H, 2.90 %; N, 20.28 %; Found C, 47.27 %; H, 2.85 %; N, 20.42 %.

Condensation of compound 12 with aromatic aldehydes:

A solution of compound 12 (0.01 mol) and (0.01 mol) of the appropriate aldehyde in

Table II

Physical and analytical data of compounds 2-12

Product N.°	Cryst. solvent	Yield/ /%	M. P./ /°C	Formula (M. W.)	Calcd. Found	Analysis C	H	N	S
2a	dioxane	78	204	$C_{22}H_{22}N_4O_3S$ (422.51)		62.54 62.70	5.24 5.10	13.27 13.15	7.59 7.63
2b	ethanol	72	205	$C_{21}H_{19}N_4O_2SCl$ (426.97)		59.07 59.20	4.49 4.20	13.12 12.91	7.51 7.49
3	ethanol/ chloroform	76	258	$C_{13}H_{11}N_3OS_2$ (289.38)		53.96 54.27	3.83 3.59	14.52 14.23	22.16 22.31
4	ethanol/ chloroform	75	184	$C_{12}H_{10}N_4OS_2$ (290.37)		49.64 49.91	3.47 3.5	19.29 19.10	22.08 22.19
7b *	ethanol	65	213	$C_9H_8N_4OS$ (220.26)		49.08 49.38	3.66 3.78	25.44 25.32	14.56 14.72
8a *	dioxane	70	212	$C_{13}H_{12}N_2O_2S$ (260.32)		59.98 59.85	4.65 4.46	10.76 10.71	12.31 12.25
8b *	dioxane	65	236	$C_{10}H_8N_2OS_2$ (236.32)		50.83 50.81	3.41 3.63	11.85 11.62	27.13 27.43
11 *	dioxane	75	260	$C_{17}H_{14}N_2O_2S$ (310.38)		65.79 66.01	4.55 4.42	9.03 9.23	10.33 10.51
12	DMF	80	240	$C_{11}H_{10}N_4O_2S_2$ (294.36)		44.85 44.88	3.53 3.42	18.79 19.03	21.56 21.8

* Recorded yields corresponding to the products of the reaction of amines with acid chlorides.

20 ml of absolute ethanol containing the catalytic amount of piperidine was heated at reflux for 3 hours. The solid product, so formed, on cooling was filtered off, washed with ethanol, dried and crystallized from DMF.

Compound 15a formed brown crystals in a 82 % yield; m. p. 253°C; IR: 3300-3100 (NH); 2200 (conjugated CN); 1680 (C = O); 1610 (C = C).

$C_{18}H_{13}N_4O_2S_2Cl$ (416.88); Calcd. C, 51.86 %; H, 3.14 %; N, 13.44 %; S, 15.38 %; Found C, 52.21 %; H, 2.95 %; N, 13.35 %; S, 15.36 %.

Compound 15b formed yellow crystals in a 75 % yield, m. p. 245°C; IR: 3400-3050 (NH); 2200 (conjugated CN); 1680 (C = O); 1620 (C = C).

$C_{19}H_{16}N_4O_3S$ (412.5); Calcd. C, 55.32 %; H, 3.9 %; N, 13.58 %; Found C, 55.12 %; H, 3.72 %; N, 13.52 %.

Compound 16 formed yellow crystals in a 62 % yield, m. p. 215°C; IR: 3400, 3060 (NH); 1680 (C = O); 1640 (C = N); 1610 (C = C).

$C_{18}H_{14}N_4O_3S_2$ (398.4); Calcd. C, 54.3 %; H, 3.54 %; N, 14.06 %; Found C, 54.22 %; H, 3.42 %; N, 14.32 %.

Coupling of diazotised amines with compound 12:

A solution of the appropriate diazonium salt (0.01 mol) was added to a cold solution of compound 12 in ethanol (30 ml) and sodium acetate (3 g) with stirring. The reaction

mixture was left in a refrigerator for two hours. The precipitated product was filtered off, washed with water, dried and crystallized from the appropriate solvent.

Compound 17a formed red crystals from DMF in a 65 % yield, m. p. 179°C; IR: 3500-3050 (NH); 2220 (conjugated CN); 1670 (C = O); 1620 (C = C).

$C_{17}H_{14}N_6O_2S_2$ (398.47); Calcd. C, 51.24 %; H, 3.54 %; N, 21.09 %; Found C, 51.40 %; H, 3.41 %; N, 20.88 %.

Compound 17b formed brown crystals from acetic acid in a 72 % yield, m. p. 205°C; IR: 3450-3050 (NH); 2200 (CN); 1680 (exocyclic CO); 1660 (antipyrinyl CO); 1610 (C = C).

$C_{22}H_{20}N_8O_3S_2$ (508.59); Calcd. C, 51.95 %; H, 3.96 %; N, 22.03 %; Found C, 52.13 %; H, 4.22 %; N, 22.34 %.

Compound 18 formed brown crystals from DMF in a 67 % yield, m. p. > 300°C; IR: 3450-3000 (NH); 1680 (C = O); 1610 (C = C).

$C_{20}H_{16}N_8O_2S_2$ (464.54); Calcd. C, 51.71 %; H, 3.47 %; N, 24.12 %; Found C, 51.57 %; H, 3.56 %; N, 24.53 %.

Received, 13th December 1985

REFERENCES

[1] M.H. ELNAGDI, M.R.H. ELMOGHAYAR, D.H. FLEITA, E. HAFEZ, S.M. FAHMEY, *J. Org. Chem.*, 3781 (1976).

[2] M.H. ELNAGDI, E.M. ZAYED, E.M. KANDEED, S.M. FAHMY, *Z. Naturforsch.*, **32b**, 430 (1977); *J. Heterocyclic Chem.*, **16**, 61 (1979).

[3] B. KOREN, B. STANOVNIK, M. TISLER, *J. Heterocyclic Chem.*, **14**, 621 (1977).

[4] J. BECHER, E.G. GRANDSEN, *Tetrahedron*, **33**, 341 (1977).

[5] M.R.H. ELMOGHAYAR, E.A. GALI, M.M.M. RAMIZ, M.H. ELNAGDI, *Liebigs Ann. Chem.*, In Press (1985).

[6] M. TISLER, B. STANOVNIK, *Khim Geterotsikl. Soedin.*, **5**, 379 (1980); C.A. **93**, 150139 (1980).

[7] A.E. DIXON, J. TAYLER, *J. Chem. Soc.*, **93**, 684 (1908).

RESUMO

Algumas reacções de isocianatos de acilo α,β-insaturados

Foram estudadas reacções de adição nucleófila de aminas aromáticas e heteroaromáticas a isocianatos de acilo α,β-insaturados. O produto de reacção 12 foi transformado em derivados de pirazolo [1,5-a]-s--triazina, de pirazolo [1,5-c]-as-triazina e de cumarina.

A.M.M. CARDOSO
M.G. SANTANA MARQUES
A.J. FERRER CORREIA
Departamento de Química, Universidade de Aveiro
3800 Aveiro, Portugal

METASTABLE MAPPING: BIDIMENSIONAL MASS SPECTROMETRY IN A REVERSE GEOMETRY INSTRUMENT

An analysis of metastable mapping in double-focusing mass spectrometers is presented, and a detailed description of this technique applied to a reverse-geometry instrument is given. The data are presented and analysed by means of tridimensional plots, contour plots and colour-coded maps, and the most significant characteristics of these representations are pointed, with emphasis to the colour-coded maps, where decompositions in the 1.st and 2.nd FFR's are identified. Consecutive decompositions in both regions are also described and located in the map.

The complete colour map is presented for bis(dimethylglyoximato) nickel(II), and the main fragmentation processes observed are identified and discussed. A brief comparison is made with other similar complexes of nickel(II), palladium(II) and platinum(II) and with the ligands themselves.

INTRODUCTION

The observation of metastable decompositions or collision induced decompositions along the flight path of a mass spectrometer has great relevance in the study of reaction mechanisms in the gas-phase, in the elucidation of ion structures and, more recently, in the direct mass spectrometric analysis of complex mixtures with little or no sample pre-treatment [1, 2].

In double-focusing mass spectrometers (Fig. 1) the electric sector disperses ions according to their kinetic energy to charge ratio ($r = m.v^2/Ee$), while the magnetic sector separates them according to their momentum to charge ratio ($r = m.v/Be$). In a conventional mass spectrum, the parameters V (acceleration potencial) and E (electric analyser field) are held constant while the magnetic field (B) is scanned to focus ions of different mass to charge ratios on the detector.

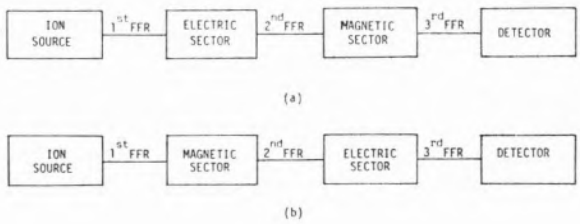

Fig. 1

Block-diagram of Double-Focusing Mass Spectrometers:

(a) *Direct Geometry.*
(b) *Reverse Geometry.*

Since the decomposition of an ion $m1^+$ outside the ion source (a metastable ion) will produce a fragment ion $m2^+$ with only a fraction of the original kinetic energy (Ve), $m2^+$ will not be detected at the same position in the mass spectrum as ions $m2^+$ formed inside the source, or will even not be detected at all. With single focusing instruments

(magnetic sector only), or in double focusing instruments of direct geometry (Fig. 1-a), the decomposition of $m1^+$ in the 2.nd FRR produces a broad and diffuse metastable peak in the conventional mass spectrum, at an apparent mass of $m^* = m2^2/m1$; such peaks are absent in the mass spectrum obtained in a reverse geometry instrument (Fig. 1-b).

SCANNING TECHNIQUES

The detection of metastable decompositions occurring in the 1.st FFR or in the 2.nd FFR of a mass spectrometer of conventional or reverse geometry can also be accomplished by alternative methods of scanning V or E independently or simultaneously, as well as by scanning any of these two parameters in conjunction with B, providing much more information than the metastable peaks observed in classical mass spectra. In Table 1 the scanning modes more frequently used are indicated, as well as the principal characteristics and information obtainable in each case. The list is by no means exhaustive, since several other possibilities exist and are used, such as B^2/V, B^2V, V/E^2, B^2E, etc. However, some of these scans provide the same type of information as the ones indicated, posing in addition several instrumental problems. The main disadvantage of the methods in wich V is varied are detuning of the source and the small usable amplitude of the ratio V/V0. Scans in wich V is held constant do not pose such problems, and consequently they are being more widely used [3, 4].

In some types of scans, information about kinetic energy released in the fragmentation is obtainable from the shape of the broad peaks present on those spectra. Although that information is lost in the daughter- or parent-ion spectra, with sharp peaks, a much better mass resolution is obtained in these cases, allowing for a more precise mass assignment [4].

Table 1

Scan	Fixed	Instrument	FFR	Information	Peak
V	E, B	Direct or Reverse	First	Parent Ion Spectrum	Broad
E	V, B	Direct	First	Daughter Ion Spectrum	Broad
		Reverse	Second		
B/E	V	Direct or Reverse	First	Daughter Ion Spectrum	Sharp
B^2/E	V	Direct or Reverse	First	Parent Ion Spectrum	Broad
$(B/E')^2 . (1-E')$ $E' = E2/E1$	V	Direct or Reverse	First	Neutral Fragment Loss	Sharp

INTERFERENCE PEAKS

A cause for considerable concern and even disagreement about the scope of validity of

many metastable based techniques is the existence of interference peaks in some unexpected circumstances. Interference peaks are due to decompositions which occur in regions of the mass spectrometer other than the field-free region that is under investigation, and may be present in the spectra obtained in any kind of scan.

The most serious interference observed in E scans is due to decompositions of other ions in the 1.st FFR [5-8]. The presence of interference peaks in V scans [9] and in B/E scans [10], due to decompositions in the 2.nd FFR, have also been reported. Interferences are also caused by decompositions involving ions of mass similar to the ion under study (e.g., $M \pm 1$, $M \pm 2$), not only in one of the field-free regions but also during acceleration of the ions, or inside the magnetic or electric sector [11].

What is common to all interference peaks is that, in fact, they correspond to ions transmitted for unexpected combinations of mass and energy. For example, the 1.st FFR interference in E scan experiments in reverse geometry mass spectrometers occurs because, while it is expected to find peaks due to decompositions in the 2.nd FFR, for a particular combination of magnetic field and electric analyser field values, ions with certain mass-to-charge ratio resulting from decompositions of other parents in the 1.st FFR may be also transmitted. The same can occur in a wide variety of other situations. In this sense, interference peaks are, therefore, inherent to a particular experiment in mass spectrometry. They may be, of course, entirely different from one instrument to another but, given reproducibility of conditions, they will be as reproducible as the «expected» metastable peaks. From this follows that the name, frequently quoted in the literature, of «Artifacts», or «Artifact Peaks», is misleading and unfortunate, as the coined name «Metastables», which resulted of a wrong interpretation, has been as well.

BIDIMENSIONAL REPRESENTATION

Most of the inconvenients associated with interference peaks can be overcome if there is an easy and prompt way of identifying the nature and origin of all signals obtainable in a mass spectrometer. Lacey and Macdonald have shown extensively [11-14] how the decompositions in different parts of different types of mass spectrometers can be represented as a three-dimensional surface, in which one of the coordinates is the ion current, or a related value, and the other two are transformations of the mass of the transmitted ions and of the electric field values for which they are transmitted (ESA and accelerating fields).

In fact, the concept of this representation was introduced by KISER *et al.* [15], and a similar treatment has been used with data acquired with a computer connected on-line to a mass spectrometer, for global analysis of all metastable transitions in the mass spectrum of a substance [16-23]. A detailed description and appraisal of the technique as used with a direct geometry mass spectrometer is given by Farncombe, Mason, Jennings an Scrivens [17].

In the present work, we describe a representation of the ion-current obtained in a reverse geometry mass spectrometer (Varian MAT 112S) by repeatedly scanning the magnetic field for several successive values of the ESA field [24]. As the resulting data consist in a series of peak intensities on a bidimensional surface of mass and ESA field, this «metastable mapping» may be, in fact, considered as a form of bidimensional mass spectrometry. It is worth establishing a correspondance between the resulting map and Lacey and Macdonald's plot. These authors used for the two axis of the representation plane $\rho = (V0/V)\ (E/E0)$ and $m^* = (V0/V).m$, which in this case are linearly related to mass and ESA field.

In Fig. 2 the bidimensional mass spectrum of bis(dimethylglyoximato) nickel(II) is represented as a colour map (described below).

The horizontal axis represents mass, and the vertical axis represents ESA field (both on a linear scale). Since the ESA voltage decreases from the bottom of the figure to the top, the main beam is in fact represented in the lower part of the map (corresponding to E0), and the metastable decompositions fill the rest of the plane. In all cases, the colour areas correspond to ion current greater than a previously defined threshold, though not all of the spectrum has the same gain, the main beam being one or two orders of magnitude attenuated as compared with the metastable area.

The main advantages of this type of representation can be readily observed. In fact, it becomes patent from the observation of the map that, as to each peak a field value and a mass can be attributed, and as the peak shape (in a bidimensional sense) can be described, its origin can be ascertained, if not always in a completely unambiguous way, at least with much greater knowledge than from simple unidimensional scans. From the figure, it is apparent that some of the colour areas, corresponding to peaks, are aligned at an angle relatively to the axis, while others form series of more round patches along a vertical line (corresponding to a constant mass). It can be demonstrated [11-14] that the first are decompositions in the 1.st FFR and during acceleration, leading to the formation of a certain ion, while the second are decompositions in the 2.nd FFR, resulting from the breakdown of the same parent ion. In some cases, as described below, decompositions inside the magnet or the ESA can also be found, and consecutive decompositions (ion formed in the 1.st FFR and breaking down in the 2.nd FFR) can also be identified.

DATA PROCESSING AND PRESENTATION

The acquisition of data to be treated in this bidimensional analysis may follow several procedures, from the very crude to the very sophisticated. In the present work, a dedicated computer interface, specifically built for this purpose, with the appropriate software, was used to acquire directly the data to a Z80 micro-computer (NEC PC8800), under CP/M. The file created in disk, is subsequently subjected to a digital filter and compression to save storage space, before treatment.

The analysis of the data can be done in three different ways: tridimensional plots, contour plots and colour maps. The tridimensional plots can be useful in particular cases, to examine closely a small portion of the spectrum, as shown in Fig. 4 for the peak corresponding to the $OH^{\cdot}$ loss from the molecular ion of the bis(dimethylglyoximato) nickel(II). Contour plots are computer-drawn curves of iso-intensity points in the mass-voltage space, and colour maps consist of a representation of the same plane in which intensities between preset values are represented by areas coloured according to a code. This has proved to be, in general, the most useful type of representation, as it provides the greatest amount of information, both visually and with the help of further computer treatment (Fig. 2).

As suggested above, in the map-type representation some «geometrical» arrangements of peaks correspond, effectively, to decomposition paths of the ions, which is easily understood as certain curves in the mass-voltage plane correspond to some of the E, B scans, single or combined, mentioned above. This can be shown most efficiently with the help of curves displayed in the monitor over the map, following certain laws depending on the relation being looked for. The most important are:

$$E = E0 \cdot M/M0$$

This curve (a straight line) connects all the ions that are parents of ion of mass M0 in the 1.st FFR, being E0 the main beam voltage.

$$E = E0 \cdot M0/M$$

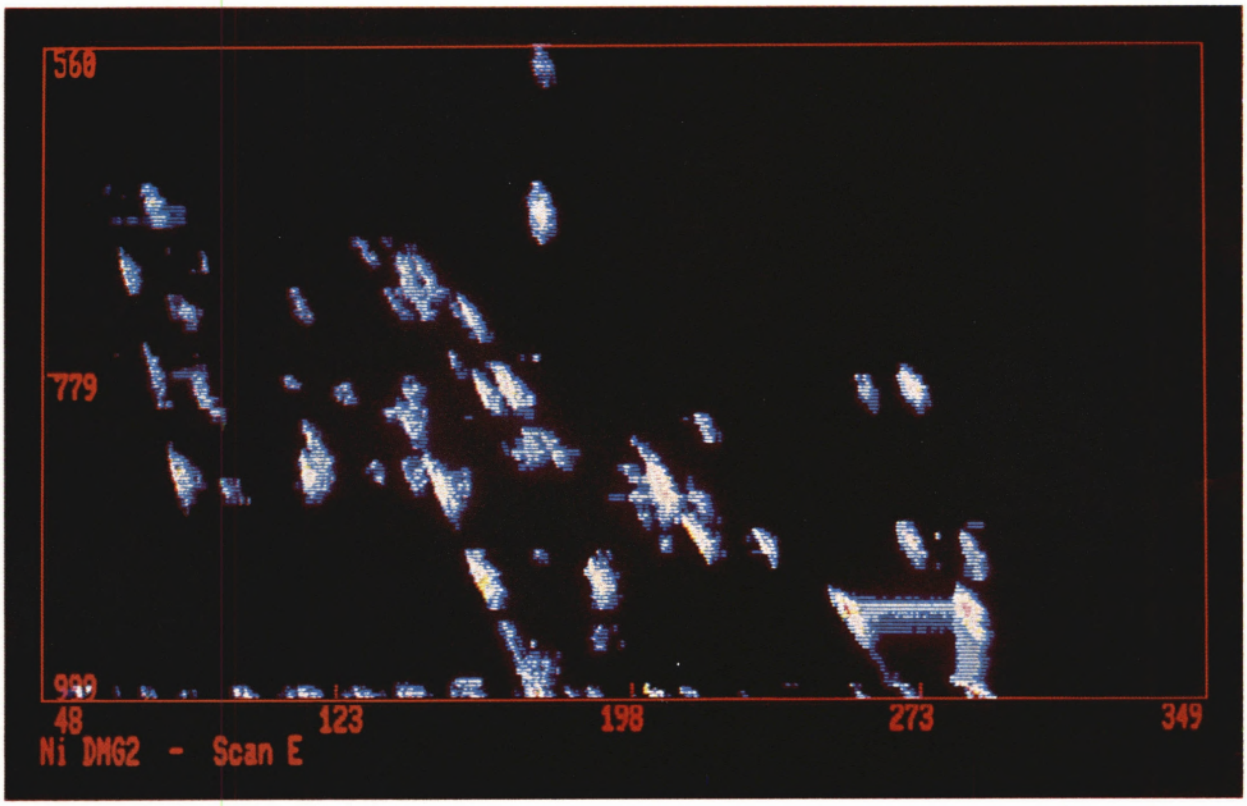

Fig. 2

Bidimensional Mass Spectrum of Bis(dimethylglyoximato) Nickel(II).

A curve connecting all the parents of ion of mass M0 in the 2.nd FFR.

$E = E0 . (1-Mn/M)$

A curve drawn across all the colour areas corresponding to loss of a neutral fragment of mass Mn.

$M = M0$

A straight vertical line, corresponding to the classical E scan at constant mass, i.e. a daughter ion spectrum in the 2.nd FFR (MIKES or DADI spectrum).

In general, of course, all the features shown in one type of representation are present in the others. However, for certain inferences and descriptions, one type may be preferred to another. For a global reference and tracing decomposition pathways, the map, with the help of the computer drawn curves, is very helpful, as it is as well for identifying the origin of the peaks (or colour areas). With the help of the map in Fig. 2, besides identification of most of the 1.st FFR and 2.nd FFR decompositions, it is possible to discover that the peak at mass 258 and E = 0.791.E0 is possibly not a 2.nd FFR «straight» decomposition, ($258^+ \rightarrow 204^+$) but a decomposition in the 2.nd FFR of an ion formed in the 1.st FFR ($288^+ \rightarrow 271^+ \rightarrow 214^+$). This is explained in Fig. 3 for the general case of $B^+ \rightarrow C^+$ in the 2.nd FFR, or $A1^+ \rightarrow B1^+$ in the 1.st FFR, $B1^+ \rightarrow C1^+$ in the 2.nd FFR. In this case, the metastable peak should be positioned at mass $B1^2/A1$ and $E = (C1/A1).E0$. A close analysis of the group represented in the lower right hand corner of Fig. 2 is shown in a tridimensional plot in Fig. 4. The tall and narrow peaks in the background are the beginning of the main beam. The broad peak in front of this represents loss of $OH^{\cdot}$ in the 2.nd FFR, while the narrower peak to the left, at an angle to the viewer, is the same decomposition in the 1.st FFR. From this peak, a narrow and small ridge going towards the main beam represents ions formed during acceleration, while the low intensity, broad barrier, connecting the 1.st and 2.nd FFR peaks, in the front of the figure and parallel

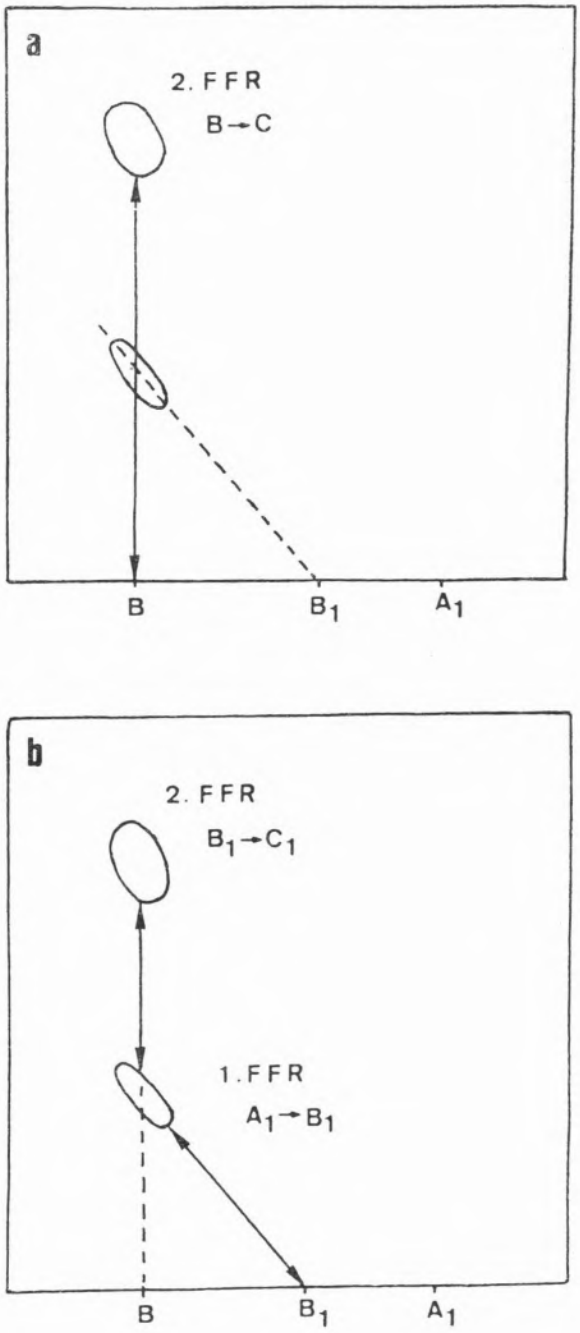

Fig. 3

Origin of a peak in a Bidimensional Map

(a) *Single decomposition in the 2.nd FFR.*
(b) *Decomposition in the 1.st FFR followed by a decomposition in the 2.nd FFR.*

to the viewer is the result of decompositions in the magnet. Finally, the broad portion connecting the 2.nd FFR peak with the main beam (perpendicular to the viewer and partly obscured by the 2.nd FFR peak) corresponds to the same decomposition taking place inside the ESA.

BIDIMENSIONAL MASS SPECTRA OF VIC DIOXIMATES

This technique of bidimensional mass spectrometry has been used to study the vic-dioximates of nickel, palladium, and platinum, and the bidimensional mass spectra for the

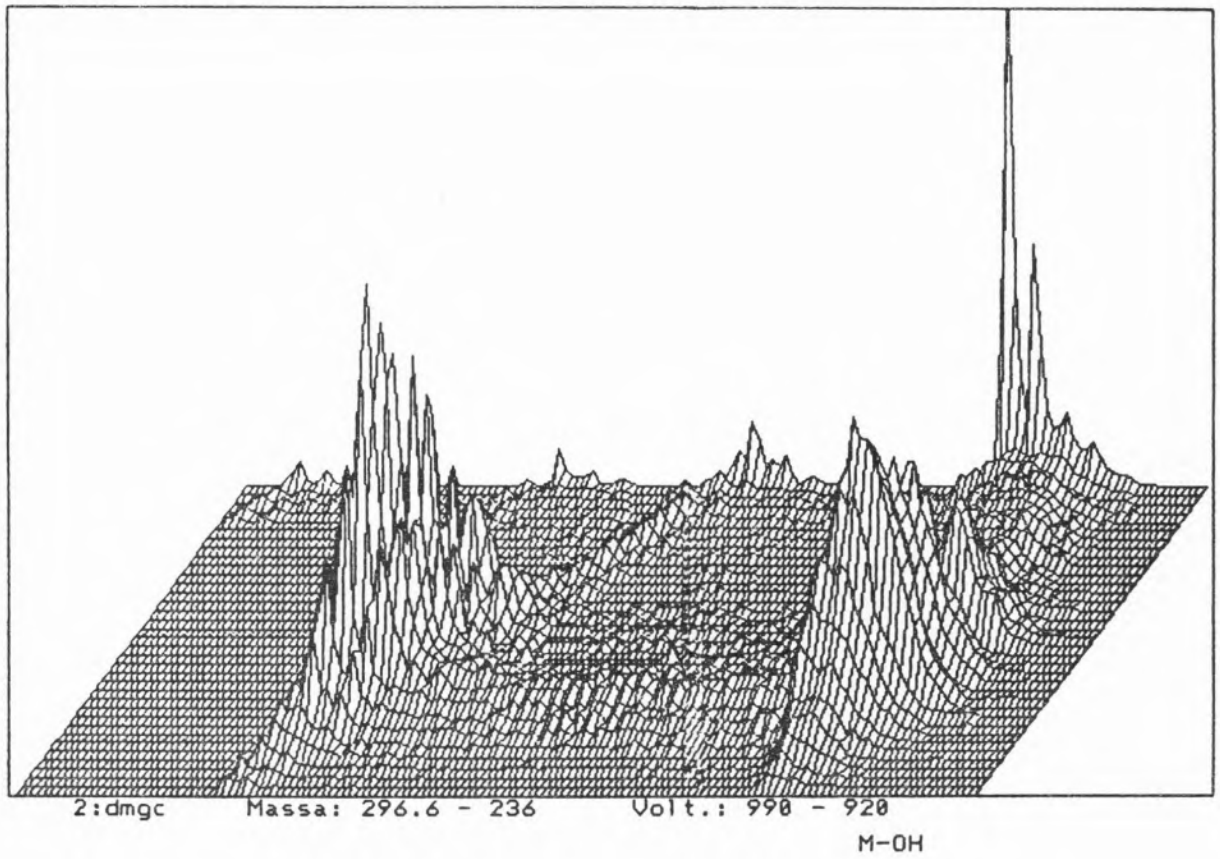

Fig. 4

Tridimensional plot of the $M^{+\cdot} \rightarrow [M\text{-}OH]^{+}$ decomposition for Bis(dimethylglyoximato) Nickel(II).

As another interesting result of the greater amount of information available at once, it should be mentioned that it is in general possible, without the loss of too much information, to work at considerably lower resolution than it would be necessary otherwise; therefore, higher intensities can be obtained, which is invaluable in the case of metastable peaks, generally of very low abundance.

dimethylglyoximato complexes of Ni(II), Pd(II) and Pt(II) and for glyoxime and dimethylglyoxime have been done and studied. Up to now, there have been relatively few mass spectrometric studies of these compounds reported in the litterature [25-28], and metastable ion evidence for fragmentation processes is scarce. From the bidimensional mass spectra we have been able to establish

metastable supported pathways leading to most of the ions that are important in the conventional mass spectra of the above men-

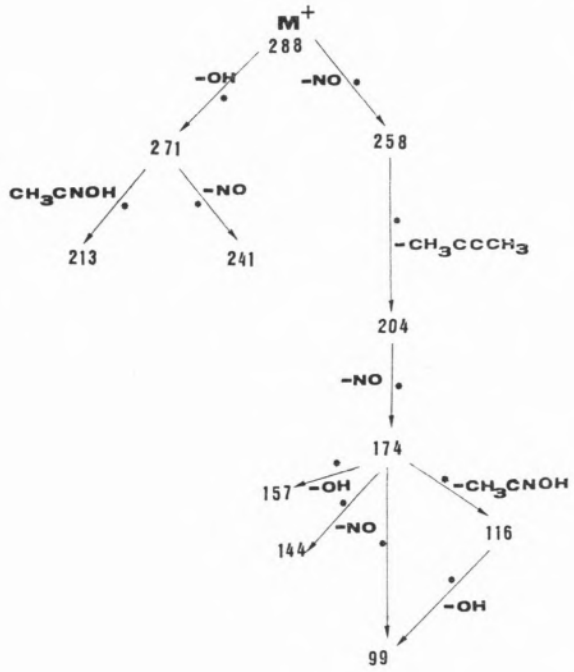

Fig. 5

Metastable supported fragmentation pattern for Bis(dimethylglyoximato) Nickel(II).

tioned compounds. As the work on the vic-dioximates as a whole will be the subject of another publication, we will here deal specifically with bis(dimethylglyoximato) nickel(II), whose bidimensional mass spectrum is shown in Fig. 2.

In Fig. 5 and 6 the metastable supported fragmentation pathways proposed are represented. In these figures we can see a proposed pathway for the formation of ion of m/e=174, being the result of successive losses of 30, 54 and 30 mass units, detected in the 2.nd FFR. In mass terms, ion 174^+ should correspond to the loss, from the molecular ion, of the equivalent to one ligand minus one mass unit. The pathway proposed for its formation [27] was a single step one, with a shift of one hydrogen atom from the lost moiety to the moiety remaining bound to the metal. However, no such reaction is supported by any metastable ion transition.

As referred above, we can not differentiate between the loss of 54 mass units in the 2.nd FFR from the ion of m/e = 258 (Fig. 5) and two successive decompositions: a loss in the 1.st FFR of 17 mass units from the molecular ion (m/e = 288), followed by a loss in the 2.nd FFR of 57 mass units (Fig. 6).

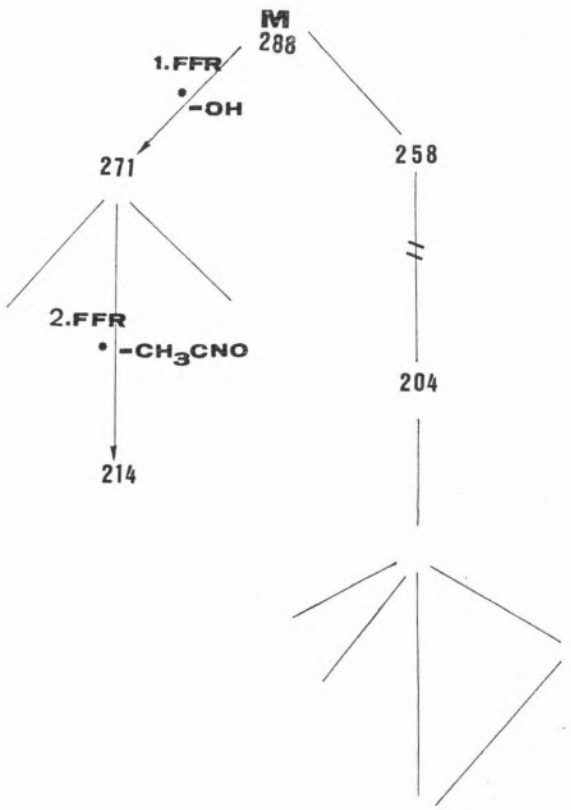

Fig. 6

Alternative fragmentation pattern for Bis(dimethylglyoximato) Nickel(II).

This is a good illustration of the help that the analysis of bidimensional mass spectra can provide, in cases where peaks from different origins can interfere with each other; in this case the possibilities of both origins become obvious, unlike the case of the conventional metastable representations [2-4].

Another significant advantage of bidimensional mass spectrometry is illustrated by

the fragmentation of ion of m/e = 174, whose daughter ion spectrum obtained by scanning the ESA electric field is shown in Fig. 7. The triple peak can be easily identified by looking

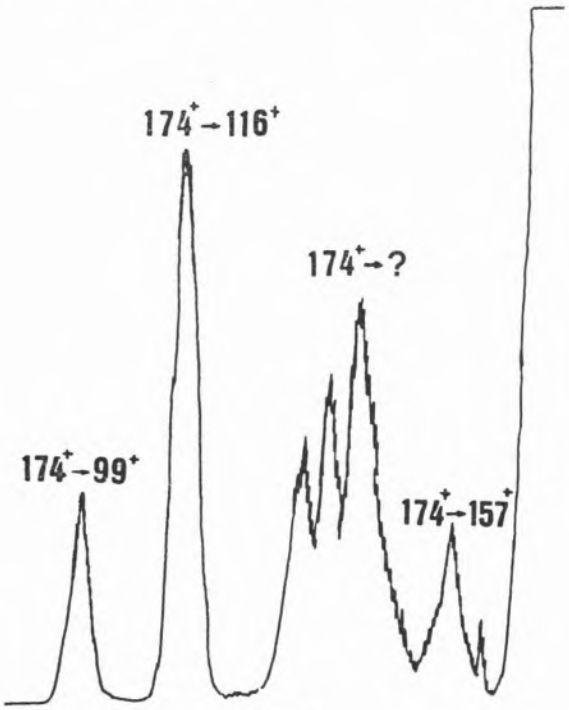

Fig. 7

Electric Field scan of ion m/e = 174.

at the bidimensional mass spectrum (Fig. 2), and it is then found to be the result of a 30 mass units loss from ion 174^+ in the 2.nd FFR, partially superimposed to peaks representing decompositions in the 1.st FFR which lead to the formation of ions of m/e = 204 and m/e = 213.

The tridimensional plot described above (Fig. 4) can also be useful in the interpretation of the metastable decompositions, and is here illustrated with the study of the only metastable supported decomposition described insofar for this class of compounds [28]: the loss of 17 mass units from the molecular ion of vic-dioximato complexes. In the figure, the substance under study is the bis(dimethylglyoximato) nickel(II), as stated.

The general features of this plot are characteristic, not only of the bis(dimethylglyoximato) complexes of Ni(II), Pd(II) and Pt(II), but also of the dimethylglyoxime itself. This will, it is hoped, allow the use of the $M^+ \rightarrow [M\text{-}OH]^+$ decomposition as an «hallmark» for the rapid identification of vic-dioximates and vic-dioximates. In this context, the use of pattern recognition is at present being implemented to extend the present work with the intention of enabling bidimensional mass spectrometry to be the basis for identification of known substances in complex mixtures. The study is currently being done with the substances mentioned above, but it is planned to extended it to a more general type of detection.

ACKNOWLEDGMENTS

The authors are indebted to the Instituto Nacional de Investigação Científica (who supported this work through grants given to the Centro de Química do Meio Aquático, Aveiro, and to one of the authors, M.G.S.M.), and to the Calouste Gulbenkian Foundation (for grants towards instrumentation).

(Received, 13th December 1985)

REFERENCES

[1] R.G. Cooks, J.H. Beynon, R.M. Caprioli, G.R. Lester — «Metastable Ions», Elsevier Sc. Publ. Co., 1973.

[2] R.G. Cooks — «Collision Spectroscopy», Plenum Press, 1978.

[3] R.K. Boyd — Spectrosc. Int. J., 1982, **1**, 169.

[4] K.R. Jennings, in «Ionic Processes in the Gas Phase», Ed. M.A. Almoster Ferreira, NATO ASI Series, 1984, 7.

[5] T. Ast, M.H. Bozorgzadeh, J.L. Wiebers, J.H. Beynon, A.G. Brenton — Org. Mass Spectrom., 1979, **14**, 313.

[6] B. Schaldach, H.F. Grutzmacher — Org. Mass Spectrom., 1980, **15**, 182.

[7] W. Heerma, M.M. Sarneel, J.K. Terlouw — Org. Mass Spectrom., 1981, **16**, 325.

[8] F.W. McLafferty, F.M. Bockhoff—Anal. Chem., 1978, **50**, 69.

[9] A. Maquestiau, Y. van Haverbeke, R. Flammang, C. de Meyer — Bull. Soc. Chim. Belg., 1977, **86**, 281.

[10] R.P. Morgan, C.J. Porter, J.H. Beynon — Org. Mass Spectrom., 1977, **12**, 735.

[11] M.J. LACEY, C.G. MACDONALD, K.F. DONCHI, P.J. DERRICK — Org. Mass Spectrom., 1981, **16**, 351.
[12] M.J. LACEY, C.J. MACDONALD — Org. Mass. Spectrom., 1978, **13**, 284.
[13] M.J. LACEY, C.J. MACDONALD — Org. Mass Spectrom., 1977, **12**, 587.
[14] M.J. LACEY, C.J. MACDONALD — Org. Mass Spectrom., 1984, **19**, 55.
[15] R.W. KISER, R.E. SULLIVAN, M.S. LUPIN — Anal. Chem., 1969, **41**, 1958.
[16] G.A. WARBURTON, R.S. STRADLING, R.S. MASON, M.J. FARNCOMBE — Org. Mass Spectrom., 1981, **16**, 507.
[17] M.J. FARNCOMBE, R.S. MASON, K.R. JENNINGS, J. SCRIVENS — Int. J. Mass Spectrom. Ion Phys., 1982, **44**, 91.
[18] M. COSGROVE, D. HAZELBY, G.A. WARBURTON, R.S. STRADLING, C.J. CHAPMAN — Int. J. Mass Spectrom. Ion Phys., 1983, **46**, 89.
[19] A. FRAEFEL, J. SEIBL — Int. J. Mass Spectrom. Ion Phys., 1983, **46**, 87.
[20] A. FRAEFEL, J. SEIBL — Int. J. Mass Spectrom. Ion Phys., 1983, **51**, 245.
[21] R.S. MASON, M.J. FARNCOMBE, K.R. JENNINGS, J. SCRIVENS — Int. J. Mass Spectrom. Ion Phys., 1983, **48**, 415.
[22] M.G. SANTANA MARQUES, A.J. FERRER CORREIA — 8th. Meet. Port. Chem. Soc., 1985.
[23] D. GAUDIN, H. VIRELIZIER, K. JANKOWSKI — Spectroscopy Letters, 1985, **18**, 243.
[24] A. FERRARI DE ALMEIDA, A.R. BORGES, N.P. DA ROCHA, J.M.S. PINTO, R.R. SILVA, A.J. FERRER CORREIA — 8th. Meet. Port. Chem. Soc., 1985.
[25] A.V. ABLOV, KH. SH. KHARITONOV, ZH. YU. VAISBEIN — Doklady Chem., 1971, **201**, 916.
[26] A.V. ABLOV, KH. SH. KHARITON, ZH. YU. VAISBEIN — Russ. J. Inorgan. Chem., 1973, **17**, 1722.
[27] J. CHARALAMBOUS, C. SOOBRAMANIEN, A.D. STYLIANOU, G. MANINI, L. OPERTI, G.A. VAGLIO — Org. Mass Spectrom., 1983, **18**, 406.
[28] J.B. WESTMORE, D.K.C. FUNG — Inorgan. Chem., 1983, **22**, 902.

RESUMO

Mapas de metastáveis: espectrometria de massa bidimensional num instrumento de geometria inversa.

Neste trabalho apresenta-se uma análise de mapas de metastáveis obtidos em espectrómetros de massa de focagem dupla, e faz-se uma descrição detalhada da técnica na sua aplicação a um instrumento de geometria inversa. Os dados são apresentados e analisados por meio de gráficos tridimensionais, curvas de iso-intensidade e mapas com cores codificadas, e as características mais significativas das diversas representações são discutidas, com relevo para os mapas com código de cores, em que são identificadas decomposições na 1.ª e 2.ª regiões livres de campo, assim como decomposições consecutivas naquelas duas regiões.

O mapa com cores codificadas é apresentado para o caso do bis(dimetilglioximato) níquel(II), para o qual é apresentado e discutido o esquema que representa as principais fragmentações identificadas. Também é feita uma breve comparação com os espectros de outros complexos semelhantes de níquel(II), paládio(II) e platina(II), assim como com os dos ligandos isolados.

ANTÓNIO R.T. CALADO
CÉSAR A.N. VIANA
LÍDIA M.P.C. ALBUQUERQUE
RAQUEL M.C. GONÇALVES

Centro de Electroquímica e Cinética da Universidade de Lisboa (I. N. I. C.)
Instituto Bento da Rocha Cabral,
Calçada Bento da Rocha Cabral, 14,
1200 Lisboa

MÉTODO ESTATÍSTICO APLICADO À CINÉTICA DE REACÇÕES DE 2.ª ORDEM

1 — Reacção de Menschutkin do iodote de etilo com a trietilamina em butanol-2.

Neste artigo analisam-se os métodos utilizados no cálculo de velocidades específicas de reacções de 2.ª ordem, suas condições de aplicabilidade e incertezas associadas. Estuda-se, em particular, a reacção de Menschutkin do iodeto de etilo com a trietilamina em butanol-2.

1 — INTRODUÇÃO

«*Mathematics is the language of Science. As Chemists learn to use the many advanced methods of statistics and data analysis, better measurements will be made and more chemical information will be extracted from those measurements.*»

B. R. Kowalski [1]

A análise estatística tem hoje importância fundamental para a interpretação de resultados experimentais em todos os domínios da Química, desde que feita de forma adequada. Há alguns anos, iniciámos um estudo sobre a aplicação de técnicas de análise estatística de resultados experimentais de cinética química à determinação da incerteza de parâmetros estimados [2]. Este tipo de análise tem vindo a ser muito desenvolvido no caso de reacções de 1.ª ordem [2-5]. No entanto, tal não tem acontecido em relação às de 2.ª ordem. Este facto justifica, por exemplo, o aparecimento, em 1981, de um artigo [6] descrevendo um novo método de determinação de velocidades específicas em tudo idêntico ao formulado por Tobey [7], dezoito anos antes. Outra consequência muito comum é o uso, por comodidade, de tratamentos de pseudo-1.ª ordem o que, implicando a utilização de um dos reagentes em excesso, pode determinar modificações do mecanismo reaccional. Neste trabalho apresentamos uma compilação dos métodos indicados para a determinação de velocidades específicas de reacções irreversíveis de 2.ª ordem, enumeramos as suas condições de aplicabilidade e, principalmente, reformulamo-los no sentido de poderem ser utilizados métodos de análise estatística que permitam (i) optimizar os valores de velocidade específica e (ii) calcular as incertezas associadas àquela grandeza.

As reacções de Menschutkin são um exemplo clássico de reacções de 2.ª ordem. Neste artigo, estudam-se, em particular, as velocidades específicas da reacção de Menschutkin do iodeto de etilo com a trietilamina em butanol-2 em função da temperatura e da pressão.

2 — MÉTODOS DE DETERMINAÇÃO DA VELOCIDADE ESPECÍFICA

A determinação da velocidade específica duma reacção irreversível de 2.ª ordem pode ser feita utilizando uma das equações apresentadas na Tabela 1. A primeira coluna desta tabela diz respeito às hipóteses subjacentes à formulação da equação integrada de velocidade. As terceira e quarta colunas indicam, respectivamente, a variável dependente e independente da relação linear y = f(x) considerada e nas sexta e sétima colunas podem ver-se as expressões que permitem obter a velocidade específica, k, e o respectivo desvio padrão, $\sigma(k)$. Descrevemos, em seguida, as características e condições de aplicabilidade específicas de cada método.

2.1 — *LEI DE VELOCIDADE INTEGRADA*

A aplicação directa da lei de velocidade integrada de reacções de 2.ª ordem é o método mais expedito de determinação da velocidade específica, k (equações | 1 | a | 5 | da Tabela 1) [6, 9]. É conveniente distinguir dois casos: a velocidade da reacção depende do quadrado da concentração de um número reagente, equação | 1 |, ou depende do produto das concentrações de dois reagentes, A e B, elevadas à potência unitária, equações | 2 | a | 5 |. Em qualquer dos casos, no entanto, a determinação da concentração de um ou de dois reagentes, em função do tempo, permite o cálculo de k, através das equações de dependência linear indicadas na Tabela 1. Note-se que, no caso dos coeficientes estequiométricos, a e b, serem unitários e as concentrações iniciais dos reagentes, $|A|_{t_o}$ e $|B|_{t_o}$, serem iguais ou muito semelhantes, a determinação de k é independente do conhecimento desses mesmos valores (equações | 2 | e | 3 |).

2.2 — *MÉTODO DE SWINBOURNE*

Swinbourne [10] propôs uma alternativa à aplicação da lei de velocidade, no caso desta depender da concentração de um único reagente.

A velocidade de uma reacção de ordem p pode escrever-se:

$$V = \frac{1}{2\,\Delta t} F(\Delta \chi) \qquad (\Delta \chi = \chi_{t+2\,\Delta t} - \chi_t)$$

na qual, Δt representa um período de tempo constante e χ uma medida física * directamente proporcional à concentração de um reagente. Consequentemente,

$$F(\Delta \chi)^{1/p} = (2k\Delta t)^{1/p}\ (\chi_{t_\infty} - \chi_t)$$

No caso particular de reacções de 2.ª ordem, e atendendo a que,

$$F(\Delta \chi)^{1/2} \simeq \Delta \chi$$

a expressão anterior toma a forma da equação | 6 | da Tabela 1. O valor de k é calculado em fun:ão de Δt não sendo, por conseguinte, necessário conhecer o valor da grandeza, física, χ, nos tempos inicial e final.

2.3 — *MÉTODO DE ROSEVEARE*

Nas reacções cuja lei de velocidade inclui as concentrações de dois reagentes, utilizando-se estes em igual concentração inicial, pode calcular-se a velocidade específica desde que se conheça a evolução da reacção em dois intervalos de tempo iguais e consecutivos (11):

$$k = \frac{(\Delta C_\alpha - \Delta C_{\alpha+1})^2}{2\ \Delta t\ (\Delta C_\alpha + \Delta C_{\alpha+1}) \Delta C_\alpha\ \Delta C_{\alpha+1}}$$

---

* É de notar que, a determinação da concentração é específica para um componente da mistura reaccional, mas, a medida de uma propriedade física reflecte o comportamento do sistema na sua globalidade; porém, a escolha desta grandeza deve ser condicionada pela sua particular sensibilidade a um, quanto muito a dois, dos componentes da mistura.

Tabela 1

*Reacções irreversíveis de 2.ª ordem: $a\,A + b\,B \rightarrow$ Produtos (P)**
Determinação de k e σ (k) através de equações do tipo: $y = m + n\,x$

	Condições	Eq.	y	x	m	k	σ(k)	Ref.
A = B		1	$1/\lvert A\rvert_t$	t	$1/\lvert A\rvert_{t_o}$	n	σ(n)	6,9
A ≠ B	$\lvert A\rvert_{t_o}=\lvert B\rvert_{t_o}$ a = b = 1	2	$1/\lvert A\rvert_t$	t	$1/\lvert A\rvert_{t_o}$	n	σ(n)	6,9
	$\lvert A\rvert_{t_o}=\lvert B\rvert_{t_o}$ a = b = 1	3	$1/C_M$	t	$1/C_{M_o}$	n/Q	$k\lvert\sigma^2(n)/n^2+\sigma^2(Q)/Q^2\rvert^{1/2}$	6,9
	$\lvert A\rvert_{t_o}\neq\lvert B\rvert_{t_o}$ a = b = 1	4	$\ln(\lvert A\rvert_t/\lvert B\rvert_t)$	t	$\ln(\lvert A\rvert_{t_o}/\lvert B\rvert_{t_o})$	$n/(\lvert A\rvert_{t_o}-\lvert B\rvert_{t_o})$	$k\{\sigma^2(n)/n^2+\lvert\sigma^2(\lvert A\rvert_{t_o})+\sigma^2(\lvert B\rvert_{t_o})\rvert/(\lvert A\rvert_{t_o}-\lvert B\rvert_{t_o})^2\}^{1/2}$	6,9
	$\lvert A\rvert_{t_o}\neq\lvert B\rvert_{t_o}$ a ≠ b ≠ 1	5	$\ln(\lvert A\rvert_t/\lvert B\rvert_t)$	t	$\ln(\lvert A\rvert_{t_o}/\lvert B\rvert_{t_o})$	$n/(b\lvert A\rvert_{t_o}-a\lvert B\rvert_{t_o})$	$k\{\sigma^2(n)/n^2+\lvert b^2\sigma^2(\lvert A\rvert_{t_o})+a^2\sigma^2(\lvert B\rvert_{t_o})\rvert/(b\lvert A\rvert_{t_o}-a\lvert B\rvert_{t_o})^2\}^{1/2}$	6,9
A = B		6	$(\chi_t-\chi_{t+2\Delta t})^{1/2}$	$\chi_{t+\Delta t}$	$-(2k\Delta t)^{1/2}\chi_t$	$n^2/2\Delta t$	$2k\sigma(n)/n$	10
A ≠ B	$\lvert A\rvert_{t_o}=\lvert B\rvert_{t_o}$ a = b = 1	7	$(\Delta C_\alpha-\Delta C_{\alpha+1})^2$	$(\Delta C_\alpha+\Delta C_{\alpha+1})\Delta C_\alpha\Delta C_{\alpha+1}$	0	$n/2\Delta t$	σ(n)	11
	$\lvert A\rvert_{t_o}=\lvert B\rvert_{t_o}$ a = b = 1	8	$\lambda_t-\lambda_{t+\Delta t}$	$(t+\Delta t)\lambda_{t+\Delta t}-t\lambda_t$	$\lvert A\rvert_{t_o}\lambda_{t_\infty}\Delta tk$	$n/\lvert A\rvert_{t_o}$	$k\lvert\sigma^2(n)/n^2+\sigma^2(\lvert A\rvert_{t_o})/\lvert A\rvert_{t_o}^2\rvert^{1/2}$	8
	$\lvert A\rvert_{t_o}\neq\lvert B\rvert_{t_o}$ a = b = 1	9	$1/\lvert A\rvert_{t+\Delta t}$	$1/\lvert A\rvert_t$	$1/(\lvert B\rvert_{t_o}-\lvert A\rvert_{t_o})\lvert e^{k\Delta t(\lvert B\rvert_{t_o}-\lvert A\rvert_{t_o})}-1\rvert$	$-J\ln n/\Delta t$	$k\sigma(n)/n\ \ln n$	12

$\lvert A\rvert_{t,t_o,t_\infty,t+\alpha\Delta t}$ - concentração do reagente A no tempo t, inicial, infinito e $t+\alpha\Delta t$, respectivamente

Δt - intervalo de tempo constante

C_{M,M_o} - concentração média entre a de A e a de B no tempo t e t_o, respectivamente

$Q = 1 - C_S / C_M$ (C_S - metade do excesso de concentração de A em relação a B no tempo t)

$\sigma(Q) = Q\{2\lvert\sigma^2(\lvert A\rvert_t)+\sigma^2(\lvert B\rvert_t)\rvert\ (\lvert A\rvert_t^2+\lvert B\rvert_t^2)\}^{1/2} / (\lvert A\rvert_t^2-\lvert B\rvert_t^2)$

χ_t - medida física directamente proporcional a $\lvert A\rvert_t$

λ_t - medida física linearmente relacionada com $\lvert A\rvert_t$

$C_\alpha = \lvert P\rvert_{t+\alpha\Delta t} - \lvert P\rvert_{t+(\alpha-1)\Delta t}$

J - ordenada (ou abcissa) do ponto de interoepção da recta y = m + n x com a bissectriz do quadrante (x,y)

Por conveniência considerou-se o esquema reaccional apenas com os dois reagentes que podem participar na lei de velocidade

ΔC_α e $\Delta C_{\alpha+1}$ representam as variações de concentração de um produto em intervalos de tempo Δt consecutivos.

De acordo com a equação | 7 | da Tabela 1, a aplicação de uma análise de regressão linear simples, possibilita o cálculo do valor mais provável de k.

O método de Roseveare, contudo, só permite a determinação rigorosa de k se se utilizar um valor de Δt correspondente a uma grande extensão de reacção.

2.4 — *MÉTODO DE TOBEY*

Partindo das condições reaccionais referidas em 2.3, deduz-se que [8]:

$$\lambda_t = \lambda_{t_o} - |A|_{t_o} k \ (\lambda_t - \lambda_\infty)$$

sendo λ o valor de uma grandeza física linearmente dependente da concentração do reagente A.

Subtraindo membro a membro expressões referidas a dois tempos arbitrários, t e $t + \Delta t$, obtém-se a equação | 8 | da Tabela 1. Determina-se o valor de k desde que o tempo de início da reacção e a concentração inicial dos reagentes sejam conhecidos e não, necessariamente, o valor da propriedade física no instante inicial.

O método recentemente proposto por Espenson [7] é, em tudo, idêntico ao de Tobey.

2.5 — *MÉTODO DE SHANK*

No caso, mais geral, da lei de velocidade incluir as concentrações de dois reagentes, sendo estas diferentes no instante inicial, Shank desenvolveu um método de intervalo de tempo constante para a determinação da velocidade específica [12].

A partir da lei de velocidade integrada pode obter-se, directamente, uma relação linear entre $f(|A|_{t+\Delta t})$ e $f(|A|_t)$, equação | 9 | da Tabela 1, cujo coeficiente angular é dado por:

$$n = \exp \{k \ (|B|_{t_o} - |A|_{t_o}) \ \Delta t\}$$

$$(|B|_{t_o} > |A|_{t_o})$$

Os valores das concentrações iniciais dos reagentes não são, contudo, necessários ao cálculo de k, uma vez que, o traçado da recta $f(|A|_{t+\Delta t}) = f(|A|_t)$ permite obter a intercepção $J = 1/(|B|_{t_o} - |A|_{t_o})$. Assim, determina-se k exclusivamente em função de J e Δt, como se pode ver na Tabela 1.

2.6 — *MÉTODO DE STURTEVANT*

Além dos métodos já referidos, para os quais foi possível conseguir uma optimização do valor de k através de uma análise estatística de minimização da soma dos quadrados dos desvios, um outro tratamento, proposto por Sturtevant como extensão do método de Roseveare, foi baseado em cálculos de geometria projectiva [13].

No caso geral de reacções cuja velocidade depende de dois reagentes, encontrando-se estes em concentrações diferentes, pode obter-se k recorrendo à seguinte expressão:

$$k = \{\cosh |(x-1)/2| \ (|A|_{t_o} - |B|_{t_o}) \ \Delta t\}^{-1}$$

$$(|A|_{t_o} > |B|_{t_o})$$

sendo,

$$x = \frac{(x_3 - x_2)\ (x_4 - x_1)}{(x_2 - x_1)\ (x_4 - x_3)} > 3$$

e

$$x_\alpha = |A|_{t_o} - |A|_{t_1} + (\alpha - 1)\ \Delta t \qquad (\alpha \ \varepsilon \ N)$$

Uma aplicação adequada da propagação de erros permite o cálculo de $\sigma(k)$:

$$\sigma(k) = k \left| \frac{\sigma^2 \left(\cosh\left(\frac{x-1}{2}\right)\right)}{\cosh^2\left(\frac{x-1}{2}\right)} + \frac{\sigma^2(|A|_{t_o}) + \sigma^2(|B|_{t_o})}{(|A|_{t_o} - |B|_{t_o})^2} \right|^{1/2}$$

na qual,

$$\sigma\left(\cosh\left(\frac{x-1}{2}\right)\right) = |2\, e^{x-1}\, \sigma^2(x)|^{1/2},$$

$$\sigma(x) = x \left| \frac{\sigma^2(x_3 - x_2)}{(x_3 - x_2)^2} + \frac{\sigma^2(x_4 - x_1)}{(x_4 - x_1)^2} + \frac{\sigma^2(x_2 - x_1)}{(x_2 - x_1)^2} + \frac{\sigma^2(x_4 - x_3)}{(x_4 - x_3)^2} \right|^{1/2}$$

e

$$\sigma(x_i - x_j) = \left| 2\,\sigma^2(|A|_{t_o}) + \sigma^2(|A|_{t_i}) + \sigma^2(|A|_{t_j}) \right|^{1/2}$$

3 — REACÇÃO DE MENSCHUTKIN DO IODETO DE ETILO COM A TRIETILAMINA EM BUTANOL-2

A reacção de Menschutkin do iodeto de etilo (EtI) com a trietilamina (Et_3N),

$$EtI + Et_3N \rightarrow Et_4N^+ I^-$$

cujo produto é o par iónico iodeto de tetraetilamónio ($Et_4N^+ I^-$), pode ser seguida por um método condutimétrico [14].

3.1 — *CURVA DE CALIBRAÇÃO CONCENTRAÇÃO-CONDUTÂNCIA*

Uma vez que a condutância eléctrica, G, do produto da reacção em BuOH-2 não é directa nem linearmente proporcional à sua concentração, c, é indispensável construir curvas de calibração. A utilização da quadrática,

$$c = a_1 G^2 + a_2 G + a_3$$

mostrou-se adequada em todas as condições experimentais de temperatura e pressão. A aplicação de uma análise de regressão linear múltipla, pelo método dos mínimos quadrados, permitiu estimar os parâmetros a_i, os respectivos desvios padrão, $\sigma(a_i)$ e as covariâncias, $\sigma(a_i, a_j)$. Nas Tabelas 2 e 3 e na Figura 1 encontram-se os valores obtidos quando se dissolvem em BuOH-2, massas de sal de amónio rigorosamente medidas, à temperatura de 40°C e à pressão de 1 atm.

3.2 — *DETERMINAÇÃO DA VELOCIDADE ESPECÍFICA E RESPECTIVO DESVIO PADRÃO*

A preparação da solução reagente requer cuidados especiais uma vez que tanto o iodeto de etilo como a trietilamina são voláteis e se pretende que as suas concentrações sejam iguais e rigorosamente determinadas.
Mediu-se a condutância da mistura reaccional em intervalos de tempo regulares. Os valores obtidos foram convertidos em concentrações do sal de amónio, recorrendo às curvas de calibração referidas em 3.1.
A aplicação da equação de velocidade integrada, no caso particular de $|A|_{t_o} = |B|_{t_o}$ e a = b = 1, equação |2| da Tabela 1, conduz aos valores de k e respectivos desvios padrão.

Tabela 2

Et_4NI em BuOH-2 ($T = 313{,}15\ K$; $P = 1\ atm$)

$c \times 10^6$ (fracção molar)	9,43354	37,3047	65,2947	92,9351	139,648
$G \times 10^6/S$	8,3982	23,622	34,450	42,784	56,244

Tabela 3

Et_4NI em BuOH-2 ($T = 313{,}15\ K$; $P = 1\ atm$)

$c = a_1G^2 + a_2G + a_3$

a_1	$\sigma(a_1)$	a_2	$\sigma(a_2)$	$a_3 \times 10^6$	$\sigma(a_3) \times 10^6$	$\sigma^2(a_1,a_2)$	$\sigma^2(a_1,a_3) \times 10^3$	$\sigma^2(a_1,a_3) \times 10^7$
25683	2388,4	1,0798	0,15778	— 1,7923	2,2758	— 366,43	4,3600	— 3,2496

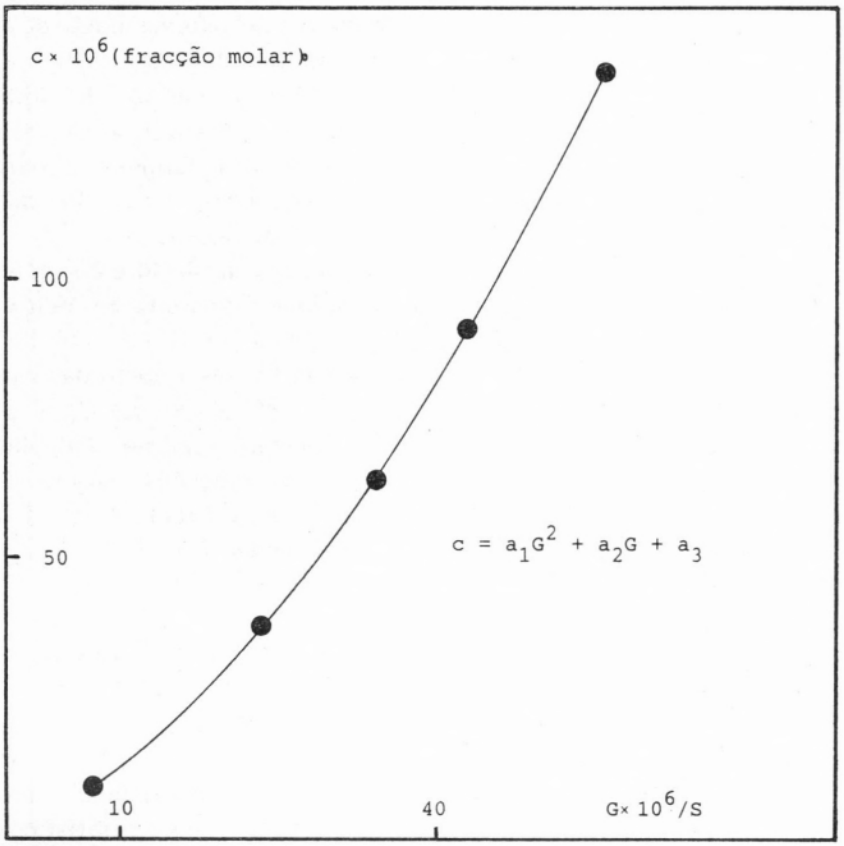

Fig. 1

Et_4NI em BuOH-2 ($T = 313{,}15\ K$; $P = 1\ atm$)

Tabela 4

EtI + Et_3N em BuOH-2

($|A|_{t_0} = 1{,}84226 \times 10^{-3}$ (fracção molar);

T = 313,15 K; P = 1 atm)

t/h	$G \times 10^6/S$	$c \times 10^6$ (fracção molar)	$(|A|_{t_0} - c)^{-1}$
5	8,9294	10,977	546,06
6	10,156	11,823	546,32
7	11,283	13,660	546,87
8	12,364	15,484	547,41
9	13,405	17,297	547,96
10	14,418	19,114	548,50
11	15,344	20,822	549,02
12	16,273	22,580	549,55
13	17,148	24,276	550,06
27	27,499	47,321	557,12
28	28,132	48,909	557,62
29	28,763	50,513	558,11
30	29,372	52,079	558,60
31	29,988	53,684	559,10
32	30,668	55,477	559,66
33	31,235	56,991	560,14
34	31,836	58,613	560,65
35	32,361	60,046	561,10
49	39,799	81,862	568,05
50	40,269	83,336	568,53
51	40,759	84,885	569,03
52	41,254	86,462	569,54
53	41,667	87,787	569,97
55	42,645	90,961	571,00
56	43,110	92,487	571,50
57	43,530	93,875	571,96
58	43,999	95,436	572,47
59	44,410	96,812	572,92
74	50,800	119,34	580,41
75	51,170	120,71	580,87
76	51,528	122,04	581,32
77	51,867	123,30	581,75
78	52,280	124,85	582,27
79	52,700	126,44	582,81
80	53,114	128,01	583,34
81	53,520	129,56	583,87
82	53,896	131,00	584,36
83	54,279	132,48	584,87
84	54,573	133,62	585,26

$m = 543{,}59$ $\quad \sigma(n) = 5{,}4653 \times 10^{-4}$

$n = 0{,}49743$ $\quad \sigma(k) = 0{,}002 \times 10^{-4}$

$k = 1{,}382 \times 10^{-4}\ s^{-1}$ (fracção molar)

Precisão de $t = \pm 0{,}00003$ h

Na Tabela 4 apresenta-se um exemplo da aplicação deste método à reacção efectuada nas seguintes condições experimentais:
$|A|_{t_0} = 1{,}84226 \times 10^{-3}$ (fracção molar);
T = 313,15 K e P = 1 atm.

3.3 — *DETERMINAÇÃO DAS FUNÇÕES TERMODINÂMICAS DE ACTIVAÇÃO E RESPECTIVOS DESVIOS PADRÃO*

Sempre que a Teoria do Estado de Transição seja aplicável, a determinação das funções termodinâmicas de activação de qualquer sistema reaccional e respectivos desvios padrão é feita a partir dos valores da velocidade específica, a qual já foi objecto de estudo em artigo anterior [2].

Na Tabela 5 encontram-se os valores de k, obtidos a várias temperaturas e pressões, relativos ao sistema iodeto de etilo-trietilamina em butanol-2.

O cálculo da energia de Gibbs de activação, $\Delta^{\neq} G^0$, e do respectivo desvio médio, $d\,\Delta^{\neq} G^0$, foi feito directamente a partir dos valores de k (equações | 15 | e | 16 | da ref. 2) e encontram-se na Tabela 5.

A equação de Wold e col. [15, 16] mostrou-se adequada ao estudo do efeito da temperatura e a equação de Hyne e col. [17] ao da pressão (Tabela 6). Os valores das funções de activação, $\Delta^{\neq} H^0$, $\Delta^{\neq} S^0$, $\Delta^{\neq} C_p^0$ e $\Delta^{\neq} V^0$ e respectivos desvios padrão, calculados de acordo com as equações estabelecidas nas colunas 3 e 4 da Tabela 3 da ref. 1, podem ver-se nas Tabelas 7 e 8.

4 — COMENTÁRIO FINAL

No estudo de mecanismos reaccionais é necessário, não só, obter valores de velocidade específica de confiança, como também, utilizar um tratamento estatístico correcto desses mesmos valores. A apresentação de um formalismo adequado e a correspondente aplicação correcta de métodos estatísticos à ciné-

Tabela 5

EtI + Et_3N em BuOH-2

(a) P = 1 atm

T/K	303,15	308,15	313,15	318,15	323,15	328,15
$(k_m \pm d\ k_m) \times 10^5$ / s^{-1}	5,10 ±0,08	8,21 ±0,13	12,84 ±0,20	20,71 ±0,36	33,26 ±0,65	53,22 ±1,54
$\Delta^{\neq}G^{\circ} \pm d\ \Delta^{\neq}G^{\circ}$ / kJ mol^{-1}	77,54 ±0,04	77,55 ±0,04	77,69 ±0,04	77,70 ±0,05	77,70 ±0,05	77,66 ±0,08

(b) T = 313,15 K

P/atm	1	100	250	500	1000	1500	2000
$(k_m \pm d\ k_m) \times 10^5$ / s^{-1}	12,84 ±0,20	15,93 ±0,16	18,63 ±0,09	23,41 ±0,06	34,43 ±0,22	49,69 ±0,40	66,20 ±0,60
$\Delta^{\neq}G^{\circ} \pm d\ \Delta^{\neq}G^{\circ}$ / kJ mol^{-1}	77,69 ±0,04	77,12 ±0,03	76,72 ±0,01	76,12 ± 0,01	75,12 ±0,02	74,16 ±0,02	73,42 ±0,02

Tabela 6

EtI + Et_3N em BuOH-2

(a) $\ln k = A_1/T^2 + A_2/T + A_3$

$A_1 \times 10^{-5}$	$\sigma(A_1) \times 10^{-5}$	A_2	$\sigma(A_2)$	A_3	$\sigma(A_3)$	$\sigma^2(A_1,A_2) \times 10^{-9}$	$\sigma^2(A_1,A_3) \times 10^{-6}$	$\sigma^2(A_2,A_3) \times 10^{-4}$
27,614	6,1568	−26843	3907,0	48,613	6,1951	−2,4053	3,8130	−2,4203

(b) $\ln k = A'_1 P^2 + A'_2 P + A'_3$

$A'_1 \times 10^7$	$\sigma(A'_1) \times 10^8$	$A'_2 \times 10^3$	$\sigma(A'_2) \times 10^5$	A'_3	$\sigma(A'_3) \times 10^2$	$\sigma^2(A'_1,A'_2) \times 10^{12}$	$\sigma^2(A'_1,A'_3) \times 10^{10}$	$\sigma^2(A'_2,A'_3) \times 10^6$
−1,6839	4,8820	1,1173	9,7671	−8,8933	3,2656	−4,6051	9,4200	−2,3106

Tabela 7

EtI + Et_3N em BuOH-2 (P = 1 atm)

T/K	303,15	308,15	313,15	318,15	323,15	328,15
$\Delta^{\neq}H^{o} \pm \sigma(\Delta^{\neq}H^{o})$ / kJ mol^{-1}	69,0 ±1,2	71,5 ±0,8	74,0 ±0,4	76,1 ±0,4	78,2 ±0,4	80,3 ±1,2
$\Delta^{\neq}S^{o} \pm \sigma(\Delta^{\neq}S^{o})$ / J K^{-1} mol^{-1}	−99 ±5	−91 ±3	−84 ±2	−77 ±2	−69 ±3	−63 ±5
$\Delta^{\neq}C_p^{o} \pm \sigma(\Delta^{\neq}C_p^{o})$ / J K^{-1} mol^{-1}	490 ±113	477 ±109	460 ±105	444 ±100	431 ±96	418 ±96

Tabela 8

EtI + Et_3N em BuOH-2 (T = 313,15 K)

P/atm	1	100	250	500	1000	1500	2000
$\Delta^{\neq}V^{o} \pm \sigma(\Delta^{\neq}V^{o})$ / cm^3 mol^{-1}	−28,7 ±2,5	−27,8 ±2,3	−26,5 ±1,9	−24,4 ±1,4	−20,1 ±0,7	−15,7 ±1,5	−11,4 ±3,1

tica de reacções de 2.ª ordem constituiu o objectivo deste trabalho.

Regressões lineares pelo método dos mínimos quadrados são as mais vulgarmente usadas no cálculo das velocidades específicas de reacções de qualquer ordem. Constata-se, no entanto, que estudos cinéticos de diferentes autores são de difícil comparação devido à não uniformidade dos métodos estatísticos utilizados, para além das divergências resultantes das técnicas experimentais escolhidas. Na verdade, se, por um lado, é inadmissível o uso de métodos dependentes do observador, por outro, verifica-se a utilização frequente de análise estatística duma forma incapaz de conduzir à determinação de parâmetros de confiança.

Pensamos que os processos de cálculo descritos neste artigo poderão ser úteis em estudos cinéticos de um grande número de reacções de 2.ª ordem, em particular nas de Menschutkin. A cinética destas reacções é um assunto familiar nos estudos de mecanismos reaccionais, quer como um exemplo clássico de uma reacção bimolecular em solução, na qual reagentes apolares dão origem a produtos polares, quer como um processo padrão na análise de efeito de solvente na reactividade química [18-21].

O número de valores experimentais e a sua distribuição ao longo do intervalo das variáveis independentes, o uso de pesos estatísticos e de critérios de concordância, a correlação entre variáveis pretensamente independentes e os seus efeitos sobre os valores das grandezas estimadas e respectivos desvios padrão são alguns dos assuntos que justificam, também, um cuidadoso exame.

Entenda-se, ainda, que não foi objectivo deste trabalho tecer considerações sobre o significado físico-químico dos valores das velocidades específicas e das funções termodinâmicas de activação aqui obtidas. Estas matérias, bem como o tratamento de outros casos concretos, são susceptíveis de posterior análise.

(Recebido em 27 de Setembro de 1985,
em versão revista, 28 de Abril de 1986)

AGRADECIMENTO

Os autores agradecem ao Instituto Nacional de Investigação Científica o apoio financeiro necessário à realização deste trabalho.

REFERÊNCIAS

[1] B.R. KOWALSKI, Chemistry and Industry, 882 (1978).
[2] C.A.N. VIANA, L.M.P.C. ALBUQUERQUE e R.M.C. GONÇALVES, Rev. Port. Quím., **22**, 117 (1980).
[3] M.J. BLANDAMER, R.L. ROBERTSON e J.M.W. SCOTT, Can. J. Chem., **58**, 772 (1980).
[4] M.J. BLANDAMER, R.E. ROBERTSON, J.M.W. SCOTT e A. VRIELINK, J. Amer. Chem. Soc., **102**, 2585 (1980).
[5] R. LOHMULLER, D.D. MACDONALD, M. MACKINNON e J.B. HYNE, Can. J. Chem., **56**, 1739 (1978).
[6] E.S. SWINBOURNE, «Analysis of Kinetic Data», Appleton, New York (1971).
[7] J.H. ESPENSON, J. Chem. Ed., **57**, 160 (1980).
[8] S.W. TOBEY, J. Chem. Ed., **39**, 473 (1962).
[9] G.M. FLECK, «Chemical Reaction Mechanism», Holt, New York (1971).
[10] E.S. SWINBOURNE, Aust. J. Chem., **16**, 170 (1963).
[11] W.E. ROSEVEARE, J. Amer. Chem. Soc., **53**, 1651 (1931).
[12] N.E. SHANK, Int. J. Chem. Kinetics, **5**, 577 (1973).
[13] J.M. STURTEVANT, J. Amer. Chem. Soc., **59**, 699 (1937).
[14] C.A.N. VIANA e A.R.T. CALADO, comunicação apresentada na 2.ª Reunião Nacional de Electroquímica, Coimbra (1981).
[15] S. WOLD e P. AHLBERG, Acta Chem. Scand., **24**, 618 (1970).
[16] S. WOLD, Acta Chem. Scand., **24**, 2321 (1970).
[17] H.S. GOLINKIN, W.G. LAIDLAW e J.B. HYNE, Can. J. Chem., **44**, 2193 (1966).
[18] M.H. ABRAHAM e P.L. GRELLIER, J. Chem. Soc., Perkin 2, 623 (1975).
[19] M.H. ABRAHAM e P.L. GRELLIER, J. Chem. Soc., Perkin 2, 1735 (1976).
[20] Y. DROUGARD e D. DECROOCQ, Bull. Soc. Chim. France, 2972 (1969).
[21] K.F. WONG e C.A. ECKERT, Ind. Eng. Chem., **62**, 16 (1970).

ABSTRACT

Statistical method applied to the kinetics of 2nd order reactions.

1 — The Menschutkin reaction of ethyl iodide with triethylamine in 2-butanol.

The different methods used to calculate the specific rates of second order reactions are reexamined. The assumptions as well as the uncertainties associated to the methods are analysed. The Menschutkin reaction of ethyl iodide with triethylamine in 2-butanol is studied.

M. TERESA S. D. VASCONCELOS
ADÉLIO A. S. C. MACHADO
C. I. Q. (U. P.), Departamento de Química
Faculdade de Ciências
4000 Porto

CALIBRAÇÃO DE ELÉCTRODO DE VIDRO PARA DETERMINAÇÃO DE CONSTANTES DE FORMAÇÃO EM MEIO NEM MUITO ÁCIDO NEM MUITO ALCALINO (pH 4-10)*

Discute-se a calibração do eléctrodo de vidro (acoplado a um eléctrodo de referência com junção líquido-líquido) em função de pc_H, usada para a determinação de constantes de formação, pondo-se em evidência as limitações de ordem prática da sua realização por titulações de ácidos muito fortes, fortes ou intermédios com base muito forte; discute-se o comportamento do eléctrodo de vidro em comparação com o de outros eléctrodos selectivos de iões.
Introduz-se um processo alternativo de calibração para o intervalo de pc_H de 4 a 10, que consiste em usar soluções tampões de pa_H com força iónica constante e igual a 0,1 M para obter uma calibração em função de pa_H, que depois se converte numa calibração em função de pc_H por meio do factor de actividade, f_H; descreve-se o trabalho realizado para avaliar a validade do processo introduzido.

(*) Parte deste trabalho foi apresentado numa comunicação ao Quarto Encontro Anual da Sociedade Portuguesa de Química, Lisboa, 1981 (ref. [1]).

1 — INTRODUÇÃO

A calibração correcta do eléctrodo de vidro é uma operação essencial na determinação de valores exactos de constantes de acidez e de formação de complexos, por potenciometria, com aquele eléctrodo.

A calibração do eléctrodo de vidro (mais precisamente, da célula electroquímica constituída por este eléctrodo e por um eléctrodo de referência com junção líquido-líquido), quando se pretende medir o pH operacional (isto é, o pH numa escala relativa de acidez), é realizada por meio de soluções tampões com actividades de catião hidrogénio (ou pa_H) conhecidas. A determinação de constantes de equilíbrio estequiométricas exige, porém, uma calibração em função de pc_H, isto é, de concentrações de catião hidrogénio. A conversão de uma calibração em função de pa_H numa calibração em função de pc_H levanta, em princípio, vários problemas, mesmo que as calibrações por meio de tampões de pa_H sejam feitas a força iónica constante (o que não é verificado nas escalas adoptadas para a medição de pH operacional) e igual à usada nas medições: não se pode garantir em absoluto que o factor de actividade do catião hidrogénio seja o mesmo nas diversas soluções tampões e nas soluções problemas, devido a variações da composição do meio iónico; pelas mesmas razões, não se pode garantir que o potencial de junção líquido-líquido entre a solução da célula e a solução do eléctrodo de referência mantenha sempre o mesmo valor. Por estas razões tem-se preferido, quando se usa a potenciometria com eléctrodo de vidro, em células electroquímicas do tipo referido, para a determinação de constantes de formação, fazer a calibração do eléctrodo de vidro directamente em função de pc_H para o que se usam séries de soluções padrões de catião hidrogénio, preparadas pela técnica da adição de quantidade conhecida [2, 3] de bases a ácidos ou vice-versa.

Em trabalho recente de determinação de constantes de formação realizado neste Departamento [4], teve-se necessidade de cali-

brar o eléctrodo de vidro em meio nem muito ácido nem muito alcalino (pH entre 4 e 10, aproximadamente), a força iónica não muito elevada (0,1 M). Quando se tentou fazer a calibração directa em função de pc_H por titulações de ácido-base, tomou-se consciência de algumas limitações práticas desta técnica, aparentemente omissas ou pouco discutidas na literatura. Este facto levou a que se desenvolvesse e avaliasse outra técnica de calibração, apropriada para as mencionadas condições experimentais, que consiste em usar tampões de pa_H com força iónica constante e igual ao valor das soluções em que se pretende fazer a medição, para obter uma calibração em função de pa_H, e converter, depois, esta última, numa calibração em função de pc_H, por meio do valor do factor de actividade do catião hidrogénio. No presente artigo descreve-se o trabalho realizado, com dois objectivos diferentes: por um lado, evidenciar as limitações da calibração do eléctrodo de vidro por titulações de ácido-base, que não têm sido suficientemente discutidas na literatura; por outro lado, relatar a técnica de calibração desenvolvida e o processo usado na sua avaliação, e discutir as suas vantagens e limitações.

2 — PARTE EXPERIMENTAL

2.1 — *EQUIPAMENTO*

MEDIÇÕES DE DIFERENÇAS DE POTENCIAL. Foram efectuadas com decimilivoltímetros de marca Orion, modelos 801A e 701A (a que se acoplaram, quando necessário, comutadores de eléctrodos da mesma marca, modelo 605), cuja sensibilidade é de $\pm 0{,}1$ mV.

ELÉTRODOS. Os resultados apresentados foram obtidos com eléctrodos de vidro de marca Philips, modelo GAH110, acoplados a eléctrodos de referência da marca Orion, modelo 90-02-00 (com solução Orion 90-00-02 no compartimento interior, o que confere ao eléctrodo o potencial do eléctrodo saturado de calomelanos, e solução de nitrato de potássio 0,1 M no compartimento exterior). Foram também usados eléctrodos de vidro das marcas Beckman, modelo PIN 39 301, e Orion, modelo 91-01-00, nos casos indicados expressamente no texto.
Entre os ensaios, os eléctrodos foram conservados em água; antes de serem utilizados, foram secos em papel adsorvente.

PREPARAÇÃO E MANUSEAMENTO DE SOLUÇÕES. Usou-se material de vidro da classe A. Para a medição de volumes usaram-se microburetas da marca Kimax (capacidade 5 cm^3) e uma microsseringa programável de marca Hamilton, modelo Microlab P, munida de seringas permutáveis de 0,5/2, 5/5 cm^3 de capacidade.

CONTROLE DE TEMPERATURAS. As determinações foram efectuadas em células de titulação de paredes duplas de marca Metrohm, modelo EA 880T, nas quais a temperatura foi mantida constante a $25{,}0 \pm 0{,}1$°C por circulação de água termostatada (termostato de circulação, marca RETSCH, modelo RST 2).

2.2 — *REAGENTES E SOLUÇÕES*

ÁGUA. Na preparação de soluções usou-se água desionizada, bidestilada por destilações simples, e fervida.

SOLUÇÕES DE NITRATO DE POTÁSSIO (utilizadas para a fixação da força iónica). Usou-se nitrato de potássio, *p. a.*, da marca Merck, que foi recristalizado três vezes em água e seco durante vários dias em exsicador com gel de sílica e cloreto de cálcio. As soluções foram preparadas por pesagem de sal e diluição em balão volumétrico, sem posterior titulação. Usaram-se sempre soluções recentemente preparadas para evitar problemas de carbonatação.

SOLUÇÕES DE ÁCIDO NÍTRICO. Foram preparadas a partir de ácido nítrico concentrado, *p. a.*, da marca Merck, por diluição conveniente, e tituladas (com bórax), volumetrica-

mente ou potenciometricamente (com um eléctrodo de vidro). Alternativamente, as soluções foram preparadas por diluição de ampolas de Titrisol Merck, ref. 9964.

SOLUÇÕES DE HIDRÓXIDO DE SÓDIO. A partir de hidróxido de sódio, *p. a.*, de marca Merck, preparou-se, no próprio dia da sua utilização, uma solução aquosa a cerca de 50 %. Diluiu-se, sob atmosfera de azoto, um volume apropriado desta solução para se obter a concentração desejada. A solução obtida foi titulada potenciometricamente com ácido nítrico ou ácido clorídrico, e a ausência de carbonato em solução foi testada pelo método de GRAN [5, 6].

SOLUÇÕES TAMPÕES DE pH. As soluções tampões usadas (hidrogenoftalato de potássio, diidrogenofosfato de potássio/hidrogenofosfato de sódio 1:1 e bórax) foram preparadas a partir de reagentes de marca Merck, *p. a.*, segundo [7], mas, quando necessária, com adição de nitrato de potássio para ajustar a força iónica a 0,1 M. Estas soluções foram guardadas ao abrigo do ar e da luz. Cada toma de solução foi usada uma única vez. As soluções foram renovadas mensalmente. Embora as soluções tampões tenham sido preparadas na escala molal, a sua utilização na escala molar, como se fez neste trabalho, não implica quaisquer erros significativos, conforme se discute pormenorizadamente em [8].

SOLUÇÕES DE ÁCIDO BÓRICO. Foram preparadas a partir de ácido bórico, *p. a.*, não condicionado, de marca Merck, e tituladas potenciometricamente com hidróxido de sódio (esta titulação permitiu simultaneamente determinar a molaridade das soluções a recolher os dados necessários à determinação das constantes de protólise do ácido).

SOLUÇÕES DE HIDROGENOFOSFATO DE POTÁSSIO. Foram preparadas a partir do sal *p.a.*, de marca Merck, seco a 110°C durante 2 horas, por pesagem e diluição rigorosas.

2.3 — *REALIZAÇÃO DOS ENSAIOS*

Os ensaios foram efectuados em atmosfera inerte, conseguida por passagem de uma corrente de azoto R, previamente purificada, sobre a solução titulada; esta foi termostatada a 25,0°C.

A força iónica das soluções foi ajustada a 0,1 M com nitrato de potássio.

Antes de se iniciarem as titulações, os eléctrodos indicador e de referência foram deixados a estabilizar, mergulhados na solução titulada, com agitação, durante cerca de uma hora (ou mais, se necessário) para atingir temperatura constante (e potencial estável).

CALIBRAÇÕES. Estas foram realizadas por titulação (método da adição da quantidade conhecida) [2, 3], excepto no caso das realizadas com soluções tampões de pH, que foram, obviamente, realizadas pelo método das soluções separadas [2, 3]. Neste último caso, as soluções foram utilizadas por ordem decrescente de pH.

DETERMINAÇÃO DE CONSTANTES DE PROTÓLISE. Foram realizadas por titulação de soluções de ácido bórico (cerca de 2×10^{-2} M), com hidróxido de sódio (cerca de 1×10^{-1} M), e de hidrogenofosfato de potássio (cerca de 2×10^{-2} M), com ácido nítrico (cerca de 3×10^{-3} M).

LEITURAS. As leituras foram efectuadas em milivolts, quer nas calibrações quer nas determinações de constantes de protólise. Considerou-se que o potencial tinha atingido um valor estável quando este se mantinha invariável a menos de $\pm 0{,}1$ mV durante 5 minutos, no mínimo, só então se procedendo ao registo do valor lido.

2.4 — *CÁLCULOS*

CALIBRAÇÕES. Os dados experimentais foram ajustados à equação $E = E^{o\prime} - s\ pC_H$ para determinação dos parâmetros $E^{o\prime}$ (potencial

normal formal) e s (declive), por mínimos quadrados, com uma calculadora Texas TI 59; o parâmetro R, apresentado juntamente com os parâmetros $E^{o\prime}$ e s, é o coeficiente de correlação do ajuste fornecido pela máquina.

DETERMINAÇÕES DE CONSTANTES DE PROTÓLISE. Os dados experimentais foram tratados pelo programa MINIQUAD [9, 10], no computador NCR 4100 ELLI0T do Laboratório de Cálculo Antomático da Faculdade de Ciências do Porto.
Os dados experimentais foram tratados sucessivamente de modo a fornecer constantes de protonação (sequência $L \mid LH \mid LH_2$)

$$L + pH \rightleftarrows LH_p \quad (p > 0)$$
$$\beta_p = |LH_p| / |L| . |H|^p \qquad (1)$$

e de desprotonação (sequência $LH_2 \mid LH \mid L$)

$$q\ LH_2 + r\ H \rightleftarrows L_qH_{2q+r} \quad (q > 0,\ r < 0)$$
$$\beta_{qr} = |L_qH_{2q+r}| . |H|^{-r} / |LH_2|^q \qquad (2)$$

Em ambas as sequências LH_2 simboliza, no caso do ácido bórico, a espécie neutra, e no caso do hidrogenofosfato de potássio, o anião diidrogenofosfato.

3 — DIFICULDADES PRÁTICAS NA CALIBRAÇÃO DO ELÉCTRODO DE VIDRO POR TITULAÇÕES DE ÁCIDO-BASE

Quando se pretende calibrar o eléctrodo de vidro em função da concentração de catião hidrogénio, nomeadamente para a determinação de constantes de equilíbrio por potenciometria, tem-se utilizado, em geral, séries de soluções padrões de ácido ou bases muito fortes, para meios fortemente ácidos ou alcalinos, e de ácidos e bases fortes ou intermédios, para a zona intermédia de pc_H; muito frequentemente, essas séries de soluções são obtidas por titulação, embora também se possam utilizar soluções separadas («soluções padrões de referência»). Os diferentes processos e técnicas experimentais usados são enumerados e discutidos em [11].

Quando, porém, se foi utilizar este processo (com soluções obtidas por titulação) deparou-se com algumas dificuldades, que se discutem nesta secção.

3.1 — *CALIBRAÇÃO COM ÁCIDO E BASES MUITO FORTES*

A titulação do meio iónico com ácido muito forte ou base muito forte é um processo de calibração do eléctrodo de vidro em função de pc_H usado desde os fins dos anos quarenta [11], posteriormente considerado [12] bem estabelecido, mas cujas limitações nem sempre são reconhecidas. Os resultados seguintes evidenciam estas limitações.

CALIBRAÇÃO DE ÁCIDO MUITO FORTE. Na fig. 1 e na tabela 1 apresentam-se resultados referentes à calibração de um eléctrodo de vidro Philips GaH110 acoplado a um eléctrodo de referência Orion 90-02-00 (com eléctrodos de vidro de outras marcas, referidas na parte experimental, obtiveram-se resultados semelhantes) com soluções padrões de ácido nítrico. Para concentrações inferiores a 10^{-3} M em catião hidrogénio, as soluções foram obtidas por adição de solução de ácido nítrico 0,1 M a 50 cm^3 de solução de nitrato de potássio 0,1 M; para concentrações superiores (tabela 1), usaram-se padrões discretos de ácido nítrico.
A fig. 1 evidencia que ocorre encurvamento da calibração para as concentrações de catião hidrogénio mais baixas (zona A); os dados referentes a concentrações superiores apresentam também encurvamento (na fig. 1 apenas se incluem dois pontos neste intervalo de concentrações superiores, zona C). Só se poderá, portanto, usar uma calibração linear num intervalo restrito de concentrações. Para determinar este intervalo consideram-se sucessivamente diversos intervalos correspondentes a variação de concentração numa década, ajustando-se uma recta ao conjunto de pontos de cada um desses intervalos. Admitindo que a dispersão aleatória dos pontos relativamente à recta se mantém aproximadamente constante, o valor do coeficiente de

correlação do ajuste, R, medirá o encurvamento, isto é, o afastamento da linearidade: quanto mais próximo da unidade for R menos encurvada será a linha. O encurvamento será, também, responsável por um abaixamento de declive a baixas concentrações e aumento do mesmo a concentrações elevadas.

forte só permite obter uma calibração linear do eléctrodo de vidro (em função de pc_H) num intervalo de concentrações restrito, de cerca de uma década.

O desvio da linearidade que a resposta do eléctrodo apresenta para concentrações de catião hidrogénio superiores a cerca de

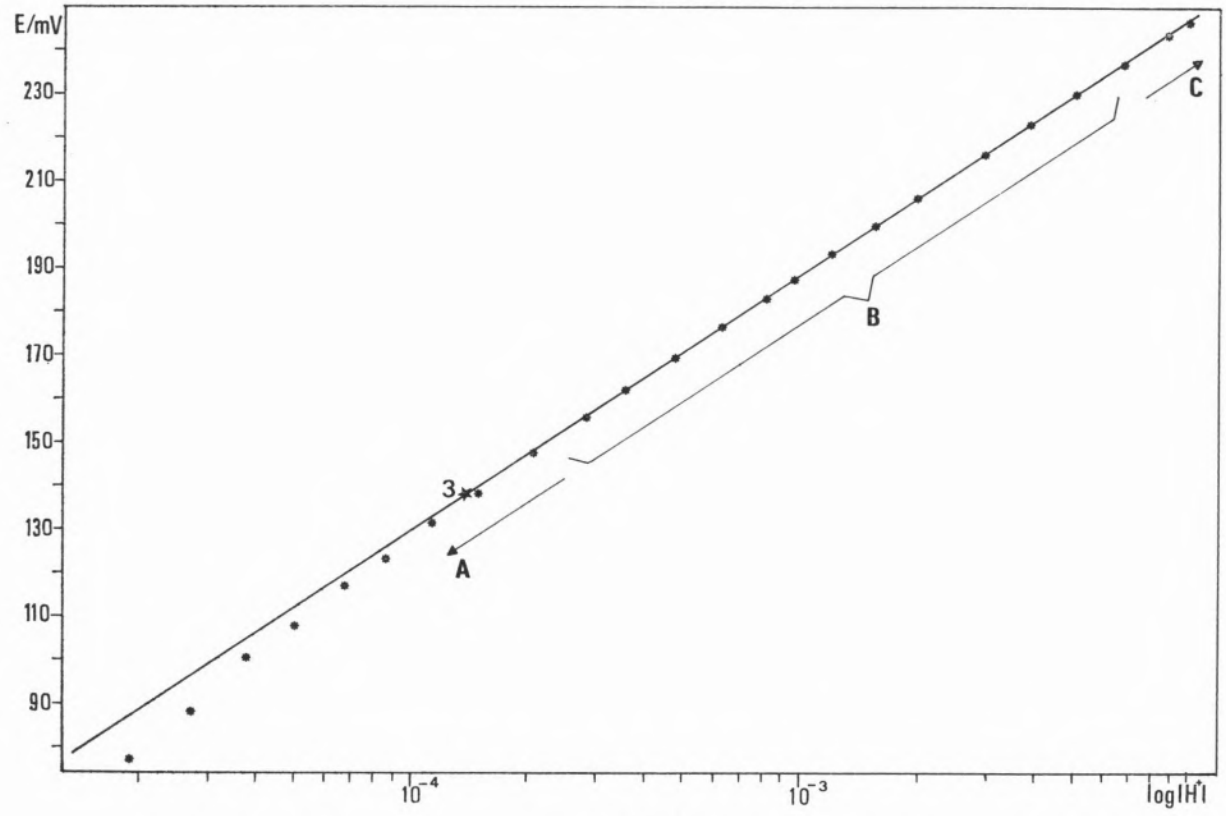

Fig. 1

Calibração do eléctrodo Philips GAH110 com ácido muito forte (ver tabela 1)

Na tabela 1 apresentam-se resultados obtidos por tratamento dos dados experimentais segundo esta estratégia. Esses resultados mostram que, para a década de concentrações de 5×10^{-4} a 5×10^{-3} M (zona B da fig. 1 e da tabela 1), se obtém um valor máximo para o coeficiente de ajuste (R = 0,99991) dos pontos a uma recta, e que, para esta, o declive é próximo do valor teórico, 59,2 mV/década (valores sublinhados na tabela 1). Em conclusão, os dados apresentados evidenciam que o uso de soluções padrões de ácido muito

5×10^{-3} M (zona C; valores de declive inferiores ao teórico e valores de R bastante inferiores à unidade, ver tabela 1) deve-se não só ao aparecimento de valores apreciáveis do potencial de junção entre o eléctrodo de referência e a solução da célula electroquímica, em consequência da concentração elevada de catião hidrogénio, mas também a variações no factor de actividade do mesmo catião, em consequência da variação da natureza do meio (a quantidade de electrólito inerte adicionada para ajustar a força iónica é cada

Tabela 1

Calibração do eléctrodo Philips GHA110 com ácido muito forte (a)

	c_H / M	s/mV.década^{-1}	$E^{o\prime}_H$/mV	R
A	$< 1.10^{-4}$ (b)	72,2	408,2	0,99789
A	1.10^{-4} - 1.10^{-3} (b)	61,9	369,7	0,99975
B	5.10^{-4} - 5.10^{-3} (b)	59,5	362,2	0,99991
C	1.10^{-3} - 1.10^{-2} (b)	57,8	357,8	0,99980
C	5.10^{-3} - 5.10^{-2} (c)	50,7	337,4	0,99881
C	1.10^{-2} - 1.10^{-1} (c)	44,2	326,6	0,99685

(a) Meio: I = 0,1 M (KNO_3); temperatura: 25°C; s, declive; $E^{o\prime}$, potencial formal, referido ao E.S.C.; R, coeficiente de correlação do ajuste.
(b) Titulação do meio iónico com ácido nítrico 0,1 M.
(c) Padrões discretos de ácido nítrico.

vez menor à medida que cresce a concentração de ácido). Os dois efeitos não são separáveis, embora frequentemente só se considere o primeiro e se discuta a situação só em termos de potencial de junção [12], por ser o mais importante quando se fixa a força iónica. Na realidade, trata-se de um «potencial de junção aparente» (designação introduzida por BATES [13]), dado por

$$\Delta E'_j = \Delta E_j + s\ \Delta\log\ f_H \qquad (3)$$

em que ΔE_j é a variação de potencial de junção e $\Delta\log f_H$ é a variação do logaritmo do factor de actividade do catião hidrogénio. O potencial de junção aparente cresce com a concentração de catião hidrogénio, podendo a variação considerar-se linear para concentrações de ácido não excessivamente elevadas [14] ($\Delta E'_j = -x\,|\,H^+\,|$). Os dados experimentais da calibração permitem determinar x [14] (em [12] descreve-se um método mais expedito que o original [14]). No caso presente (calibrações a 25°C, com soluções de ácido nítrico com concentrações no intervalo 10^{-3} a 10^{-1} M com força iónica ajustada a 0,1 M), o valor obtido para x foi x = 148,5 mV/M. Este valor implica que o encurvamento da calibração devido ao potencial de junção aparente seja observado para concentrações de catião hidrogénio superiores a cerca de 5×10^{-2} M. A força iónica mais elevada, o valor de x é menor [15], o que significa que ocorre resposta linear do eléctrodo até valores de concentração de catião hidrogénio um pouco acima deste valor, mas ainda da sua ordem de grandeza. Finalmente, será de referir que, já que se pode determinar experimentalmente x, estes desvios da linearidade a concentrações elevadas são corrigíveis; para isso, a determinação experimental do valor de x tem de ser feita exactamente nas mesmas condições experimentais que as medições.

A concentrações de catião hidrogénio inferiores a cerca de 5×10^{-4} M, a resposta do eléctrodo apresenta também desvios de linearidade (ver fig. 1 e tabela 1, zona A; valores de declive superiores ao teórico e valores de R muito baixos, ver tabela 1; estes últimos resultam não só do encurvamento mas tam-

bém da dispersão dos pontos, ver fig. 1). Verifica-se, ainda, que, nesta zona de baixas concentrações de catião hidrogénio, a resposta do eléctrodo não é reprodutível (ao contrário do que sucede na zona de resposta nernstiana); para as concentrações mais baixas, o eléctrodo responde muito lentamente, não chegando sequer a estabilizar completamente, o que dá origem a leituras erráticas. Este comportamento resulta da ausência de poder tampão das soluções diluídas de ácido forte, que incentiva a lexiviação de componentes alcalinas da superfície da membrana de vidro do eléctrodo [16]. Uma das consequências deste facto é a imprecisão de resposta do eléctrodo de vidro na zona de variação brusca de potencial na titulação de um ácido com uma base (ou vice-versa), razão pela qual não devem ser colhidos pontos nesta situação para a determinação de constantes de formação.

CALIBRAÇÃO COM BASE MUITO FORTE. Nesta calibração (feita em função de pc_{OH}) verifica-se que a zona de resposta linear do eléctrodo de vidro é, também, limitada a cerca de uma década, devido a problemas do mesmo tipo que os discutidos acerca da calibração com ácido muito forte, acrescidos de alterações do potencial de assimetria da membrana de vidro (devidas principalmente ao ataque da superfície da membrana pelo anião hidróxido) e a interferências de catiões de metais alcalinos (introduzidos na solução como constituintes da base forte ou lexiviados da superfície da membrana de vidro pelo referido ataque) [17].

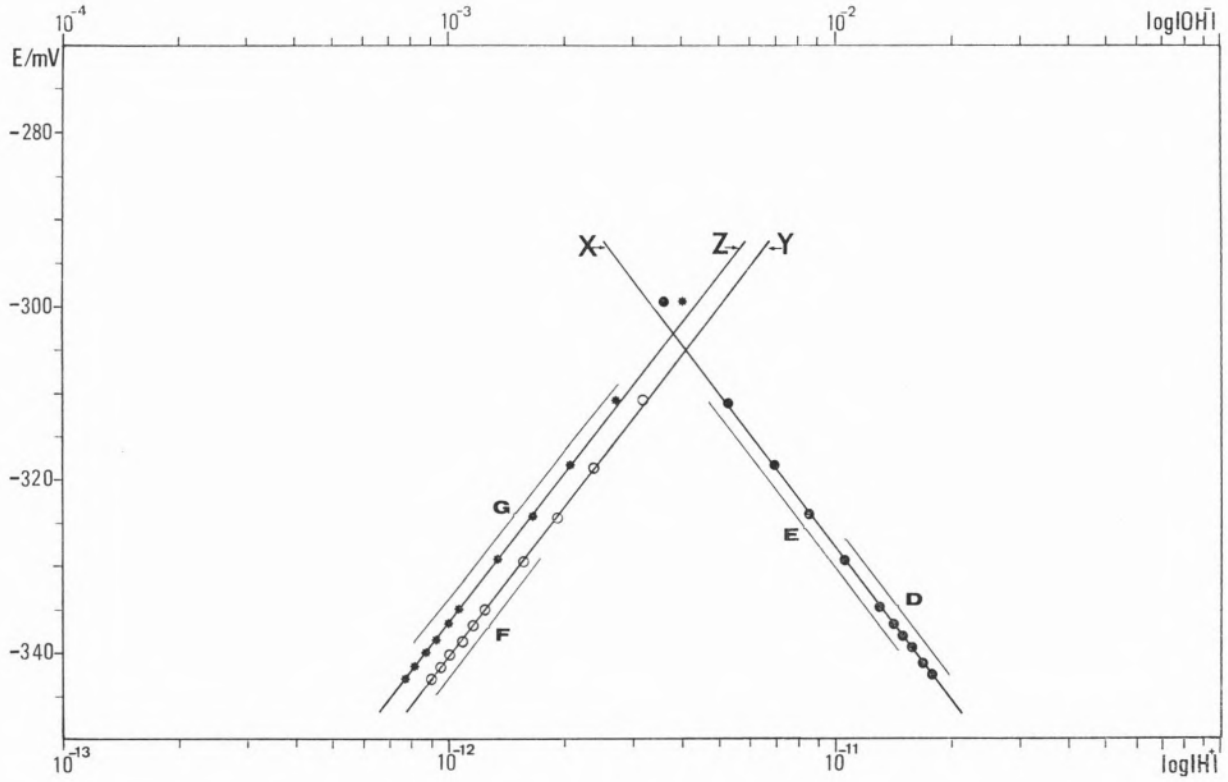

Fig. 2

Calibração do eléctrodo Philips GAH110 com base muito forte (X: $E = f\ (pc_{OH})$; Y e Z: $E = f\ (pc_H)$, ver nota (b) da tabela 2)

Tabela 2

Calibração do eléctrodo Philips GHA110 com base muito forte (a)

		c_{OH}/M	c_H / M	s/mV.década^{-1}	E°′/mV	R
X	D	$1{,}0.10^{-2}$ - $2{,}0.10^{-2}$		−56,7	−441,9	0,99996
	E	$5{,}2.10^{-3}$ - $1{,}5.10^{-2}$		−60,1	−448,2	0,99973
Y (b)	F		$9{,}3.10^{-13}$ - $1{,}6.10^{-12}$	56,7	339,7	0,99996
	G		$1{,}1.10^{-12}$ - $3{,}2.10^{-12}$	60,1	379,3	0,99973
Z (b)	F		$7{,}8.10^{-13}$ - $1{,}3.10^{-12}$	56,7	343,6	0,99996
	G		$9{,}3.10^{-13}$ - $2{,}7.10^{-12}$	60,1	384,1	0,99972

(a) Ver nota (a) da tabela 1.

(b) No cálculo dos valores da concentração de catião hidrogénio, c_H, a partir dos correspondentes valores da concentração de anião hidróxido, c_{OH}, usaram-se os seguintes valores da constante de autoprotólise estequiométrica da água: (Y): $1{,}667 \times 10^{-14}$ ref. [19]); (Z): $1{,}398 \times 10^{-14}$ (determinado experimentalmente neste trabalho).

Os resultados da calibração em meio nitidamente alcalino evidenciam, porém, um outro facto muito importante. Na fig. 2 e na tabela 2 apresentam-se resultados referentes à calibração da célula com base forte, por titulação de uma solução de hidróxido de sódio 0,02 M (I = 0,1 M) com ácido nítrico 0,1 M (curva X). Os resultados mostram que também em meio alcalino ocorre encurvamento da calibração (agora em função da concentração de anião hidróxido); um tratamento dos dados em sucessivos segmentos, semelhante ao que se usou em meio ácido, mostrou, porém, que, no intervalo em que o eléctrodo responde mais linearmente à concentração de anião hidróxido de 1×10^{-2} M a 2×10^{-2} M (zona D da fig. 2 e da tabela 2), isto é, para o qual o coeficiente de correlação do ajuste tem maior valor (R = 0,99996), o declive da recta ajustada é nitidamente inferior ao valor teórico (valor sublinhado na tabela 2).

Este abaixamento de declive em meio alcalino, cujas causas são as referidas no penúltimo parágrafo, é uma característica habitual do eléctrodo de vidro, que, por isso, é tolerada, dentro de certos limites; para a sua especificação usa-se a chamada «eficiência electromotriz» [18], que é dada, aproximadamente, pelo declive experimental expresso como percentagem do teórico. O valor desta grandeza encontrado para o eléctrodo Philips GHA110 (95,7 %) está nitidamente dentro dos limites aceites para eléctrodos deste tipo (de «intervalo de pH alargado», zona de operacionalidade de catálogo pH = 0-14): o valor mínimo exigido pelas especificações para a eficiência electromotriz é 95 % (pH = 11-12) ou 90 % (pH = 12-13) [18].

O facto de o declive do eléctrodo de vidro, na sua calibração com base forte (em função de pc_{OH}), ser inferior ao teórico, mantém-se quando a calibração é convertida numa calibração em função de pc_H, através da constante de autoprotólise da água (fig. 2 e tabela 2, ver secção seguinte), e, por si só, impede que se possa fazer uma calibração linear única envolvendo quer a zona de concentrações ácidas quer a zona de concentrações alcalinas. A conversão levanta, porém,

problemas adicionais, como se passa a discutir.

IMPORTÂNCIA DO VALOR DA CONSTANTE DE AUTOPROTÓLISE DA ÁGUA NA EXACTIDÃO DA CALIBRAÇÃO COM BASE MUITO FORTE. Na fig. 2 e tabela 2 incluem-se resultados da calibração do eléctrodo com base muito forte em função de pc_H, em que esta grandeza foi obtida por cálculo, através da constante estequiométrica de autoprotólise da água K_{ag} ($pc_H = pK_{ag} - pc_{OH}$). Usaram-se dois valores diferentes para esta constante estequiométrica (a 25°C e I = 0,1 M), concretamente $1{,}667 \times 10^{-14}$ [19] (resultados Y) e $1{,}398 \times 10^{-14}$ (resultados Z), determinado neste trabalho por aplicação do método de GRAN [5] à titulação de base forte com ácido forte — pontos da zona alcalina (ver adiante).

A não coincidência das calibrações Y e Z (fig. 2) evidencia a importância do valor da constante de autoprotólise da água utilizado na conversão de pc_{OH} para pc_H, na presente situação: embora os declives das duas calibrações sejam iguais (56,7 mV/década na zona de linearidade), os valores dos respectivos potenciais normais $E^{o\prime}_H$ diferem cerca de 4 mV (tabela 2). A esta diferença de potencial entre as duas curvas corresponde uma diferença de concentrações apreciáveis (16 % ou 0,07 unidades em pc_H).

A exactidão do valor da constante estequiométrica de autoprotólise da água é, portanto, essencial para se obter uma calibração exacta do eléctrodo de vidro com base muito forte, expressa em função de pc_H. Dadas as discrepâncias de valores encontrados, em geral, na literatura (quando existem para as condições experimentais usadas!), é preferível determinar aquela constante experimentalmente. Não é fácil, porém, realizar esta determinação experimental simultaneamente com a calibração do eléctrodo de vidro (ver a secção 3.3), e obter resultados isentos de erro. ROSSOTTI [12], por exemplo, aconselha que o valor da constante seja obtido por $K_{ag} = \text{antilog}\,[\mathcal{F}\,(E^{o\prime}_{OH} - E^{o\prime}_H)/RT \ln 10]$ (os símbolos têm o significado habitual), sendo $E^{o\prime}_H$ e $E^{o\prime}_{OH}$ obtidos, respectivamente, de calibrações com soluções padrões de ácido muito forte (em função de pc_H) e de base muito forte (em função de pc_{OH}); no entanto, a atribuição do valor teórico, ($RT \ln 10/\mathcal{F}$), ao declive, implica um erro, já que o valor do declive pode não ser o teórico, nomeadamente não é o teórico em meio alcalino, como se referiu. Esta mesma limitação pode ser apontada a outros métodos de calibração em que se admite o valor teórico para o declive do eléctrodo em meio alcalino [20].

Em virtude da discrepância observada entre o valor de K_{ag} determinado experimentalmente por nós, $1{,}398 \times 10^{-14}$ ($pK_{ag} = 13{,}85$), e valores de literatura nas mesmas condições experimentais (25°C e I = 0,1 M), nomeadamente o já referido valor de JAMESON e WILSON [19], $1{,}667 \times 10^{-14}$ ($pK_{ag} = 13{,}778$) e os de EILBECK e colaboradores [21], $1{,}66 \times 10^{-14}$ ($pK_{ag} = 13{,}78$), e MOTEKAITIS e MARTELL [22], $1{,}614 \times 10^{-14}$ $pK_{ag} = 13{,}792$), foi-se analisar até que ponto as diferenças poderiam resultar de diferentes processos de recolha e tratamento dos dados experimentais. Verificou-se que, se admitisse o valor teórico (59,2 mV/década) para o declive da resposta do eléctrodo (em vez do obtido experimentalmente na calibração do eléctrodo com soluções tampões com força iónica ajustada, 58,4 mV/década) e se se definisse a calibração pela resposta do eléctrodo na solução tampão de diidrogenofosfato de potássio/hidrogenofosfato de sódio ($pc_H = 6{,}784$) (ver secção 4), a aplicação do método usado na determinação da constante de autoprotólise da água (tratamento pelo método de GRAN dos dados da titulação de base forte com ácido forte — pontos de zona alcalina [5]) conduzia ao valor $1{,}622 \times 10^{-14}$ ($pK_{ag} = 13{,}79$). Este valor concorda perfeitamente com os recolhidos na literatura para as mesmas condições experimentais, já referidos. Estes factos sugerem que a discrepância de valores observada resulta de se ter usado o valor experimental do declive (esta conclusão não é, porém, segura, porque os artigos donde se colheram os valores da literatura não fornecem detalhes suficientes quanto à determinação dos mesmos).

DISCUSSÃO. O uso de soluções padrões de ácidos e bases muito fortes para a calibração do eléctrodo de vidro em função da concentração de catião hidrogénio, com vista a determinação de constantes de acidez e de formação de complexos, tem sido discutido e avaliado por diversos autores [20, 23-26] (ver também [27]).

No que diz respeito ao afastamento da linearidade a baixas concentrações de catião hidrogénio, McBRYDE [24], tendo feito o estudo para valores desta concentração inferiores a 10^{-3} M, salienta a ocorrência de desvios quando ela se aproxima de 10^{-4} M, sem discutir a sua causa; DUNSMORE e MIDGLEY [26] usam valores de pc_H inferiores a 3,5 sem mencionar qualquer razão para este limite.

No que respeita ao afastamento da linearidade para concentrações elevadas de catião hidrogénio, estes últimos autores [26] corrigem a resposta para atender ao potencial de junção. No entanto, McBRYDE [24] parece ignorar o encurvamento da calibração verificado nestas condições, o que pode explicar o facto de os valores do declive das rectas pH (experimental) $= m(-\log c_H) + b$ (tabela 1 de [24]) serem quase sempre inferiores à unidade. Semelhantemente, a correcção dos valores lidos de pH mediante adição do chamado parâmetro A, usado muito frequentemente [27, 23] (McBRYDE [24, 25] usa o parâmetro alternativo Γ = antilog A), que pode ser definido a partir da expressão (3) por

$$A = \Delta E'_j / s = (\Delta E_j / s) + \Delta \log f_H \qquad (4)$$

pressupõe linearidade de resposta do eléctrodo de vidro. Em soluções de força iónica elevada [27], para as quais a zona de resposta linear do eléctrodo é relativamente mais ampla do que a referida atrás, a correcção por uso daquele parâmetro pode ter interesse prático; quando a força iónica é mais baixa ($I \lesssim 0{,}5$ M), a zona de resposta linear é mais restrita, e só é lícito usar o parâmetro se quer a sua determinação quer as medições problema estiverem contidas nesta zona. Note-se que, em qualquer destes casos [23-25], as medições foram feitas em unidades de pH, pelo que estava em jogo, simultaneamente, a calibração do elécrodo e a calibração do pHmetro. DUNSMORE e MIDGLEY [26] reconheceram a importância do encurvamento da calibração e, corrigindo-a pelo processo de BIEDERMANN e SILLEN [14], apresentam um processo iterativo de cálculo do pc_H (a partir dos valores lidos de potenciais), o qual, porém, não é simples de realizar.

De um modo geral, estes estudos sobre a calibração do eléctrodo de vidro com ácidos (e bases) muito fortes, em função da concentração de catião hidrogénio, não encaram o eléctrodo de vidro como qualquer outro eléctrodo selectivo. Na calibração de um eléctrodo selectivo há lugar à determinação experimental de três parâmetros: declive, potencial normal e limite inferior de resposta linear. Para o eléctrodo de vidro, tem-se admitido frequentemente que o declive é o teórico e têm-se ignorado, quase completamente, os problemas ligados à determinação experimental do limite inferior de resposta linear e à influência das condições experimentais no seu valor. Os resultados obtidos neste trabalho mostram que, quando se consideram *soluções não tamponadas* do ião primário, o valor do limite inferior de resposta linear do eléctrodo de vidro (a catião hidrogénio), da ordem de 5×10^{-4} M a força iónica 0,1 M (ver tabela 1 e fig. 1), é bastante elevado, se comparado com os de outros eléctrodos selectivos quando respondem aos respectivos iões primários em soluções não tamponadas, nomeadamente os de membrana cristalina. Isto significa que, quanto a linearidade da resposta, o eléctrodo de vidro não pode ser considerado um eléctrodo selectivo dos de melhor qualidade.

3.2 — *CALIBRAÇÃO COM ÁCIDOS E BASES FORTES OU INTERMÉDIOS*

Para calibrar o eléctrodo de vidro no intervalo de concentrações de catião hidrogénio compreendido entre, aproximadamente 10^{-3}

e 10^{-11} M, não é possível utilizar ácidos e bases muito fortes porque estes, às concentrações a que teriam de ser usados, não asseguram à solução o poder tampão necessário à obtenção de uma resposta estável do eléctrodo. Por esta razão, para se resolver o problema da calibração no referido intervalo de concentrações de catião hidrogénio, recorre-se, geralmente [11], à titulação de ácidos ou bases de força intermédia cujas constantes de protólise estequiométricas sejam conhecidas, com base ou ácido muito forte, respectivamente, sendo o poder tampão garantido pela presença em solução de, pelo menos, um par conjugado de ácido-base. Este processo de calibração tem, no entanto, alguns inconvenientes que serão apontados com o apoio de resultados obtidos num caso concreto.

CALIBRAÇÃO COM UM ÁCIDO INTERMÉDIO. Na fig. 3 e na tabela 3 apresentam-se resultados referentes à calibração da célula electroquímica com soluções de ácido acético/anião acetato (HA/A^-). Estas foram obtidas por titulação, com solução de ácido acético 1 M, de uma solução de hidróxido de sódio 4×10^{-3} M (I = 0,1 M), de modo a cobrir a gama de concentrações 6×10^{-3} M $< c_{HA} < 3 \times 10^{-2}$ M). Os resultados obtidos (zona I da fig. 3) são apresentados na tabela 3 e na fig. 3, juntamente com os resultados obtidos numa calibração com ácido muito forte realizada no mesmo dia (zona H da fig. 3). Na fig. 3, para evidenciar bem certos pormenores de comportamento que serão discutidos a seguir, duplicou-se (mediante uma translação de 20 mV na escala das ordenadas), a repre-

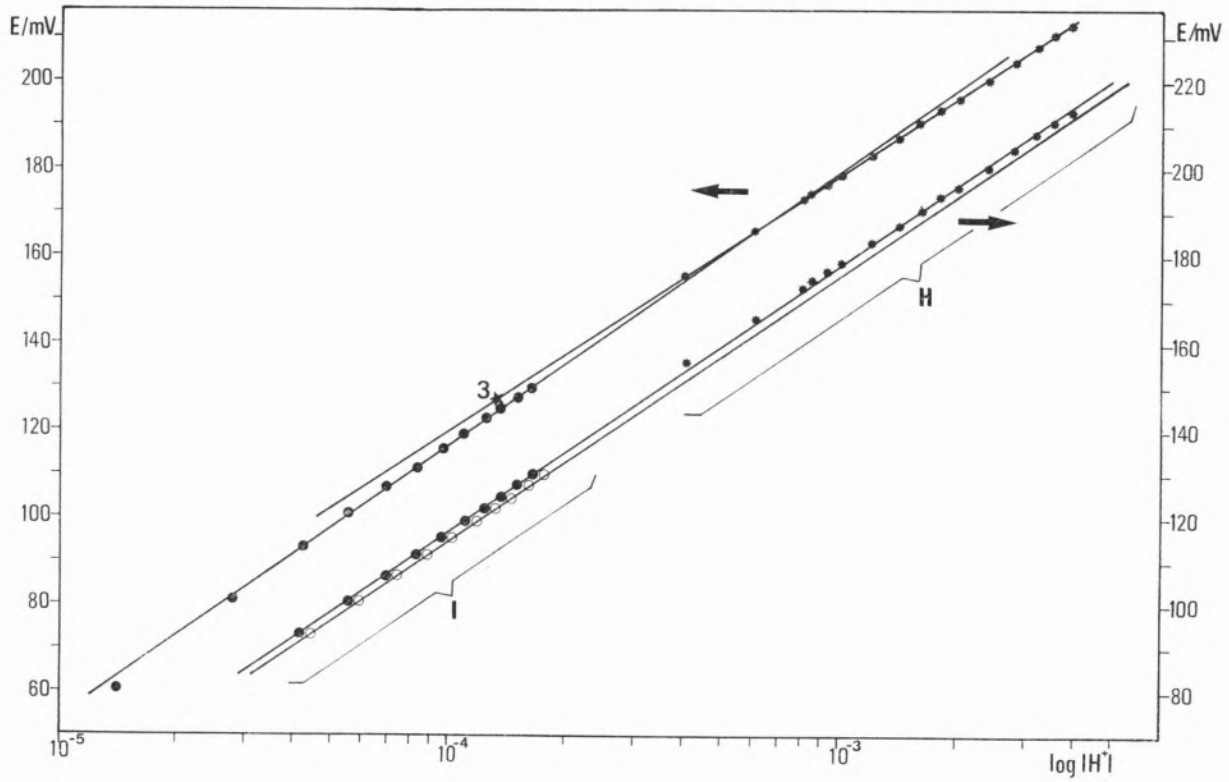

Fig. 3

*Calibração do eléctrodo Philips GAH110 com ácidos intermédios (Zona I: $pK_a = 4{,}551$ [28], ●, e $pK_a = 4{,}58$ [29, 30], o) e muito forte (Zona H, *) (ver detalhes no texto)*

Tabela 3

Calibrações do eléctrodo Philips GAH110 com ácidos muito forte (a) *e com constante de protólise* (b, c)

	c_H / M	s/mV.década^{-1}	$E^{o\prime}_H$ / mV	R
H	4.10^{-4} - 4.10^{-3} (a)	58,5	354,1	0,99998
I	4.10^{-5} - 2.10^{-4} (b)	63,3	369,3	0,99996
H + I	4.10^{-5} - 4.10^{-3} (a, b)	61,3	361,8	0,99984

(a) Soluções padrão de ácido nítrico.
(b) Soluções padrão de ácido acético/anião acetato, $pK_a = 4{,}551$ [28].
(c) Ver nota (a) da tabela 1.

sentação gráfica dos pontos experimentais correspondentes às referidas calibrações. Na fig. 3 incluem-se ainda duas calibrações na zona I, obtidas com os mesmos valores experimentais, mas com dois valores diferentes para a constante de protólise estequiométrica do ácido acético, obtidos na literatura (ver adiante).

Os resultados obtidos ilustram dois inconvenientes típicos deste processo de calibração, que se discutem a seguir.

EXACTIDÃO DA CONSTANTE DE PROTÓLISE. A fig. 3 evidencia que os valores de pc_H calculados com base em calibrações deste tipo são muito sensíveis ao valor da constante de protólise em jogo, neste caso a constante de acidez estequiométrica do ácido acético (a 25°C, I = 0,1 M). Concretamente, usaram-se dois valores de pK_a diferindo apenas de 0,02 unidades (4,551 [28], símbolos círculo fechado na fig. 3, e 4,53 [29, 30], símbolos círculo aberto, ambos referentes à força iónica 0,1 M, embora não ajustada com nitrato de potássio), observando-se na curva de calibração uma translacção de cerca de 0,08 unidades de pc_H, ou seja, aproximadamente, 2 mV. A exactidão de uma calibração obtida por este processo exige, portanto, que os valores das constantes de protólise usados, válidos para as condições experimentais em jogo, sejam muito rigorosos. Esta exigência levanta muitas dificuldades já que, se acaso existem valores publicados de constantes estequiométricas nas condições experimentais desejadas, é frequentemente difícil avaliar a sua qualidade.

CONTINUIDADE DOS TROÇOS DE CALIBRAÇÃO. A fig. 3 e a tabela 3 mostram que o ajuste simultâneo dos conjuntos de pontos referentes a dois ácidos diferentes (ácido acético/anião acetato, zona I, e ácido nítrico, zona H) é aceitável (R = 0,99984, ver tabela 3; ver, também, na fig. 3, a curva de calibração referente à escala das ordenadas à direita). No entanto, os ajustes separados diferem significativamente entre si (tabela 3, comparem-se os valores do declive e do potencial normal formal correspondentes aos troços de calibração H e I; ver, também, na fig. 3, os troços de calibração referentes à escala das ordenadas à esquerda).

A necessidade de proporcionar à solução um certo poder tampão implica que cada par conjugado ácido/base só permita calibrar o eléctrodo de vidro num intervalo de cerca de uma unidade de pc_H, em torno do valor de pK_a do respectivo ácido. Decorrente deste facto surge um problema que está,

aliás, intimamente ligado ao da exactidão da constante de protólise: a continuidade (ou falta de continuidade!) dos troços da curva de calibração obtidos com diferentes pares conjugados ácido/base (ou ácido ou base muito fortes). Na realidade, como o exemplo apresentado evidencia, a continuidade pode ser mais aparente que real. Quando se quer calibrar o eléctrodo num intervalo de várias unidades de pH, há necessidade de se usar vários pares conjugados ácido/base, e o problema acentua-se.

DISCUSSÃO. A titulação de ácidos (ou bases) fortes ou intermédios como processo de calibração do eléctrodo de vidro em função da concentração de catião hidrogénio, foi avaliada por POWELL e colaboradores [28, 31] e, mais recentemente, por AVDEEF e BUCHER [32]. Embora as limitações anteriormente referidas não sejam postas em evidência pelos autores destes artigos, elas estão implícitas nos resultados. POWELL e CURTIS [31] empregaram na calibração soluções de etilenodiamina/ácido perclórico com valores de pc_H entre 4 e 10, obtendo uma curva de calibração com um «ligeiro encurvamento em S», usando o seu «declive médio»; os valores de constantes de acidez foram obtidos da literatura, admitindo que alterações da natureza do electrólito inerte e das proporções dos constituintes da solução não teriam influência neles. HEDWIG e POWELL [28] usaram para a calibração, sucessivamente, soluções de cloreto de hidrogénio, ácido acético e dicloreto de etilenodiamónio (em todos os casos preparadas por titulações com hidróxido de sódio), referindo que há, nitidamente, diferenças entre as calibrações obtidas com as soluções de ácido acético e as dos outros dois compostos (*). AVDEEF e BUCHER [32] usaram para a calibração diversas soluções padrões («tampões universais»), preparados a partir de acetato de potássio, diidrogenofosfato de potássio, dicloreto de etilenodiamónio e bórax (isolados ou em misturas duplas ou triplas), por titulação com base forte; os resultados mostram, também, discrepâncias entre as calibrações obtidas a partir de diferentes soluções.

Em qualquer destes casos [28, 31, 32], as medições foram feitas em unidades de pH, o que exigiu uma calibração prévia do pHmetro e complicou a situação; isto é, como já foi referido a propósito dos estudos sobre as calibrações com ácido muito forte, discutidos atrás, não se encarou o eléctrodo de vidro como qualquer outro eléctrodo selectivo. No entanto, o comportamento do eléctrodo de vidro é semelhante ao dos outros eléctrodos selectivos: em primeiro lugar, a zona de resposta linear obtida na calibração com soluções não tamponadas pode ser ampliada para concentrações mais baixas por calibração com soluções tamponadas; em segundo lugar, um sistema tampão permite fazer a calibração numa zona restrita de concentrações, pelo que se põe, quer no caso do eléctrodo de vidro quer no caso dos outros eléctrodos selectivos [33], o problema da continuidade dos troços de calibração.

Em qualquer dos casos, a extrapolação de uma calibração para fora da zona de concentrações coberta pelo sistema tampão usado pode introduzir erros apreciáveis, pelo que não é lícita. Por outro lado, quanto mais longo for o intervalo em que se pretende fazer a calibração (por recurso a um número crescente de sistemas tampões) menos exacta será, em geral, a calibração obtida. É de referir, finalmente, a este propósito, que o eléctrodo de vidro é usado frequentemente em intervalos de concentração de catião hidrogénio muito largos (por exemplo, em titulações para determinações de constantes de equilíbrio), o que agudiza o problema da respectiva calibração.

(*) Embora, nestes dois artigos [28, 31], se afirmasse que as calibrações obtidas a diferentes valores de força iónica (no intervalo 0,04 a 0,2 M [28] ou 0,35 M [31]) coincidiam, posteriormente [32] foi demonstrado que elas dependiam da força iónica, segundo o que era de esperar atendendo à dependência do factor de actividade relativamente a esta grandeza.

3.3 — *REFINAMENTO COMPUTACIONAL DA CALIBRAÇÃO USADA NA DETERMINAÇÃO DE CONSTANTES DE EQUILÍBRIO*

A discussão anterior leva naturalmente à conclusão de que o problema da calibração do eléctrodo de vidro (excepto no intervalo restrito de concentrações em que a calibração pode ser feita com soluções padrões de ácido forte) é um problema que não pode ser resolvido autonomamente: a calibração do eléctrodo exige o conhecimento dos valores das constantes de protólise dos sistemas escolhidos para a realizar, determinados, pelo menos idealmente, nas condições experimentais pretendidas; a determinação destas, por sua vez, se realizada por potenciometria, exige uma calibração prévia nas mesmas condições experimentais!

No que respeita à realização da calibração do eléctrodo de vidro para a determinação de constantes de equilíbrio, quando os dados experimentais destas determinações são tratados pelo método dos mínimos quadrados não lineares por via computacional, tem-se adoptado a atitude de calibrar o eléctrodo por meio de titulações envolvendo ácidos e/ou bases muito fortes, de modo a obter valores iniciais para os parâmetros de calibração (nomeadamente, $E^{o\prime}$, já que para o declive se pode usar o valor teórico) e optimizar, depois, os valores destes parâmetros (ou só parte deles) conjuntamente com os das constantes de equilíbrio a refinar. Vários programas aparecidos recentemente seguem esta estratégia [34-36].

Num processo de optimização deste tipo pode-se, também, incluir, como variáveis a optimizar, a constante de autoprotólise da água (o que permitirá a determinação simultânea desta e dos parâmetros de calibração do eléctrodo, impossível de realizar pelos processos clássicos, ver a secção 3.1) e até as próprias concentrações analíticas dos reagentes. Na prática, porém, o número de parâmetros a optimizar tem de ser limitado, pois, se for muito elevado, os resultados obtidos podem ser falsos [34, 36]. Há, portanto, vantagens em limitar a optimização às variáveis que não possam ser determinadas experimentalmente com rigor suficiente, principalmente quando se trata de sistemas bastante complexos (AVDEEF e BUCHER [32] afirmam que o refinamento de valores de concentrações analíticas conhecidas *à priori* produz essencialmente um «efeito cosmético»!).

Independentemente de se refinar um maior ou menor número de variáveis, num procedimento deste tipo admite-se que os valores refinados finais para $E^{o\prime}$ e s (declive) definem uma calibração válida para todo o intervalo de concentrações em que se realizam medições. Se este for muito alargado, a calibração obtida pode estar afectada de erro, já que o declive do eléctrodo de vidro é menor em meio alcalino do que em meio ácido. Por outras palavras, o procedimento pode implicar uma extrapolação, que deve ser sempre encarada com cautela.

4 — CALIBRAÇÃO COM SOLUÇÕES PADRÕES DE REFERÊNCIA IDÊNTICAS A TAMPÕES PRIMÁRIOS MAS COM FORÇA IÓNICA AJUSTADA

Os resultados discutidos anteriormente mostraram que a calibração do eléctrodo de vidro no intervalo pretendido ($pc_H = 4\text{-}10$), por meio de titulações de ácidos ou bases, levantaria muitas dificuldades, porque se teriam de usar vários pares conjugados ácido/base para se cobrir totalmente este intervalo. Em face disto, procurou-se estabelecer um processo alternativo de calibração, mais rápido e mais cómodo que o anterior.

4.1 — *BASE DO PROCESSO E SUA DESCRIÇÃO*

Os tampões primários de pa_H do «National Bureau of Standars» [37] apresentam valores de força iónica variáveis de tampão para tampão, o que impede o seu uso para calibrações em termos de pc_H, para as quais se exigem soluções com força iónica constante. Verifi-

cou-se, porém, que o tampão «diidrogenofosfato de potássio 0,025 M/hidrogenofosfato de dissódio 0,025 M» («tampão de fosfato» (1 : 1), $pa_H = 6{,}865$, a 25°C) tem força iónica 0,1 M, enquanto que os tampões «hidrogenoftalato de potássio 0,05 M» («tampão de ftalato», $pa_H = 4{,}008$, a 25°C) e «bórax 0,01 M («tampão de bórax», $pa_H = 9{,}180$, a 25°C) têm forças iónicas inferiores, respectivamente 0,05 M e 0,02 M [37]; e, por outro lado, que para estes dois últimos casos existem descritos na literatura valores de pa_H para soluções com valores de força iónica superiores (obtidas por adição de electrólito inerte), iguais ou próximos a 0,1 M [38, 39].

A disponibidade destes dados sugeriu que se poderia fazer a calibração à força iónica 0,1 M com os três tampões referidos, que cobriam razoavelmente bem a zona de calibração pretendida, desde que se usasse o «tampão de fosfato» tal e qual, e se ajustasse os valores da força iónica dos dois outros tampões a 0,1 M, usando-se correcções de pa_H aos valores tabelados, obtidas na literatura, para obter os valores das respectivas actividades de catião hidrogénio. Os valores de pa_H para as três soluções com o mesmo valor da força iónica seriam convertidos em pc_H por meio do factor de actividade do catião hidrogénio à referida força iónica:

$$pc_H = pa_H + \log f_H \qquad (5)$$

Uma estratégia deste tipo foi recentemente seguida na medição do pc_H do sangue e soro sanguíneo [40] e permitiu a eliminação de erros resultantes da diferença na força iónica entre as soluções tampões usadas na calibração e as amostras [41].

4.2 — *CÁLCULO DE VALORES DE pa_H E pc_H DE SOLUÇÕES TAMPÕES COM FORÇA IÓNICA AJUSTADA A 0,1 M*

«TAMPÃO DE FOSFATO». Como este tampão tem força iónica 0,1 M, foi usado tal e qual; o valor de pc_H foi calculado a partir do de pa_H usando o valor de KIELLAND [42] para o factor de actividade do catião hidrogénio (a 25°C e $I = 0{,}1$ M), $f_H = 0{,}83$. O resultado obtido é apresentado na tabela 4.

Tabela 4

Cálculo da concentração de catião hidrogénio das soluções tampões com força iónica 0,1 M, a 25°C

Tampão	Δpa_H	pa_H	pc_H	c_H
1. Bórax $Na_4B_4O_7$ 0,01 M	−0,056	9,124	9,043	$9{,}056 \times 10^{-10}$
2. Fosfato KH_2PO_4 0,025 M Na_2HPO_4 0,025 M	—	6,865	6,784	$1{,}644 \times 10^{-7}$
3. Ftalato $KHC_8O_4H_4$ 0,05 M	−0,044	3,964	3,883	$1{,}309 \times 10^{-4}$

«TAMPÃO DE FTALATO». HAMER e ACREE [38] estudaram o efeito da adição de cloreto de potássio no pa_H desta solução tampão, no intervalo de valores de força iónica 0,06-0,1 M (a 25°C). Observaram uma variação quase linear em que a correcção para força iónica 0,1 M era $\Delta pa_H = -0{,}044$. Admitiu-se que, quando a força iónica é ajustada com nitrato de potássio, esta correcção se mantém, hipótese esta que é trivial em situações análogas [p. ex., 32], pelo que se obteve o valor corrigido $pa_H = 3{,}964$, a partir do qual se calculou pc_H (tabela 4).

«TAMPÃO DE BÓRAX». MANOV e colaboradores [39] estudaram o efeito da adição de cloreto de sódio no pa_H desta solução, no intervalo de valores de força iónica 0,02-0,07 M (a 25°C), observando uma variação linear. Admitindo que, tal como sucede no caso do «tampão de ftalato» e, também, no caso do «tampão de fosfato» (no intervalo de valores de força iónica 0,1-0,15 M fixada com cloreto de sódio) [43], a linearidade se mantém até força iónica 0,1 M, pode-se determinar, por extrapolação da representação gráfica de pa_H em função da força iónica, o valor da correcção de actividade para a força iónica 0,1 M, obtendo-se $pa_H = 9{,}124$ ($\Delta pa_H = -0{,}056$) (fig. 4). Procedendo-se como no caso anterior,

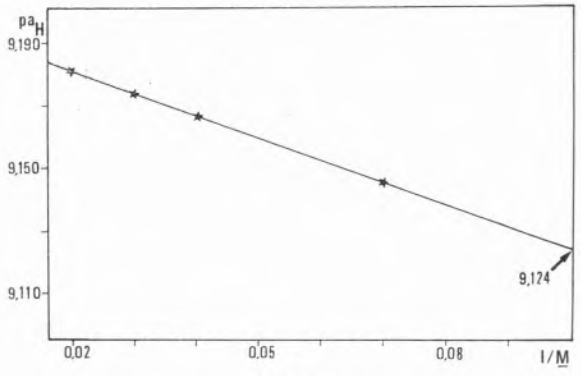

Fig. 4

Variação do pa_H da solução tampão de bórax 0,1 M com a força iónica (ajustada com cloreto de sódio) [39, 44]

calculou-se o valor de pc_H para a solução com a força iónica ajustada (tabela 4).

4.3 — *RESULTADOS E SUA DISCUSSÃO*

Os resultados obtidos na calibração da célula, com as soluções tampões de força iónica ajustada a 0,1 M são apresentados na fig. 5 e tabela 5. Para a análise de resultados, consideraram-se as rectas de calibração obtidas a partir das três soluções ou apenas de duas delas (o «tampão de fosfato», de pc_H intermédio e, sucessivamente, cada um dos outros dois).

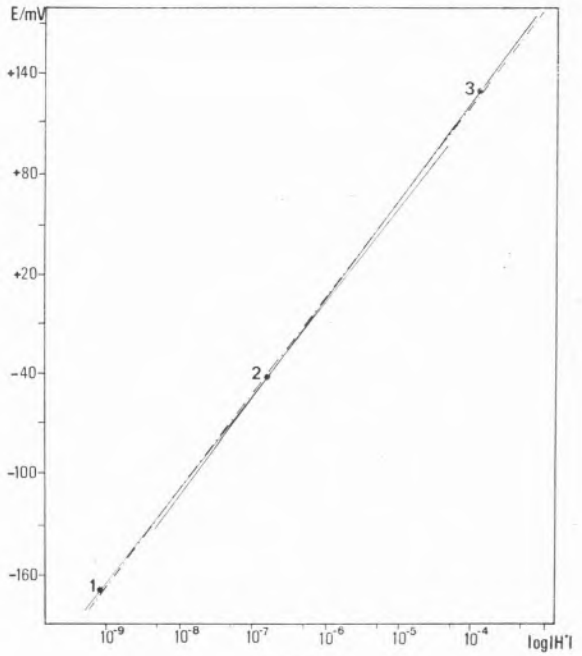

Fig. 5

Calibração do eléctrodo Philips GAH110 com soluções tampões com força iónica 0,1 M (ver composição das soluções na tabela 4)

Os resultados contidos na tabela 5 evidenciam que a recta de calibração obtida com as três soluções tampões apresenta um coeficiente de correlação aceitável (R = 0,99990). No entanto, esta recta de calibração (na fig. 5 a traço-ponto) não coincide com as obtidas a partir de duas soluções tampões (na fig. 5 a cheio): há diferenças apreciáveis, que nos declives quer nos potenciais normais (tabela 5). Quando se consideram as rectas de calibração obtidas a partir apenas de duas soluções tampões, verifica-se que o declive da

Tabela 5

Calibração do eléctrodo Philips GAH110 com soluções tampões de força iónica 0,1 M [a, b]

Tampão	c_H / M	s/mV.década^{-1}	$E_H^{o\prime}$ / mV	R
2	$1{,}644.10^{-7}$			
3	$1{,}309.10^{-4}$	59,6	361,6	—
1	$9{,}056.10^{-10}$			
2	$1{,}644.10^{-7}$			
3	$1{,}309.10^{-4}$	58,4	355,8	0,99990
1	$9{,}056.10^{-10}$			
2	$1{,}644.10^{-7}$	56,7	341,9	—

(a) Ver composição das soluções na tabela 4.
(b) Ver nota (a) da tabela 1.

recta associada aos tampões «de fosfato» e «de bórax», a que corresponde a zona de pc_H mais elevado, é inferior ao obtido para a recta referente aos tampões «de ftalato» e «de fosfato», a que corresponde uma zona de pc_H ácido (56,7 e 59,6 mV/década, respectivamente, tabela 5). Este comportamento é semelhante ao observado em calibrações com soluções de base muito forte relativamente a calibrações com ácido muito forte, discutido na secção 3.1.

Devido ao decréscimo de sensibilidade do eléctrodo de vidro à medida que a concentração de catião baixa, nomeadamente para meio alcalino, é que, quando se pretende usar o eléctrodo de vidro num intervalo limitado de pa_H para a determinação do pH operacional, se deve calibrá-lo com duas soluções tampões perto dos extremos desse intervalo. Quando, como no caso presente, a zona de utilização pretendida é bastante ampla, e se usam mais de duas soluções tampões na calibração, parece preferível dividir a calibração em segmentos sucessivos definidos por dois tampões cada. Por exemplo, nos estudos de equilíbrio químico a que o presente caso diz respeito, usou-se a recta de calibração definida pelos tampões «de fosfato» e «de bórax» para a medição de valores de pc_H superiores a 7 e a recta definida pelos tampões «de ftalato» e «de fosfato» para a medição de valores de pc_H inferiores a este valor.

É interessante referir que os resultados obtidos com este processo de calibração acompanham os obtidos quando se usaram soluções de ácido e de base muito forte para realizar a calibração. Na verdade, os parâmetros da recta da calibração obtida com soluções tampões «de fosfato» e «de ftalato» (tampões 2 e 3) ($s = 59{,}6$ mV/década, $E_H^o = 361{,}6$ mV, tabela 5) são muito próximos dos da recta de calibração com ácido muito forte na zona de resposta estritamente linear ($s = 59{,}9$ mV/década, $E_H^{o\prime} = 362{,}2$ mV, tabela 1); à escala da fig. 1 as duas rectas coincidiram (nesta figura inclui-se o ponto

referente à solução «tampão de ftalato»). Algo de semelhante se verificou para a recta de calibração com as soluções tampões «de bórax» e «de fosfato» (tampões 1 e 2) ($s = 56{,}7$ mV/década, $E_H^{o\prime} = 341{,}9$ mV, tabela 5) relativamente à recta de calibração com base muito forte ($s = 56{,}7$ mV/década, $E_H^{o\prime} = 343{,}6$ mV, tabela 2), embora, neste caso, a diferença entre os potenciais normais seja já de 1,7 mV (os valores de declive, inferiores aos teóricos, coincidem!).

Quando se comparam os parâmetros da recta de calibração obtida com as soluções tampões «de fosfato» e «de ftalato» (tampões 2 e 3) com os da obtida com soluções de ácido acético/anião acetato ($s = 63{,}5$ mV/década, $E_H^{o\prime} = 369{,}3$ mV, tabela 3 e fig. 3, zona H), não há concorlância dos valores dos parâmetros de calibração (na fig. 3, o ponto representativo da solução tampão «de ftalato» está afastado da recta de calibração com ácido acético/anião acetato cerca de 2 mV). A discordância resulta, provavelmente, das dificuldades encontradas neste último processo de calibração, discutidas em 3.2.

Um aspecto que merece também discussão específica é o do valor do factor de actividade usado para o catião hidrogénio, já que os factores de actividade dos iões isolados não são determináveis por via experimental, podendo-se dispor apenas de valores calculados. A concordância encontrada nas calibrações a partir das soluções tampões com força iónica ajustada e de soluções de ácido muito forte prova que o valor usado [42] é correcto. Por exemplo, o afastamento do ponto referente à solução «tampão de ftalato» da calibração com ácido muito forte (fig. 1) é de 0,5 mV, a que corresponde uma diferença em pc_H de menos de 0,1 unidades, o que sugere que não há erro apreciável proveniente do valor escolhido para os factores de actividade do catião hidrogénio. HEDWING e POWELL [28] discutem este aspecto com mais pormenor, referindo que o valor para o factor de actividade do catião hidrogénio de KIELLAND [42] conduz a resultados mais aceitáveis que valores calculados de outro modo.

4.4 — *AVALIAÇÃO INDIRECTA DO PROCESSO DE CALIBRAÇÃO*

A avaliação do processo de calibração foi completado por um processo indirecto: análise dos resultados obtidos na determinação de constantes de protólise de espécies previamente determinadas por potenciometria, por titulações em que o eléctrodo de vidro foi calibrado pela utilização das soluções tampões com força iónica ajustada. Usaram-se, para este fim, o ácido bórico e o anião hidrogenofosfato, por os valores das constantes de protólise envolvidas terem ordens de grandeza semelhantes aos das espécies cujas constantes de protólise se pretendia determinar [4]. Uma pesquisa bibliográfica [45-47] revelou que, embora não existissem valores publicados exactamente para as condições de meio usadas no presente estudo, havia valores de confiança para 25°C e força iónica 0,1 ou 0,15 M, que permitiriam comparações.

Os resultados de ensaios típicos, obtidos por tratamento dos dados experimentais com o programa MINIQUAD [10, 11] são apresentados na tabela 6 (que inclui, também, detalhes experimentais). Os valores repetidos das constantes de equilíbrio, obtidos, para cada modelo ensaiado, em cálculos realizados sucessivamente com as duas sequências de cálculo usadas, são coincidentes, o que comprova a convergência do programa para mínimos reais da função ajustada.

Apesar do ácido bórico ser considerado um ácido monoprótico, usou-se, entre os modelos ensaiados, um que incluía um segundo equilíbrio de desprotonação, correspondente a um hipotético $pK_{a_2}(H_3BO_3)$, a fim de testar a ausência de constantes de acidez fantasmas (de valor da ordem de grandeza 10^{-12} ou inferior); este equilíbrio foi rejeitado, o que comprovou a não obtenção destas. O valor obtido para $pK_{a_1} = p\beta_{1-1}$ foi 8,94 (literatura, $I = 0{,}1$ M, ajustada com perclorato de sódio [48]: 8,98; $I = 0{,}1$ M, ajustada com nitrato de potássio [49]: 9,11, valor este de menor confiança por, entre outras razões, não terem sido consideradas espécies polinucleares). Foi ajustada, também, a constante de

Tabela 6

Determinação das constantes de protólise do ácido bórico (LH_2) e do anião diidrogenofosfato (LH_2^-) a 25°C (resultados típicos) (a)

Espécie	A			B				R	χ^2	pc_H	N.º de pontos
	$\log \beta_1$	$\log \beta_2$	$\log \beta_3$	$\log \beta_{1,-1}$	$\log \beta_{1,-2}$	$\log \beta_{3,-1}$	$\log \beta_{5,-4}$				
H_3BO_3	Valores determinados										
	r (b)	r	(c)					—	—		
				−8,9410(24)	r	(c)	(c)	0,0039	7,90	7,70 - 9,48	21
				−8,93849(75)	(c)	−6,379(32)	r	0,0011	9,05		
	Valores da literatura (d) [48]										
				−8,98		−7,29	6,77				
$H_2PO_4^-$	Valores determinados										
	11,586(31)	18,340(31)	r	(−6,754(31)) (e)				0,00011	6,28		
	(11,592(34)) (f)			−6,75325(69)	−18,345(32)	(c)	(c)	0,00012	16,29	7,85 - 8,76	29
				−6,7482(16)	(c)	(c)	(c)	0,00034	16,86		
	Valores da literatura (g) [50]										
	11,545(5)			−6,638(3)							

(a) Os dados experimentais foram tratados usando os diversos modelos de cálculo indicados e as sequências (ver texto)

A: $L \mid LH \mid LH_2$ $\quad L + pH \rightleftarrows LH_p$ $\quad (p > 0)$ $\quad \beta_p$

B: $LH_2 \mid LH \mid L$ $\quad q\ LH_2 + r\ H \rightleftarrows L_q H_{2q+r}$ $\quad (q > 0, r < 0)$ $\quad \beta_{qr}$

Fixou-se a constante $K_{ag} = 1{,}398 \times 10^{-14}$ (valor determinado neste trabalho).

Incluem-se os valores dos parâmetros R (factor de concordância) e χ^2, fornecidos pelo programa, que dão indicações quanto à qualidade dos resultados obtidos.

Os números entre parêntesis a seguir aos valores da constante (logarítmos) são os respectivos desvios padrões.

(b) r: constante rejeitada.

(c) Espécie não incluída no modelo de cálculo.

(d) A 25°C, I = 0,1 M ($NaClO_4$) [48].

(e) Valor calculado a partir do tratamento pela sequência A.

(f) Valor calculado a partir do tratamento pela sequência B.

(g) A 25°C, I = 0,16 M (NaCl) [50].

formação β_{3-1} (log $\beta_{3-1} = -6{,}38$), associada à formação da partícula $L_3H_5^-$ ($LH_2 = H\ BO_3$) anteriormente também detectada [48] (valor: log $\beta_{3-1} = -7{,}29$), num estudo em que também foi detectada a espécie de constante β_{5-4}. Esta espécie não foi ajustada no presente estudo, o que pode ser causa da grande diferença (quase uma unidade logarítmica) encontrada nos valores de β_{3-1} obtidos nos dois estudos. Note-se que discrepâncias deste tipo para espécies polinucleares (quer em termos de número de espécies detectadas quer nos valores das constantes) são vulgares (veja-se, a seguir, a discussão sobre uma situação semelhante).

No caso do hidrogenofosfato, foram determinadas a segunda e a terceira constantes de acidez do ácido fosfórico, $pK_{a_2} = 6{,}75$ e $pK_{a_3} = 11{,}59$ (literatura, $I = 0{,}15$ M, ajustada com cloreto de sódio [50]: 6,63 e 11,55, respectivamente). Foi também ajustada a primeira constante de protólise, mas com um grau de precisão muito baixo (concretamente $pK_{a_1} = 2{,}09$, $\sigma = 0{,}55$), o que resulta de as determinações terem sido feitas a pc_H elevado (7,85-8,76), o que arrasta como consequência que as concentrações do ácido não protolisado sejam muito baixas. Neste sistema não se incluíram equilíbrios de associação detectados num outro estudo anterior, noutras condições experimentais [51], por, segundo VACCA e colaboradores [50], não serem significativas para a descrição do sistema nas presentes condições.

Em conclusão, as diferenças encontradas entre os valores obtidos e os valores de literatura das constantes de protólise do ácido bórico e do anião hidrogenofosfato são mínimas (e esperadas, dadas as diferenças de meio iónico, e, até, força iónica, e de detalhes de técnica experimental e de cálculo usadas), o que depõe a favor do processo de calibração usado.

5 — DISCUSSÃO FINAL E CONCLUSÕES

Os resultados apresentados na secção 3 mostram que, quando se considera o eléctrodo de vidro como um eléctrodo selectivo para catião hidrogénio (o que se faz com propriedade, pois que de um eléctrodo selectivo se trata), e se faz a sua calibração usando a estratégia vulgarmente utilizada na calibração de eléctrodos selectivos, se tornam evidentes certas limitações deste tipo de eléctrodo. Por um lado, em soluções não tamponadas, a zona de resposta linear tem amplitude muito limitada (o limite inferior de resposta linear é de cerca de 5×10^{-4} M a força iónica 0,1 M). Por outro lado, quando se usam solução tamponadas para estender a zona de resposta linear para valores inferiores, cada sistema tampão só permite varrer uma ou duas décadas de concentração de catião hidrogénio; se se pretende fazer a calibração numa zona de concentrações muito larga há que usar vários sistemas conjugados, pelo que se põe, na prática, um problema de continuidade dos diversos troços de calibração. Além disso, verifica-se que, em soluções de catião hidrogénio muito diluídas (meio bastante alcalino), o declive de resposta do eléctrodo observado experimentalmente é significativamente inferior ao teórico. Em conclusão, a calibração linear do eléctrodo de vidro, num intervalo de concentrações que envolva várias unidades de pa_H ou pc_H, pode implicar inexactidão da calibração, pelo menos em parte do intervalo considerado, que poderá ser tanto maior quanto mais esse intervalo se estender para zona alcalina.

Os resultados apresentados e discutidos na secção 4 mostram que o processo de calibração do eléctrodo de vidro, em função da concentração de catião hidrogénio, que utiliza soluções tampões de pa_H com força iónica constante (ajustada), permite obter, no intervalo de pc_H de 4 a 10, aproximadamente, uma calibração suficientemente exacta para poder ser usada na determinação de constantes de equilíbrio do «tipo aplicado» [12], isto é, que são obtidas para permitir o cálculo da distribuição das espécies numa solução particular, por exemplo, para planificar um processo analítico.

O processo de calibração proposto é bastante rápido e cómodo, o que constitui uma grande vantagem relativamente aos processos, muito vulgarmente utilizados, que envolvem titulações de ácido-base.

Quanto às limitações do processo de calibração descrito, deve-se começar por referir que, como se baseia na escala de pH do «National Bureau of Standards» (em que o pH operacional das soluções padrões primárias usadas para definir a escala funciona como pa_H sem introduzir erros apreciáveis [52]), não poderá ser implementado em meios muito ácidos (pc_H inferior a cerca de 3,5) ou muito alcalinos (pc_H superior a cerca de 10), já que, para estes, não existem padrões primários (os erros provenientes dos potenciais de junção residuais são demasiado elevados). Por outro lado, este processo de calibração só se poderá aplicar quando a força iónica for fixada ao valor 0,1 M (o valor da força iónica das soluções tampões de fosfato 1 : 1 e 1 : 3,5) ou a valores apenas um pouco superiores a este (por exemplo, 0,6 M, o valor da força iónica no sangue e soro sanguíneo [41]): para valores mais elevados de força iónica, a convenção de Guggenheim-Bates para o factor de actividade do anião cloreto, em que se baseia a definição das escalas de pH, em particular a do «National Bureau of Standards», deixa de ser válida, pelo que estas escalas perdem significado [41, 52].

Note-se, também, que não existem alternativas para implementação do processo que permitam, por exemplo, apertar o intervalo de medição de pc_H, já que não parece dispor-se de dados sobre a variação de pa_H com a força iónica para qualquer outro padrão primário da escala do «National Bureau of Standards», além dos três usados.

Apesar destas limitações, o processo é útil, pois, se se pretende calibrar o eléctrodo de vidro nas condições para que aquele é adequado, permite fazê-lo facilmente num amplo intervalo de pc_H, em zona nem muito ácida nem muito alcalina. O estudo realizado mostrou que a calibração obtida é razoavelmente concordante com a obtida por titulação do meio iónico com ácido forte, que só permite a calibração para valores de pc_H inferiores a cerca de 3 unidades. O uso adjacente dos dois processos permite, portanto, alargar a amplitude do intervalo de calibração.

(Recebido, 13 de Dezembro de 1983,
versão revista em 25 de Setembro de 1985)

AGRADECIMENTOS

Este trabalho foi realizado no âmbito da Linha de Acção 4A (Construção e Aplicações de Eléctrodos Selectivos de Iões) do Centro de Investigação em Química da Universidade do Porto, que tem o suporte económico do Instituto Nacional de Investigação Científica, Lisboa.

Agradece-se ao Laboratório de Cálculo Automático da Faculdade de Ciências do Porto as facilidades de computação concedidas.

Agradece-se ao Sr. António J. T. Sousa a colaboração prestada na execução de tarefas laboratoriais de rotina.

BIBLIOGRAFIA

[1] M.T.S.D. VASCONCELOS, A.A.S.C. MACHADO, «Resumos das Comunicações ao Quarto Encontro Anual da Sociedade Portuguesa de Química», Comunicação PC12, Lisboa, 1981.

[2] I.U.P.A.C., Analytical Chemistry Division, Comission on Analytical Nomenclature, «Recommendations for Nomenclature of Ion-Selective Electrodes», *Pure Appl. Chem.*, 48, 129 (1976).

[3] J.L.F.C. LIMA, A.A.S.C. MACHADO, «Nomenclatura sobre Eléctrodos Selectivos de Iões», Centro de Investigação em Química (UP), Porto, 1977.

[4] M.T.S.D. VASCONCELOS, «Determinação potenciométrica (pH e pM) de Constantes de Formação de Complexos», Tese de Doutoramento, Faculdade de Ciências do Porto, Porto, 1983.

[5] G. GRAN, *Analyst*, **77**, 661 (1952).

[6] F.J.C. ROSSOTTI, H. ROSSOTTI, *J. Chem. Ed.*, **42**, 375 (1965).

[7] R.G. BATES, «Determination of pH, Theory and Practice», 2.ª ed., Wiley & Sons, Nova Iorque, 1973, p. 94.

[8] R. G. BATES, *J. Res. Nat. Bur. Stand.*, **66A**, 179 (1962).

[9] A. SABATINI, A. VACCA, P. GANS, *Talanta*, **21**, 53 (1974).

[10] P. GANS, A. VACCA, A. SABATINI, *Inorg. Chim. Acta*, **18**, 237 (1976).

[11] Ref. [7], p. 254-276.

[12] H.S. ROSSOTTI, *Talanta*, **21**, 809 (1974).

[13] Ref. [7], p. 264.

[14] G. BIEDERMANN, L.G. SILLEN, *Ark. Kemi*, **5**, 425 (1953).
[15] H.S. ROSSOTTI, «Chemical Applications of Potentiometry», 2.ª ed., Van Nostrand, Londres, 1969, p. 110.
[16] N. LINNET, «pH Measurements in Theory and Practice», Radiometer, Copenhaga, 1970, p. 84.
[17] Ref. [7], p. 360 e 364.
[18] Ref. [7], p. 342.
[19] R.F. JAMESON, M.F. WILSON, *J.C.S. Dalton*, 2607 (1972).
[20] M. MOLINA, C. MELIOS, J.O. TOGNOLLI, L.C. LUCHIARI, M. JAFELICCI Jr., *J. Electroanal. Chem.*, **105**, 237 (1979).
[21] W.J. EILBECK, F. HOLMES, G.G. PHILLIPS, A.E. UNDERHILL, *J. Chem. Soc.*, **A**, 1161 (1967).
[22] R.J. MOTEKAITIS, A.E. MARTELL, *Inorg. Chem.*, **13**, 550 (1974).
[23] H.M. IRVING, M.G. MILES, L.D. PETTIT, *Anal Chim. Acta*, **38**, 475 (1967).
[24] W.A.E. MCBRYDE, *Analyst*, **94**, 337 (1969).
[25] W.A.E. MCBRYDE, *Analyst*, **96**, 739 (1971).
[26] H.S. DUNSMORE, D. MIDGLEY, *Anal. Chim. Acta*, **61**, 115 (1972).
[27] Ref. [7], p. 262 e referências aí contidas.
[28] G.R. HEDWING, H.K.J. POWELL, *Anal. Chem.*, **43**, 1206 (1971).
[29] L.G. SILLEN, A.E. MARTELL, «Stability Constants of Metal-Ion Complexes», Special Publication 17, The Chemical Society, Londres, 1964, p. 364.
[30] M. YASUDA, K. YAMSAKI, H. OHTAKI, *Bull. Chem. Soc. Japan*, **23**, 1067 (1960).
[31] H.K.J. POWELL, N.F. CURTIS, *J. Chem. Soc.*, **B**, 1205 (1966).
[32] A. AVDEEF, J.J. BUCHER, *Anal. Chem.*, **50**, 2137 (1978).
[33] M.G.P. SILVA, J.L.F.C. LIMA, A.A.S.C. MACHADO, «Resumos de Comunicações da Quarta Reunião Nacional de Electroquímica», Braga, 1983, Comunicação C30.5.
[34] G. ARENA, E. RIZZARELLI, S. SAMMARTANO, C. RIGANO, *Talanta*, **26**, 1 (1979).
[35] F. GAIZER, A. PUSKAS, *Talanta*, **28**, 565 (1981).
[36] P.M. MAY, D.R. WILLIAMS, P.W. LINDER, R.G. TORRINGTON, *Talanta*, **29**, 249 (1982).
[37] Ref. [7], p. 71-84, 90-99, 118-122.
[38] W.J. HAMER, S.F. ACREE, *J. Res. Nat. Bur. Stand.*, **32**, 215 (1944).
[39] G.G. MANOV, N.J. DELOLLIS, P.W. LINDVALL, S.F. ACREE, *J. Res. Bur. Stand.*, **36**, 543 (1946).
[40] A.K. COVINGTON, *Anal. Chim. Acta*, **127**, 1 (1981).
[41] R.C. BATES, C.A. VEGA, D.R. WHITE JR., *Anal. Chem.*, **50**, 1295 (1978).
[42] J. KIELLAND, *J. Am. Chem. Soc.*, **59**, 1675 (1937).
[43] R.G. BATES, S.F. ACREE, *J. Res. Nat. Bur. Stand.*, **34**, 373 (1945).
[44] Ref. [7], p. 120.
[45] Ref. [29], p. 104.
[46] L.G. SILLEN, A.E. MARTELL, «Stability Constants of Metal-Ion Complexes, Supplement n.º 1, Special Publication 23, The Chemical Society, Londres, 1971, p. 52.
[47] E. HOGFELDT, «Stability Constants of Metal-Ion Complexes, Part A: Inorganic Ligands», IUPAC Chemical Data Series, N.º 21, Pergamon Press, Oxford, 1982, p. 76.
[48] N. INGRI, *Acta. Chem. Scand.*, **16**, 439 (1962).
[49] A. IVASKA, E. WÄNNIMEN, *Anal. Letters*, **6**, 931 (1973).
[50] A. VACCA, A. SABATINI, L. BOLOGNI, *J.C.S. Dalton*, 1246 (1981).
[51] C.W. CHILDS, *J. Phy. Chem.*, **73**, 2956 (1969).
[52] R.G. BATES, *Crit. Rev. Anal. Chim.*, **10**, 247 (1981).

ABSTRACT

Calibration of glass electrodes for measurement of hydrogen ion concentration in the range of pc_H from 4 to 10.

Experimental difficulties found in procedures for calibration of glass electrodes (in cells with liquid junction) for the measurement of hydrogen ion concentration, with standards obtained by titration of strong or weak acids with base, have been discussed. A comparison of the calibration behaviour of the glass electrode with that of other ion selective electrodes is included.

An alternative procedure for calibration of glass electrodes in the range of pc_H from 4 to 10, which uses pa_H standard with ionic strength fixed to 0,1 M, from which hydrogen ion concentrations are obtained through activity coefficients, has been introduced and evaluated.

INSTRUCTIONS FOR AUTHORS

1. The **Revista Portuguesa de Química** accepts for publication original papers, research notes and review articles.

2. All manuscripts will be sent to referees for assessment.

3. Manuscripts should be written either in Portuguese or English.

4. Three complete copies of the manuscript should be submitted to one of the Editors. The manuscript should be typed on only one side of the paper with double spacing throughout the text, tables, figure legends, footnotes, and list of references, and with a margin of not less than 4 cm on the left-hand side of each page. The title page should carry the title of the paper, the authors' names, the name and address of the laboratory where the work was done, the name and address of the person to whom proofs should be sent, and a short resuming title for printing at the head of each right-and printed page. An abstract, both in Portuguese and English, in not more than about 300 words should be included; it should be typed on a separate page. A list of figure legends, begining on a new page, should be included. Finally, a list of references in numerical sequence, also begining on a new page, should be included. References should be given in the *current* style of *Chemical Abstracts,* particular care being taken always to give authors' initials.
Research notes should be brief, no more than five typed pages, and need no abstract.

5. Authors are strongly advised to adhere to international conventions in the choice of symbols, units and notation.
A few non-SI units are acceptable without definition; these include Å, cm^{-1}, eV and u (unified atomic mass unit). Atomic units are also acceptable provided they are stated explicitly as in the IUPAC recommendations (*Pure and Applied Chemistry,* 1978, **50**, 75). In general, however, non-SI units should be avoided, but in the rare cases where this is particularly inconvenient the non-SI units should be defined once in each paper.
When numerical values of a physical quantity are tabulated, the expression placed at the head of the comumn should be a pure number. For example, a table of entropies could have as a heading $S/(JK^{-1}\ mol^{-1})$. Similarly, the axis labels for graphs should also be pure numbers, such as the quotient of the symbols for the physical quantity and the symbol for the unit used. Manuscripts which do not conform to these conventions will be edited appropriately and in some cases may be returned to the authors for editing, after they have been accepted.

6. There are no page charges for the journal. Offprints may be ordered from the editors at the proof stage.